Use of Radio Frequency Identification Tags in Pavements

PUBLICATION NO. FHWA-HRT-14-061

APRIL 2015

U.S. Department of Transportation
Federal Highway Administration

Research, Development, and Technology
Turner-Fairbank Highway Research Center
6300 Georgetown Pike
McLean, VA 22101-2296

FOREWORD

This document presents the results of evaluations of radio frequency identification (RFID) for a set of pavement applications: tracking of placement of truckloads of hot mix asphalt (HMA) in the pavement, tracking of placement of truckloads of Portland cement concrete (PCC) in the pavement, real-time measurement of pavement temperature versus depth and time during intelligent compaction, early detection of reflection cracking in overlays, and guidelines for integration of material property data from construction and pavement performance data during service via RFID-assisted geolocation. RFID tracking of HMA placement was the most successful application and the one with potential for immediate commercial implementation. RFID tracking of PCC placement was unsuccessful, at least with the RFID systems evaluated in this study; the high dielectric constant of the hydrated cement paste severely attenuates the RFID signals. Real-time measurement of pavement temperatures with depth and time during intelligent compaction shows promise, but further work is required to develop faster and more reliable reader software/hardware and RFID tags. Laboratory and limited field evaluation of an RFID-based sensor for early detection of reflection cracks in HMA overlays also shows promise, but additional development work and field trials are required. The guidelines for data integration outline in generic terms the necessary steps to integrate RFID-tagged material property data collected during construction with pavement management system data collected during service; implementation details will be dependent on the materials and pavement systems used by each individual agency. The intended audience for this report is transportation engineers involved in pavement construction, quality acceptance testing for paving materials, pavement design, and pavement management.

Jorge E. Pagán-Ortiz
Director, Office of Infrastructure
Research and Development

TECHNICAL DOCUMENTATION PAGE

1. Report No. FHWA-HRT-14-061	2. Government Accession No.	3. Recipient's Catalog No.
4. Title and Subtitle Radio Frequency Identification Applications in Pavements		5. Report Date August 2014
		6. Performing Organization Code
7. Author(s) Charles W. Schwartz, Junaid S. Khan, Grant H. Pfeiffer, Endri Mustafa		8. Performing Organization Report No.
9. Performing Organization Name and Address University of Maryland—College Park Department of Civil and Environmental Engineering 1173 Glenn L. Martin Hall College Park, MD 20742		10. Work Unit No. (TRAIS)
		11. Contract or Grant No. DTFH61-06-D-00036
12. Sponsoring Agency Name and Address Office of Infrastructure Research and Development Federal Highway Administration 6300 Georgetown Pike McLean, VA 22101-2296		13. Type of Report and Period Covered Final Report, September 2006–July 2013
		14. Sponsoring Agency Code

15. Supplementary Notes
The Contracting Officer's Technical Representative (COTR) was Katherine Petros.

16. Abstract
Radio frequency identification (RFID) technology is widely used for inventory control, tool and material tracking, and other similar applications where line-of-sight optical bar codes are inconvenient or impractical. Several applications of RFID technology to pavements are evaluated in this report: tracking of placement of truckloads of hot mix asphalt (HMA) within the pavement, tracking of placement of truckloads of Portland cement concrete (PCC) within the pavement, real-time measurement of pavement temperature versus depth and time during intelligent compaction, and early detection of reflection cracking in overlays. RFID tracking of HMA placement was the most successful application and the one with potential for immediate commercial implementation. RFID tracking of PCC placement was unsuccessful, at least with the RFID systems evaluated in this study; the high dielectric constant of the hydrated cement paste severely attenuates the RFID signals. Real-time measurement of pavement temperatures with depth and time during intelligent compaction shows promise but further work is required to develop reader software/hardware and RFID tags with more reliable and faster response rates. Laboratory and limited field evaluation of an RFID-based sensor for early detection of reflection cracks in HMA overlays also shows promise, but additional development work and field trials are required. Guidelines for integration of material property data from construction and pavement performance data during service via RFID-assisted geolocation are also provided. The necessary steps required to integrate RFID-tagged material property and pavement management data are outlined in generic terms. Implementation details will depend on the materials and pavement systems used by each individual agency.

17. Key Words Radio frequency identification; pavement instrumentation; pavement construction; materials management; pavement management; intelligent compaction; reflection cracking	18. Distribution Statement No restrictions. This document is available to the public through NTIS: National Technical Information Service 5301 Shawnee Road Alexandria, VA 22312

19. Security Classif. (of this report) Unclassified	20. Security Classif. (of this page) Unclassified	21. No. of Pages 208	22. Price

Form DOT F 1700.7 (8-72) Reproduction of completed page authorized

SI* (MODERN METRIC) CONVERSION FACTORS

APPROXIMATE CONVERSIONS TO SI UNITS

Symbol	When You Know	Multiply By	To Find	Symbol
		LENGTH		
in	inches	25.4	millimeters	mm
ft	feet	0.305	meters	m
yd	yards	0.914	meters	m
mi	miles	1.61	kilometers	km
		AREA		
in^2	square inches	645.2	square millimeters	mm^2
ft^2	square feet	0.093	square meters	m^2
yd^2	square yard	0.836	square meters	m^2
ac	acres	0.405	hectares	ha
mi^2	square miles	2.59	square kilometers	km^2
		VOLUME		
fl oz	fluid ounces	29.57	milliliters	mL
gal	gallons	3.785	liters	L
ft^3	cubic feet	0.028	cubic meters	m^3
yd^3	cubic yards	0.765	cubic meters	m^3
	NOTE: volumes greater than 1000 L shall be shown in m^3			
		MASS		
oz	ounces	28.35	grams	g
lb	pounds	0.454	kilograms	kg
T	short tons (2000 lb)	0.907	megagrams (or "metric ton")	Mg (or "t")
		TEMPERATURE (exact degrees)		
°F	Fahrenheit	5 (F-32)/9 or (F-32)/1.8	Celsius	°C
		ILLUMINATION		
fc	foot-candles	10.76	lux	lx
fl	foot-Lamberts	3.426	$candela/m^2$	cd/m^2
		FORCE and PRESSURE or STRESS		
lbf	poundforce	4.45	newtons	N
lbf/in^2	poundforce per square inch	6.89	kilopascals	kPa

APPROXIMATE CONVERSIONS FROM SI UNITS

Symbol	When You Know	Multiply By	To Find	Symbol
		LENGTH		
mm	millimeters	0.039	inches	in
m	meters	3.28	feet	ft
m	meters	1.09	yards	yd
km	kilometers	0.621	miles	mi
		AREA		
mm^2	square millimeters	0.0016	square inches	in^2
m^2	square meters	10.764	square feet	ft^2
m^2	square meters	1.195	square yards	yd^2
ha	hectares	2.47	acres	ac
km^2	square kilometers	0.386	square miles	mi^2
		VOLUME		
mL	milliliters	0.034	fluid ounces	fl oz
L	liters	0.264	gallons	gal
m^3	cubic meters	35.314	cubic feet	ft^3
m^3	cubic meters	1.307	cubic yards	yd^3
		MASS		
g	grams	0.035	ounces	oz
kg	kilograms	2.202	pounds	lb
Mg (or "t")	megagrams (or "metric ton")	1.103	short tons (2000 lb)	T
		TEMPERATURE (exact degrees)		
°C	Celsius	1.8C+32	Fahrenheit	°F
		ILLUMINATION		
lx	lux	0.0929	foot-candles	fc
cd/m^2	$candela/m^2$	0.2919	foot-Lamberts	fl
		FORCE and PRESSURE or STRESS		
N	newtons	0.225	poundforce	lbf
kPa	kilopascals	0.145	poundforce per square inch	lbf/in^2

*SI is the symbol for the International System of Units. Appropriate rounding should be made to comply with Section 4 of ASTM E380.
(Revised March 2003)

TABLE OF CONTENTS

LIST OF FIGURES

LIST OF TABLES

LIST OF ACRONYMS AND ABBREVIATIONS

CMOD	Crack Mouth Opening Displacement
CPVC	Chlorinated Polyvinyl Chloride
DC	Direct Current
FHWA	Federal Highway Administration
GPS	Global Positioning System
HMA	Hot Mix Asphalt
ICT	International Coding Technologies
IDT	Interdigital Transducer
IRI	International Roughness Index
LIMS	Laboratory Inventory Management System
LTS	Log Track System
MB	Megabyte
MDSHA	Maryland State Highway Administration
MMS	Materials Management System
MTV	Material Transfer Vehicle
NCAT	National Center for Asphalt Technology
PCC	Portland Cement Concrete
PDA	Personal Digital Assistant
PDE	Partial Differential Equation
PMMA	Polymethyl Methacrylate
PMS	Pavement Management System
QA	Quality Assurance
QC	Quality Control
RF	Radio Frequency
RFID	Radio Frequency Identification
SAW	Surface Acoustic Wave
TFHRC	Turner-Fairbanks Highway Research Center
UHF	Ultrahigh Frequency
UMD	University of Maryland
W/C	Water-to-Cement

EXECUTIVE SUMMARY

PROJECT OBJECTIVES

The original objective of this project was to demonstrate that inexpensive expendable radio frequency identification (RFID) tags could be used to identify the spatial location along the pavement alignment of specific truckloads of hot mix asphalt (HMA) production. These tags are placed in the truckload as it leaves the production plant, pass through the paver, and are compacted into the finished mat. Cross-referencing these tags with Global Positioning System (GPS) latitude and longitude coordinates after construction allows spatial referencing of quality assurance (QA) material property data measured at the production plant, enabling linkage to other spatially referenced in-place test results and pavement management system (PMS) pavement performance data. This use of the large QA and PMS datasets already collected by highway agencies will permit more robust analyses and insights into the relationships between HMA material properties and actual pavement performance.

Phases I and II of this project addressed the development of techniques for making the RFID tags sufficiently rugged to withstand the harsh thermal and mechanical conditions of HMA paving and for evaluating the survival and read performance of the tags after construction. Phase I focused on identifying feasible RFID devices for HMA tracking, identifying candidate projects for field testing, and formulating a field evaluation work plan. Phase II executed the work plan developed in Phase I.

During the Phase I and II work, some additional applications of RFID technologies to pavements were identified for evaluation:

- Evaluation of potential problems caused by surfaced tags.
- Exploration of surface acoustic wave (SAW) RFID technology for improved performance of small format tags.
- Demonstration of RFID tracking of placement of Portland cement concrete (PCC) loads in pavements.
- Provision of guidance to agencies on data integration.

The evaluation of these additional topics was the focus of the additional and final Phase III of the project.

This report documents all work done over all three phases of the project.

RFID TECHNOLOGY

Two types of RFID technology were employed in this study: conventional passive ultrahigh frequency (UHF) RFID tags and the newer SAW RFID tags. The passive UHF RFID technology encodes a digital signature on a small microchip attached to a copper foil antenna—the RFID "tag." This passive tag receives energy from UHF radio waves transmitted by a RFID "reader"; the tag harvests this incoming radio frequency (RF) energy to transmit its encoded digital

signature back to the reader. These RFID tags, although small, can be read several yards away from the reader's antenna.

SAW RFID tag consists of an interdigital transducer (IDT) and a series of acoustic reflector traps etched into a piezoelectric substrate. The tag reader emits a radio wave pulse to the IDT that is converted piezoelectrically into a nanoscale acoustic wave. The wave travels past the reflectors to produce a unique pattern of reflected pulses. These travel back to the IDT, where they are piezoelectrically converted into an encoded electronic reply signal to the reader. The SAW chip operates in a purely passive mode and does not require supplementary direct current (DC) power (i.e., battery). The principal advantages of the SAW RFID technology for pavement construction include better inherent ruggedness, smaller formats, and longer read ranges for a given tag antenna size compared with conventional RFID. In addition, and most relevant to this study, SAW RFID technology is capable of wireless measurement of temperature via the perturbation of the return wave signal caused by the influence of thermal strains on the spacing of the acoustic reflectors.

PRACTICAL APPLICATIONS OF RFID TECHNOLOGY

RFID technology is widely used today for supply chain inventory management, security, equipment tracking, among other applications. However, in construction, RFID technology is primarily used for tracking equipment and materials. Specific RFID applications identified in the literature review include the following:

- Tracking of PCC test specimens.
- Maturity monitoring of in-place PCC.
- Tracking of construction materials at project site (e.g., fabricated pipe).
- Construction tool inventory/usage control/monitoring.
- Location identification of buried infrastructure (cables and pipes).

Several new applications of RFID technology to pavements were evaluated in this study: RFID tracking of HMA and PCC placement, measurement of pavement temperature with depth and time during intelligent compaction, and early detection of reflection cracks in HMA overlays.

KEY FINDINGS

Key findings of this work are summarized here, organized by the following topical areas:

- RFID tracking of HMA placement (chapters 2, 3, and 4).
- RFID tracking of PCC placement (chapter 5).
- Pavement temperature measurement using SAW RFID (chapter 6).
- Reflection crack detection (chapter 7).
- Guidance on data integration (chapter 8).

RFID Tracking of HMA Placement

The feasibility of using RFID tags to track HMA placement was evaluated via: 1) literature review, 2) identification of appropriate RFID technology, and 3) prototype tag development and

evaluation. The feasibility evaluation identified UHF passive RFID technology as best suited to the hot mix asphalt paving application. After considerable research of available products, a ThingMagic Mercury® 5 RFID system and related hardware were acquired for use in this project. Suitable RFID tags were identified, and a feasible encapsulation system was developed that adequately protects the RFID tags from the temperatures and compaction stresses inherent in HMA transport and paving. An Alien® Gen 2 2x2 RFID tag curled and encapsulated in high-temperature epoxy inside a ¾-inch (19-mm) nominal outside diameter chlorinated polyvinyl chloride (CPVC) pipe provided a hardened tag of appropriate size and adequate read range.

The encapsulated RFID tags were field tested to evaluate the following issues: survivability in real-world paving scenarios, read range under actual field conditions; required redundancy, construction practicality issues, and construction quality issues. The encapsulated RFID tags were evaluated at three parking lot locations on the University of Maryland (UMD) campus and in two stages in a new pavement constructed by the Maryland State Highway Administration (MDSHA). The field trials confirmed the very high survival rate of the encapsulated tags. Read success rates varied significantly with tag size and less significantly on other details such as antenna configuration and vehicle speed. The field trials consistently demonstrated that post-construction read success rates of 60 to 80 percent or higher are achievable from a bumper-mounted antenna array, even on a vehicle moving at traffic speeds.

It was observed during the HMA field trials that some of the encapsulated RFID tags "floated" to the surface of the compacted mat. This raised the possibility of a decrease in in-place compacted density or an increase in the in situ permeability or both in the local region around the tag. Extensive density and permeability testing was performed to evaluate these possibilities. No localized decrease in density, increase in permeability, or any detrimental effects of the surfaced tags were found. These findings confirm that the encapsulated RFID tags are a successful low-impact and inexpensive technology for tracking placement of HMA in the roadway.

RFID Tracking of PCC Placement

The successful application of RFID tags to track placement of HMA immediately suggested the parallel use for PCC placement. Preliminary laboratory evaluation of the passive UHF RFID tags in concrete cylinders showed promise. The reconstruction of a section of I-90 near Syracuse, NY, provided an opportunity for field evaluation. A large number of RFID tags similar to those used in the HMA application were placed in the PCC delivery trucks as they left the batch plant near the paving site. These tags were deposited with the PCC ahead of the slip form paver and incorporated into the concrete slabs. Unfortunately, on the return visit to the site about 1 month after paving, none of the tags could be read. The causes of this surprising and disappointing result were investigated in the laboratory. The most plausible explanation supported by the laboratory results is that the hydrated cement paste causes the cured concrete to have a very high dielectric constant. The penetration depth (i.e., read range) of the UHF RFID radio waves diminishes sharply as the dielectric constant increases. A different technology is therefore needed for the PCC tracking application.

Pavement Temperature Measurement Using SAW RFID

SAW RFID technology has the intrinsic capability to measure thermal expansion and thus temperature. Real-time measurement of pavement temperature distributions is necessary to interpret the stiffness feedback data in intelligent compaction because the stiffness of HMA is extremely temperature dependent. The temperature measurement capability of SAW RFID was evaluated through laboratory and field testing. For the field testing, various configurations of SAW RFID tags were encapsulated in thermally conductive epoxy, attached with quick-set epoxy to the surface of a milled existing pavement, and then covered with a 1.5-inch (38-mm) thick compacted HMA overlay. Although limitations of the SAW RFID reader system made it difficult to measure the temperature versus time trends during the first few minutes after placement, mat temperatures were recorded starting at about 10 min after placement until the mat was too cool for continued compaction. The measured temperatures versus time compared favorably with predictions from analytical/numerical models, and an approach for using the SAW RFID field temperature measurements for calibrating these analytical/numerical models is proposed. Overall, the SAW RFID technology has potential for in situ temperature measurement in HMA pavement layers.

Reflection Crack Detection

Reflection cracking is a dominant distress in rehabilitation overlays. Early detection of these cracks before they reach the pavement surface can be important to highway agencies both for rehabilitation planning purposes and for enforcing construction contract warranties. The development of an early-onset reflection crack detector was originally intended as another application of the SAW RFID technology. However, it was subsequently determined that conventional RFID was a more appropriate technology choice, in part because of the current relatively high cost of SAW RFID tags.

The reflection crack sensor concept is to implement a switch in the antenna circuit of the RFID tag: when there is no crack, the RFID tag signal can be read at a distance, but after a crack forms the signal becomes too weak to be read. A prototype reflection crack detector was developed and tested in the laboratory and, under more limited conditions, in the field. In the laboratory, the prototype detector was shown to be capable of detecting a reflection crack before it reached the pavement surface. The limited field trials also showed that the detector had the required survivability and read range for real-world applications. This approach shows considerable promise, but it will require additional and more rigorous field evaluation that was beyond the scope and resources of the present project.

Guidance on Data Integration

The motivation for this entire study was the application of RFID technology for tracking HMA placement. This is also the application that is most suited to near-term commercial implementation. The major benefit of this application is the integration of agency QA materials testing data with their pavement management database. This integration could provide insights into the relationships between good material properties and construction techniques and superior pavement performance. This integration could also permit much more powerful forensic investigations of poorly performing road sections by enabling easy and quick access to the

associated material properties measured during construction. However, several steps are needed to effect this data integration, and given the wide range of materials and pavement management systems in use among the States, these steps will be slightly different for each agency. General guidelines are provided for the data integration steps that can be easily adapted to each agency's specific databases and policies and procedures.

CONCLUSIONS AND RECOMMENDATIONS

RFID tracking of HMA placement was the most successful application in this study and the one with the most potential for immediate commercial implementation. RFID tracking of PCC placement was unsuccessful, at least with the RFID systems evaluated in this study; the high dielectric constant of the hydrated cement paste severely attenuates the RFID signals. Real-time measurement of pavement temperatures with depth and time during intelligent compaction shows promise, but further work is required to develop faster and more reliable reader software/hardware and RFID tags. Laboratory and limited field evaluation of an RFID-based sensor for early detection of reflection cracks in HMA overlays also shows promise, but additional development work and field trials are required.

Recommendations for additional research and development include the following:

- Commercialization of the RFID system for tracking HMA placement. This research has demonstrated the success of the concept. However, it was impossible to generate commercial interest in it during the course of the project.

- Evaluation of other RFID systems (e.g., different frequency range, active instead of passive system) for use in tracking PCC placement. The high dielectric constant of the cement paste coating the aggregates in PCC makes it impossible to pass a sufficiently strong signal to/from the passive UHF RFID tags used so successfully for HMA tracking.

- Refinement of the techniques for temperature measurement using SAW RFID tags. More work is required to determine the minimum thickness of the epoxy coating to maximize tag readability and minimize thermal lag while still ensuring survivability. Additional work in collaboration with the SAW RFID system manufacturer is required to optimize the temperature window in the reader so that the early rapid cooling trends of the mat can be captured. Field trials should also be repeated on thicker HMA layers in which the variation of temperature with depth is more pronounced.

- Laboratory evaluation of the reflection crack detector should be conducted using a Texas Overlay Tester instead of three-point bending to better simulate how overlays fail. Through these tests, the crack mouth opening displacement (CMOD) as a function of vertical crack propagation can be determined more accurately and the crack detector design can be adjusted as needed. Laboratory evaluation should then be followed by field trials on in-service pavements. The duration of these field trials would need to be on the order of 5 to 10 years to allow sufficient time for reflection cracks to initiate and propagate.

CHAPTER 1: INTRODUCTION

PROJECT OBJECTIVES

The original objective of this project was to demonstrate that inexpensive expendable RFID tags can be used to identify the spatial location along the pavement alignment of specific truckloads of HMA production. These tags are placed in the truckload as it leaves the production plant, pass through the paver, and are compacted into the finished mat. Cross-referencing these tags with GPS latitude and longitude coordinates after construction allows spatial referencing of QA material property data measured at the production plant, enabling linkage to other spatially referenced in-place test results and PMS pavement performance data. This use of the large QA and PMS datasets already collected by highway agencies will permit more robust analyses and insights into the relationships between HMA material properties and actual pavement performance.

Phases I and II of this project addressed the development of techniques for making the RFID tags sufficiently rugged to withstand the harsh thermal and mechanical conditions of HMA paving and for evaluating the survival and read performance of the tags after construction. Phase I focused on identifying feasible RFID devices for HMA tracking, identifying candidate projects for field testing, and formulating a field evaluation work plan. Phase II executed the work plan developed in Phase I.

During the Phase I and II work, some additional applications of RFID technologies to pavements were identified for evaluation:

- Evaluation of potential problems caused by surfaced tags.
- Exploration of SAW RFID technology for improved performance of small format tags.
- Demonstration of RFID tracking of placement of PCC loads in pavements.
- Provision of guidance to agencies on data integration.

The evaluation of these additional topics was the objective of the additional and final Phase III of the project.

REPORT ORGANIZATION

This report documents the work and findings from all three phases of the project. The subsequent chapters, along with brief descriptions of the work in each and highlights of the findings, are described below. Each chapter is intended as standalone document of its respective work area.

Chapter 2: Feasibility Evaluation. The feasibility of using RFID tags to track HMA placement was evaluated via: 1) literature review, 2) identification of appropriate RFID technology, and 3) prototype tag development and evaluation. The feasibility evaluation identified UHF passive RFID technology as best suited to the hot mix asphalt paving application. After considerable research of available products, a ThingMagic Mercury® 5 RFID system and related hardware were acquired for use in this project. Suitable RFID tags were identified and a feasible encapsulation system was developed that adequately protects the RFID tags from the temperatures and compaction stresses inherent in HMA transport and paving. An Alien® Gen 2

2x2 RFID tag curled and encapsulated in high-temperature epoxy inside a ¾-inch (19-mm) nominal outside diameter CPVC pipe provided a hardened tag of appropriate size for adequate read range.

Chapter 3: RFID Tracking of HMA Placement. The encapsulated RFID tags were field tested to evaluate the following issues: survivability in real-world paving scenarios, read range under actual field conditions, required redundancy (i.e., how many tags must be added to a truckload to locate the mix reliably along the pavement alignment; this is related to the survivability issue, but also includes delays in passing through the paver), construction practicality issues (e.g., do the tags interfere with normal paving operations), and construction quality issues (e.g., do the tags impair the quality of the compacted mat by inducing segregation or other defects). The encapsulated RFID tags were evaluated at three parking lot locations on the UMD campus and in two stages in a new pavement constructed by the MDSHA. The field trials confirmed the very high survival rate of the encapsulated tags. Read success rates varied significantly with tag size and less significantly on other details such as antenna configuration and vehicle speed. The field trials consistently demonstrated that post-construction read success rates of 60 to 80 percent or higher are achievable from a bumper-mounted antenna array, even on a vehicle moving at traffic speeds.

Chapter 4: Evaluation of Surfaced Tags. It was observed during the HMA field trials that some of the encapsulated RFID tags "floated" to the surface of the compacted mat. This raised the possibility of a decrease in in-place compacted density or an increase in the in situ permeability or both in the local region around the tag. Extensive density and permeability testing was performed to evaluate these possibilities. No localized decrease in density, increase in permeability, or any detrimental effects of the surfaced tags were found. These findings confirm that the encapsulated RFID tags are a successful low-impact and inexpensive technology for tracking placement of HMA in the roadway.

Chapter 5: RFID Tracking of PCC Placement. The successful application of RFID tags to track placement of HMA immediately suggested the parallel use for PCC placement. The reconstruction of a section of I-90 near Syracuse, NY, provided an opportunity to evaluate this in the field. A large number of RFID tags similar to those used in the HMA application were placed in the PCC delivery trucks as they left the batch plant near the paving site. These tags were deposited with the PCC ahead of the slip form paver and incorporated into the concrete slabs. Unfortunately, on the return visit to the site about 1 month after paving, none of the tags could be read. The causes of this surprising and disappointing result were investigated in the laboratory. The most plausible explanation supported by the laboratory results is that the hydrated cement paste causes the cured concrete to have a very high dielectric constant. The penetration depth (i.e., read range) of the UHF RFID radio waves diminishes sharply as the dielectric constant increases. A different technology is therefore needed for the PCC tracking application.

Chapter 6: Pavement Temperature Measurement Using SAW RFID. SAW RFID technology has the intrinsic capability to measure thermal expansion and thus temperature within a pavement layer as a function of depth and time. This is particularly useful for intelligent compaction, where estimates of HMA stiffness using sensor data from the vibrating roller must consider the instantaneous distribution of temperature in the mat. The temperature measurement capability of SAW RFID technology was evaluated through laboratory and field testing. For the

field testing, various configurations of SAW RFID tags were encapsulated in thermally conductive epoxy, attached with quick-set epoxy to the surface of a milled existing pavement, and then covered with a 1.5-inch (38-mm) thick compacted HMA overlay. Although limitations of the SAW RFID reader system made it difficult to measure the temperature versus time trends during the first few minutes after placement, mat temperatures were recorded starting at about 10 min after placement until the mat was too cool for continued compaction. The measured temperatures versus time compared favorably with predictions from analytical/numerical models, and an approach for using the SAW RFID field temperature measurements for calibrating these analytical/numerical models is proposed. Overall the SAW RFID technology was judged to have high potential for in situ temperature measurement in HMA pavement layers.

Chapter 7: Reflection Crack Detection. Reflection cracking is a dominant distress in rehabilitation overlays. Early detection of these cracks before they reach the pavement surface can be important to highway agencies both for rehabilitation planning purposes and for enforcing construction contract warranties. The development of an early-onset reflection crack detector was originally intended as another application of the SAW RFID technology. However, it was subsequently determined that conventional RFID was a more appropriate technology choice, in part because of the current relatively high cost of SAW RFID tags. A prototype reflection crack detector was developed and tested in the laboratory and, under more limited conditions, in the field. The prototype detector was shown in the laboratory to be capable of detecting a reflection crack before it reached the pavement surface. The limited field trials also showed that the detector had the required survivability and read range for real-world applications. This approach shows considerable promise, but it will require additional and more rigorous field evaluation that was beyond the scope and resources of the present project.

Chapter 8: Guidance on Data Integration. The motivation for this entire study was the application of RFID technology for tracking HMA placement. This is also the application that is most suited to near-term commercial implementation. The major benefit of this application is the integration of agency QA materials testing data with their pavement management database. This integration could provide insights into the relationships between good material properties and construction techniques and superior pavement performance as well as enable more powerful forensic investigations of poorly performing pavements. This integration could also permit much more powerful forensic investigations of poorly performing road sections by enabling easy and quick access to the associated material properties measured during construction. However, several steps are needed to effect this data integration, and given the wide range of materials and pavement management systems in use among the States, these steps will be slightly different for each agency. General guidelines are provided for the data integration steps that can be easily adapted to each agency's specific databases and policies and procedures.

Chapter 9: Conclusions. The key findings and recommendations from each topic area are consolidated and summarized.

Chapters 2 and 3 summarize the work completed in Phases I and II, and chapters 4 through 8 document the work completed in Phase III.

RFID TECHNOLOGIES IN THIS STUDY

RFID technology is widely used today for supply chain inventory management, security, equipment tracking, among other applications. However, in construction, RFID technology is primarily used for tracking equipment and materials. General surveys of RFID applications in construction are provided by Jaselskis et al., Jaselskis and El-Misalami, and Sawyer.[1,2,3] Two types of RFID technology were employed in this study: conventional UHF passive RFID tags and the newer SAW RFID tags. Each of these technologies is briefly described in the following subsections.

UHF RFID Technology

The UHF RFID technology employed in this study is the basis for the work in Phases I and II. The RFID technology encodes a digital signature on a small microchip attached to a copper foil antenna—the RFID "tag." This passive tag receives energy from UHF radio waves transmitted by a RFID "reader"; the tag harvests this incoming RF energy to transmit its encoded digital signature back to the reader. These RFID tags, although small, may be read several yards away from the reader's antenna. The primary objectives of Phases I and II were to evaluate the feasibility of using UHF RFID tags in laboratory asphalt specimens and in the field during paving construction.

SAW RFID Technology

One of the major objectives of Phase III was to evaluate the feasibility of using SAW-based RFID technology to measure HMA temperatures. SAW-based RFID sensors are inherently capable of measuring and transmitting temperatures as well as a digital signature. This is in contrast to the conventional RFID technology used in Phases I and II, which is capable of only transmitting digital signatures. In addition, the SAW RFID technology is inherently capable of operating successfully at lower energy inputs than the conventional silicon-based integrated circuit RFID technology.

SAW RFID tag consists of an IDT and a series of acoustic reflector traps etched into a piezoelectric substrate. The tag reader emits a radio wave pulse to the IDT that is converted piezoelectrically into a nanoscale acoustic wave. The wave travels past the reflectors to produce a unique pattern of reflected pulses. These travel back to the IDT, where they are piezoelectrically converted into an encoded electronic reply signal to the reader. The SAW chip operates in a purely passive mode and does not require supplementary DC power (i.e., battery).[4]

Overall, the principal advantages of the SAW RFID technology for pavement construction include better inherent ruggedness, smaller formats, and longer read ranges for a given tag antenna size compared with conventional RFID. Unlike conventional RFID tags, the incoming RF signal does not need to be converted to DC in SAW RFID. Therefore, the incoming RF signal strength does not need to exceed the minimum threshold required for the rectifier operation. This is the principal theoretical reason for the inherently longer read ranges in the SAW RFID technology.

In addition, and most relevant to this study, SAW RFID technology is capable of wireless measurement of temperature via the perturbation of the return wave signal caused by the influence of thermal strains on the spacing of the acoustic reflectors.

CHAPTER 2: FEASIBILITY EVALUATION

The feasibility evaluation encompassed the following components: 1) literature review, 2) identification of appropriate RFID technology, and 3) prototype tag development and evaluation. Each of these is described in the following sections.

LITERATURE REVIEW

The literature review focused on RFID technology and applications in the general areas of civil engineering and construction. Specific RFID applications identified in these areas include the following:

- Tracking of PCC test specimens.
- Maturity monitoring of in-place PCC.
- Tracking of construction materials at project site (e.g., fabricated pipe).
- Construction tool inventory/usage control/monitoring.
- Location identification of buried infrastructure (cables and pipes).

An annotated bibliography of the reviewed articles is provided at the end of this report.

IDENTIFICATION OF APPROPRIATE RFID TECHNOLOGY

Aspects of RFID technology of relevance to this project include the following:

- Physical size of the tag.
- Operating frequency (low, high, ultrahigh, and microwave; this influences tag size and read range).
- Type of tag (active or passive; this influences cost, power consumption, and maximum read range).
- Read range (including high-gain antenna design).
- Durability/survivability (e.g., strength of tag encapsulation; maximum/operating temperature ranges).
- Cost of the expendable tag.

Some light was shed on these aspects by articles from the literature review. However, other lines of inquiry were also pursued: 1) consultations with Dr. Marc Cohen, a research scientist at the Center for Engineering Logistics and Distribution in UMD's Institute for Systems Research and 2) exploratory laboratory studies.

Dr. Cohen has extensive experience in RFID technology. Discussions with him confirmed and expanded the conclusions reached from the literature review (see also table 1):

1. For a physical tag size on the order of 1 inch (25 mm), the UHF range is optimal.

2. Passive tags, which are preferred because of their cost differential relative to active tags, should be able to provide the requisite read range performance.

3. Commercial RFID readers are readily available for vehicle mounting (e.g., antennas on a front bumper) with read ranges on the order of 3 ft (1 m) or more, which is sufficient for this study's applications.

4. Possible attenuation of the RFID signal by the asphalt concrete could be an issue and therefore needed to be explored early.

5. Thermal and mechanical survivability are key challenges. The maximum temperature range tolerable for short periods (e.g., the time required to truck a load of asphalt from the production plant to the paver) is significantly higher than the typical rated operating and/or storage temperatures for RFID tags.

Table 1. Characteristics of different RFID technologies.

Type	Frequency	Pros/Cons	Read Range (ft)	
			Passive	Active
Low Frequency	125 KHz	Requires less power, better penetration of nonmetallic, and/or high water content substances	1	—
High Frequency	13.56 MHz	Works well on metal objects	3	—
UHF	860–960 MHz	Better range, faster data transfer. Uses more power. More "directed," requires a clear path between tag and reader. Largest application area, widest installed base in industry.	10–20	100–300
Microwave	2.45 GHz	Little experience to date.	—	—

— Indicates no information available
1 ft = 0.0305 m
KHz = kilohertz
MHz = megahertz
GHz = gigahertz

Preliminary Evaluations

Potential attenuation of the RFID signal by the asphalt surrounding the embedded tag could have a major impact on read range and thus system practicality. Because this aspect is vital to the project, it was evaluated early on in a very preliminary way as part of the identification of appropriate RFID technologies. Jaselskis et al. describe the theoretical aspects of electromagnetic wave interaction with materials, with a particular focus on asphalt concrete.[(2)] The key material property governing the transmission of dielectric materials is the permittivity. A dielectric material is an electrical insulator. A vacuum is the ideal insulator, but many materials (e.g., asphalt concrete) also fall into this category. When an electric field interacts with a dielectric

medium, redistribution of charges within its atoms or molecules alters the shape of the field both inside and around the medium. The absolute permittivity, ε_a, is the fundamental physical quantity governing the interaction between and electric field and a dielectric medium. It is a measure of the ability of the medium to polarize and thus reduce the strength of the field. In other words, permittivity defines a materials ability to transmit or "permit" an electric field. The relative permittivity or dielectric constant, ε, is the permittivity of a material relative to that of an ideal vacuum, ε_0, as shown in the equation in figure 1.

$$\varepsilon = \frac{\varepsilon_a}{\varepsilon_0}$$

Figure 1. Equation. Definition of relative permittivity or dielectric constant ε.

According to Maxwell's equations for nonmagnetic media, the electric field E induced by the incident electromagnetic wave is defined in the equation in figure 2.

$$E = E_0 e^{i\omega}$$

Figure 2. Equation. Electric field E.

The displacement vector D is calculated using the equation shown in figure 3:

$$D = \varepsilon_0 \varepsilon(\omega) E$$

Figure 3. Equation. Displacement vector D.

where:

ω = circular frequency of the wave.
ε_0 = permittivity of vacuum.
$\varepsilon(\omega)$ = frequency dependent dielectric constant of the medium
$= \varepsilon_a(\omega)/\varepsilon_0$, where $\varepsilon_a(\omega)$ = absolute permittivity.
$i = \sqrt{-1}$.

The displacement field D represents how the electric field E influences the organization of electrical charges in a given medium. The total current flowing within a medium is divided into conduction and displacement components. The displacement current can be thought of as the elastic response of the material to the applied electric field. As the magnitude of the applied field is increased, an increasing amount of energy is stored in the displacement field. If the electric field is subsequently decreased, the material will release the stored energy.

Owing to inertia processes in fluctuating electromagnetic fields, the displacement field D for most materials is not in phase with the electric field E. As a consequence, the dielectric constant is the complex frequency-dependent quantity $\varepsilon^*(\omega)$ defined in the equation in figure 4.

$$\varepsilon^*(\omega) = \varepsilon'(\omega) - i\varepsilon''(\omega)$$

Figure 4. Equation. Complex relative permittivity (dielectric constant).

The real part of the permittivity, $\varepsilon'(\omega)$, is a measure of polarization and is thus a measure of the energy stored in the medium while the imaginary part, $\varepsilon''(\omega)$, defines the average power absorbed and/or scattered by the medium and thus is a measure of energy loss. This energy loss can also be related to the electrical conductivity σ for the given frequency as shown in the equation in figure 5.

$$\varepsilon''(\omega) = \frac{\sigma}{\varepsilon_0 \omega}$$

Figure 5. Equation. Relationship between imaginary portion of complex dielectric constant and electrical conductivity.

The net effect of all of the above is that electromagnetic wave propagation is impeded as the permittivity increases. Maximum RFID read range occurs when the RFID electromagnetic waves travel through a material with a low dielectric.

For asphalt concrete, both the real and imaginary permittivity components will be functions of the mixture composition, moisture content, and density. Jaselskis et al. measured the complex relative permittivity components as functions of frequency and temperature for several asphalt concrete mixtures.[2] Values of the real and imaginary relative permittivity components for a sand asphalt mixture varied between about 4.5 and 5.5, and 0.2 and 0.3, respectively.

The theoretical description of electromagnetic wave propagation and losses in terms of relative permittivity is placed in better context through comparisons with other materials. Table 2 summarizes relative permittivity values for construction and related materials. Asphalt concrete typically has a relative permittivity of between 3.5 and 5.0, comparable to Portland cement concrete, aggregates, and other similar materials. This range lies closer to the properties of good UHF media (e.g., vacuum and air), and relatively far away from poor UHF media (e.g., water)—suggesting that attenuation losses of RFID signals through asphalt concrete should be modest.

Table 2. Typical dielectric constant (relative permittivity) values for common materials.

Material	Dielectric Constant	Frequency Range
Vacuum	1.0	—
Air	1.00054	—
Teflon (polytetrafluorethelene)	2.0 to 2.1	—
Polyethylene	2.25	—
Bitumen	**2.38**	**—**
Polystyrene	2.4 to 2.7	—
Polyvinylchloride	3.3 to 4.55	—
Porous asphalt concrete	3.6 to 4.1	50 MHz to 1.6 GHz
Dense graded asphalt concrete	**4.4 to 5.0**	**50 MHz to 1.6 GHz**
Concrete	**4.5**	**—**
Quartzite aggregate	4.95	—
Granite	6.25 to 5.75	60 MHz to 1.4 GHz
Glass	6.775	—
Rubber	7	—
Silicon	11.68	—
Cement mortar	20 to 30	1 MHz to 300 MHz
Water	80	—

— Indicates no information available
Note: Bold font indicates materials most relevant to the present study.
MHz = megahertz
GHZ = gigahertz

RFID System

Based on a careful review of the specifications and available product reviews for various manufacturers' systems, the Mercury® 5 RFID reader from ThingMagic was selected as most suitable for this project. Key specifications of the Mercury® 5 reader include the following:

Hardware

Name: ThingMagic Mercury® 5
Processors: Intel© IXP4xx Network Processor
Texas Instruments Digital Signal Processor
Memory: 64 Megabyte (MB) DRAM, 16 MB FLASH
Connectivity: RS-232 serial interface
10/100 Base-T Ethernet interface

Mechanical and Environmental

Dimensions: 10 by 10 by 1.5 inches (250 by 250 by 38 mm)
Temperature: 32–104 °F (0–40 °C) operating
-4–158 °F (-20–70 °C) storage
Humidity: 0–90 percent relative humidity (noncondensing)
Weight: 3 lb 10 oz (1.6 kg)
Power: 24V DC 2A unregulated

Radio Frequency

Operating Frequencies:	902–928 MHz
Air Interface Protocols:	EPC Class 0 EPC Class 1 EPC Generation 2 ISO 18000-6B/Unicode 1.19 Rewritable Class 0+
RF Power:	+32.5 dBm (1 Watt (30 dBm)) in accordance with Federal Communications Commission Part 1.5; +2.5 dB attenuation due to antenna cables)

The ThingMagic Mercury® 5 was purchased as a complete start-up system, including the reader, two bistatic circular antennas, four 25-ft (7.6-m) cables, a startup CD, and a selection of RFID tags.

Suitable tags compatible with the Mercury® 5 reader and meeting size limits were also identified. Key features of these tags are summarized in table 3. Sample quantities were obtained for the Alien® Gen 2 1x1 and Alien® Gen 2 2x2 tags. Attempts to purchase small trial quantities of the Avery-Dennison™ AD-812 tags were unsuccessful.

Table 3. Candidate RFID tags (all passive).

Vendor	Model	Frequency (MHz)	Size (inches)	Temperature Range (^{o} F)		Comments
				Operating	Storage	
Alien®	Gen 2 1x1	902–928	1 by 1	-13 to +149	—	Small form factor optimized for plastic packaging such as pill bottles; nominal read range of 1.25 to 2.5 m.
Alien®	Gen 2 Mini-Squiggle®	902–928	1.1 by 0.39	-13 to +149	—	Nominal read range of 1 to 1.5 m.
Alien®	Gen 2 2x2	860–960	1.85 by 1.65	-13 to +149	—	Omni-directional
Avery-Dennison™	AD-812	902–928	1 by 1	-40 to +149	-40 to +185	Designed for superior edge-on read performance.

— Indicates no information available
MHz = megahertz
°C = (°F – 32)/1.8
1 m = 3.28 ft

Linking the RFID tag identifier with GPS latitude and longitude coordinates is also an important component of this project. A Garmin™ GPS 12 transponder was initially evaluated for linking GPS with RFID. Preliminary findings suggested that a data logger would be an easier technology for linking the RFID tag data to latitude and longitude coordinates. A GPS data logger records a constant stream of latitude/longitude/time values that can then be matched post facto to the time stamps on the RFID tag data. An inexpensive Pocket Tracker Pro system from Brickhouse® Security (www.brickhousesecurity.com) was therefore acquired for use on the project. Key features of the Pocket Tracker Pro system useful for this project include: 1) location accuracy to

within 8.2 ft (2.5 m); 2) read rate of one location point per second; 3) magnetic vehicle mount; 4) universal serial bus computer interface; 5) 100-h battery life (AAA batteries); and 6) low cost.

PROTOTYPE TAG DEVELOPMENT AND EVALUATION

Fabrication

Encapsulation of the RFID tags to protect them from temperature extremes and compaction stresses is key to their use in asphalt paving applications. Two candidate encapsulation media were considered: ceramics and high-temperature epoxy. Upon evaluation of these two materials, the ceramics were discarded because of high cost and fabrication difficulties. A high temperature epoxy, Durapot™ 866 from Contronics, Inc. (www.contronics.com), was selected as a suitable encapsulating material. Durapot™ 866 is a thermally and electrically insulating compound that forms a low-density nonporous foam for high-temperature applications. This two-part epoxy, after proper curing at room temperature for 24 h followed by oven curing at 248 °F (120 °C) for 4 h, has an upper temperature limit of 500 °F (260 °C), more than adequate for asphalt applications.

Suitable molds for encapsulating the RFID tags in the high-temperature epoxy are also required. CPVC pipe was found to be suitable for this purpose. CPVC is a thermoplastic commonly used for cold and hot piping systems in building construction. It has a glass transition temperature of approximately 230 °F (110 °C) and a melting point of 414 °F (212 °C), which is sufficient for use with hot mix asphalt. The Alien® 1x1 and 2x2 tags were curled respectively inside 1-inch (25-mm) and 2-inch (50 mm) long sections of 3/4-inch (19-mm) nominal diameter CPVC pipe. The inside diameter of this pipe is sufficiently large that the ends of the curled tags did not overlap. Curling the tag with the antenna facing outward or inward had no influence on the read range. The pipe with tag was then filled with the high-temperature epoxy and cured. Because the CPVC pipe is transparent to the RFID signal and has a melting point higher than the HMA compaction temperature, there was no need to extrude the tag after curing of the epoxy.

The epoxy molding and curing process was further refined to minimize problems caused by air bubbles during curing. The original procedure followed the epoxy manufacturer's suggestions: the mold was filled with epoxy at room temperature, then cured at room temperature for 24 h followed by oven curing at 248 °F (120 °C) for 4 h. This process often resulted in voids between pipe wall and tag during filling (figure 6) and air bubbles within the epoxy during the room temperature curing (figure 7). These defects would then expand and cause tag failure during the subsequent oven curing (figure 8 and figure 9). A post-mortem examination of tags compacted into gyratory HMA cylinders also found bulges along the edges of the encapsulated tags (figure 10). However, the compaction force of 88 psi (608 kPa) over 160 gyrations did not appear to cause any significant damage to the tag encapsulation.

In the refined encapsulation method, the epoxy resin is first preheated for 15 to 30 min at 104 °F (40 °C) to reduce its viscosity. The hardener is then added to the preheated resin. The tags are placed in CPVC pipe molds in a circumferential orientation (see figure 16 later) and the bottom pipe opening is sealed with duct tape. Epoxy is then poured in three lifts into the pipe, with the pipe tapped vigorously on the laboratory bench after each lift to eliminate any trapped air bubbles. The encapsulated tags are then placed upright in the oven at 122 °F (50 °C) for up to 1 h

until hardened. Occasionally, escaping air bubbles could be observed during this stage, and in a few cases (fewer than 1 in 10), some of the epoxy was pushed out of the pipe owing to entrapped air. After hardening, the tags are removed from the oven, the duct tape seal removed, and the tags cooled for 2 h at room temperature. The tags are then checked for survival through the first stage of the curing process. Observed survival rates at this stage were very high, especially for the Alien® 2x2 tags. Surviving tags are then cured in a second stage at 257 °F (125 °C) for 4 h.

Figure 6. Photo. Voids between epoxy and CPVC pipe wall after filling at room temperature.

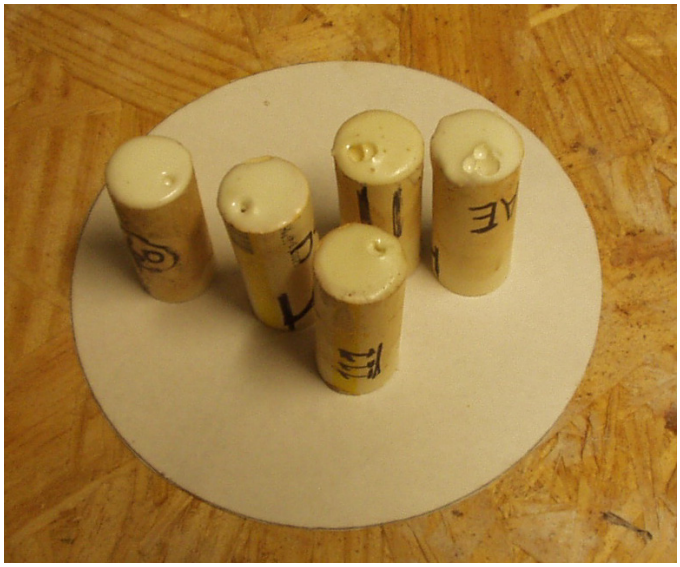

Figure 7. Photo. Air bubbles at ends of epoxy filler after room temperature curing.

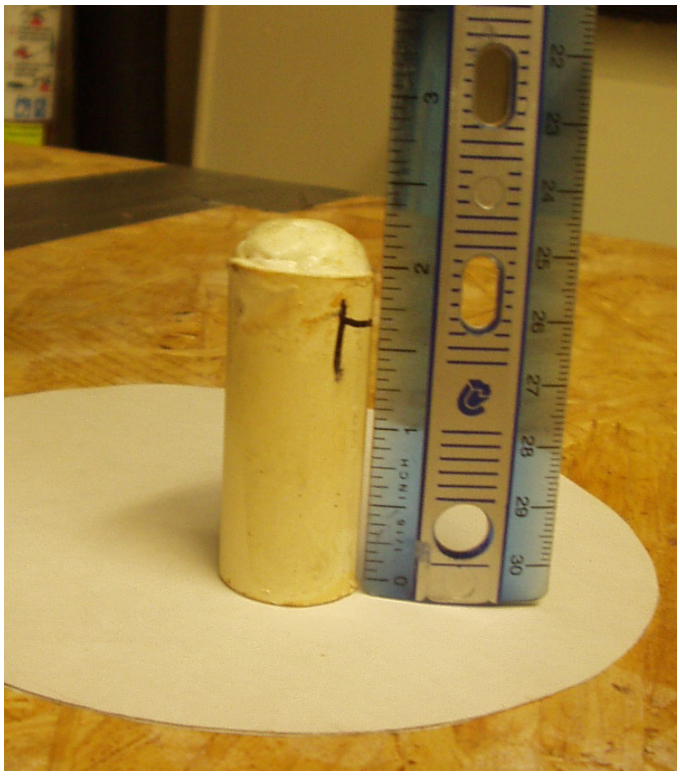

Figure 8. Photo. Extrusion of epoxy from end of pipe after oven curing.

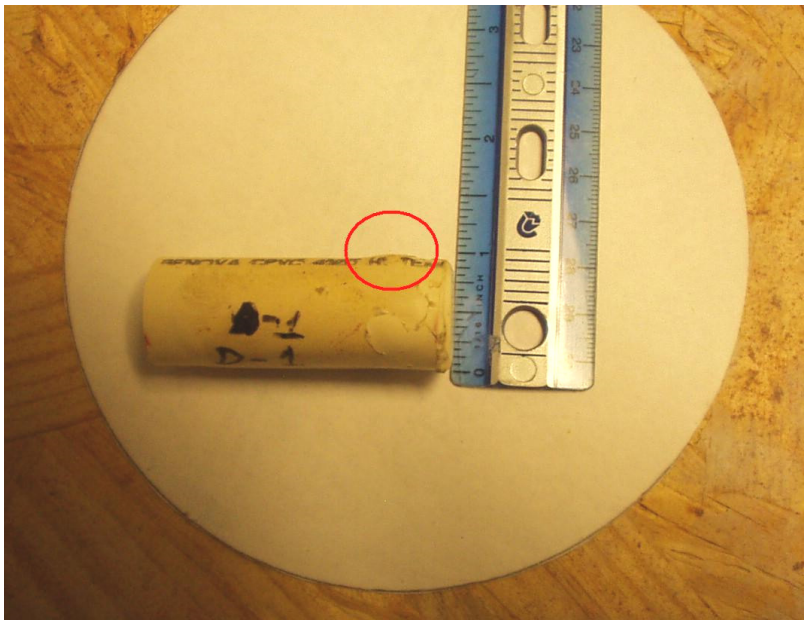

Figure 9. Photo. Bulge in sidewall of encapsulated tag after oven curing.

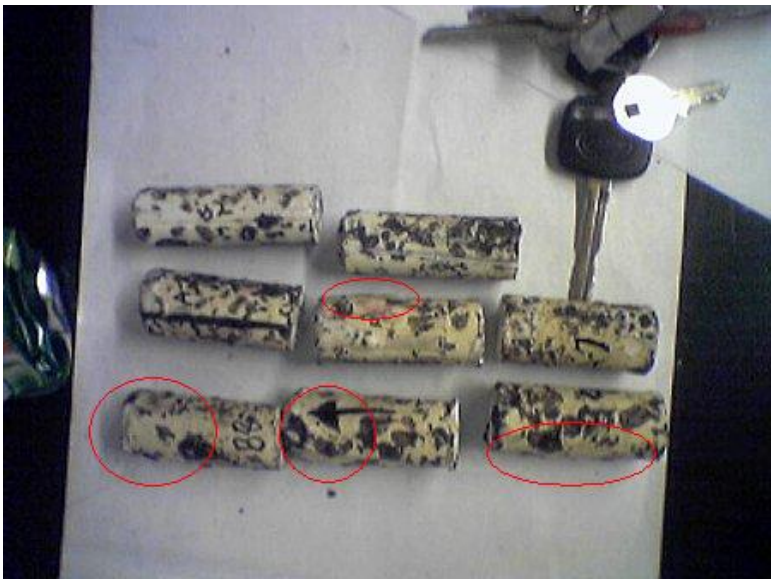

Figure 10. Photo. Post-mortem examination of tags retrieved from compacted HMA with bulges in encapsulated tags circled.

Evaluation of Read Range

Initial Evaluation

Read range was evaluated initially using the Alien® 2x2 tags curled in the CPVC pipe sections. During this initial evaluation, it was discovered that there are several sources of interference that can alter the measured effective read range as follows:

1. There appears to be a "body antenna" effect. Tags held by hand were discovered to have different read ranges than tags placed on an inanimate object with all persons removed to a distance. Even body movements 8 ft (2.5 m) away from the tag would trigger a read when none had been observed before.

2. Placing the tags on the floor and then stepping some distance away gave more controlled conditions and consistent read data. The disadvantage of placing the tags on the floor and then reading them in a horizontal direction to determine maximum read distance is that the tags are slightly off the centerline of the antenna. This tends to decrease the measured read range. The advantage, of course, is that placing everything on the laboratory floor is much easier than elevating everything several feet off the floor.

3. When a half-filled bucket of aggregate was accidentally placed behind one of the tags, the read range increased considerably. This may have beneficial implications for field versus laboratory performance of the tags.

The read range tests were designed to minimize these compounding influences. The 1 by 2 ft (0.3 by 0.6 m) RFID antenna was oriented perpendicular to the floor, supported along its long edge directly on the floor. A grid was laid out on the floor in front of the antenna. Tags were placed at each grid point, and the observer stepped aside before tag read success was assessed.

Replicate specimens and multiple reads were employed to improve the robustness of the test results.

The first series of tests employing this protocol were conducted on flat Alien® 2x2 tags before curling or encapsulation. Six read attempts were made at each grid point. Three of these were with the tag facing the antenna, and three were with the tag facing away. The tag orientation was found to have no effect on the read success rate. Each grid point was assigned a value of 1 if the read success rate was greater than 50 percent for the six read attempts, a value of 0.5 if the tag could be read but the success rate was less than 50 percent, and a value of 0 if the tag could not be read at all. A total of six tags were tested using this scheme. The results from this test series are summarized in figure 11. Each block in the figure represents a 1 by 1 ft (0.3 by 0.3 m) cell on the floor as viewed from above. The antenna is perpendicular to the floor (i.e., vertical), resting along its 2-ft (0.6-m) long edge. Note that the antenna assembly contains separate transmit and receive antennas along its length, as indicated by the "T" and "R" designations in the figure. The numeric values in figure 11 represent the total score in each cell for the six tags, and the color coding depicts the read success rate category (all tags read, >50 percent tags read, <50 percent tags read, no tags read). Overall, the results in figure 11 suggest an effective read range of approximately 7 ft (2.1 m) for the flat Alien® 2x2 tags in air. There is some slight asymmetry in the read success pattern that may be due to experimental variability, local interference, and/or the asymmetric antenna design.

The next series of tests was conducted on the curled Alien® 2x2 tags inside the CPVC pipe but before encapsulation in epoxy. This test series was designed to evaluate the effects of the curved tag geometry on read success. The pipes containing the curved tags were placed on the floor and parallel to the plane of the antenna in all tests. However, two orientations of the tags relative to the antenna were considered: 1) the pipe axis horizontal with respect to the floor and parallel to the long axis of the antenna and 2) the pipe axis vertical and parallel to the short axis of the antenna. The results from this test series are summarized in figure 12 and figure 13 for the horizontal and vertical orientations, respectively. It is clear from these figures that curling the tags does reduce the read range, and by a larger amount for the vertical orientation. Maximum effective read range in air in front of the antenna is approximately 5 ft (1.5 m) for the horizontal orientation and 3 ft (1 m) for the vertical, compared with approximately 7 ft (2.1 m) for the flat tag configuration.

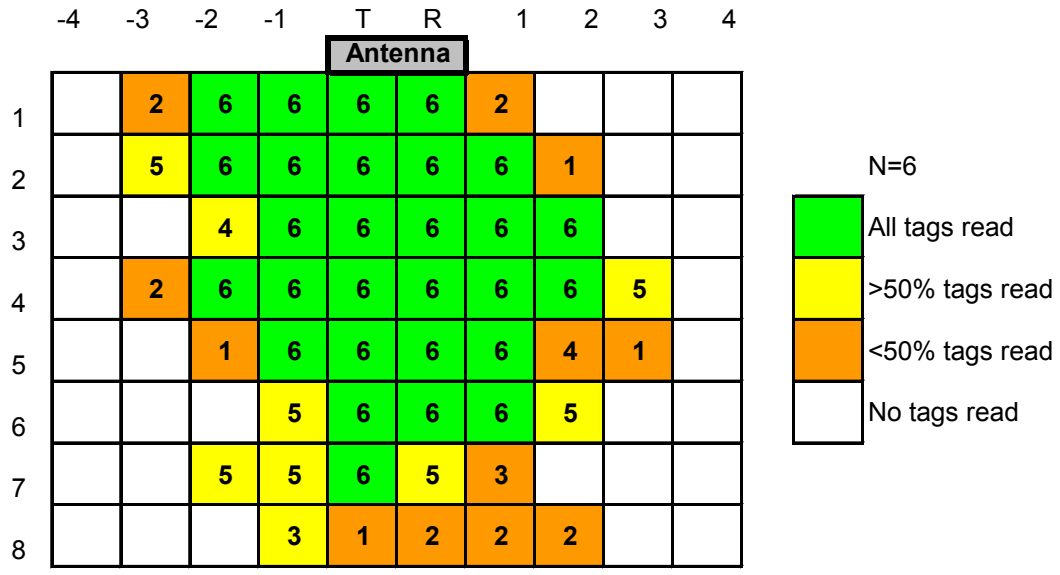

All distances in ft (1 ft = 0.305 m)
T=transmit side of antenna
R=receive side of antenna

Figure 11. Diagram. Read range for flat Alien® 2x2 tags in air with tags oriented parallel to reader antenna.

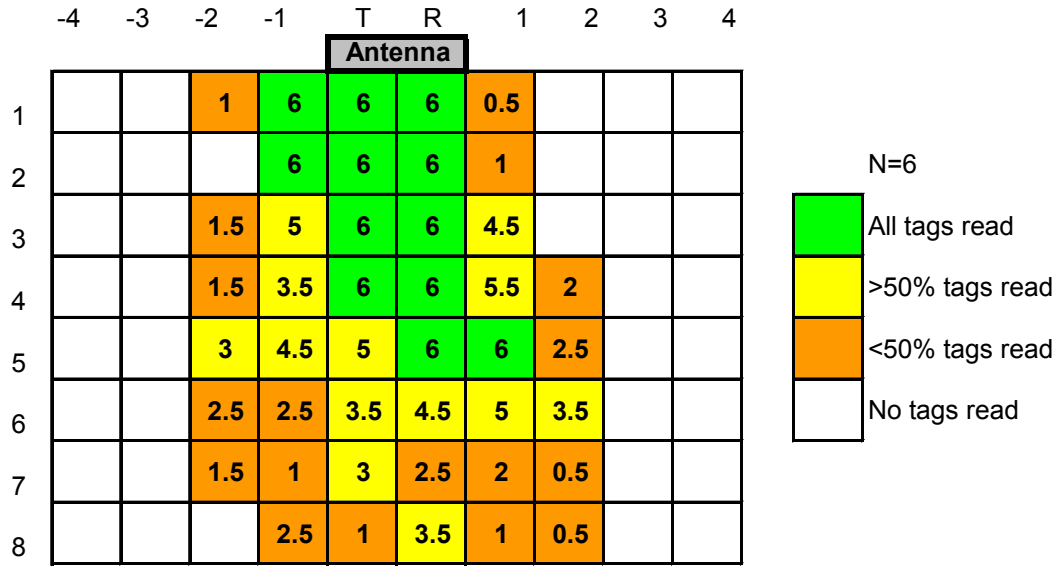

All distances in ft (1 ft = 0.305 m)
T=transmit side of antenna
R=receive side of antenna

Figure 12. Diagram. Read range for curled Alien® 2x2 tags in CPVC pipe before encapsulation and curing with tags oriented in horizontal direction.

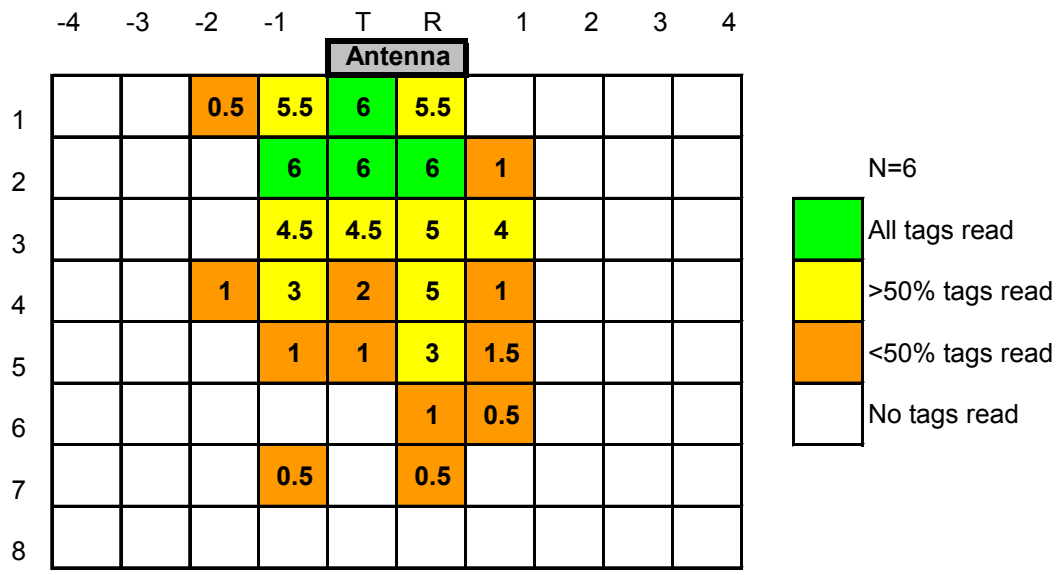

All distances in ft (1 ft = 0.305 m)
T=transmit side of antenna
R=receive side of antenna

Figure 13. Diagram. Read range for curled Alien® 2x2 tags in CPVC pipe before encapsulation and curing with tags oriented in vertical direction.

Read ranges after encapsulation with epoxy and curing, the next stage in the fabrication process, are summarized in figure 14 and figure 15 for the horizontal and vertical tag orientations, respectively. Effective read range limits are reduced even further by the epoxy and curing process to approximately 2 ft (0.6 m) for the horizontal orientation and 1 ft (0.3 m) for the vertical. This may be because the Alien® 2x2 tags were curled with the antenna and chip facing inward and the paper backing facing outward. It is possible that there may have been some signal leakage from the antenna into the epoxy that is responsible for the reduced read range. Unfortunately, the initial supply of tags was nearly exhausted when this phenomenon was discovered.

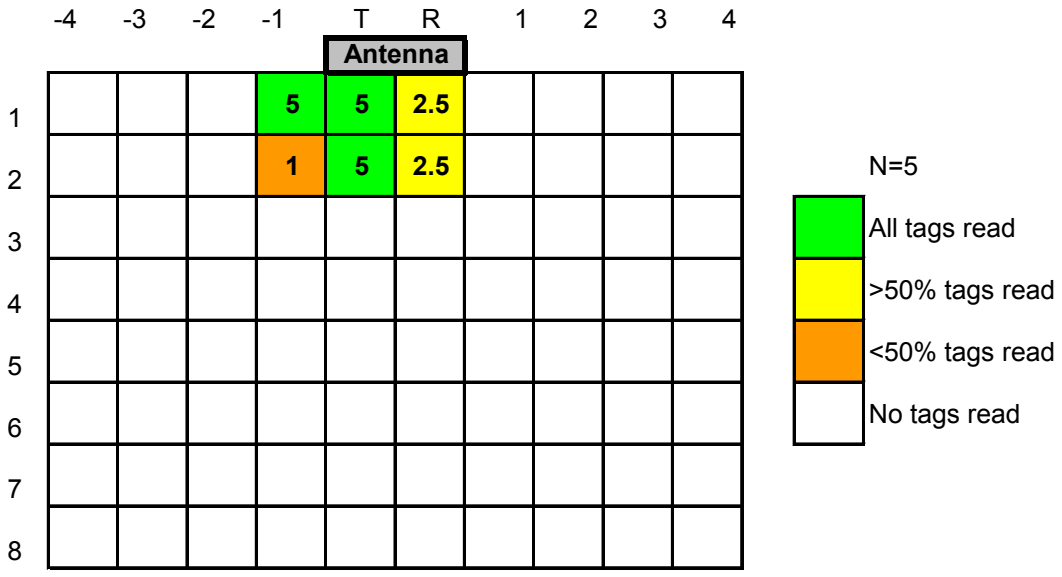

All distances in ft (1 ft = 0.305 m)
T=transmit side of antenna
R=receive side of antenna

Figure 14. Diagram. Read range for curled Alien® 2x2 tags in CPVC pipe after encapsulation and curing with tags oriented in horizontal direction.

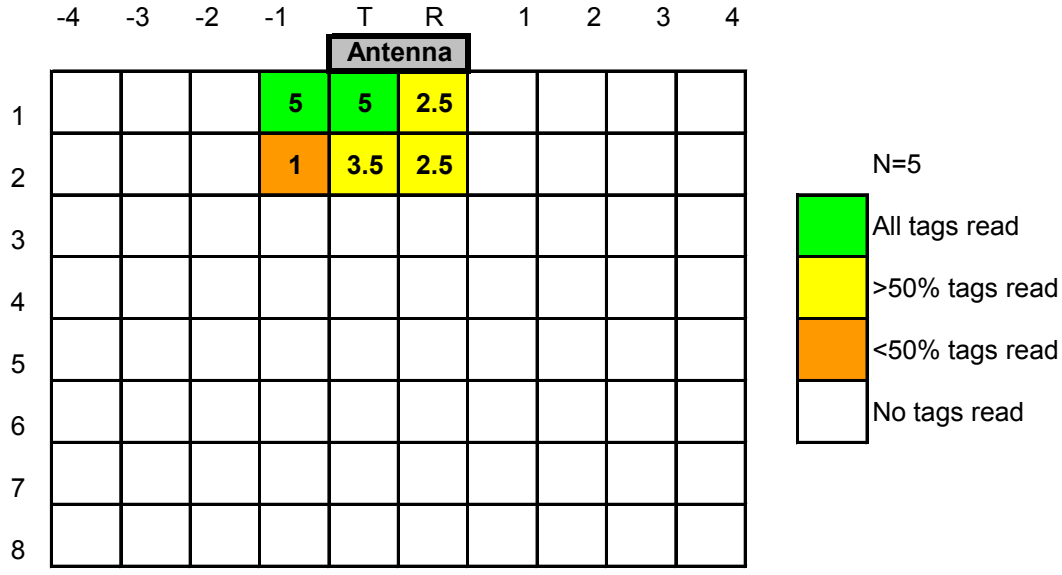

All distances in ft (1 ft = 0.305 m)
T=transmit side of antenna.
R=receive side of antenna

Figure 15. Diagram. Read range for curled Alien® 2x2 tags in CPVC pipe after encapsulation and curing with tags oriented in vertical direction.

Additional Evaluation

After receiving more RFID tags, additional evaluations were performed to examine the effects on read performance of orientation of the tag within the CPVC mold cylinder and of the

encapsulated cylindrical tag relative to the antenna geometry. All tags were now curled with the antenna surface outward and against the CPVC pipe wall. As shown in figure 16, two orientations can be defined for the tags depending on whether the antenna dipoles are oriented in an axial or circumferential direction with respect to the CPVC pipe axis (CPVC pipe axis is vertical in figure 16). In addition, the cylindrical encapsulated tag itself can have varying orientations relative to the antennae. Two limiting cases were considered: both had the axis of the cylindrical encapsulated tag parallel to the plane of the antenna unit, but in one orientation, the axis was parallel to the line connecting the centers of the transmit and receive antennae (i.e., parallel to the long dimension of the antenna unit) and in the other, the axis was perpendicular to this line (i.e., parallel to the short dimension of the antenna unit). Note that in reality, one can only control the orientation of the RFID tag within the CPVC mold; the orientation of the cylindrical tag relative to the antenna geometry will depend on the final random orientation of the encapsulated tag within the compacted pavement.[1]

Table 4 summarizes the influence of tag and cylinder orientation on maximum read range for the encapsulated Alien® 1x1 tags after oven curing at 248 °F (120 °C) for 24 h and subsequent oven heating to 247 °F (175 °C) for 1.5 h. Table 5 presents similar data for the Alien® 2x2 tags. Recall that the maximum read range for the nonencapsulated flat tags through air ranged between 2.5 to 4 ft (0.6 to 1.2 m) and 6 to 13 ft (2 to 4 m) for the Alien® 1x1 and 2x2 tags, respectively. Conclusions that can be drawn from these data include the following:

- The maximum read range of the Alien® 1x1 tags is substantially less than that of the Alien® 2x2 tags under all conditions.

- Regardless of orientation details, curling the RFID tag inside the CPVC pipe and/or encapsulating it in high-temperature epoxy significantly degrades the maximum read range. The 4-ft (1.2-m) maximum read range of the flat Alien® 1x1 tag decreased to a maximum of 2-ft (0.6-m) when encapsulated; the 13-ft (4-m) maximum read range of the flat Alien® 2x2 tag decreased to a maximum of 9 ft (2.7 m) when encapsulated.

- In nearly all cases the circumferential orientation of the RFID tag inside the CPVC pipe gives longer maximum read ranges. The differences between circumferential and axial orientation are modest to nonexistent for the smaller Alien® 1x1 tags but significant for the larger Alien® 2x2 geometry.

- The effect of orientation of the tag axis relative to the T-R antenna line appears to be quite small, with no consistent trends except for a small benefit of the perpendicular alignment for the circumferentially oriented Alien® 2x2 tags. It is fortunate that this influence is small because there is no way to consistently control the orientation of the tags relative to the antennae in the field.

[1] During the subsequent field trials (chapter 3), it was observed that most of the in-place tags appeared to lie within a horizontal plane, i.e., parallel to the plane of the antenna unit during field reading.

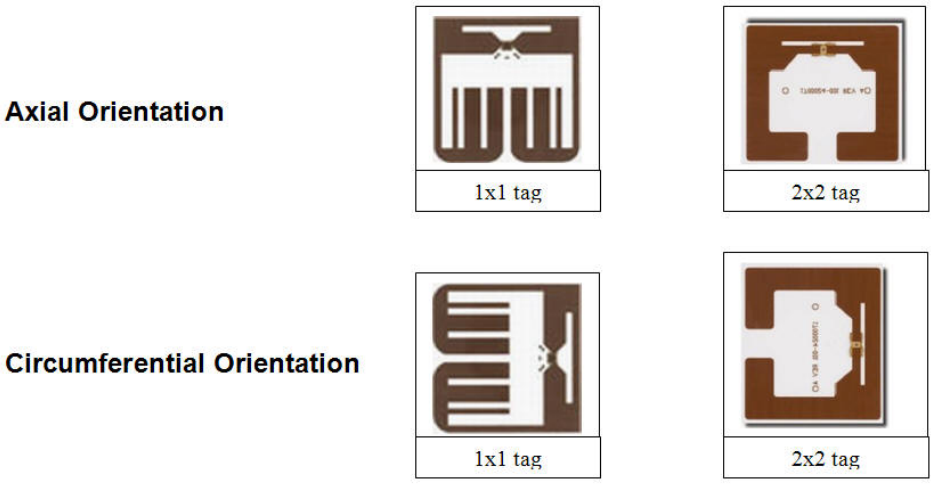

Figure 16. Drawing. Orientation options for RFID tags inside CPVC pipe molds (axis of CPVC pipe mold is vertical in all drawings).

Table 4. Maximum read range (ft) for Alien® 1x1 tags after 24-h oven cure at 248 °F (120 °C), cooling, then reheating for 1.5 h at 247 °F (175 °C).

Alignment of RFID Tag Within CPVC Pipe (Figure 16)	Orientation of Cylindrical Tag Axis Relative to T-R Antenna Line	
	Parallel	Perpendicular
Axial	1–1.6	0.5–1
Circumferential	0.5–1	1.6–2

Note: Cylindrical tag axis parallel to plane of antenna unit in all cases.

Table 5. Maximum read range (ft) for Alien® 2x2 tags after 24-h oven cure at 248 °F (120 °C), cooling, then reheating for 1.5 h at 247 °F (175 °C).

Alignment of RFID Tag Within CPVC Pipe (Figure 16)	Orientation of Cylindrical Tag Axis Relative to T-R Antenna Line	
	Parallel	Perpendicular
Axial	2–2.5	0.5–2
Circumferential	5–7	8–9

Note: Cylindrical tag axis parallel to plane of antenna unit in all cases.

Evaluation of the tag read performance continued to be plagued by sporadic problems with RF interference/reflections, proximity of the floor and/or people in the laboratory, and other factors. Consequently, an improved procedure for evaluating read performance and range in the laboratory was standardized. Nonconductive supports were constructed for the RFID antenna and tags to elevate them approximately 3.28 ft (1 m) above the laboratory floor. All laboratory personnel move several meters away from the antenna and tags prior to conducting read tests to minimize body interference.

Figure 17 and figure 18 summarize typical read rate performance as measured using the new standardized procedure. The two samples represent Alien® 2x2 tags encapsulated in CPVC molds and compacted into a single gyratory HMA cylinder. At each position, the cylinder was

oriented horizontally (axis parallel to floor) and then rotated through six different angles relative to the antenna. The figure summarizes the read success rate over all angles at various positions from the antenna for the two embedded tags. In general, the tags in these trials could be read up to a distance of approximately 5 ft (1.5 m) from the antenna and at angles off the antenna axis. Note that there are some slight differences in the read performance between the two samples; variability in individual tag read performance has been observed consistently throughout this study. Note also that the read success rate is biased toward the transmitter ("T") side of the antenna. Apparently, it is important to position the tag closer to the transmitter antenna so that it receives maximum impinging RF energy.

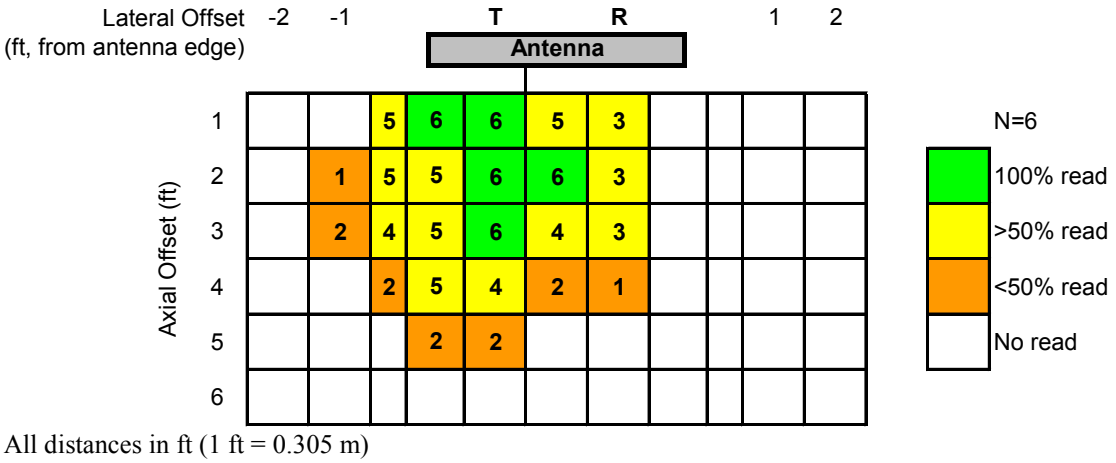

All distances in ft (1 ft = 0.305 m)

Figure 17. Diagram. Read performance for sample 7 as evaluated using standardized laboratory procedure.

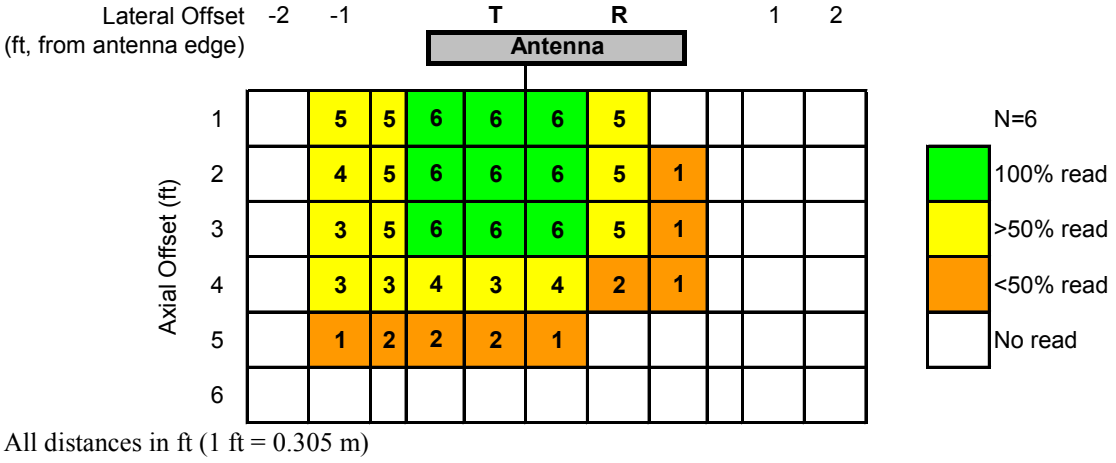

All distances in ft (1 ft = 0.305 m)

Figure 18. Diagram. Read performance for sample 8 as evaluated using standardized laboratory procedure.

Thermal Survivability

Thermal survivability is the first hurdle for the RFID tags because typical mixing and compaction temperatures in HMA of up to 356 °F (180 °C) are well above their operating and long-term storage temperature limits. Thermal survivability was investigated in a preliminary way using the Alien® 1x1 encapsulated tags. Only one replicate was tested for each condition.

All tags were left in the oven for 1.5 h at the target temperature. The time duration was chosen to duplicate the longest time between placement of the tags in the truckload of hot mix at the plant to final cooling of the compacted mat in the field. Immediately after removal from the oven, none of the tags could be read. However, all tags could be read to a distance of 3 ft (1 m) in air after being allowed to cool for 20 min. This is very similar to the baseline read for the Alien® 1x1 encapsulated tag prior to heating.

The preliminary investigation of thermal survivability was repeated with two encapsulated Alien® 2x2 tags. The first was heated for 1.5 h at 302 °F (150 °C); as with the Alien® 1x1 tags, the 2x2 tag could not be read immediately after removal from the oven but was readable up to a range of 10 ft (3 m) after 20 min of cooling. The second Alien® 2x2 tag was heated to 347 °F (175 °C) and appeared to fail because it could not be read even after cooling. However, visual inspection suggested that the encapsulation may have been flawed, directly exposing part of the tag to the high temperatures.

Mechanical Survivability

Mechanical survivability was independently evaluated via gyratory compaction of the encapsulated tags into a cold mix asphalt product. Mechanical survivability was investigated in a preliminary way using the Alien® 1x1 encapsulated tags. Each tag was placed in the loose cold mix near the center of the mold and then compacted to between 50 and 100 gyrations in the compactor. This is intended to simulate the stresses that the tags would feel during compaction in the mat in the field. All of the encapsulated tags survived the compaction. The average read range of 26 inches (670 mm) represents an approximately 30-percent decrease from the greater than 3 ft (1 m) baseline read range prior to compaction. It is speculated that this reduction is due to the additional attenuation of the RFID signals through the asphalt rather than any effect from the compaction itself.

The preliminary investigation of mechanical survivability was repeated with one encapsulated Alien® 2x2 tag compacted in the cold mix asphalt to 100 gyrations. Read range after compaction was approximately 10 ft (3 m). Again, this represents a decrease from the baseline read range through air of approximately 25 ft (7.6 m) for the 2x2 tag.

One of the cold mix gyratory plugs was saturated in water after initial testing to evaluate the influence of pavement moisture on signal attenuation. No significant difference in read range was discerned between the dry and wet conditions.

Combined Thermal and Mechanical Survivability

Once the survivability of the tags under only thermal or mechanical torture had been established, the final test was survivability under combined conditions in the laboratory. This test is intended to simulate the actual field scenario of transport of the tag in the truckload of hot mix asphalt followed by compaction into the mat behind the paver.

The hot mix asphalt used for this evaluation was a dense graded mix with a PG 64-22 unmodified binder. Tags were placed in an oven along with the loose mix for 1.5 h at a temperature of 320 °F (160 °C) before compaction. Two tags were placed in the loose mix in each gyratory mold near the axis at approximately the third points of the mold height. After

compaction, the gyratory plugs were extruded from the molds and then scanned in the axial direction by the RFID reader.

Figure 19 summarizes the read tests for three gyratory plugs, each containing two tags that had been encapsulated in the CPVC pipe. For two of the plugs, only one of the two tags survived the heating and compaction. During the read tests, the gyratory plug was rotated through six different positions (12:00, 2:00, 4:00, 6:00, 8:00, and 10:00). Each of the tags was read in each position. Given that there were only four surviving tags among the three gyratory plugs, there was a maximum of 24 possible successful reads. For the one plug in which both tags survived, there were no trends in read success or range between the closer versus more distant tag. As shown in the figure, the maximum effective read range was approximately 2 ft (0.6 m). This is roughly consistent with the effective read range for this tag type through air after encapsulation and curing (figure 14 and figure 15). In other words, the additional heating and compaction for the tags depicted by figure 19 did not significantly degrade the effective read range.

Six tags in all were oven heated and compacted into gyratory plugs. Of these, four survived and were able to transmit their identification numbers to the RFID reader when scanned. This corresponds to a survival rate of 75 percent. This is sufficient for field application because it is envisioned that multiple tags will be tossed into the truckload of HMA for redundancy.

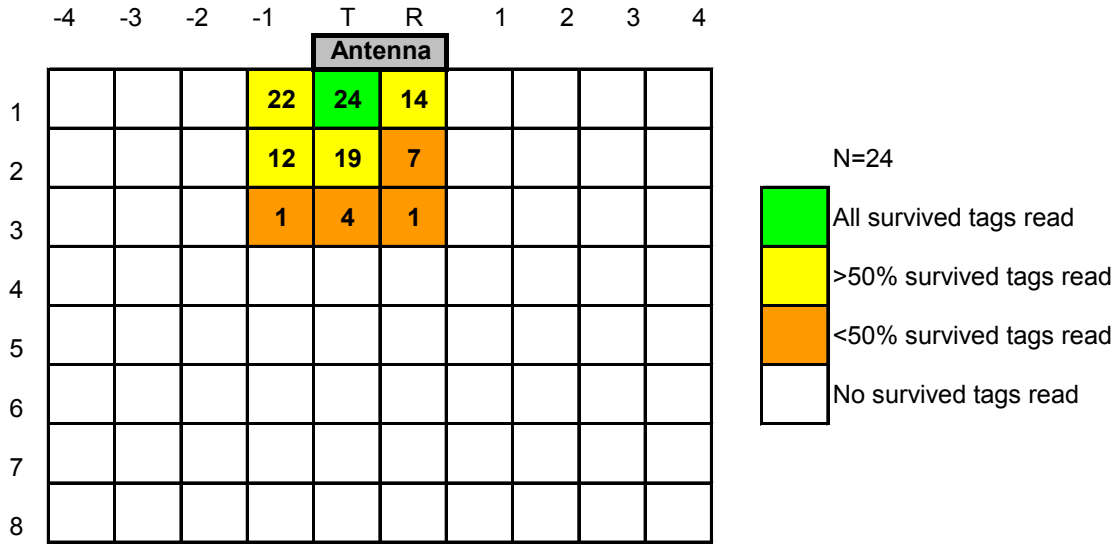

All distances in ft (1 ft = 0.305 m)
T=transmit side of antenna
R=receive side of antenna

Figure 19. Diagram. Read range for curled Alien® 2x2 tags in CPVC pipe after HMA oven heating and gyratory compaction.

CONCLUSIONS FROM FEASIBILITY EVALUATION

- Conventional passive UHF (860–960 MHz) RFID technology was determined as the most promising for paving applications. The advantages of passive UHF RFID included small tag size, low cost, adequate read range, and wide commercial availability. Potential attenuation of the UHF radio signals by HMA and survivability of the tags in the harsh

thermal and mechanical environment during paving were identified as the two key challenges to be addressed in the research.

- Based on theoretical considerations and data from the literature, it was determined that HMA was likely a good UHF medium in terms of attenuation losses. This was confirmed through laboratory studies, which concluded that UHF RFID signal attenuation by asphalt concrete should not be a serious issue in the field.

- Based on a careful review of the specifications and available product reviews for various manufacturers' systems, a Mercury® 5 RFID reader system from ThingMagic, Inc. was purchased for this project. Alien® Technologies Gen 2 1x1 and 2x2 tags were selected for initial evaluation because of their compatibility with the Mercury® 5 reader and their suitable dimensions.

- Various encapsulation schemes were evaluated for hardening the RFID tags against the thermal and mechanical stresses of paving. The final scheme consisted of encapsulation of rolled tags inside ¾-inch (19-mm) nominal outside diameter CPVC pipe subsequently filled with cured Cotronics Durapot™ 866 high-temperature epoxy.

- The read ranges of the encapsulated tags were thoroughly evaluated. The read range for the Alien® 1x1 tags in the optimal circumferential orientation inside the CPVC pipe varied between 0.5 and 2 ft (0.15 and 0.6 m), which is inadequate for the intended application. The corresponding read range for the Alien® 2x2 tags varied between 5 and 9 ft (1.5 and 2.7 m), which is more than adequate for the HMA tracking application.

- Thermal and mechanical survivability of the encapsulated tags was evaluated in the laboratory via oven heating and gyratory compaction. The encapsulated tags survived oven heating for 1.5 h at temperatures up to 347 °F (175 °C), adequate for paving applications. Survival rate for combined thermal and mechanical effects was approximately 75 percent. This is sufficient for field application because multiple tags will be placed into each truckload of HMA for redundancy.

- One gyratory plug was saturated in water after initial testing to evaluate the influence of pavement moisture on signal attenuation. No significant difference in read range was discerned between the dry and wet conditions.

CHAPTER 3: RFID TRACKING OF HMA PLACEMENT

INTRODUCTION

The encapsulated RFID tags were field tested to evaluate the following issues:

- Survivability under real-world paving scenarios.
- Read range under actual field conditions.
- Required redundancy (i.e., how many tags must be added to a truckload to locate the mix reliably along the pavement alignment; this is related to the survivability issue, but also includes delays in passing through the paver).
- Construction practicality issues (e.g., do the tags interfere with normal paving operations?).
- Construction quality issues (e.g., do the tags impair the quality of the compacted mat by inducing segregation or other defects?).

The pavement sections selected for the Phase II field trials included the following:

1. UMD Parking Lot XX1 (figure 20).
2. UMD Parking Lot EE (figure 20).
3. UMD Parking Lot T (figure 20).
4. Hampstead Bypass/MD 30 (figure 21).

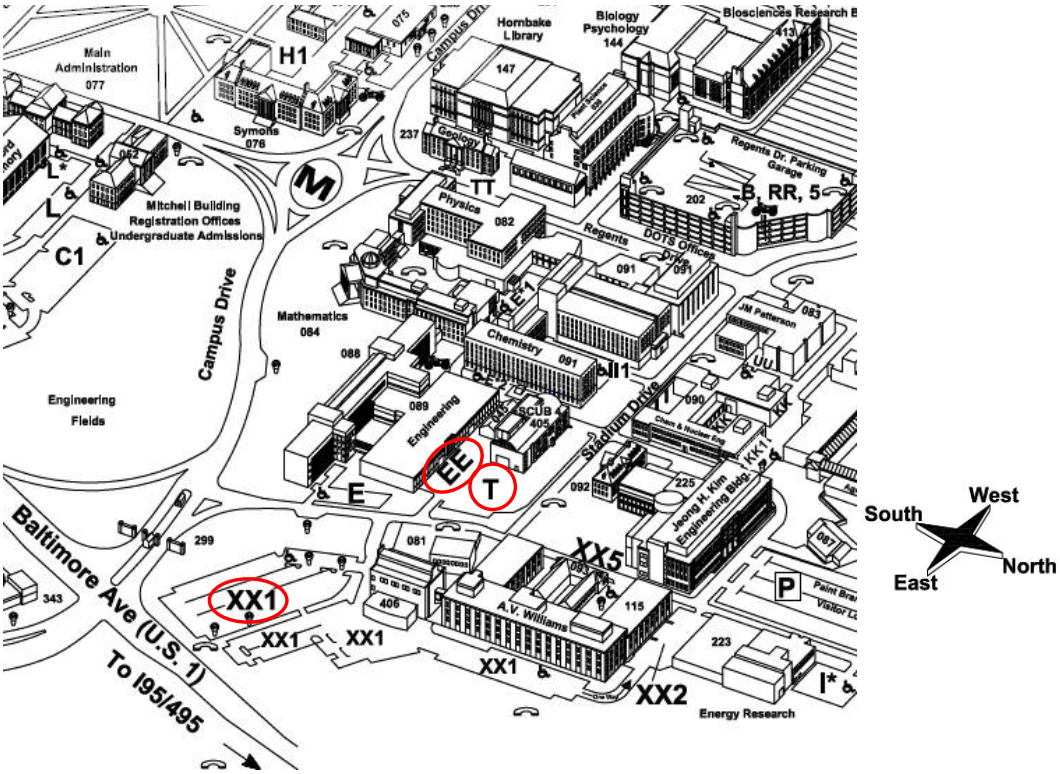

Source: http://dots.umd.edu/parking/maps/map_campus.pdf
Annotations added study team.

Figure 20. Map. Location of UMD parking lot paving projects.

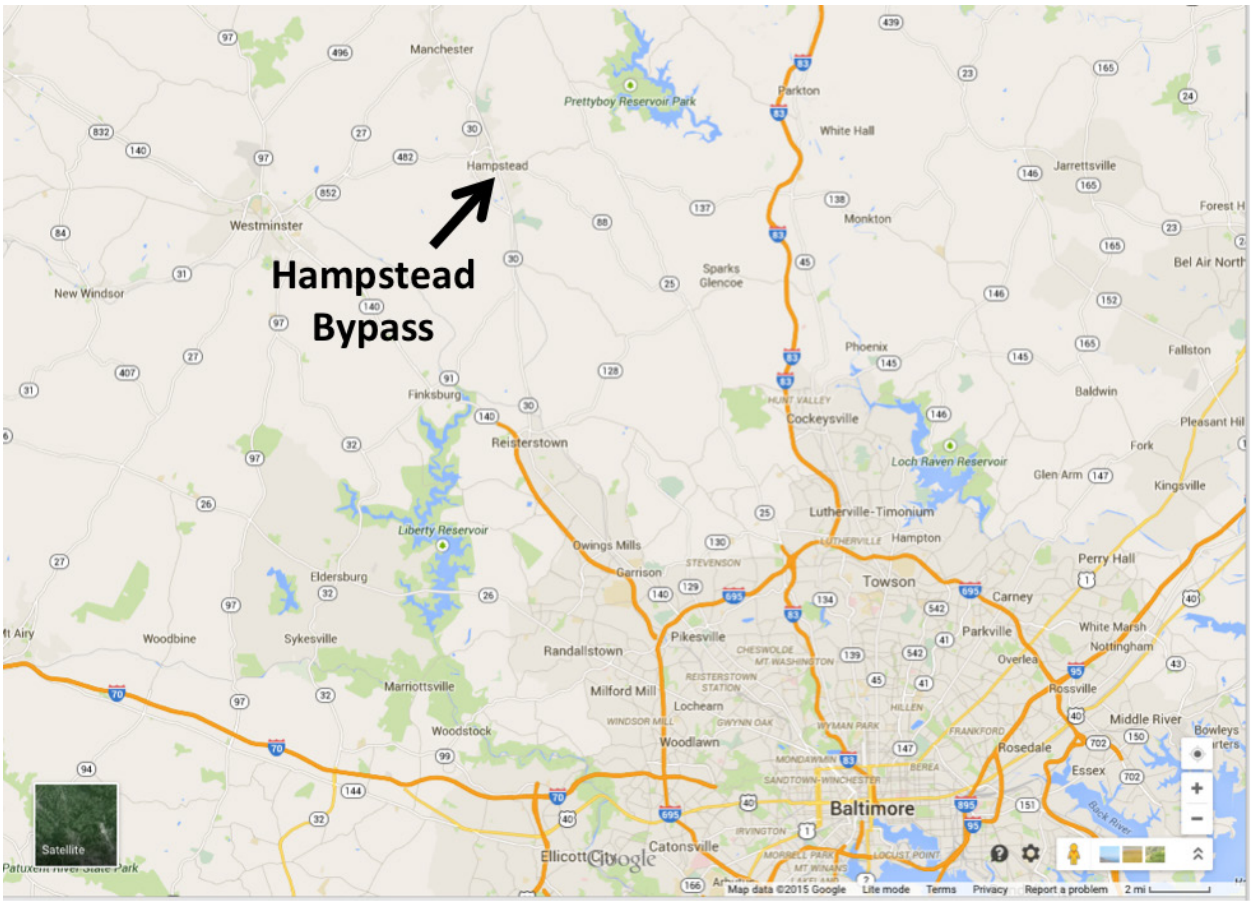

Original image: ©2015 Google®; map annotations provided by University of Maryland

Figure 21. Map. Location of Hampstead Bypass project.[(5)]

UMD PARKING LOT XX1

UMD Parking Lot XX1 is across Paint Branch Drive from the Civil Engineering Department's Pavement Materials Laboratory. The August 2007 paving work was to patch a large trench from storm drain replacement. Paving consisted of both a base and surface course. The paving contractor for the job was College Park Paving (foreman: Mr. Dennis Wilder).

Construction was begun just as Phase II of this project got underway, so there was insufficient time to prepare any tags for the base course paving and only a limited number of tags were ready in time for placement in the surface course. Six Alien® 2x2 and six Alien® 1x1 tags were pre-placed on top of the previously paved HMA base course and/or milled existing pavement. Pre-placement was performed in this initial trial so that the locations of the tags could be determined precisely during post-construction reading. The tags and their locations are summarized in table 6 and figure 22.

All tags were successfully heat tested at 347 °F (175 °C) for 1.5 h prior to placement in the field. Initially, half of the tags were placed before application of the tack coat (figure 23). However, because of the risk of sticky tags being picked up by the tires on the asphalt delivery trucks, the remaining tags were placed immediately ahead of the paver as it approached (figure 24). The

tags were then covered with a 2-inch (50-mm) thick lift of 0.5-inch (12.5-mm) surface mix by the paver (figure 25) and compacted under the rollers. In a few locations, the surface lift thickness was less than 2 inches (50 mm). None of the tags protruded above or were visible within the pavement surface after compaction.

Table 6. RFID tag identification in UMD Parking Lot XX1.

Tag Type	Label	Digital Signature
Alien® 1x1	2	0200989E
	3	0300ABAF
	4	04003238
	5	05000109
	6	0600545A
	7	0700676B
Alien® 2x2	AB	01ABC94C
	AD	01ADA98A
	BD	01BDBBBB
	BE	01BE8BD8
	CA	01CAB5CB
	CE	01CEF54F

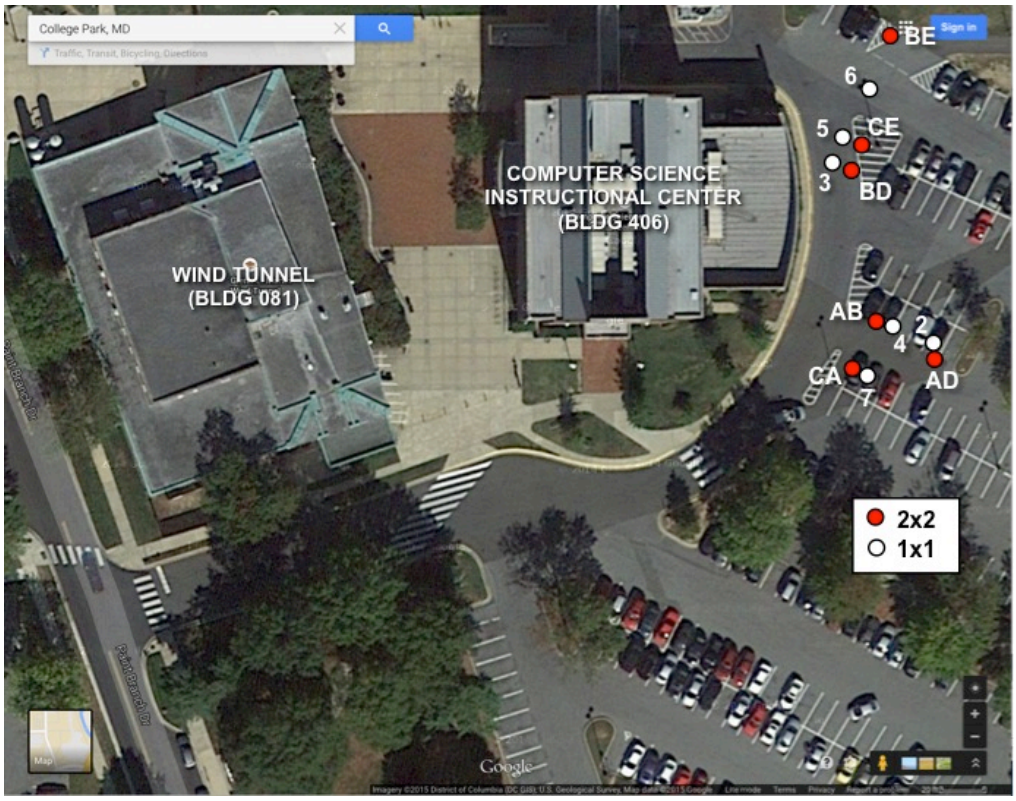

Original image: ©2015 Google®; map annotations provided by University of Maryland
Note: Locations are approximate. Image predates August 2007 paving; the HMA patch evident in the image is not the patch in which the encapsulated RFID tags were embedded.

Figure 22. Photo. Location of pre-placed RFID tags in UMD Lot XX1.[6]

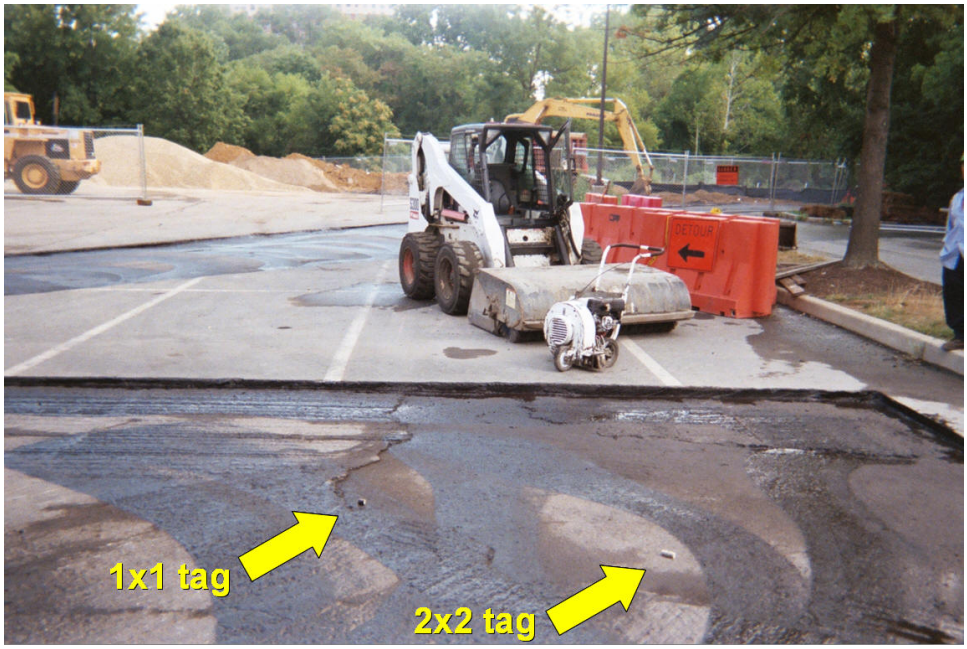

Figure 23. Photo. Pre-placement of tags at UMD Lot XX1 paving project.

Figure 24. Photo. Paving over pre-placed encapsulated tags.

Figure 25. Photo. Encapsulated tag beneath paver.

The tags were read in the field a few days after construction. A rolling support for the electronics was improvised using a plastic laboratory cart with one RFID antenna secured using nonmetallic rope to cantilevered wooden boards. The RFID reader and laptop computer were also placed on the cart. Power was supplied from an automobile via a power inverter and long extension cable. The cart was manually pushed in overlapping passes over the paved area. Figure 26 illustrates the final improvised apparatus for reading the RFID tags in the UMD parking lots. One complication was that Parking Lot XX1 was placed back in service immediately after paving, so the read evaluation had to be conducted at night when there were few parked cars.

The read success rate was evaluated at two antenna heights of 32 inches (810 mm) and 10 inches (250 mm) above the pavement surface. At the time of the field data collection, a portion of the parking lot containing one each of the Alien® 2x2 and Alien® 1x1 tags was fenced off and inaccessible, leaving only five each of the 2x2 and 1x1 tags available for evaluation. Details of the read success for all of the tags are given in table 7. The read success rate at the 32 inches (810 mm) antenna height was 100 percent for the Alien® 2x2 tags (i.e., all five of the 2x2 tags could be read), and 0 percent for the Alien® 1x1 tags. The lower 10-inch (250-mm) antenna height yielded better results, with 100 percent of the Alien® 2x2 tags and 40 percent (i.e., two of the five) of the 1x1 tags successfully read.

Figure 26. Photo. Hand cart for reading RFID tags in UMD parking lots with antenna in the lower position (10 inches above pavement surface).

Table 7. Read success for RFID tags in UMD Parking Lot XX1.

Tag Type	Label	Digital Signature	Read From 32-Inch Height?	Read From 10-Inch Height?
Alien® 1x1	2	0200989E	No	No
	3	0300ABAF	No	No
	4	04003238	No	Yes
	5	05000109	No	No
	6	0600545A	Inaccessible	Inaccessible
	7	0700676B	No	Yes
Alien® 2x2	AB	01ABC94C	Yes	Yes
	AD	01ADA98A	Yes	Yes
	BD	01BDBBBB	Yes	Yes
	BE	01BE8BD8	Inaccessible	Inaccessible
	CA	01CAB5CB	Yes	Yes
	CE	01CEF54F	Yes	Yes

1 inch = 25.4 mm

UMD PARKING LOT EE

This parking lot is immediately adjacent to the Pavement Materials Laboratory. Similar to the work on Parking Lot XX1, paving consisted of base and surface courses to patch a large trench from storm drain replacement. This paving was originally scheduled for late September 2007. However, construction was subsequently delayed until October. The 4-inch (100-mm) thick layer of 0.75-inch (19-mm) dense-graded base mix was placed on October 16; the 2-inch (50-mm) thick lift of 0.5-inch (12.5-mm) dense-graded surface mix was paved the following day, October 17. The paving contractor for the job was College Park Paving (foreman: Mr. Dennis Wilder).

Two methods of tag placement were employed in Lot EE. For the base lift, 10 each of the Alien® 1x1 and 2x2 tags were pre-placed ahead of the paver, and an additional 10 each of both tag sizes were placed in the paver hopper and run through the paver. For the surface course, 10 each of both tag sizes were tossed in the paver hopper and run through the paver; none of the tags was pre-placed ahead of the paver for the surface lift. All tags were compacted into the mat by rollers behind the paver. A total of 40 tags were placed in the base course and 20 in the surface layer.

After paving of the surface lift was complete, the mobile cart with antenna, RFID reader, and computer (figure 26) was used to evaluate the read success rate for the tags. Based on the findings from Lot XX1, the height of the antennae above the pavement surface was kept constant at approximately 10 inches (250 mm). The read success rates for the different tag sizes as a function of layer (base versus surface) and method of placement (pre-placed versus through-the-paver) are summarized in figure 27. In this figure, "Placed" refers to the pre-placed tags (base lift only), and "Paver" designates the tags tossed into the pavement hopper (both base and surface lifts). Some key observations that can be drawn from figure 27 include the following:

- The Alien® 1x1 "Paver" tags in the base lift had a higher read success rate (70 percent) than did the same size tags placed in the surface lift (40 percent), despite the fact that the surface lift was at a shallower depth and thus closer to the antenna and had less potential for signal attenuation through the HMA. It is believed that this simply illustrates the high variability inherent in the small format Alien® 1x1 tags.

- The Alien® 2x2 "Paver" tags in the base lift had a slightly lower read success rate (90 percent) than did the same size tags placed in the surface lift (100 percent). This matches physical reasoning, but again the discrepancy could also be simply due to variability among the different sets of tags.

- The discrepancies between the read rates for the Alien® 1x1 and the 2x2 tags in the base lift was greater for the "Placed" set (100 percent versus 10 percent) than for the "Paver" set (100 percent versus 70 percent). There is no objective physical reason for this because none of the pre-placed tags was observed to be damaged by truck and/or paver tires, etc. Again, this may simply be a consequence of variability among the different sets of tags.

- Overall, the Alien® 1x1 tags had an average read success rate of about 40 percent while the larger Alien® 2x2 tags had a much higher read success rate of more than 95 percent. These rates are comparable to those observed in Lot XX.

Some of the tags in Lot EE were observed to have migrated to the surface of the mat. While no tags were seen on the surface of the finished base course, one of the small tags and three of the larger tags were observed at the top of the surface course. Examples are shown in figure 28 and figure 29. Other than aesthetics, it is unclear whether these surfaced tags will have any detrimental effect on the performance of the pavements. They arguably could provide a preferential pathway for local intrusion of water into the asphalt that could produce accelerated stripping or other problems. This issue should be investigated further in the future.

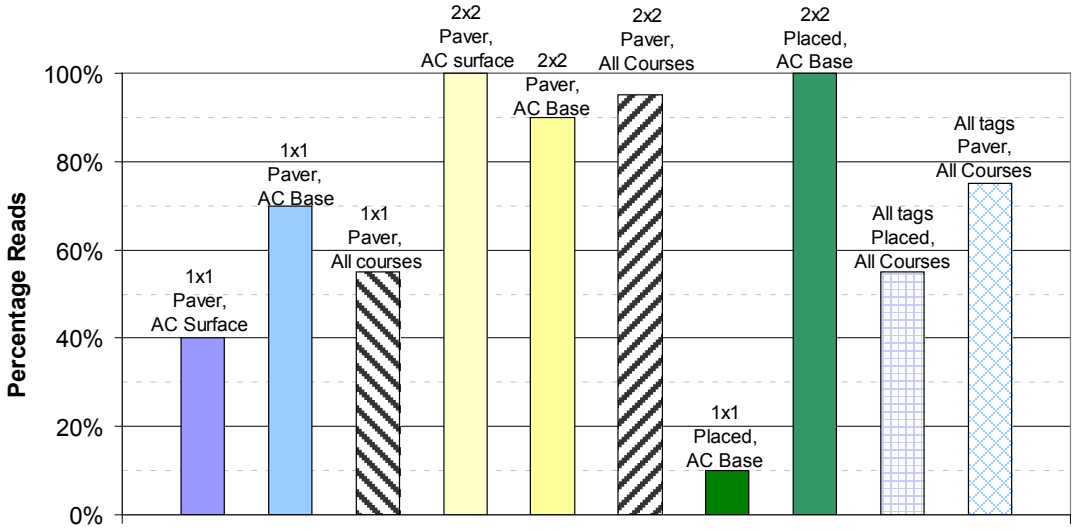

Figure 27. Chart. Summary of read success rates for tags in Parking Lot EE.

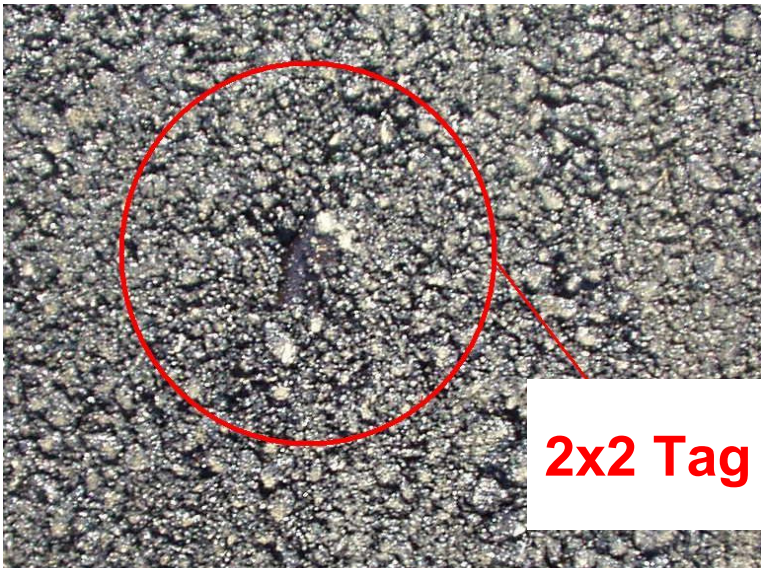

Figure 28. Photo. Examples of surfaced RFID tags in Lot EE.

Figure 29. Photo. Worst-case example of surfaced RFID tag in Lot EE.

UMD PARKING LOT T

This parking lot is near the Pavement Materials Laboratory. Paving conditions are similar to those for Lots XX1 and EE, although the area of patch is smaller, and therefore only a few tags were placed. This area was paved in late October 2007. Results were comparable to those from Lot XX1 and Lot EE.

HAMPSTEAD BYPASS/MD 30

The Hampstead Bypass project lies to the east of MD 30 around the town of Hampstead, MD (figure 30). The route runs from south of Wolf Hill Drive to north of the town of Hampstead. The project included construction of two lanes of MD 30 on new alignment for approximately 4.4 mi (7 km). The new alignment incorporates three roundabouts: one near the southern terminus to provide a connection to existing MD 30; one at MD 482; and one near the northern terminus to provide a connection to existing MD 30.

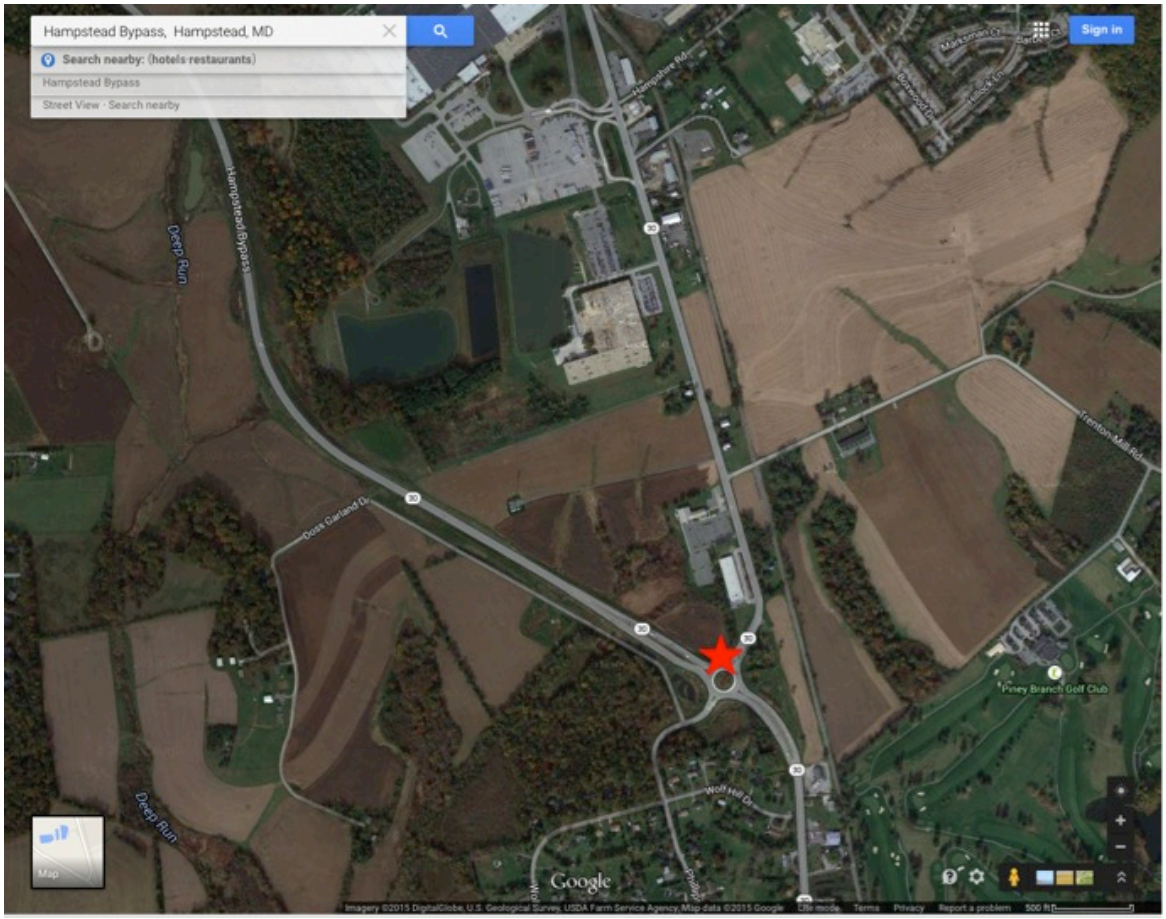

Original image: ©2015 Google®; map annotations provided by University of Maryland

Figure 30. Map. Location of Hampstead Bypass project with star marking approximate location of southern entrance to construction site.[(5)]

The new pavement construction consisted of two 4-inch (100-mm) thick base lifts and a 2-inch (50-mm) surface layer. Nominal maximum sizes for the HMA mixtures were 0.75 inches (19 mm) for the base lifts and 0.5 inches (12.5 mm) for the surface layer. Project specifications called for a material transfer vehicle (MTV) as an intermediary between the unloading trucks and the paver. Because this project involved multiple lifts and was scheduled to be closed to traffic for several months after paving, it was ideal for detailed field evaluations.

A significant problem developed with regard to tag availability prior to construction. The smaller Alien® 1x1 tags were taken out of production by Alien Technologies. A search of RFID tag suppliers identified several alternatives. The most promising of these were an approximately 1 by 2 inches (30 by 50 mm) "Rafsec® Web" tag from UPM Raflatac® (figure 31—see also http://www.upmraflatac.com/). Sample quantities of these tags were ordered for laboratory evaluation. The UPM Raflatac® tags had the advantage that they could still be curled into the pipe molds similar to the Alien® 1x1 tags. Laboratory read performance of the UPM Raflatac® tags was comparable to, and in some cases slightly better than, that for the Alien® 1x1 tags. The read performance of the UPM Raflatac® tags was still lower than for the larger Alien® 2x2 tags, however.

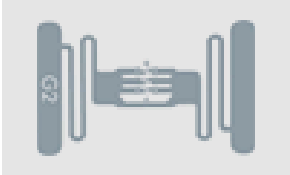

Figure 31. Drawing. UPM Raflatac® RFID tag.

The Hampstead Bypass project was constructed in phases, the first phase of which was the leg near the southern terminus with MD 30 (figure 32). Construction delays postponed the start of paving until November 2007, and as a consequence, only the lower base lift could be placed before the end of the construction season. Both UPM Raflatac® and Alien® 2x2 tags were placed in this lower 4-inch (100-mm) base lift. Additional Alien 2x2 tags were placed in the upper 4-inch (100-mm) base lift in April 2008 at the start of the new construction season. All tags were placed in the section of pavement just north of the lane merge at the southern terminus roundabout. This is designated as the "Study Area" in figure 33.

Image from http://www.sha.state.md.us/WebProjectLifeCycle/ProjectMaps.asp?projectno=CL416536# with annotations by the University of Maryland

Figure 32. Photo. Hampstead Bypass project site.

.

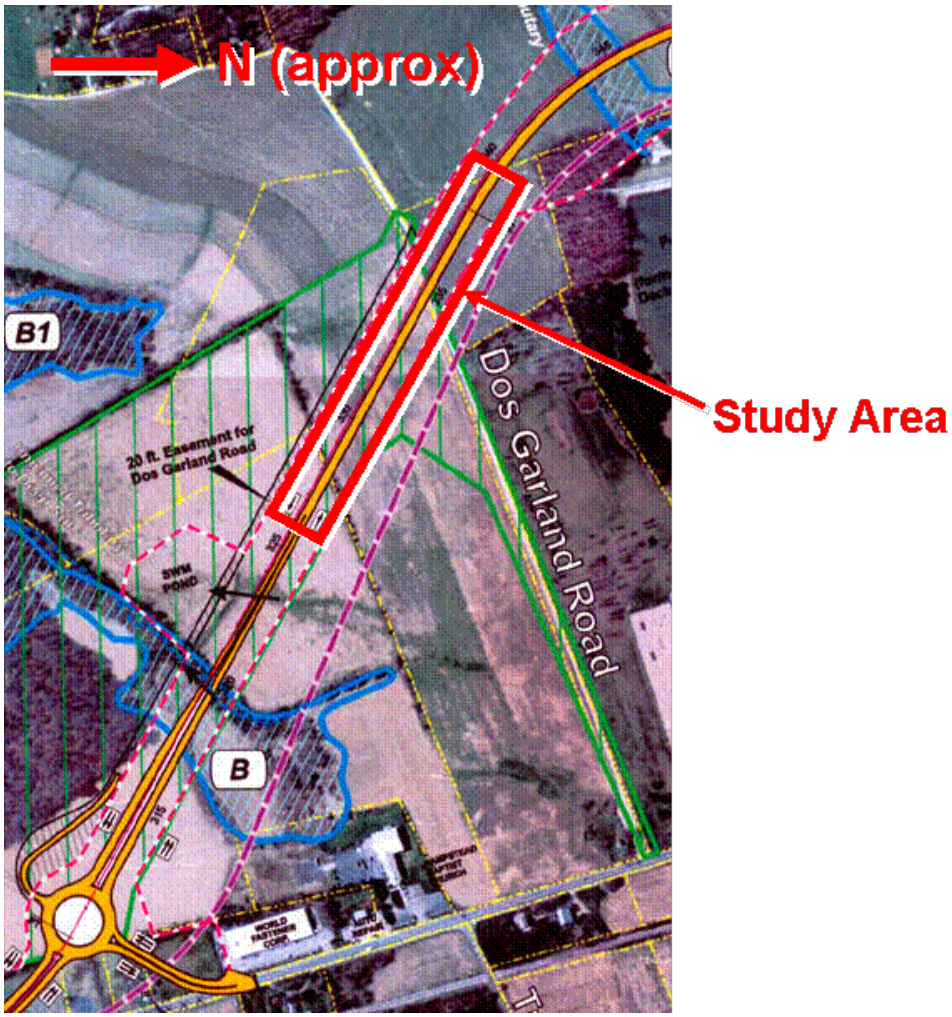

Image from
http://www.sha.state.md.us/WebProjectLifeCycle/ProjectMaps.asp?projectno=CL416536#
with annotations by the University of Maryland

Figure 33. Photo. Magnified view of study area at the Hampstead Bypass project site (boxed area in figure 32).

November 2007 Paving

Both UPM Raflatac® and Alien® 2x2 tags were placed in the lower base lift of the southbound travel lane in the study area (figure 33) during paving on November 28, 2007. Paving and tag placement began at the lane merge at the southern edge of the study area and proceeded northward. Note that the MTV was not used for the lower base lift because it was too heavy for the unprotected aggregate base.

The experimental plan for this field trial was as follows:

1. Ten Alien® 2x2 tags with prerecorded digital IDs were placed into each of six sequential truckloads. The tags were placed between the second and third drop in each load. The license plate number of the truck was recorded by a student research assistant and

reported by telephone to other student research assistants at the job site awaiting its arrival.

2. Upon arrival of each tagged truck at the paving site, the license plate number of the truck and the station and GPS coordinates at which it began unloading into the paver were recorded. The GPS coordinates were recorded both with a conventional handheld GPS transceiver (Garmin® GPS-12) and with a GPS logger (Pocket Track Pro Magnetic from Brickhouse® Security) cross-referenced by time stamp. A log of all tag locations is provided in table 8.

3. Steps 1 and 2 were repeated using 40 UPM Raflatac® tags (10 each in 4 sequential trucks).

4. The mat was inspected visually for surfaced tags. Although few tags were observed at the surface after extrusion of the mat behind the paver, more were observed on the surface after compaction.

Table 8. Log of tags in lower 4-inch (100-mm) base lift at Hampstead Bypass project (November 2007).

Truck Number	Truck License Plate	Tag Size (inches)	Tag IDs	Time at Unload	Station at Unload	Coordinates of Unload Point			
						Handheld GPS		GPS Logger	
						N	W	N	W
1	109-ED97	2x2	1–10	02:00pm	320+50	*39° 44′ 59.6″*	76° 50' 44.1"	39° 34'5 9.6431"	76° 50' 44.0653"
2	039-ED20	2x2	11–20	02:04pm	321+00	39° 35' 00.0"	76° 50' 44.6"	39° 34' 59.7440"	76° 50' 44.5930"
3	152-ED09	2x2	21–30	02:09pm	321+50	*39° 40′ 70.8″**	*76° 22′ 37.0″**	39° 35' 00.1638"	76° 50' 45.3763"
4	127-ED60	2x2	31–40	02:21pm	322+50	39° 35' 01.0"*	76° 50' 774"*	39° 35' 00.6391"	76° 50' 46.6820"
5	052-ED56	2x2	51–60	02:30pm	323+00	39° 35' 01.0"	76° 50' 47.0"	39° 35' 01.0212"	76° 50' 47.0927"
6	152-ED10	2x2	41–50	02:43pm	325+50	39° 35' 02.4"	76° 50' 49.8"	39° 35' 02.3407"	76° 50' 49.8822"
1	162-ED77	1x2	1–10	02:45pm	326+25	39° 35 '02.6"	76° 50' 50.4"	39° 35' 02.4377"	76° 50' 50.2902"
2	155-ED61	1x2	11–20	02:50pm	328+50	39° 35' 03.9"	76° 50' 53.2"	39° 35' 02.5480"	76° 50' 50.8996"
3	039-ED17	1x2	21–30	—	—	—	—	—	—
4	092-ED62	1x2	31–40	03:02pm	329+50	39° 35' 04.2"	76° 50' 54.3"	39° 35' 04.2766"	76° 50' 54.4862"

* Indicates coordinates were read with a different GPS device
— Indicates no data collected
Note: Italics indicates possible error in data recording
1 inch = 25.4 mm

The project team returned to the Hampstead Bypass site on December 3 for preliminary read trials. The vehicle-mounted read system consisted of an adjustable wooden frame suspending the antennae above the pavement surface behind the test vehicle (figure 34). A slow vehicle speed of less than about 5 mi/h (8 km/h) was maintained for all trials. The antennae were arranged with the transmitter sides inboard (i.e., toward the centerline of the car) and the receiver ends outboard. Two antenna heights of approximately 3 inches (75 mm) and 12 inches (300 mm) were evaluated. Because the limited tag read range and antenna configuration made it unlikely that the entire lane width could be read successfully from a single position, three vehicle passes along the southbound travel lane were made for each antenna at each height. Note that a production data collection system could be designed with a wider antenna array that would minimize or eliminate the need for multiple passes.

Figure 34. Photo. Vehicle-mounted antennae and RFID reader.

Key observations from the read trials include the following:

- No overlap of tags was observed—i.e., the tags were ordered in the same order as the truck deliveries to the paver.

- For the Alien® 2x2 tags, six tags that were detected at the 3-inch (75-mm) antenna height were not detected at the 12-inch (300-mm) height, and 12 tags detected at the 12-inch (300-mm) height were not detected at the 3-inch height.

- For the UPM Raflatac® tags, three tags each were detected from one antenna height but not from the other antenna height.

- One truck containing UPM Raflatac® tags (tag numbers 21 to 30) was "lost" at the job site during paving, and the station location at which it unloaded was not recorded. However, from the RFID tag read, it was confirmed that it unloaded between the trucks containing tags 1 to 10 and 11 to 20. This confirms the effectiveness of RFID in providing a definitive location for the load when manual methods fail for any reason (paper record errors, miscommunication, etc.).

- Fifteen percent of the Alien® 2x2 tags were observed at the surface of the base lift.

- No UPM Raflatac® tags were observed at the surface of the lift.

- For the UPM Raflatac® tags, 10 percent or more of the tags in all truckloads were detected at both antenna heights (figure 35).

- For the Alien® 2x2 tags, 30 percent or more of the tags in all truckloads were detected at the 3-inch (75-mm) antenna height, and 50 percent or more of the tags in all truckloads were detected at the 12-inch (300-mm) antenna height (figure 36).

- Overall read success rates were slightly less than 20 percent for the UPM Raflatac® tags, and approximately 60 percent for the larger Alien® 2x2 format (figure 37).

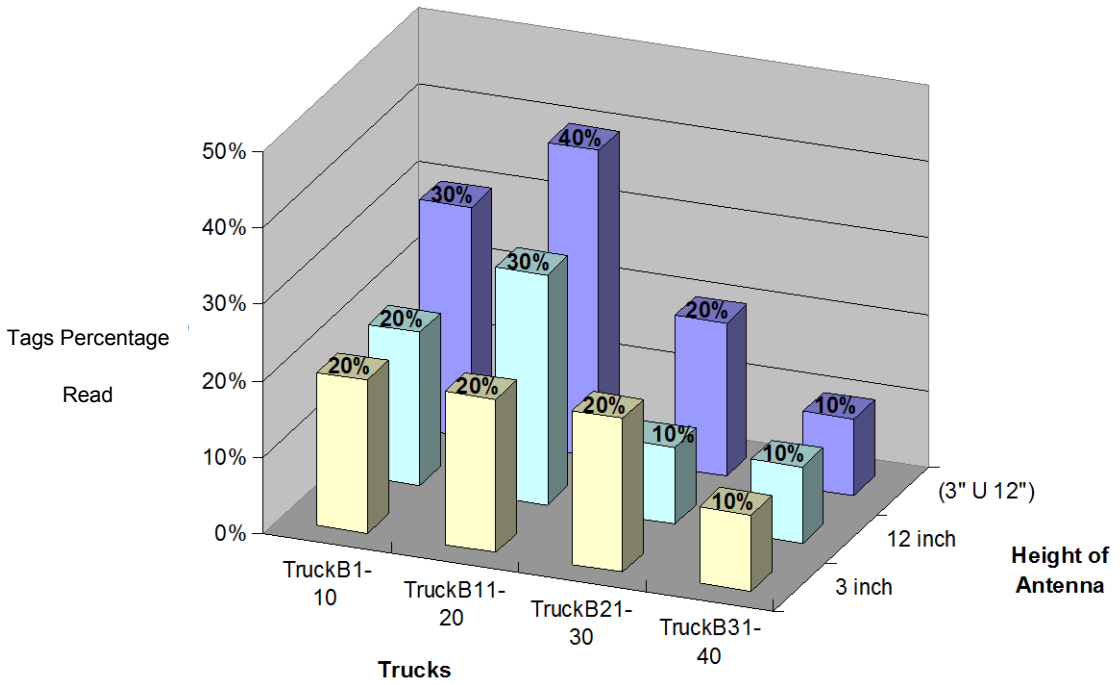

Figure 35. Chart. Percentage of UPM Raflatac® tags read in each truck versus height of antennae (Hampstead Bypass, November 2007).

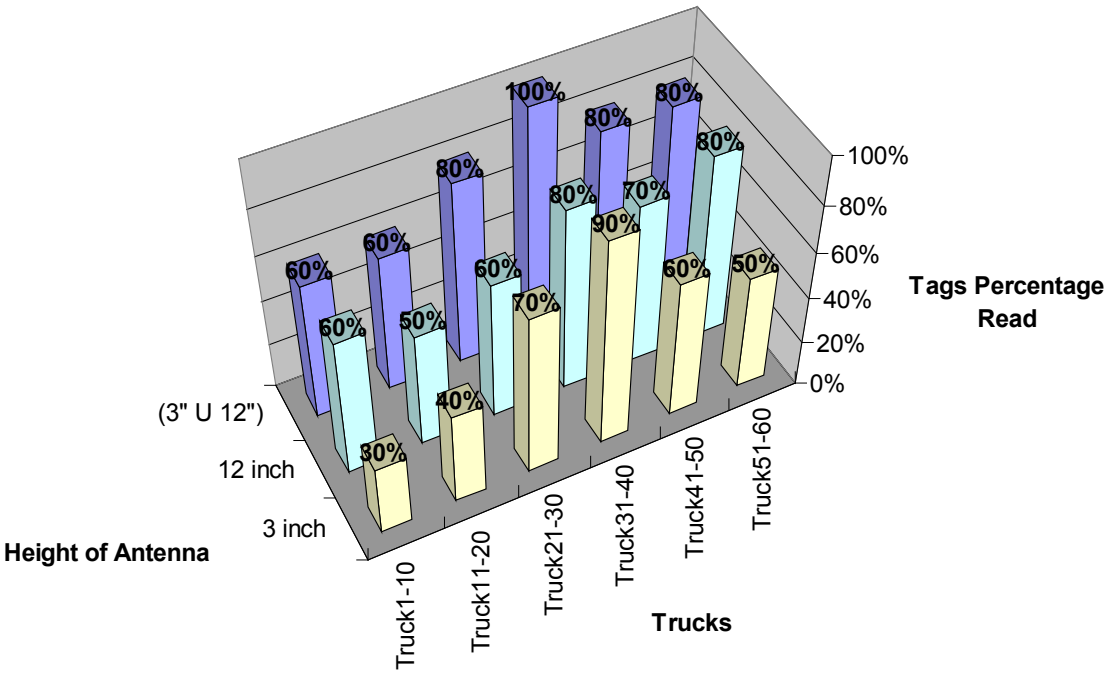

Figure 36. Chart. Percentage of Alien® 2x2 tags read in each truck versus height of antennae (Hampstead Bypass, November 2007).

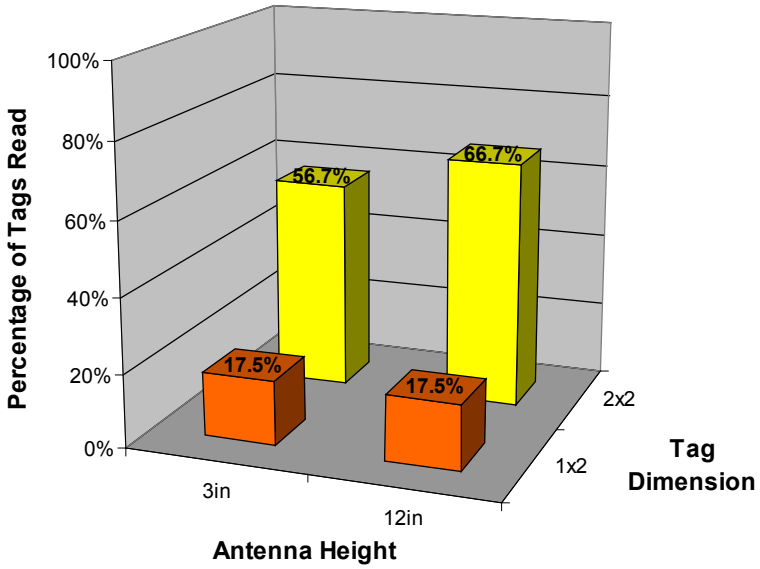

Figure 37. Chart. Overall read success rate for lower base lift at Hampstead Bypass (November 2007).

April 2008 Paving

Thirty-two Alien® 2x2 tags were placed in the upper base lift of the northbound travel lane in April 2008. The experimental plan for this field trial was similar to that for the lower base lift

placed the preceding November: eight Alien 2x2 tags with prerecorded digital IDs were placed into each of four sequential truckloads, and spatial location of each truck along the alignment during unloading was recorded. A key difference for the upper base lift paving was the use of the MTV. The RoadTec® SB-2500D MTV used on this project (figure 38) is more than 50 ft (15 m) long and has a 25-T (22.7-t) surge capacity; potential spatial lag and mixing of HMA truckloads because of the use of the MTV were among the issues evaluated in this field trial.

Figure 38. Photo. RoadTec® SB-2500D material transfer vehicle used in April 2008 paving at the Hampstead Bypass project.

The vehicle-mounted read system (figure 34) was again used to scan the tags immediately after construction. The antenna configurations were similar to those in the November 2007 trials except that only the lower 3-inch (75-mm) antenna height was used, and the influence of antenna orientation (receive sides inbound/outbound) was evaluated. Three passes (edge, centerline, and edge of lane) were performed at each of several vehicle speeds. Additional passes were made over the southbound travel lane containing the tags placed during the November 2007 paving to ascertain whether they were still functioning and readable.

The delivery and read locations for all tags that could be read are summarized in figure 39. Overall, 78 percent of the Alien® 2x2 tags placed in the upper base lift could be found by the reader; this is a slightly higher percentage than for the lower base lift paved the preceding November. GPS coordinates were not recorded during this field trial, so instead, all position information is referenced to station. The station at which the haul truck began unloading into the MTV defines the beginning of the delivery range, and the station at which the unloaded haul truck pulled away from the MTV defines the end. Read locations are recorded only within a station (100 ft (30 m)) interval, although many of the tag locations could be pinpointed more precisely. The data in figure 39 indicate that most of the tags were found in roughly the correct

sequence in the completed mat. The fact that the MTV itself is more than 50 ft (15 m) long and that it can carry (and potentially mix) more than one truckload of HMA means that there will inevitably be a spatial lag of unknown length between the truck unloading range and the final location of the tags in the mat. Tag IDs in bold italics in figure 39 indicate tags that were offset more than one station interval from the delivery range; 80 percent of the tags were found within one station interval of their delivery, with the longest offset of the remaining 20 percent between four to five stations (tags 81, 90).

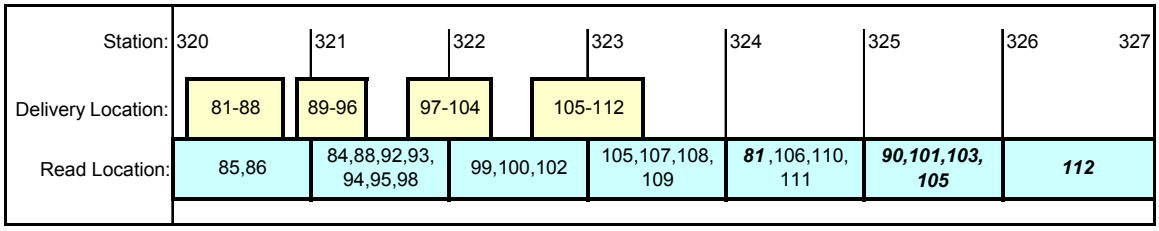

Note: Bold italics identify tag IDs that are displaced more than one station (100 ft (30 m)) from their delivery location.

Figure 39. Chart. Delivery and read locations for RFID tags paved into the upper base lift at the Hampstead Bypass (April 2008).

Note that even without the MTV, there will always be a significant spatial distribution of tags from a given truckload along the alignment. One truckload of HMA for a 4-inch (100-mm)-thick lift corresponds to approximately 70 lane-ft (21 lane-m) of paving; tags in the truckload can end up anywhere along this length. This lack of spatial resolution—even when magnified by use of an MTV—is not significant in practical terms because the material properties from the sampled truckload are intended to represent an entire lot of material (e.g., 1,000 T (907 t), corresponding to about 0.5 lane-mi (0.8 lane-km) of paving).

Some of the tags in figure 39 are in the incorrect sequence. For example, tag 81 from the first truckload was found in the same interval of pavement as tags 106, 110, and 111 from the fourth truck. Similarly, tag 90 from the second truck and tags 101 and 103 from the third truck appear in the same interval as tag 105 from the fourth truck. This may be due to the variable nature of the spatial lag between delivery and read location, or it may be a consequence of mixing of HMA from different loads in the MTV. Regardless of the cause, this incorrect sequencing would not be an issue for production use when only random (as opposed to sequential) truckloads would be tagged.

Additional key observations drawn from the read trials in April 2008 include the following:

- As summarized in figure 40, the read success rate was significantly better when the dual antennae were oriented with their receive (R) ends inboard (and therefore their transmit (T) ends outboard). Placing the transmit ends of the antennae outboard may provide a better distribution of incoming RF energy to the tags.

- Read success rate decreased slightly with increasing vehicle speed. As shown in figure 41, the read success rate at 45 mi/h (72 km/h) was approximately 65 percent of the rate at slow speeds.

- The read success rate for the Alien® 2x2 placed in the southbound lane paved the preceding November was approximately 60 percent when read in April. This was approximately equal to the read success rate during the initial reading in early December 2007, suggesting little degradation of the embedded RFID tags during the intervening 4 months.

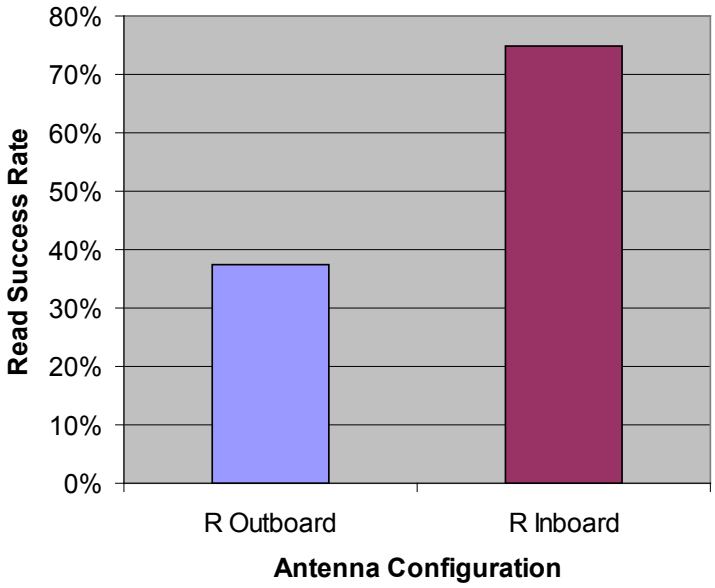

R = receive

Figure 40. Chart. Influence of antennae orientation on read success rate.

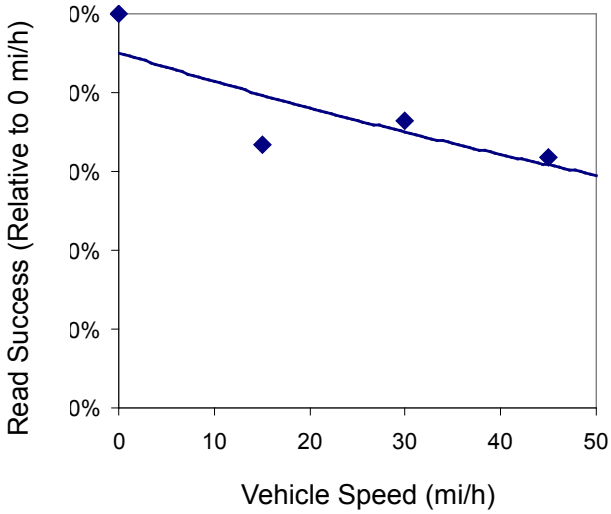

1 mi/h = 1.6 km/h

Figure 41. Graph. Influence of vehicle speed on read success rate.

CONCLUSIONS

Field trials at several projects confirmed the very high survival rate of the encapsulated tags. Read success rates varied significantly with tag size and less significantly on other details such antenna configuration and vehicle speed. Nonetheless, the field trials consistently demonstrated that post-construction read success rates of 60 to 80 percent or higher are achievable from a bumper-mounted antenna array, even on a vehicle moving at traffic speeds. A major secondary advantage of the approach is its minimal intrusion in the usual paving construction sequence. The only potential drawback observed was the occasional surfacing of tags at the top of the compacted mat. All surfaced tags were aligned parallel to the mat surface; no tags were observed in an upright orientation protruding above the mat in any of the trials.

CHAPTER 4: EVALUATION OF SURFACED TAGS

INTRODUCTION

During field trials for tracking HMA placement described in chapter 3, a small number of the RFID tags rose to the surface of the compacted pavement. This raised the question of whether this would compromise the durability of the pavement by increasing water infiltration or decreasing density locally.

The in-place permeability and density in the local area surrounding surfaced RFID tags were measured to answer this question. The assumption in this evaluation is that if the permeability and density of the pavement around the surfaced tags are similar to that in other areas, it can be assumed that the surfaced tags will not compromise the integrity of the pavement. All of the density and permeability tests were conducted in the UMD Parking Lot EE, where multiple tags surfaced in the 2-inch (50-mm)-thick lift of 0.5-inch (12.5-mm) surface mix (see figure 42).

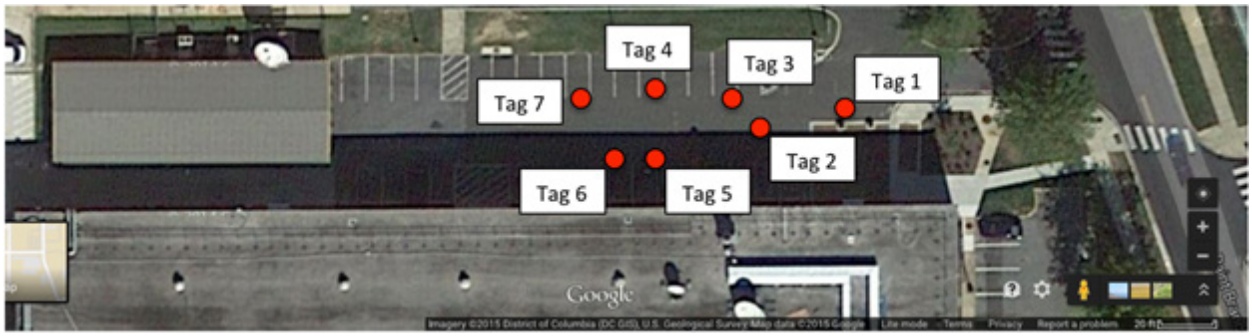

Original image: ©2015 Google®; map annotations provided by University of Maryland

Figure 42. Photo. Location of permeability and density tests at parking Lot EE at UMD.[7]

DENSITY TESTING

Methodology

In-place density measurements were obtained using the Troxler® Model 3440 nuclear density gauge shown in figure 43. Dr. Nelson Gibson and Mr. Dennis Sixbey of the Federal Highway Administration (FHWA) Turner-Fairbank Highway Research Center (TFHRC) provided the nuclear density gauge and performed the readings at the UMD campus. Mr. Sixbey is a certified nuclear gauge technician as well as the Radiation Safety Officer at the TFHRC. Testing was conducted on July 29, 2009, under generally clear weather conditions.

All nuclear density measurements were conducted in the backscatter mode. It was not possible to calibrate the nuclear gauge because the mix properties were unknown. As a consequence, the absolute density measurements would not be accurate. However, because the main focus of these tests is the relative density near the surfaced tag relative to the density at some distance away, an accurate absolute density reading is not necessary. Two readings were recorded on top of each tag, and 4 additional readings were recorded at distances of approximately 5 inches (125 mm), 9 inches (225 mm), and 16 inches (400 mm) away from the tag (see pattern in figure 44) for a total of 98 readings. Another eight readings were taken at random locations remote from any of

the tags. All density measurements were based on 1-min readings. Care was taken to ensure that no vehicles, people, or other potential sources of interference were near the nuclear gauge during the readings. Some of the readings may have suffered some indeterminable loss of accuracy when the roughness of the asphalt surface made it difficult to completely stabilize the device.

Figure 43. Photo. Troxler® Model 3440 nuclear density gauge.

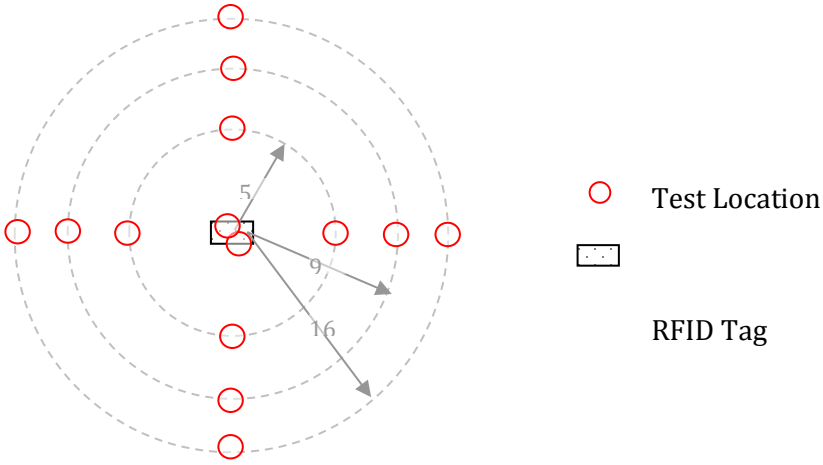

Figure 44. Diagram. Location of tests relative to tag.

Density Results

Figure 45 through figure 51 summarize the full set of density readings taken on top of and around each tag. These graphs also indicate which readings might be compromised because of irregularities in the pavement surface.

A linear regression analysis of density versus distance from the surfaced tag was performed for each set of test results. The results are shown as the trend lines in figure 45 through figure 51. The regression line was fit to the entire density data at each distance. However, the slopes of density trends versus distance are the key indicator of interest. The slopes ranged from a minimum of 0.03 for Tag 6 (i.e., essentially no variation of density with distance) to a maximum of 0.18 for tag 3 (i.e., modest variation of density with distance).

There are two reasons to suspect that the measurements directly on top of the tags (i.e., radial distance r equal to 0) may be biased: 1) the tags themselves have lower density than the HMA, so even if the HMA were completely uniform surrounding the tag, the measurements directly on the tag would indicate a lower density for the zone; and 2) the surface irregularities directly surrounding the tag made it more difficult to place the nuclear gauge in a stable configuration directly on top of the tags than in locations away from the tags. To investigate this potential bias, the regression analyses were rerun with the points at r = 0 removed. The slopes for the trend lines with the r = 0 data retained and with the r = 0 data removed are compared in table 9. It is clear that removing the data at r=0 significantly reduces the slope of the density versus distance trend, with some tags now even showing a decrease in density with increasing distance (i.e., tags 5 and 7). The average slope of the trend lines across all tags drops from 0.09 when the r = 0 data are retained to 0.03 when the r = 0 data are removed. In either case, these small slope values suggest very little impact of the tags on in-place density.

As a further check, *t*- and *F*-tests were conducted to determine whether there were any statistically significant differences in density at different distances from the tags. These tests compare the means (*t*-test) and variances (*F*-test) of two groups of data.

Data for all tags were combined for the purposes of performing the *t*- and *F*-tests. To compensate for normal spatial variability of in-place density, the measured density at each location for a given tag was normalized by the average of all density readings for that tag. Any remaining spatial variability after this normalization can then be attributed to distance from the tag. The *t*- and *F*-tests were conducted in pairs of datasets: r = 0 (i.e., on top of the tag) and r = 5 inches (125 mm); r = 0 and r = 9 inches (225 mm); r = 0 and r = 16 inches (400 mm); and r = 16 inches (400 mm) and random far-field readings. The results of the *t*- and *F*-tests are shown in table 10. The t_{crit} and F_{crit} values in the table are for a significance level α =0.01. In all but one case, both the *t*- and *F*-test statistics are smaller than the critical values, indicating that the differences in the means and variances respectively of the two datasets in each pair are not statistically significant. The only exception is the 0 versus 125 mm (5 inches) pair, where the *F*-test is satisfied but the *t* value slightly exceeds t_{crit}. The overall conclusion is that there is very little statistical difference between the density measurements at the various locations from the tag.

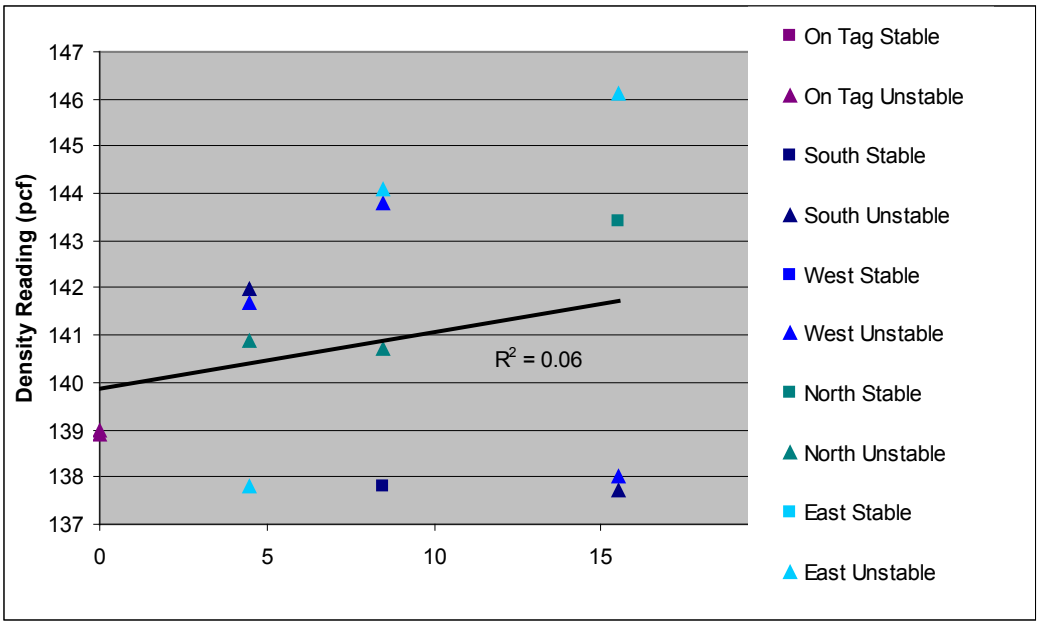

pcf = pounds per cubic ft
1 inch = 25.4 mm

Figure 45. Graph. Density as a function of radial distance for tag 1 (slope=0.12).

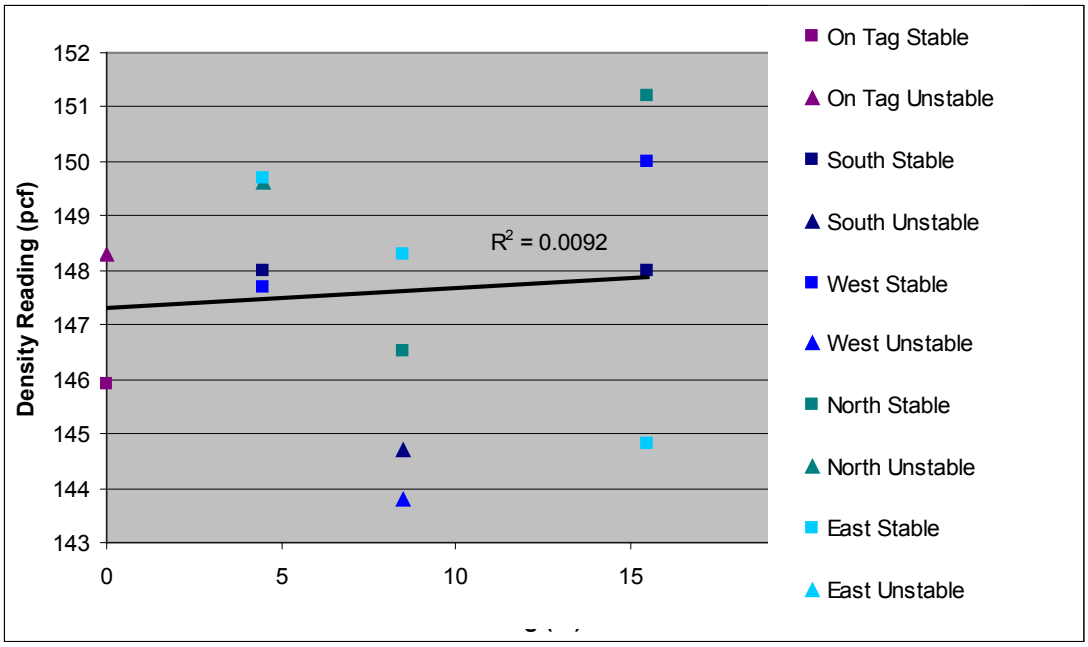

pcf = pounds per cubic ft
1 inch = 25.4 mm

Figure 46. Graph. Density as a function of radial distance for tag 2 (slope=0.04).

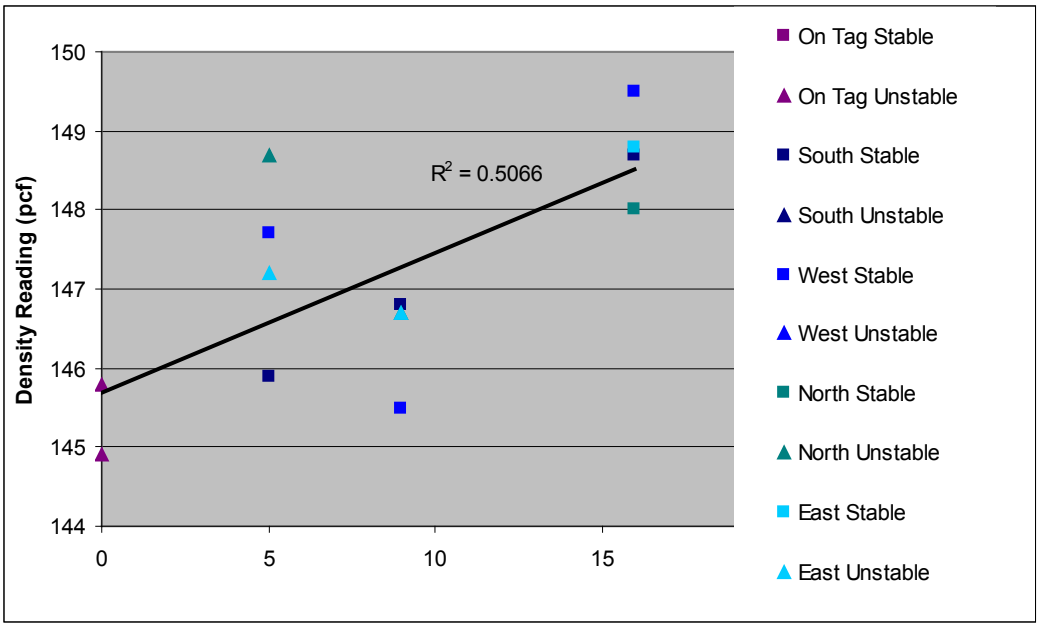

pcf = pounds per cubic ft
1 inch = 25.4 mm

Figure 47. Graph. Density as a function of radial distance for tag 3 (slope=0.18).

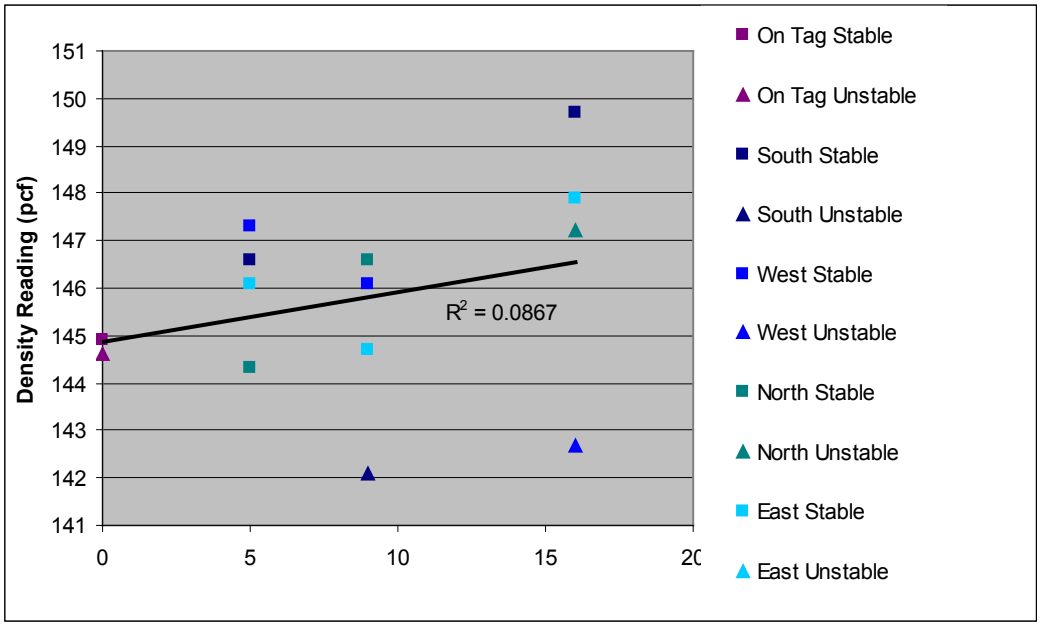

pcf = pounds per cubic ft
1 inch = 25.4 mm

Figure 48. Graph. Density as a function of radial distance for tag 4 (slope=0.11).

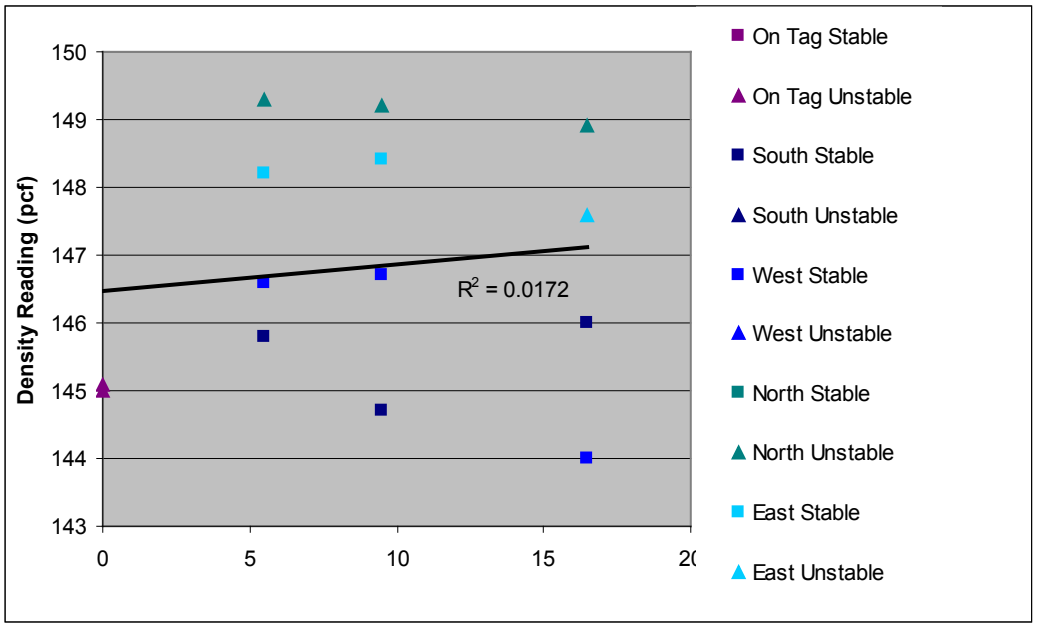

pcf = pounds per cubic ft
1 inch = 25.4 mm

Figure 49. Graph. Density as a function of radial distance for tag 5 (slope=0.04).

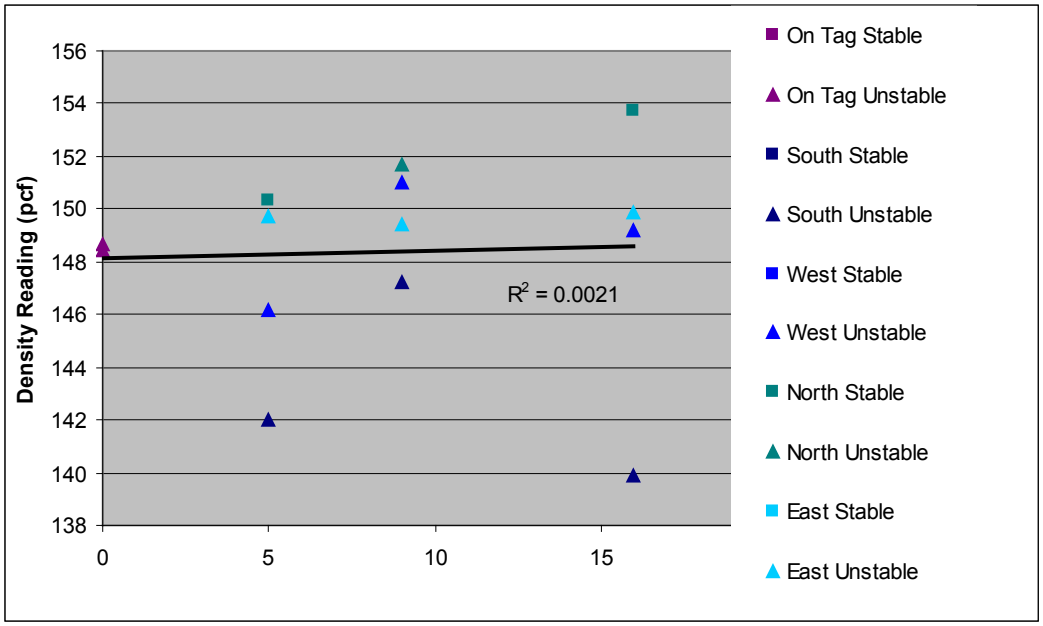

pcf = pounds per cubic ft
1 inch = 25.4 mm

Figure 50. Graph. Density as a function of radial distance for tag 6 (slope=0.03).

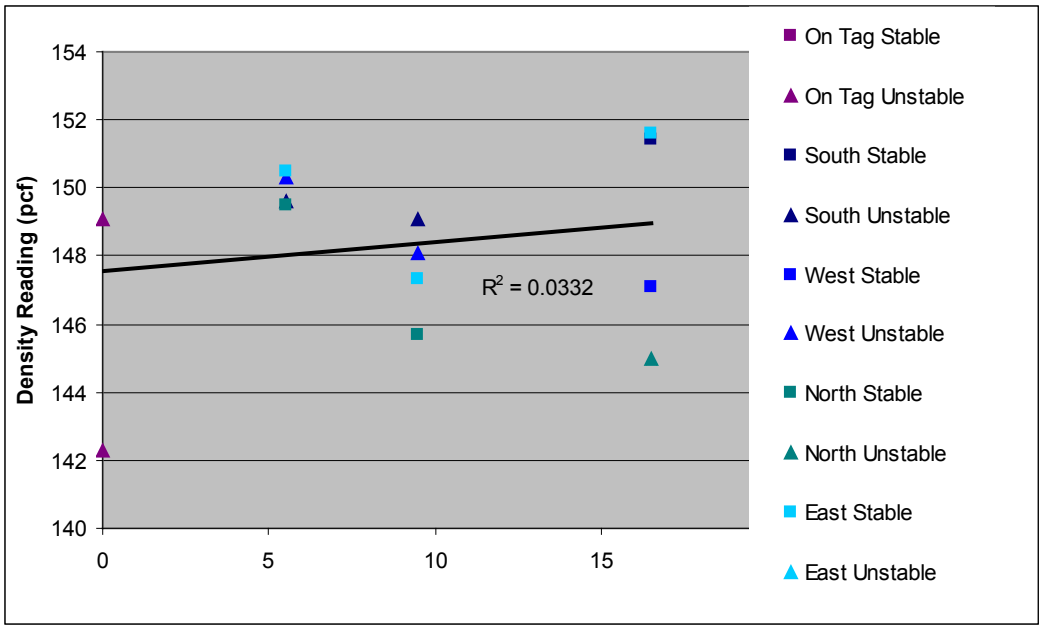

Pcf = pounds per cubic ft
1 inch = 25.4 mm

Figure 51. Graph. Density as a function of radial distance for tag 7 (slope=0.08).

Table 9. Slopes of in-place density versus distance trend lines with and without data at r = 0.

Tag	Slope	
	With r = 0 Data Points	Without r = 0 Data Points
1	0.12	0.05
2	0.04	0.02
3	0.18	0.15
4	0.11	0.10
5	0.04	-0.08
6	0.03	0.06
7	0.08	-0.08
Average	0.09	0.03

r = radial distance

Table 10. The *t*- and *F*-test results for in-place density tests.

Combination	t	t_{crit}	F	F_{crit}
0 versus 5 inches	2.833	2.704	1.265	4.06
0 versus 9 inches	1.741	2.704	1.538	4.06
0 versus 16 inches	2.173	2.704	3.417	4.06
16 inches versus far field	0.465	2.727	1.049	3.86

1 inch = 25.4 mm

Conclusions Regarding In-Place Density

The linear regression analyses of density versus distance at each tag produced very small slope and R^2 values in nearly all cases. These both imply little or no relationship between density and distance from the RFID tag. In other words, there do not appear to be any localized variations in in-place density caused by the RFID tags.

The t-tests of the pooled in-place density measurements for all distance combinations except the 0 versus 5 inches (125 mm) case found that any differences in the means were not statistically significant. Even for the 0 versus 5 inches (125 mm) case, the *t*-statistic exceeded the t_{crit} value at the 0.01 significance level by only a very small margin. The *F* values were smaller than F_{crit} for all distance combinations, indicating that any differences in variance are not statistically significant. As with the linear regression results, the *t*- and *F*-test results suggest that there are no localized variations in in-place density caused by the RFID tags.

PERMEABILITY TESTING

Methodology

In-place permeability tests were conducted on each of the seven surfaced tags using an National Center for Asphalt Technology (NCAT) (Auburn University) field permeameter. The device is centered over the tag and measures the permeability over a diameter of approximately 5.75 inches (145 mm). Seven additional tests were conducted at random locations in the parking lot far from any tags.

The procedure used to conduct the in-situ permeability tests followed the test protocol developed by NCAT.[8] As shown in figure 52, the permeameter consists of four tiers of different diameter cylinders separated in two sections. The sealant used for these tests was plumber's putty. A small 1 ft (0.3 m) square area was identified and brushed clear of debris. A thin layer of the moldable sealant was applied to the rubber gasket on the base plate of the permeameter. Next, a uniform 0.5-inch (12.5-mm)-thick layer of moldable sealant is applied approximately 3 inches (76.2 mm) around the outside diameter on the base plate. Some sealant was reused in other tests after slicing off the top part contaminated by debris. The permeameter is carefully placed on the asphalt test area so that the rubber gasket surrounds the outside diameter of the base plate. Uniform foot pressure is then applied around the perimeter of the base to create a watertight seal with the asphalt.

Many tests were redone because of concern that water observed outside the test area was a leak in the sealant rather than lateral drainage through the HMA. It was sometimes difficult to create a watertight seal because the pavement was uneven. In an effort to improve the seal, four 5-lbf (22.25 N) weights were distributed on the base plate to compensate for the head pressure from the water column. Extra weight was exerted by placing four bricks on the base plate as shown in figure 52.

A thin layer of sealant was used to connect the two sections of the permeameter. The filling tube assembly was inserted all the way to the bottom, and water was added at a steady rate while minimizing bubbles. Water was added until it filled a tier that made it possible for accurate

observation of head drop. The time required for the water to drop a given distance in the selected tier was recorded.

Figure 52. Photo. In-place permeability test setup.

Using the measured time and distance for the water drop, the coefficient of permeability was calculated using the falling head permeability equation shown in figure 53:

$$k = \frac{aL}{At} \ln\left(\frac{h_1}{h_2}\right)$$

Figure 53. Equation. Permeability determination from falling head permeability test.

where:

k = coefficient of permeability.
a = inside area of standpipe (depends on tier used for testing).
L = thickness of asphalt mat.
A = area of permeameter base through which water can flow into the pavement.
h_1 = initial head.
h_2 = final head.
t = elapsed time between h_1 and h_2.

Permeability Results

Figure 54 summarizes the results of the 14 permeability tests, which consisted of 7 tests on top of the surfaced RFID tags and 7 random readings far from the tags. Only the reading on top of tag 1 showed a more permeable surface compared with all the other readings. This could be caused by segregation because larger size aggregates were observed on the surface at this location only. Excluding this tag, the readings on top of the RFID tags ranged from 4.92×10^{-5} to 41.6×10^{-5}

inches/s (12.5×10^{-5} to 105.6×10^{-5} cm/s), which is very similar to the random far-field readings, which ranged from 4.76×10^{-5} to 36.8×10^{-5} inches/s (12.1×10^{-5} to 93.4×10^{-5} cm/s). Statistical *t*- and *F*-tests were performed to see whether there was any significant difference between the means and standard deviations of these two sets of data. The *t*-test gave a value of $t=0.00813$ with $t_{crit}=3.055$ at a significance level $\alpha=0.01$. The *F*-test gave a value of $F=6.87$ and $F_{crit}=8.89$. In both cases, the test statistics were less than the critical values, implying no statistically significant differences in the means and variances for the in-place permeability values on top of the RFID tags versus values at random far-field locations.

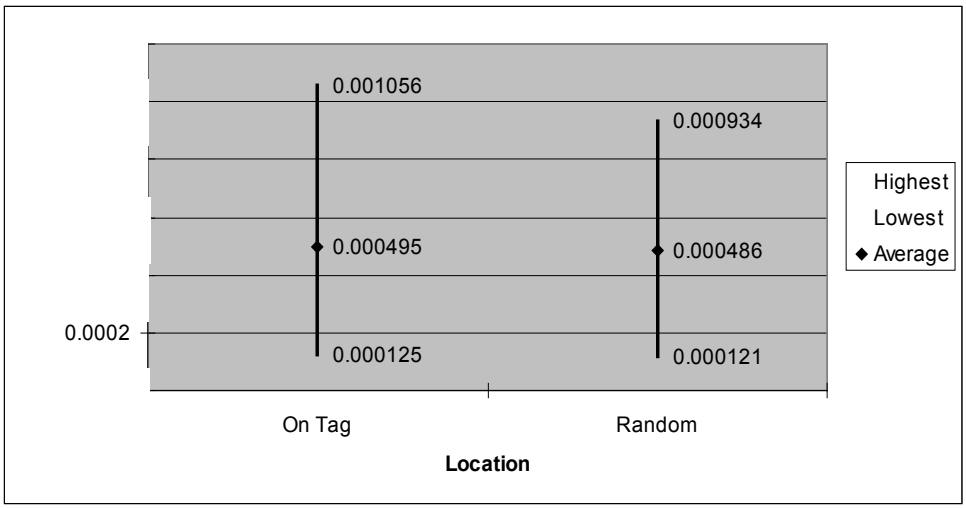

1 inch/s = 25.4 mm/s

Figure 54. Chart. Coefficient of permeability on top of the tags and at random locations.

Conclusions Regarding In-Place Permeability

Based on the very similar ranges in measured permeabilities and the results from the *t*- and *F*-tests, it is concluded that there is no detrimental effect of the surfaced RFID tags on in-place permeability for the HMA.

OVERALL CONCLUSIONS REGARDING SURFACED TAGS

The test results show that there are no practical or statistical impacts on in-place density or permeability from the surfaced RFID tags. Consequently, the tags should not be causes of local damage due to reduced stiffness/strength (correlated with density) or water inflows (related to permeability). Other than aesthetic concerns, the surfaced RFID tags do not appear to have a detrimental effect on asphalt pavements.

There is the possibility for long-term deterioration around the tags due to degradation of the bonds between the asphalt binder and the CPVC pipe encapsulation. However, qualitative observations of the surfaced tags in Lot EE at the time of this writing show no evidence of deterioration over the intervening 6 years.

CHAPTER 5: RFID TRACKING OF PCC PLACEMENT

INTRODUCTION

To ensure and ideally to improve the performance of concrete pavements, it is vital that the influence of material properties on performance be clearly understood. Correlations between as-constructed properties of PCC in construction databases and field performance in PMSs can quantify the link between material quality and pavement performance.

PCC is produced at a production facility and then trucked to the highway construction site for offloading. As part of an overall QA program, PCC producers sample their production periodically from delivery trucks as they leave the plant to perform various quality control (QC) tests to ensure that the mixture properties remain within acceptable limits. Agencies typically take additional samples for quality acceptance testing to corroborate the producer's QC test results and to establish pay factors.

Knowledge of where the sampled truckload of material is deposited along the roadway is critical when attempting to correlate as-constructed material properties with measured performance from a PMS because pavement management data are typically referenced to a specific spatial location (milepoint, latitude/longitude). Unless the PCC QA data can also be tied to a spatial location along the pavement, they cannot be correlated accurately with pavement management data.

Similar to the HMA tracking application considered in chapters 2 through 4, sensors based on RFID technology could be used to tag truckloads of PCC as they left the production plant. The sensors would be cast into the slab during the concrete paving operation. After construction, a vehicle-mounted scanner would be used to electronically "read" the identity tags to link them to the material properties measured from samples obtained from the truck that brought the concrete to that location. The data could then be directly linked to future pavement performance data in the agency's PMS, enabling robust statistical analyses of the correlations between material properties and actual performance.

LABORATORY EVALUATION

A preliminary laboratory evaluation of read range was conducted by embedding conventional UHF passive RFID tags in 4-inch (100-mm) diameter by 12-inch (300-mm)-high concrete cylinders. Alien® Gen 2 2x2 and Alien® Gen 2 1x1 tags were encapsulated using the same techniques as for the HMA tracking tags and then embedded in the middle of the cylinders in an upright position. Two replicates of each tag type were embedded in a one tag per cylinder basis. After the tags were embedded, read ranges were measured periodically as the cylinders were curing. All readings were conducted using a Mercury® 5 ThingMagic reader. No relationship between the curing of the cylinders and the read range of the RFID tags was observed. To determine the orientation effect on the readings, the read range was recorded for the cylinders in vertical and horizontal positions relative to the antennae. The results are shown in table 11 and table 12 for readings taken at 20-s intervals after 13 days of curing. The best read range results obtained when the RFID tags where in front of the transmit side of the antenna are given.

Table 11. Read range for vertically positioned cylinders.

Size	Maximum Distance	Number of Readings
2x2	3 ft	12
2x2	4 ft	2
1x1	1 ft	5
1x1	1.5 ft	8

1 ft = 0.305 m

Table 12. Read range for horizontally positioned cylinders.

Size	Maximum Distance	Number of Readings
2x2	5 ft	26
2x2	1 ft	215
1x1	1 ft	5
1x1	0	0

1 ft = 0.305 m

Based on these results, it can be seen that the larger format 2x2 tags have much longer read ranges through concrete compared with the smaller format 1x1 tags. Orientation is also a very important factor in the consistency of the readings. The read range for the second replicate of the 2x2 tags in the horizontal position was only 1 ft (0.3 m). Because the orientation of the tags in the field is purely random, it should be anticipated that some of the tags could end up in the worst orientation and may not be readable; this appears to be what happened for one of the 1x1 tags. Nonetheless, these preliminary results show the potential of this application in PCC tracking.

FIELD EVALUATION

The concept of PCC tracking was evaluated in the field in conjunction with the reconstruction of a section of the New York State Thruway I-90 outside Syracuse, NY. The Syracuse Project was located between exits 39 and 40 on I-90 as shown in figure 55. Three different types of tags were studied: Alien® Gen 2 Higgs® 2 2x2, Alien® Gen 2 1x1, and Gen 2 Titan™ tags. A total of 80 tags were used in this project, with seven Alien® 2x2, seven Alien® 1x1, and six Titan™ tags in each truck.

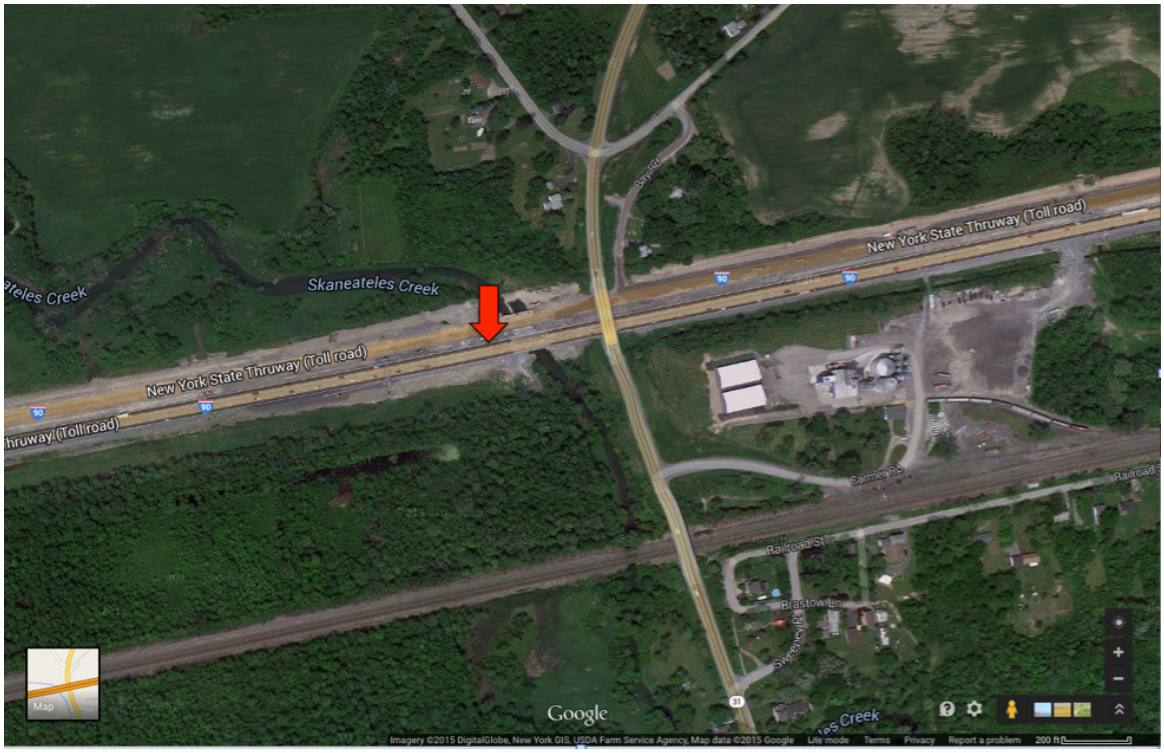

Original image: ©2015 Google®; map annotations provided by University of Maryland

Figure 55. Photo. Location on the Syracuse project where the RFID tags were embedded.[9]

Methodology

The Syracuse field trial was performed in two steps. The first was the embedment of the RFID tags in the concrete pavement, which took place on October 8, 2009. Four sets of tags, each consisting of three different types of tag, were used for this project. The Alien® Gen 2 Higgs® 2 2x2 and 1x1 tags were pre-encapsulated in CPVC pipes with high-temperature epoxy following the procedure explained in chapter 2. The tags were curled inside of the CPVC pipes in an effort to keep the final product in the size and shape of an aggregate, thus maintaining the integrity of the concrete. The Titan™ tags were already encapsulated by the manufacturer to endure high humidity and pressure.

The first three sets of tags, each including seven Alien® Gen 2 2x2 tags, seven Alien® Gen 2 1x1 tags, and six Gen 2 Titan™ tags, were sown in three consecutive trucks as they were being loaded with concrete at the plant. These were the last trucks to unload before a bridge deck. After unloading, the tags in the concrete mix went through the slip form paver and were finished into the 13-inch (325-mm) slab. Some concern was raised about whether the concrete unloaded from these three trucks would be cut and replaced with manually finished concrete next to the bridge deck because bridge obstacles might interfere with the progress of the slip form paver. However, it was later confirmed that there was no slip form concrete removed from in front of the bridge. The fourth set of tags was sown in the sixth truck after the bridge. The finished pavement with the tags embedded is shown in figure 56.

The second step was to read the embedded tags after the concrete had cured for 24 days. Two antennae were connected to the reader and mounted on the outside of a cargo van at a height of approximately 6 inches (150 mm) from the pavement, as shown in figure 57. The antennae each contain a receive side and a transmit side. In the laboratory evaluation, the best readings were received when the tags were in front of the transmit side of the antenna. Therefore, the most efficient way to cover the pavement area was to position the antenna sequence across the width as T/Transmit-R/Receive-T/R. Overlapping passes at very low speeds were performed to cover the entire width of the pavement. The overlapping passes were repeated three times. The pavement area was also manually checked for tags by moving the antennae by hand over the pavement surface.

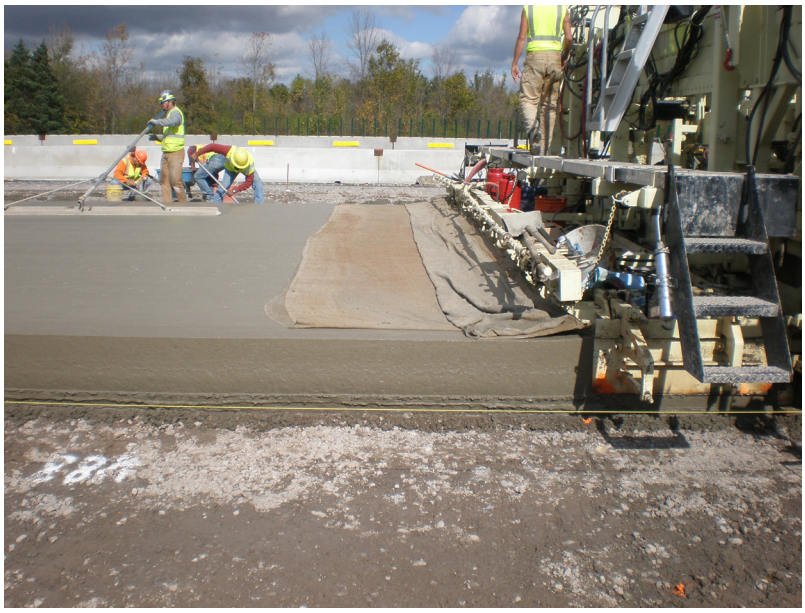

Figure 56. Photo. Finished concrete pavement.

Figure 57. Photo. Antenna configuration.

Field Test Results

None of the embedded tags were read in any of the passes. This was not unexpected for the Alien® Gen 2 1x1 tags because as shown in table 11 and table 12, their read range was much lower than that of the Alien® 2x2 tags. However, the inability to read any of the Alien® Gen 2 2x2 or the Titan™ tags was a surprise. The Titan™ tags could be read up to approximately 6 ft (1.8 m) in air.

It is unlikely that the failure to read any tags was due to equipment malfunction. The reader was checked and worked in the laboratory immediately before and after the test, and it passed all diagnostics in the field on the day of the test. The possibility that all of the tags ended up in the bottom of the 13-inch (325-mm) slab and could not be read because of severe attenuation was also highly unlikely.

The inability to read any of the tags in the field was particularly surprising because RFID tags have been used successfully in tracking precast concrete. Trackcon®, a division of International Coding Technologies (ICT), uses passive UHF tags to track precast concrete components. The tags are UPM Raflatac® Dogbone tags incorporating the Monza® 3 chip, the newest chip at the time from Impinj®, Inc. They are molded into the surface of precast concrete components. Trackcon® has also tried to embed them in concrete, and according to Tom Tilson, CEO of ICT, the tags can be read through 6 inches (150 mm) of concrete and sporadically even through 12 inches (300 mm) of concrete. However, for these tags to be read, the 9090 Motorola® handheld reader had to be no farther than 3 to 4 inches (75 to 100 mm) away from the tag. Falken Secure Networks, Inc. markets another commercial system for tracking precast concrete components using RFID. Company representatives confirm reading through precast concrete of thicknesses of 6 to 8 inches (150 to 200 mm) using the latest generation tags such as Alien® Higgs® 3 or UPM Raflatac® Dogbone Monza® 3 with the 9090 Motorola® handheld reader.

The following are two possible reasons that these two companies were able to read tags through concrete but the current study could not:

- The two companies used tags incorporating the newest chips available such Monza® 3 and Higgs® 3.

- The tags they used are encapsulated flat instead of curled as the ones used for PCC tracking in this study were.

Even though ICT was able to read some tags through concrete, the company is not pursuing the idea of inserting passive tags in concrete because it has concluded that the read ranges and read success are not good enough for successful application. ICT continues to place RFID tags only on the surface of precast components.

Because these puzzling insights from similar applications were inconclusive, further investigations were conducted to determine why the tags in the present study could be read satisfactorily through HMA but not at all through PCC.

FURTHER INVESTIGATIONS

Laboratory Evaluation

Encapsulated RFID tags were embedded in a concrete block in the laboratory to simulate conditions in the field. Only the Alien® Gen 2 2x2 tags were used for the laboratory evaluation because they had the best read range in air. An 8-ft^3 (0.23-m^3) wooden box was built for the laboratory evaluation.

Because coarse aggregate is the largest component of concrete and often has a high dielectric constant, 12 tags were first placed in known positions inside the box as it was filled with coarse aggregate. The coarse aggregate was a limestone from the Millville quarry in West Virginia. This aggregate had an estimated dielectric constant of 7 (dry) or 8 (wet).[10] The RFID tags were placed in three layers as shown in figure 58 through figure 61. The box was then read with the antenna positioned at the mid-height of the box at distances of 1 and 2 ft (0.3 and 0.6 m) away from the box. The antenna was positioned horizontally with the transmitter on the right side. Readings were taken with the middle of the antenna located between 24 inches (600 mm) to the left of the box and 24 inches (600 mm) to the right in 4-inch (100-mm) intervals for all four sides. All the read ranges were conducted in the laboratory, so there was the inevitable random interference due to metal objects.

Because the box is symmetrical, the readings on each side should have theoretically been identical. However, owing to interferences and possible inconsistencies when placing the tags in the box, there were slight variations in the readings from one side to the other.

The number of tags read at each offset averaged for each side is shown in figure 62. It can be seen that the number of tags read is skewed, with more tags being read on the left side of the box (negative values for distance). From previous read range studies, it was known that the RFID tags read best if they are closer to or in front of the T (transmit) side of the antenna. Because the T side of the antenna was on the right, increasing the offset on the right side increased the distance from the T side to the tags, which explains the skewed readings.

Another important fact is that, although the antenna was placed only 1 or 2 ft (0.3 or 0.6 m) away from the box, that is not the actual antenna-to-tag distance. The distance to the tags also included an extra 4 to 20 inches (100 to 500 mm) of coarse aggregate based on their position inside the box.

The maximum distance at which any of the tags was read was generally on the order of 6 ft (1.8 m).

Figure 58. Photo. Tags located 8 inches (200 mm) from the bottom and 4 inches (100 mm) from the sides.

Figure 59. Photo. Tags located 12 inches (300 mm) from the bottom and 12 inches (300 mm) from the sides.

Figure 60. Photo. Tags located 8 inches (200 mm) from the top and 8 inches (200 mm) from the sides.

Figure 61. Photo. Box filled with aggregate and 12 RFID tags.

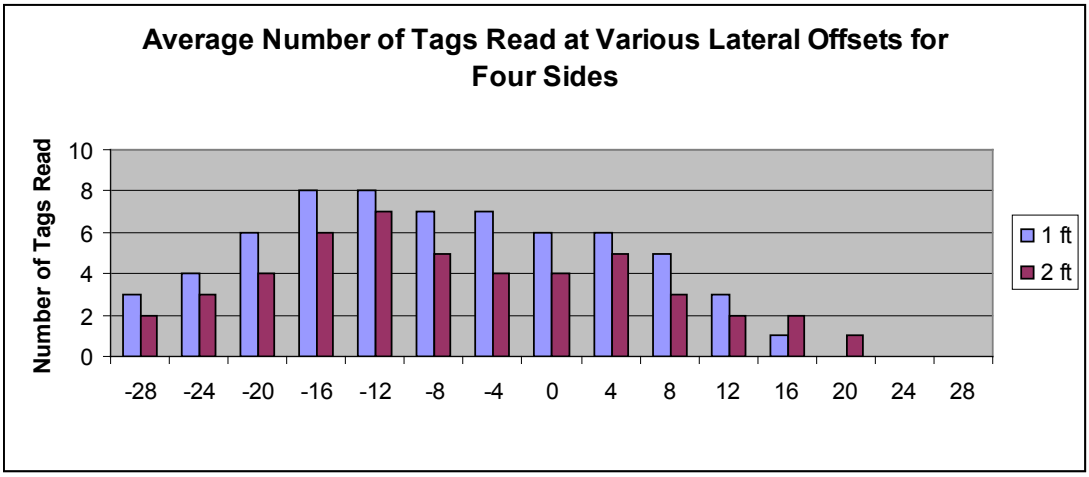

1 ft = 0.305 m
1 inch = 25.4 mm

Figure 62. Chart. Average read range of four sides of the box for the RFID tags embedded in coarse aggregate.

Next, the same tags were placed in the same locations as in the aggregate tests as the box was filled with concrete. None of the tags could be read after encapsulation in concrete, even after the concrete had cured for 1 month. To check the survivability of the tags, they were extracted from the concrete block via demolition. The tags could be read after extraction, so survivability was not the issue.

Additional tests were performed in an effort to determine the reason these passive RFID tags could not be read through concrete. Because the tags could be read through the coarse aggregate, the next logical step was to determine whether the moisture present in the concrete attenuated the electromagnetic waves enough so that the chip could not be activated. The dielectric constant of water is about 80, which makes it one of the most difficult media for the electromagnetic waves to penetrate.

A 32 gal (121 L) plastic bucket was filled with sand at about 9.5-percent water content, which was similar to the water content for the concrete mixture. Sixteen tags were embedded at various depths in the sand at a maximum of 7 inches (175 mm) in from the sides of the bucket. All of these tags were read successfully from at least 2 ft (0.6 m) away. This finding shows that moisture by itself is not the reason there were no readings through concrete.

As a final test, six tags were embedded at three different depths in a 5-gal (19 L) plastic bucket of cement paste prepared at a water-to-cement (w/c) ratio of 0.4. The tags closest to the surface were embedded only to about 3.5 to 4 inches (87 to 100 mm). None of these tags could be read even after 12 days of hydration. These findings clearly indicated that the cement paste was the reason for the unsuccessful readings through concrete.

The Dielectric Constant of Cement Paste

Using mixture theory, the dielectric constant of concrete is approximately 11, which alone would not account for the poor read performance. Therefore, in an effort to determine the reasons that

the RFID tags could not be read through the cement paste and ultimately through the concrete block, a thorough literature review was performed on the dielectric constant of cement.

Zhang et al. used a microwave technique to determine the dielectric constant of cement pastes with different w/c ratios at frequencies between 8.2 and 12.4 GHz for up to 30 hours of hydration.[11] The w/c ratio of 0.4 is the closest to the one used in the present study. Because attempts to read the tags embedded in the concrete block were made after 1 month of hydration—i.e., after most of the water was hydrated—the dielectric constant of interest from Zhang et al.'s study was the latest one after 30 hours of hydration. Zhang et al.'s measured dielectric constant for the cement paste was about 20 at 8.5 GHz, which is the closest frequency to the 915 MHz UHF frequency used in the present study. Other results by Zhang et al. show that the dielectric constant increases as frequency decreases, which means that the dielectric constant will be greater than 20 for frequencies close to 1 GHz.

Wen and Chung examined the dielectric constant of cement pastes with different admixtures.[12] Table 13 summarizes their key results. The first row gives the dielectric constant of Portland cement mixed only with water, which is the value of interest for the present study. At 1 MHz, this value is 23.7±2.8. For frequencies of about 1 GHz, the dielectric constant would be slightly lower, approaching perhaps 20.

From these two papers, it is seen that the dielectric constant of cement is much higher than that of the coarse aggregate and coarse aggregate and water as estimated using mixture theory. Although the coarse aggregate is the main component of concrete, the cement paste covers all of the aggregate. The electromagnetic waves coming from the antenna must first go through the cement paste, which could strongly attenuate the signal due to its high dielectric constant. After that, the electromagnetic waves experience still more attenuation from the aggregate, making it hard for the signal to reach the RFID tags and power the chip.

Table 13. Dielectric constants for various cement pastes (after Wen and Chung[12]).

Fiber Type	Fiber Content		Admixture	Relative Dielectric Constant		
	Percentage by Mass of Cement	Percentage by Volume		10 KHz	100 KHz	1 MHz
—	0	0	—	28.6 ± 3.4	24.8 ± 3.6	23.7 ± 2.8
—	0	0	SF	20.8 ± 3.4	19.6 ± 3.2	16.5 ± 0.8
—	0	0	L	34.9 ± 4.5	31.5 ± 2.9	24.3 ± 2.9
Carbon	0.5	0.48	SF	53.7 ± 7.0	38.3 ± 4.8	28.1 ± 2.9
Carbon	0.5	0.41	L	63.2 ± 5.2	40.4 ± 5.9	33.2 ± 6.8
Carbon	1.0	0.95	SF	48.7 ± 4.8	29.6 ± 5.0	25.0 ± 5.0
Steel	0.5	0.10	—	19.6 ± 4.8	19.0 ± 1.0	13.7 ± 2.4

— Not applicable
Admixtures: L = Lime, SF = Slag Flyash
KHz = kilohertz
MHz = megahertz

CONCLUSIONS REGARDING PCC TRACKING

Preliminary laboratory evaluation of concrete cylinders suggested that the Alien® Gen 2 2x2 tags could be read through about 2 inches (50 mm) of concrete at a distance of up to 5 ft (1.5 m). Although this suggests that PCC tracking should therefore be successful, negative results were obtained during the Syracuse project field trials. None of the encapsulated RFID tags embedded in the concrete pavement were read even after 24 days of concrete curing.

In an effort to determine the reason for this failure, an extensive laboratory evaluation was conducted. Twelve encapsulated RFID tags were embedded in three layers in an 8-ft^3 (0.23-m^3) box filled with coarse aggregate. These tags were all successfully read as the antenna was moved around all sides of the box. This suggests that attenuation of the radio signals by the coarse aggregate, the main component of concrete, is not the reason the tags could not be read in the field.

Next, the same configuration as for the aggregate box was applied to the box filled with concrete. None of the tags could read after 1 month of curing, even though four tags were embedded only 4 inches from the box side. All tags could be successfully read when extracted after demolition of the concrete box.

The next test consisted of inserting 16 tags in a bucket filled with sand and water. All of the tags could be read from at least 2 ft (0.6 m) away. Finally, six RFID tags were embedded at different depths in a 5-gal (19-L) bucket of cement paste. None of the tags could be read even after 12 days of hydration. This indicates that the cement paste, which has a dielectric constant of about 20, is the main factor attenuating the electromagnetic waves in the concrete.

In light of these results, it can be said that passive RFID tags, although successful in tracking HMA, are not suitable for tracking PCC. Active tags, with their much higher transmitting power, could possibly work for this application; however, because they are needed in large quantities, their high price would make them unsuitable for the PCC tracking application.

CHAPTER 6: PAVEMENT TEMPERATURE MEASUREMENT USING SAW RFID

INTRODUCTION

There have been efforts since the late 1960s to model HMA temperatures as a function of time as an aid to optimizing compaction. Compaction is a densification process in which the air voids in an HMA mixture are reduced by the application of mechanical energy, commonly via a vibratory steel-drum roller. It is widely recognized that compaction is a critical factor in flexible pavement performance. Achieving optimal compaction for any particular mix depends primarily on temperature (for a given asphalt viscosity) and compactive effort. Inadequate compaction may result in reduced pavement stiffness, fatigue life, and durability.

Temperature versus time during compaction is especially important when using state-of-the-art intelligent compaction techniques. One of the principal advantages of intelligent compaction is the estimated stiffness of the compacted material as determined from the feedback sensors on the vibrating drum. The stiffness of HMA (and also warm mix asphalt) is extremely dependent on temperature. Analysis of the feedback data from the sensors on the intelligent compactor thus requires knowledge of the temperature distributions with depth and time in the cooling mat. The conventional infrared temperature measurements taken during compaction measure only the temperature at the surface—the coolest location in the mat—and may be biased by the water sprayed on the rollers. A technique for measuring temperature throughout the mat thickness in real time has potential for improving the effectiveness of intelligent compaction for asphalt concrete.

The specific objectives of the investigations reported in this chapter are as follows:

1. Evaluate the feasibility of using SAW-based RFID technology to measure HMA temperatures versus depth and time via wireless sensors.

2. Demonstrate, both in the laboratory and the field, the survivability and temperature measurement capabilities of the SAW RFID sensors.

3. Perform analyses of the measured field data to develop asphalt cooling curves (temperature versus time) and compare these results with analytical mat cooling models. The coupling of some limited field measurement data with analytical models leverages the value of the sensor data.

4. Perform a sensitivity analysis on the input parameters for the traditional mat cooling models and calibrate, via the sensitivity analysis, input parameters that provide reasonable and close agreement with the measured temperatures from the field.

This work was performed in conjunction with the FHWA Pooled Fund Study on Intelligent Compaction and specifically with an intelligent compaction demonstration project conducted in Maryland.[13]

PREVIOUS WORK

A literature review of all previous work related to the development mat cooling models was performed. Although numerous journal articles and technical reports were reviewed, only the most relevant to the present study are discussed here.

Heat Flow Formulations

Corlew and Dickson pioneered methods for predicting HMA temperatures as a function of time from when the asphalt leaves the paver to the end of compaction.[14] Their mat cooling model is based on the principles of one-dimensional transient heat flow as illustrated in figure 63.

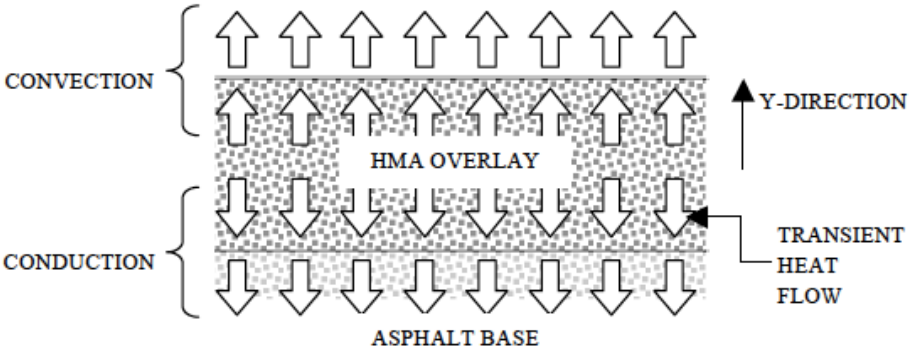

Figure 63. Drawing. Cross section of an HMA overlay indicating directional flow of thermal energy.

Transient heat flow is described by the partial differential equation (PDE) relating temperature T, time t, and depth y shown in figure 64.

$$\frac{\partial T}{\partial t} = \alpha \frac{\partial^2 T}{\partial y^2}$$

Figure 64. Equation. Differential equation for transient heat flow.

The parameter α in figure 64 is the thermal diffusivity—the ability of a material to conduct thermal energy compared with its ability to store thermal energy. The equation in figure 65 defines thermal diffusivity:

$$\alpha = \frac{k}{\rho C_p}$$

Figure 65. Equation. Definition of thermal diffusivity.

where:

k = thermal conductivity of the material.
ρ = material density.
C_p = specific heat capacity.

The units for thermal diffusivity are area per unit of time (e.g., ft^2/h).

Although Corlew and Dickson proposed an analytical solution to the equation in figure 64, they found that the interactions of the various modes of thermal energy transfer at the pavement surface were better modeled using numerical techniques.

Figure 66 illustrates the numerical solution scheme for the transient heat flow analysis. The pavement thickness is divided into sublayers (sections divided by isothermal lines) and the PDE in figure 64 is approximated using finite difference equations at the nodes located at the midpoints of each sublayer. As shown in figure 66, the nodes extend from the pavement surface boundary through the overlay and continue for some depth through the asphalt base to the lower boundary. The boundary conditions consist of a constant ambient air temperature (T_{Air}) above the surface of the overlay (depth location i=n) and a constant base temperature at the bottom of the analysis domain (i=1). The lower boundary is located at a sufficient depth where conduction no longer affects the temperature of the base material over the duration of the transient analysis—i.e., the bottom boundary condition is $T_{1j} = T_{Initial}$ for all time steps j.

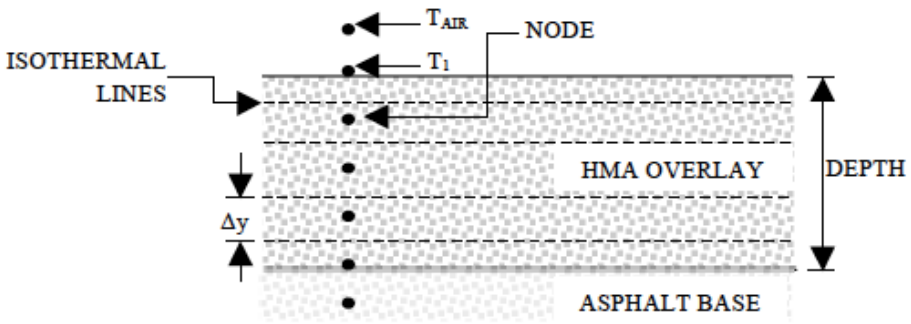

Figure 66. Drawing. Typical incremental elements of HMA overlay used in numerical solution.

Figure 67 expresses the finite difference approximation of the heat balance equation within the mat:

$$\frac{\partial T}{\partial t} = \alpha \frac{\partial^2 T}{\partial t^2} \Rightarrow \frac{T_{i,j+1} - T_{ij}}{\Delta t} = \alpha \left(\frac{T_{i+1.j} - 2T_{ij} + T_{i-1,j}}{\Delta y^2} \right)$$

Figure 67. Equation. Finite difference approximation to heat balance equation.

where:

i =2…n-1 = the node number in the interior.
T_{ij} = temperature (^oF) at node i and time j.

The equation in figure 68 solves for $T_{i,j+1}$.

$$T_{i,j+1} = \frac{\alpha \Delta t}{\Delta y^2}\left(T_{i+1,j} - 2T_{ij} + T_{i-1,j}\right) + T_{ij}$$

Figure 68. Equation. Equation for $T_{i,j+1}$.

These one-dimensional conduction equations are used to calculate temperatures within both the HMA overlay and the asphalt base. Corlew and Dickson point out that the thermal diffusivity might be different for the two materials. However, this difference is expected to be small for most asphalt mixtures. Therefore, the thermal diffusivity is assumed uniform for the overlay and base material.

Similarly to conduction, heat loss from the surface *i=n* due to convection and radiation is based on the energy balance equation shown in figure 69:

$$T_{n,j+1} = T_{nj}\left[1 - \frac{2\alpha \Delta t}{\Delta y^2}\left(N_B + 1\right)\right] + \frac{2\alpha \Delta t}{\Delta y^2}\left(T_{n-1,j} + N_B T_{Air}\right) + \frac{2\alpha \Delta t}{k \Delta y^2}\left[aH_s - \varepsilon\sigma\left(T_{nj} + 459.67\right)^4\right]$$

Figure 69. Equation. Energy balance equation for convective and radiation heat losses at pavement surface.

where:

N_B = Biot number (described below).
k = thermal conductivity (BTU/ft^2-h-°F/ft).
T_{Air} = ambient air temperature (°F).
a = solar absorptivity.
H_S = solar heat flux (BTU/ft^2-h).
ε = emissivity.
σ = Stefan-Boltzman constant—1.713x10^{-9} (BTU/ft^2-h-°R^4).

The Biot number is a dimensionless value commonly used in transient heat flow and mass transfer analysis.[15] It is the ratio of heat transfer resistances *within* and *at the surface* of a mass undergoing convection. This number indicates whether temperatures within the body will vary significantly in space while the mass heats or cools over time due to thermal energy transfers at its surface. Mathematically, the Biot number is defined as the equation shown in figure 70.[15]

$$N_B = \frac{hs}{k}$$

Figure 70. Equation. Definition of Biot number.

The convective heat transfer coefficient h in figure 70 relates convective heat flow with temperature difference and surface area via Newton's law of cooling. The effective length s is the ratio between volume and surface area, and k is the thermal conductivity. The final radiation term in figure 69 includes parameters that account for the absorption of radiant solar energy ($a\ H_S$) and for the radiant energy emitted by the pavement ($\varepsilon\ \sigma$).

Corlew and Dickson developed a computer program to simulate mat cooling based on this finite difference formulation. To validate this model, they performed field experiments in which thermocouples were embedded throughout the depth of an HMA overlay to measure mat cooling versus time. Wind velocity, ambient air temperature, initial base temperature, solar radiation, and overlay thickness were also measured in their experiments. Corlew and Dickson found very close correlations between measured and predicted temperatures.

Overall, Corlew and Dickson's study suggested the following:

1. When using proper environmental conditions, modeling mat cooling is feasible and accurate using finite difference analysis techniques.

2. The heat flux from the overlay into the underlying base layer is initially greater than the heat flux into the atmosphere. Therefore, the lower region of the overlay expels heat faster than the upper region. However, Jordan and Thomas found that with increasing time, the cooling of the surface becomes dominant.[16]

Wolfe and Colony expanded on Corlew and Dickson's approach and converted the mat cooling models into a format more suitable for the portable handheld computers of the time and for tabular and graphical summary.[17] In an attempt to streamline the conductive heat flow calculations in figure 68, Wolfe and Colony used Saul'yev's method for conduction, a numerical technique based on forward and backward finite differences. Saul'yev's method requires less memory than that needed by Corlew and Dickson's formulation and thus was better suited to the comparatively primitive handheld computers available in the 1970s. Wolfe and Colony also developed an explicit form of convective heat transfer energy balance at the mat surface.

Wolfe and Colony also employed the slightly different finite difference energy balance equation shown in figure 71 for the heat flows at the surface of the mat. All terms were as defined previously.

$$-\varepsilon\sigma\left(T_{nj}+459.67\right)^4+aH_S+\frac{k\left(T_{n-1,j}-T_{nj}\right)}{\Delta y}-h\left(T_{nj}-T_{Air}\right)=\frac{\Delta y\rho C_p\left(T_{n,j+1}-T_{nj}\right)}{2\Delta t}$$

Figure 71. Equation. Modified version of finite difference energy balance for heat flows at surface of mat.

Figure 71 includes energy losses due to radiation and convection and gains from solar radiation. Figure 71 can then be rearranged as shown in figure 72 to solve for the temperature at the next time step, $T_{n,j+1}$.

$$T_{n.j+1}=T_{nj}+\frac{2h\alpha\Delta t}{k\Delta y}\left(T_{Air}-T_{nj}\right)+\frac{2\alpha\Delta t}{\Delta y^2}\left(T_{n-1,j}-T_{nj}\right)+\frac{2a\alpha\Delta tH_S}{k\Delta y}-\frac{2\varepsilon\sigma\alpha\Delta t}{k\Delta y}\left(T_{nj}+459.67\right)$$

Figure 72. Equation. Modified equation for $T_{n,j+1}$ at mat surface.

Figure 68 and figure 72 are used in this study as the finite difference solution for the transient heat flow in the overlay.

Wolfe and Colony argued that both free and forced convection effects should be included when calculating the convective heat transfer coefficient.[17,18] Free convection occurs when there is no wind velocity, as opposed to forced convection that includes wind velocity. Wolfe, Heath, and Colony recommended the relationship shown in figure 73 for convection[19]:

$$h = 1.3 + 0.62V^{0.75}$$

Figure 73. Equation. Relationship for forced convection.

where V is the wind velocity in mi/h.

Wolfe and Colony state that solar heat flux emitted by the Sun can range up to about 400 BTU (422 kJ) per hour at local solar noon.[17] However, it is dependent on the time of the year, the Sun's declination, and the location (latitude) of the surface being considered. They suggest the the equation in figure 74 for estimating solar heat flux[18]:

$$H_S = R\left(1 - NW/100\right)$$

Figure 74. Equation. Relationship for estimating solar heat flux.

where:

R =incident solar radiation (direct and diffuse).
N = a cloud base factor, which varies from 0.80 to 0.90.
W = percentage cloud cover, which is visually estimated.

The value for incident radiation is obtained from historical data. The authors provide a graph of solar heat flux versus time for typical incident radiation in Ohio between 38°50' and 42°00' latitude (the location of their study).

Alternative methods for determining solar heat flux have been proposed in the literature. Rather than modifying solar radiation for cloud effects and cover, radiation can also be quantified in terms of the effective sky temperature.[20]

Wolfe, Heath, and Colony performed laboratory and then field tests to demonstrate that their numerical predictions correlated favorably to measured mat cooling curves.[19] The field trials were performed in November 1979 at a project site in Ohio. The field instrumentation at the project site included a radiation pyrometer to measure base surface temperatures, a pyrheliometer to measure solar insolation, an anemometer to measure wind speed, temperature probes, and recording devices. Field temperatures were measured near and at the interface of the newly placed HMA and its base layer. Surface temperatures were also measured but were dismissed because of instrument inaccuracies. The field test found generally close correlations between calculated and measured temperatures.

Wolfe, Heath, and Colony concluded that their predictive equations were adequate for the purpose of making "go/no-go" decisions in the field for placing and compacting HMA under adverse site conditions.[19] Specific findings from the study included the following:

- Based on the simulation results, solar radiation and cloud cover are not major influences on the placement of HMA. In other words, solar radiation should not be considered in making a "go/no-go" decision in the field.

- The convective heat transfer coefficient is relatively difficult to measure. There are numerous equations and experimental methods to estimate this parameter. However, the study generally confirmed the recommendations in figure 73 for this value.

- Prior to the actual paving, the surface of the base material is subjected to heat from the paver as it passes. The authors suggested that, depending on the speed of the paver (and if it pauses), the initial interface temperature between the asphalt and base material may not be accurate. Temperatures should be recorded once the paver passes the test area.

Thermal Property Values

Wolfe and Colony, based on a review of several sources, recommended typical values for other thermophysical material properties of asphaltic mixtures.[17] These are summarized in table 14.

Table 14. Typical thermal property values.[17]

Property	Units	Symbol	Suggested	Minimum Value	Maximum Value
Thermal conductivity	BTU/ft-h-°F	k	0.80	0.58	1.01
Thermal diffusivity	ft^2/h	α	0.0215	0.0215	0.0337
Absorptivity	Dimensionless	a	0.85	0.85	0.90
Emissivity	Dimensionless	ε	0.95	0.90	0.95
Stefan-Boltzman constant	BTU/ft^2-h-°F (R^4W/m^2-K^{-4})	σ	$1.713x10^{-9}$ ($5.670x10^{-8}$)	N/A	N/A

N/A = Not Applicable
1 BTU/ft-h-°F = 1.73 W/m-°K
1 ft^2/h = 0.093 m^2/h

Luca and Mrawira performed a series of laboratory tests to measure the thermal diffusivity α and thermal conductivity *k* for Superpave HMA mixtures and compared their measured values with values reported previously in the literature.[21] Their measured values generally agreed favorably with those in the literature; the values fit within a general range of $1.35x10^{-2}$ to $3.20x10^{-2}$ ft^2/h ($1.25x10^{-3}$ to $2.98x10^{-3}$ m^2/h) for thermal diffusivity and 0.70 to 2.24 BTU/ft-h-°F (1.21 to 3.88 W/m-°K) for thermal conductivity. The authors highlight that these parameters are generally difficult to measure. Table 15 and table 16 summarize Luca and Mrawira's findings.

Table 15. Typical values for thermal diffusivity.[21]

Author	Year	Thermal Diffusivity, α, x 10^{-2} (ft^2/h)
Luca and Mrawira[21]	2005	1.56–2.13
Wolfe et al.[19]	1983	1.99–3.20
Fwa et al.[22]	1997	2.07–2.24
Highter and Wall[23]	1983	1.35–2.90
Corlew and Dickson[14]	1968	2.27

1 ft^2/h = 0.093 m^2/h

Table 16. Typical values for thermal conductivity.[21]

Author	Year	Thermal Conductivity, k (BTU/ft-h-°F)
Luca and Mrawira[21]	2005	0.94–1.19
Wolfe et al.[19]	1983	0.58–1.01
Fwa et al.[22]	1997	2.07–2.24
Highter and Wall[23]	1983	0.75–0.82
Corlew and Dickson[14]	1968	0.70

1 BTU/ft-h-°F = 1.73 W/m-°K

LABORATORY EVALUATION OF SAW RFID TAGS

The differences between surface SAW and conventional RFID were described in chapter 1. A series of laboratory tests were performed to evaluate the suitability of SAW RFID technology for pavement applications. These tests were organized into the following subtopics:

- Development of an encapsulation process using thermally conductive epoxy that will promote the transfer of thermal energy while protecting the tag from physical damage.
- A read range study to evaluate the signal strength/readability of the SAW RFID tags. The read range study includes testing for tag orientation (including rotation) to the antenna and position/distance from the antenna.
- A thermal sensitivity study to evaluate the thermal response of the tags when exposed to elevated temperature transients. More specifically, this study evaluates the time required for a tag to heat up and then equilibrate to the temperature of the surrounding material/ environment.

Tag Encapsulation

Encapsulating the RFID tags with a thin coating of thermally conductive epoxy protects them from paving and compaction stresses while only minimally interfering with heat transfer during mat cooling. The encapsulation medium selected for this study is Durapot 865™ epoxy from Cotronics, Inc. This encapsulant has a thermal conductivity of about 1 BTU/ft-h-ºF (1.73 W/m-°K) and is electrically insulating. To put this parameter into perspective: the thermal conductivity of copper is about 230 (400), standard epoxy is about 0.20 (0.35), and asphalt is about 0.433 BTU/ft-h-ºF (0.75 W/m-°K). Durapot 865™ is a two-component epoxy (resin and hardener) that cures at room temperature. The following encapsulation procedure was used:

- The epoxy resin component is preheated for about 40 min at 122 °F (50 °C) to reduce its viscosity.
- The epoxy components are then combined at 100 parts resin to 21 parts hardener and thoroughly mixed.
- The wooden mold (fabricated in advance) is lined with standard kitchen plastic wrap secured using masking tape.

- A layer of epoxy is poured at the bottom of the mold prior to tag placement to create a thin protective base layer.

- The tag is placed in the mold on top of the bottom epoxy layer and pressed downward into the encapsulant. The tag is then covered in the epoxy to completely encase it.

- The wood mold, with epoxy and tag, is then placed in a vacuum dessicator to remove any air pockets in the epoxy.

- After removing the air and curing for 24 hours, the tags are removed and sanded for smoothness.

Figure 75 shows the unencapsulated tags used in this study. As will be described more fully later, the larger tag on the left of figure 75 is the single patch antenna tag (with larger receiving antenna) approximately 45 by 45 mm (1¾ by 1¾ inches) in size. The tag on the right is the monopole antenna tag approximately 8 by 45 mm (1/3 by 1¾ inches) in size. Figure 76 shows the encapsulated tags prior to final sanding. Both unencapsulated and encapsulated tags were evaluated in the read range and thermal sensitivity studies.

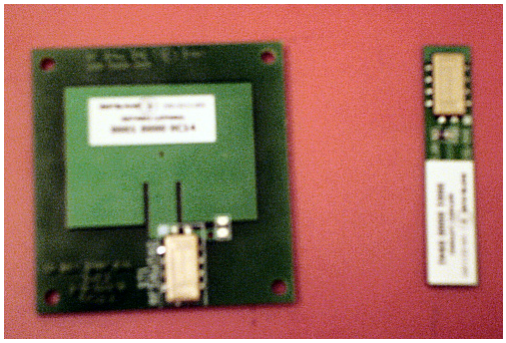

Figure 75. Photo. Unencapsulated RFID tags (left: single patch, right: monopole).

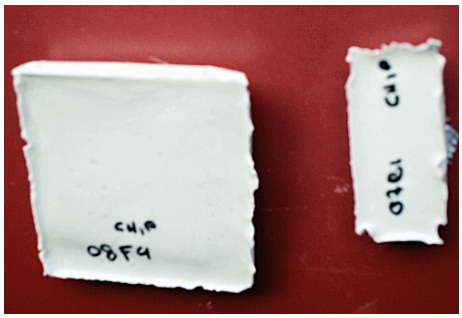

Figure 76. Photo. Encapsulated RFID tags before finish sanding (left: single patch, right: monopole).

Signal Strength and Readability

A series of read range tests were performed to evaluate the signal strength and readability of the SAW RFID tags in both the monopole and single patch antenna configurations. The monopole

and single patch tag antennae differ primarily in the shape of their RF field distributions (for transmission) and sensitivities (for reception).

The monopole antenna is formed by replacing half of its dipole antenna with a ground plane normal to the antenna axis. If the ground plane is sufficiently large, the monopole behaves like a dipole with its reflection in the ground plane providing the missing symmetric half. A dipole antenna has a toroidal field strength/sensitivity distribution with omnidirectional field strength/ sensitivity in the midplane and normal to the antenna axis, and with dead zones at the ends of the dipole.

Patch antennae, on the other hand, are designed for a more directional RF radiation/sensitivity. A simple patch antenna consists of a looped antenna one-half wavelength long, separated by a constant thickness over a ground plane. The ground plane is typically only modestly larger than the active patch. The simple patch antennae of this type radiate a linearly polarized wave. The typical radiation pattern for a linearly polarized patch antenna is unidirectional with a beam width angle of about 65 degrees. An infinitely large ground plane would prevent any radiation toward the back of the antenna. But, with the more usual finite ground plane, power loss through the back side of the antenna is about -20 dB compared with the front side.

Two types of reader antennae were supplied with the SAW RFID system—linearly and circularly polarized. Both reader antenna types were evaluated for the following tag configurations: unencapsulated tags in air, encapsulated tags in air, and encapsulated tags in an asphalt specimen.

Unencapsulated Tags in Air

To determine the full read range capacity of the unaltered SAW RFID tags, an "open-floor" read range study was performed. The following diagrams illustrate the read range capacity for the unencapsulated tags in air. Each cell within the diagram represents a 1 ft (0.3 m) interval of lateral offset or distance ahead of the antenna. Note that the antenna is fixed 1 ft (0.3 m) away from the test grid in front of cells L-A and R-A. For example, cell "-2, B" is located 2 ft (0.6 m) to the left and 3 ft (1 m) ahead of the face of the antenna. The numbers in each cell are the number of read responses from the tag at that location during a 20s interval.

A uniform tag orientation was used throughout this study. The tag was affixed to the back of a plastic board, antenna oriented vertically, facing toward the reader antenna (unless otherwise noted). Figure 77 and figure 78 display the results of the read range study performed on a single patch tag using a linearly polarized antenna and circularly polarized antenna, respectively. The green cells indicate strong reliable readings, yellow are more unpredictable, and red are zero or unlikely readings. Figure 79 and figure 80 summarize the corresponding read range results for unencapsulated monopole tags using a linearly and circularly polarized antenna.

Comparing these four figures, it is apparent that the single patch tags have a stronger readability than the monopole tags, both in terms of the number of reads and the width of the readable zone ahead of the antenna. This is because of the larger size and higher sensitivity of their antennae. However, all of the unencapsulated tags (patch and monopole) exhibited read ranges greater than 8 ft (2.4 m) in air.

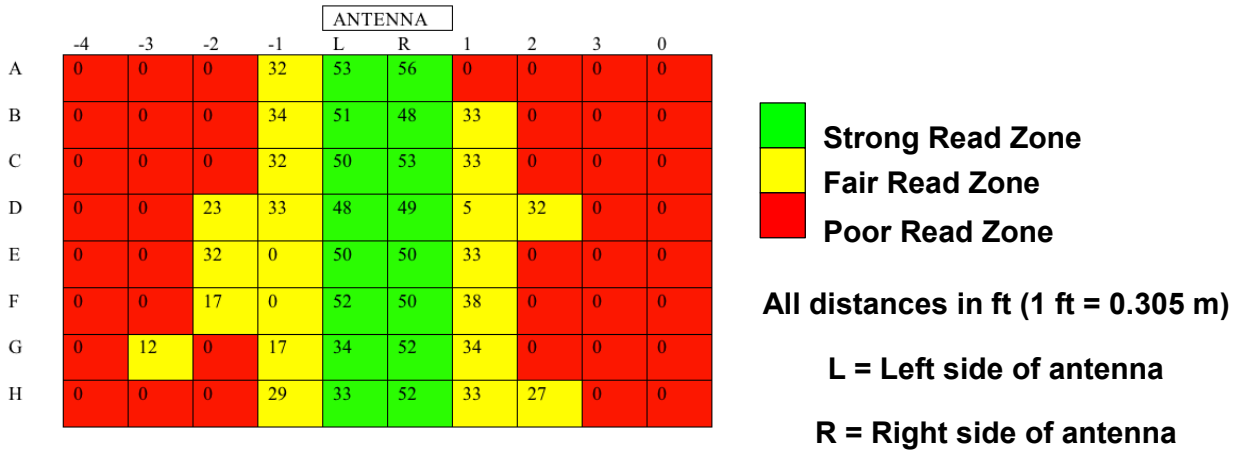

Figure 77. Diagram. Unencapsulated single patch tag, linear polarization.

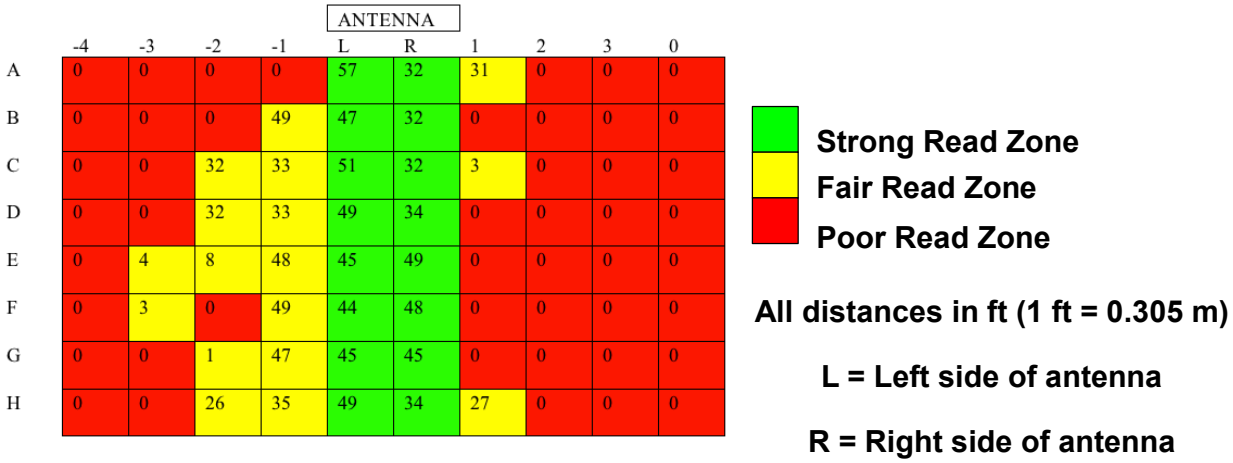

Figure 78. Diagram. Unencapsulated single patch tag, circular polarization.

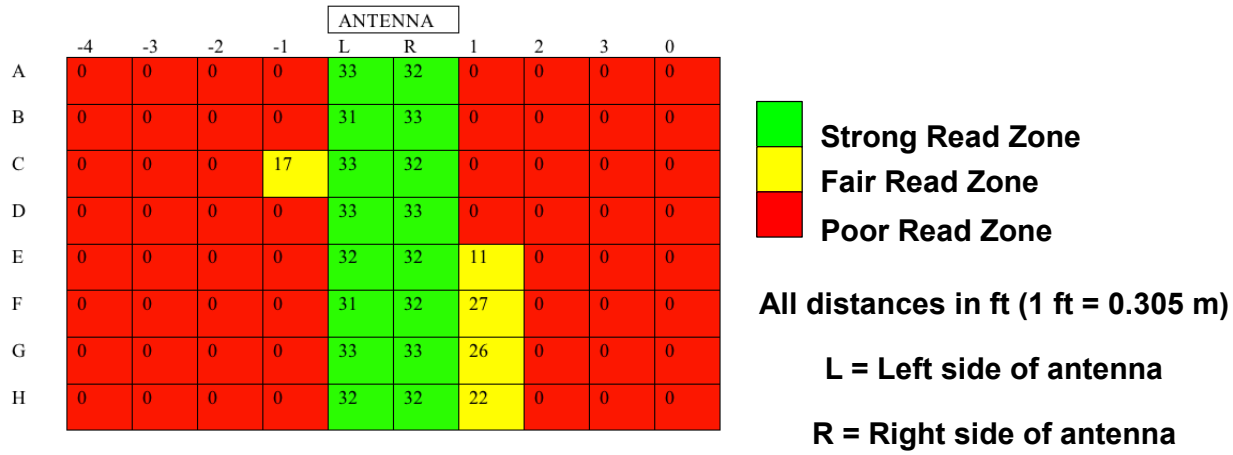

Figure 79. Diagram. Unencapsulated monopole tag, linear polarization.

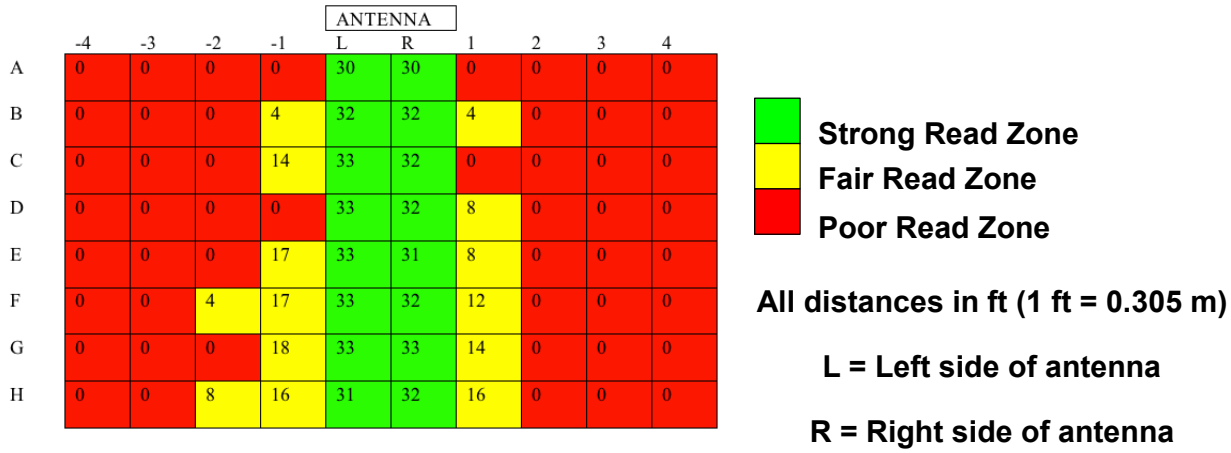

Figure 80. Diagram. Unencapsulated monopole tag, circular polarization.

Encapsulated Tags in Air

Similar read range testing was performed on tags after encapsulation in thermally conductive epoxy. Figure 81 and figure 82 summarize the measured read ranges for the encapsulated single patch tag using linear and circular reader antenna polarization, respectively. Figure 83 and figure 84 summarize similar results for the encapsulated monopole tag.

Based on the results in these figures, it is again apparent that the single patch tags have better readability than the monopole tags. In addition, the polarization of the reader antenna influences read performance. A linearly polarized antenna has more directionality than the circularly polarized antenna. This means that, all else being equal, the linearly polarized antenna will have better read performance for some orientations of the tag (relative to the plane of the antenna polarization) and worse read performance for others, compared with the circularly polarized antenna. In general, the circularly polarized antenna will have slightly lower read performance but with much less sensitivity to the orientation of the tag relative to the antenna. The latter characteristic is more important for field applications, so all subsequent testing was conducted using only the circularly polarized reader antenna.

It is also apparent from these results that while encapsulating the RFID tags within epoxy increases their likelihood of survival in the field, it is detrimental to their readability in air. Based on the read range results, the encapsulated monopole tags are likely to perform marginally for field use while the encapsulated patch tags are anticipated to perform well.

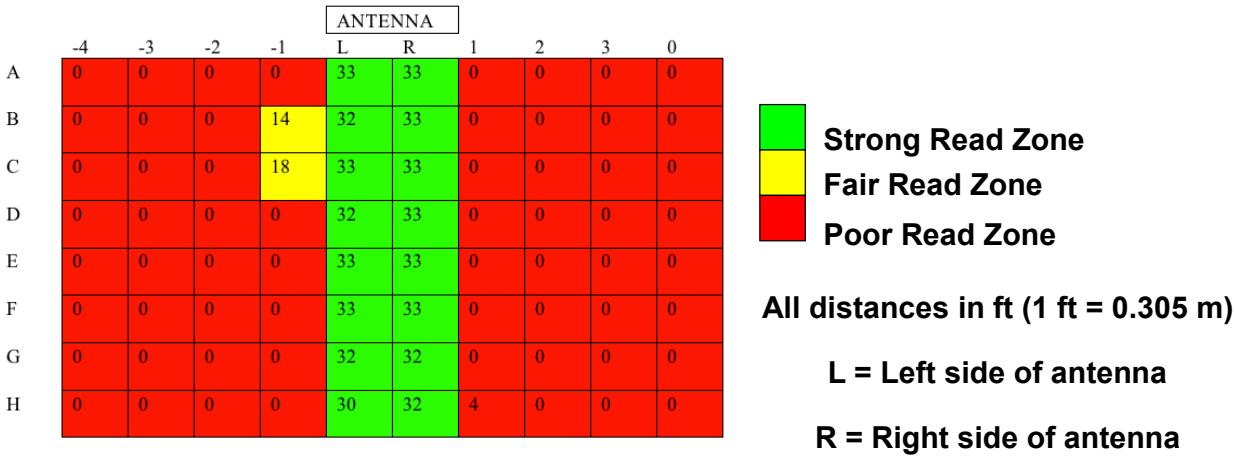

Figure 81. Diagram. Encapsulated single patch tag, linear polarization.

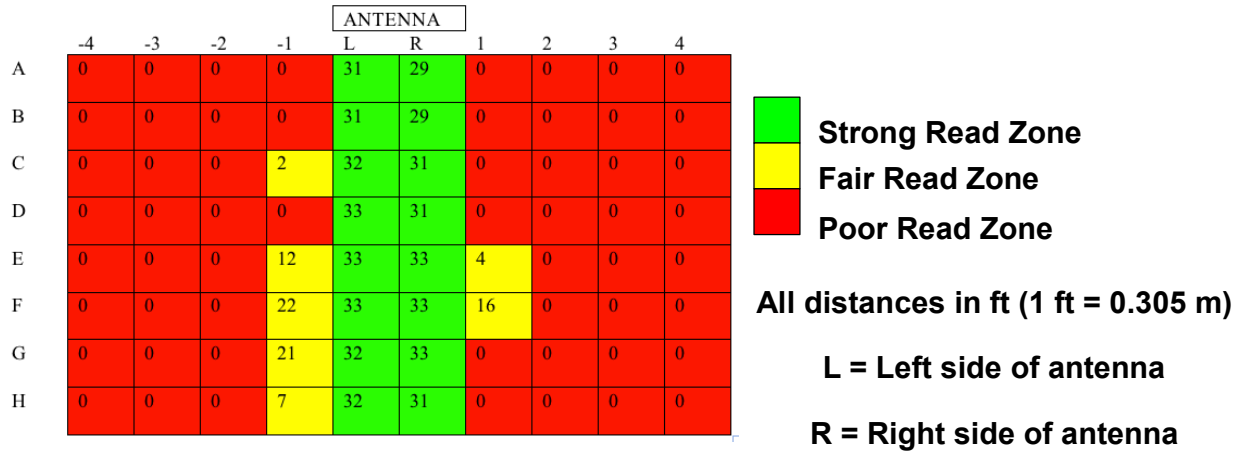

Figure 82. Diagram. Encapsulated single patch tag, circular polarization.

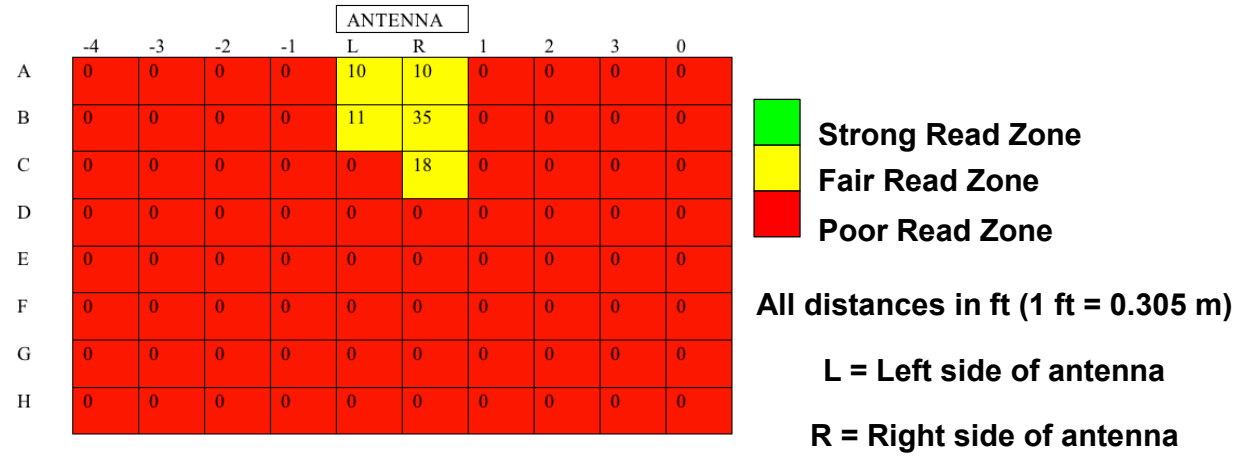

Figure 83. Diagram. Encapsulated monopole tag, linear polarization.

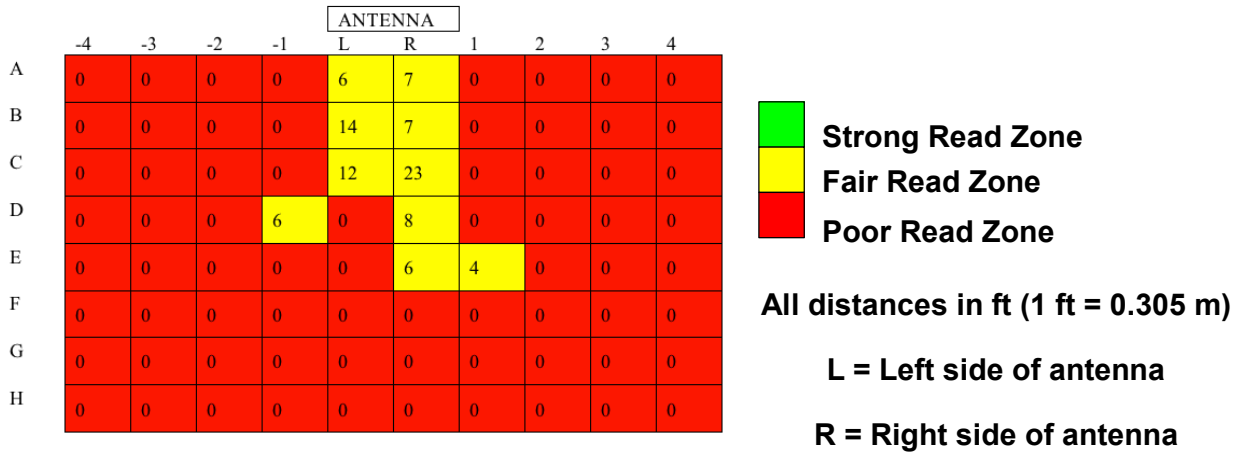

Figure 84. Diagram. Encapsulated monopole tag, circular polarization.

Encapsulated Tags Within Asphalt

In an effort to simulate survivability and readability under field conditions, the SAW tags were placed in HMA at about 392 °F (200 °C) and compacted in a gyratory compactor. All specimens were compacted at about 88 psi (600 kPa) pressure for 150 gyrations. Initially, unencapsulated patch and monopole tags were positioned in the gyratory specimens to evaluate their inherent survivability. Two of three unencapsulated tags were destroyed during compaction. Therefore, all subsequent tags evaluated in this read range study were encapsulated in thermally conductive epoxy.

The encapsulated tags were placed near the center of the gyratory plugs. As shown in figure 85, a variety of tag orientations were explored to determine which would provide the best readability. In addition to these orientations, the encapsulated tags were also rotated about the cylinder's axis to evaluate any further potential signal degradation. Figure 86 depicts the rotational positions of the asphalt sample.

Overall, the testing revealed that the strongest signal strength and readability were produced in orientation #1 (face side of the tag facing the antenna) for both the single patch and monopole tags. In this orientation, rotation #1 (figure 86) provided the best and most consistent results. Figure 87 and figure 88 summarize typical testing results for orientation #1 for both the monopole and single patch tags. Note that the single patch tag was read up to about 12 ft (3.6 m) from the antenna using this orientation. Although not shown, orientations #2 and #4 were also considered strong and reliable for both types of tags. In addition, the monopole tags performed well in orientations #4 and #6.

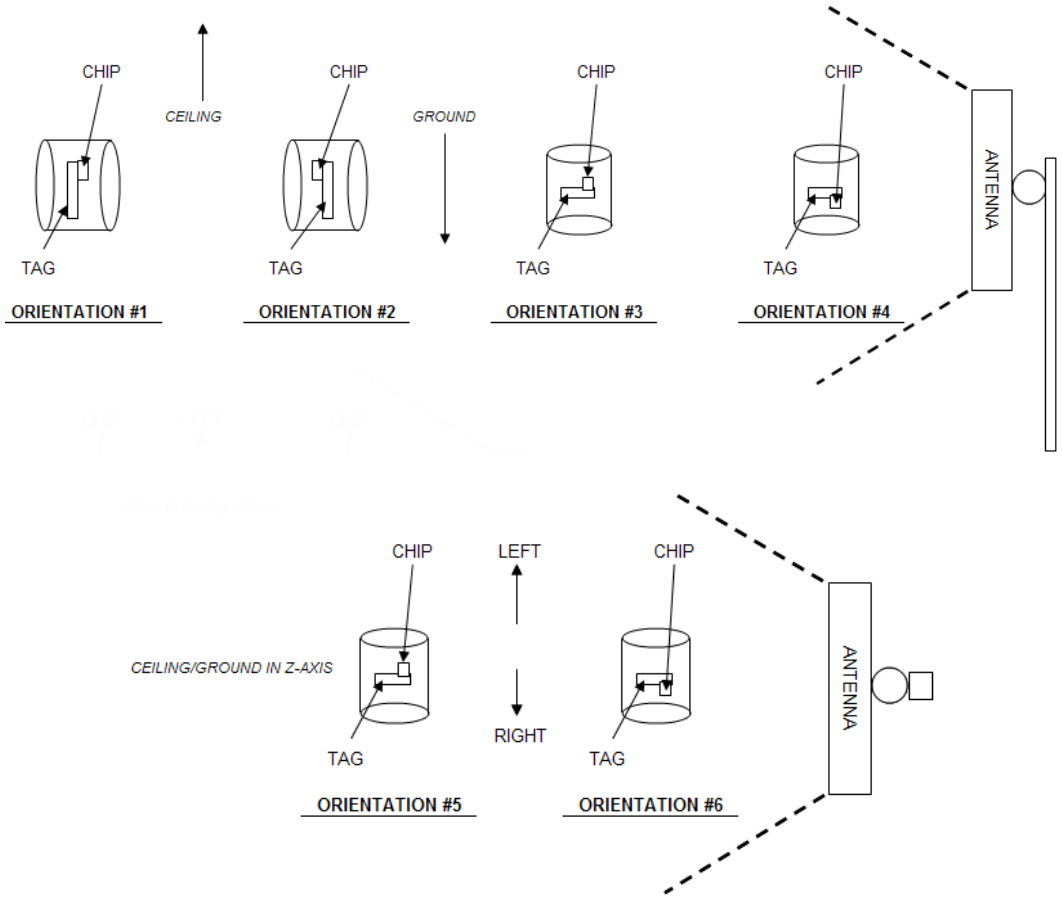

Figure 85. Drawing. Orientation guide for tags within asphalt specimens.

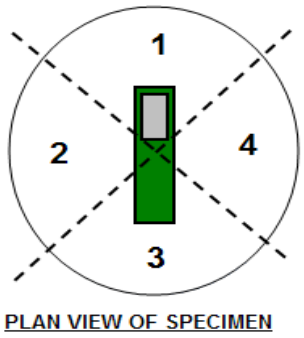

Figure 86. Drawing. Rotation scheme for tags within asphalt specimens (monopole and single patch).

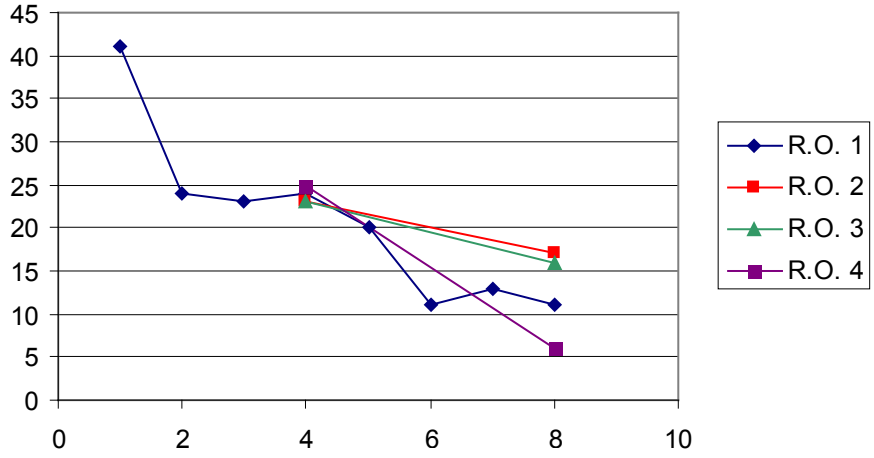

R.O. = rotational orientation
1 ft = 0.305 m

Figure 87. Graph. Orientation #1 for monopole tag using circular polarization.

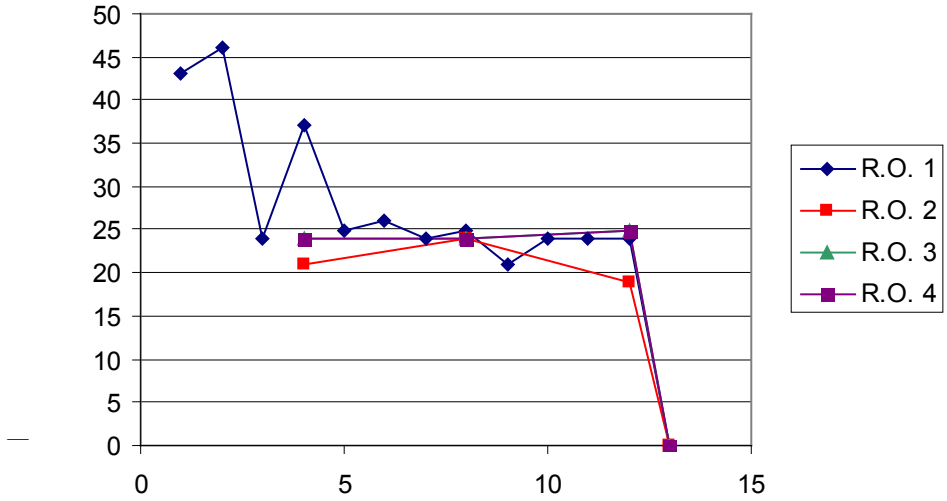

R.O. = rotational orientation
1 ft = 0.305 m

Figure 88. Graph. Orientation #1 for single patch tag using circular polarization.

Conclusions: Signal Strength and Readability

Overall, both the encapsulated monopole and patch antenna tags showed acceptable performance when encased in HMA. The monopole tags, while more practical and compact in size, did not perform as reliably as the patch tags in terms of signal strength and readability. Based on the entire laboratory read performance testing, both the monopole and patch tags warrant further

investigation in field trials. Because they are to be pre-positioned ahead of the asphalt paver, they can be placed in the optimum location: orientation #1/rotational position #1.

Thermal Sensitivity

To simulate field conditions within a laboratory, the testing apparatus shown in figure 89 was developed for measuring the temperature sensitivity and transient response of the SAW RFID tags. As shown in the figure, the SAW RFID tags were pre-positioned on a flat wood plank covered in foil (to isolate temperatures and increase signal strength) and exposed to preheated materials. The selected materials used for testing included generically graded asphalt aggregate and HMA with about 5-percent binder content by weight. These materials were preheated to about 284 to 338 °F (140 to 170 °C) and placed over the test tag at room temperature. Upon exposure, tag temperatures were recorded over time via the RF SAW reader and software. Independent temperature measurements were collected using a Fluke® thermocouple probe affixed to the foil adjacent to the tag. Because our initial small supply of SAW RFID tags was limited, the tags tested here were the same as those used previously for the survivability and read performance testing; they were recovered from the gyratory plugs after completion of the survivability testing.

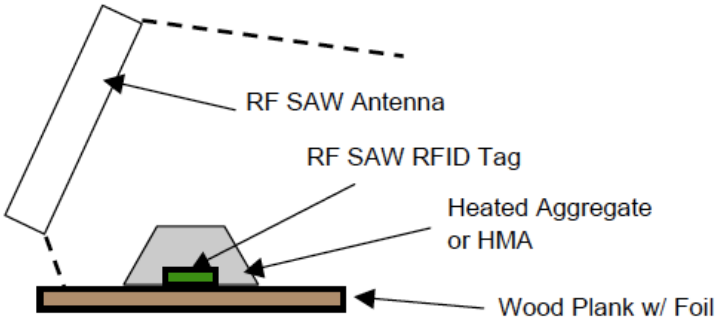

Figure 89. Drawing. Thermal testing apparatus.

Table 17 describes the tags used for this study. figure 90 through figure 92 summarize the thermal sensitivity study results for hot aggregate material. Time zero corresponds to ambient (room temperature) conditions immediately before covering the RFID tag and Fluke® thermocouple with the hot aggregate. The test results show that the unencapsulated monopole tag (tag 0A21, figure 90) quickly matched the temperature readings from the thermocouple. The encapsulated monopole tag (tag 0443, figure 91) required about 5 to 6 min to reach aggregate temperature, as measured by the thermocouple. This thermal lag is assumed to be due to the additional thermal mass and relatively low thermal conductivity from the encapsulating epoxy. The thermal lag even more pronounced for the encapsulated patch tag (tag 09FE, figure 92) because of its larger format and corresponding larger mass of encapsulating epoxy. Even after 6 min, the encapsulated patch was 104 °F (40 °C) cooler than the reference measurement. Note that no unencapsulated patch tag was evaluated in this thermal study because it had been destroyed in the gyratory compactor during the first stage of the testing.

Table 17. Tags employed in thermal testing.

Tag Name	Type	Encapsulated
0A21	Monopole	No
0443	Monopole	Yes
09FE	Single Patch	Yes

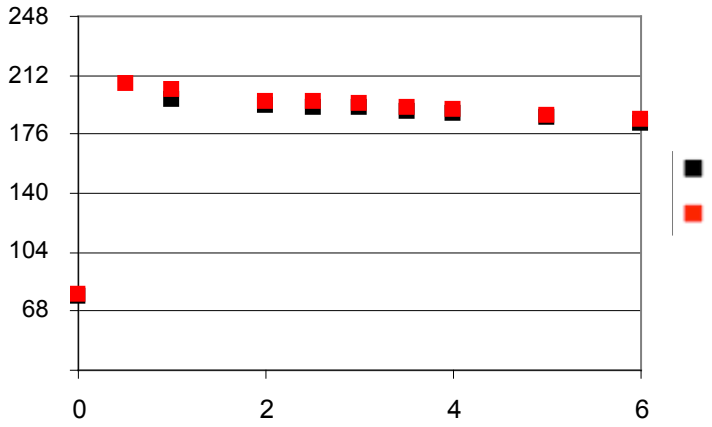

°C = (°F – 32)/1.8

Figure 90. Graph. Thermal response from tag 0A21 using hot aggregate.

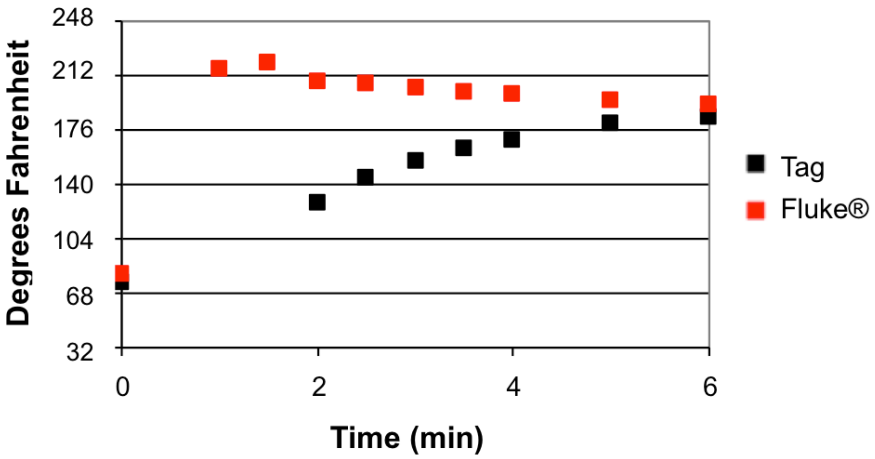

°C = (°F – 32)/1.8

Figure 91. Graph. Thermal response from tag 0443 using hot aggregate.

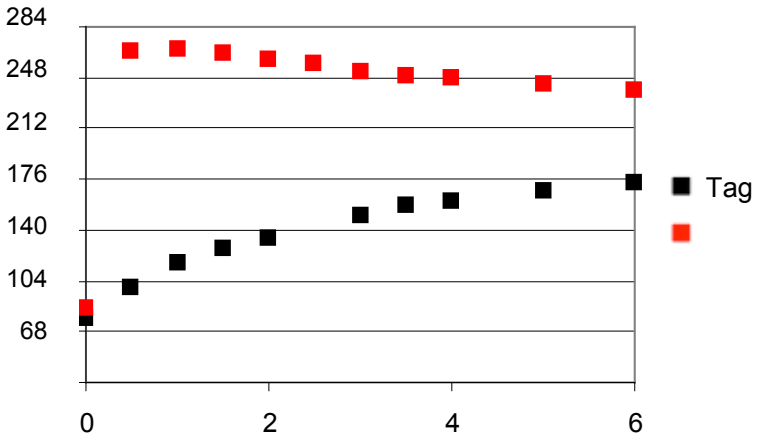

°C = (°F – 32)/1.8

Figure 92. Graph. Thermal response from tag 09FE using hot aggregate.

Figure 93 through figure 95 summarize the thermal sensitivity study results for the HMA material. Similar conclusions can be drawn here as for the hot aggregate: the unencapsulated monopole tag responds quickly and accurately, the encapsulated monopole tag responds with an acceptable time delay, and the encapsulated patch tag responds much more slowly and was still far from the equilibrium temperatures when the measurements ended at 6 min. This thermal lag may prove to be detrimental for field use.

Once the tags have equilibrated from the initial thermal shock (i.e., starting at ambient temperature and being covered with 284 to 338 °F (140 to 170 °C) HMA, they then match the thermocouple measurements for the continued slow cooling with time. This is most evident for the monopole tags (figure 93 and figure 94); readings were not continued for a long enough time period to completely confirm this for the encapsulated single patch tag (figure 95).

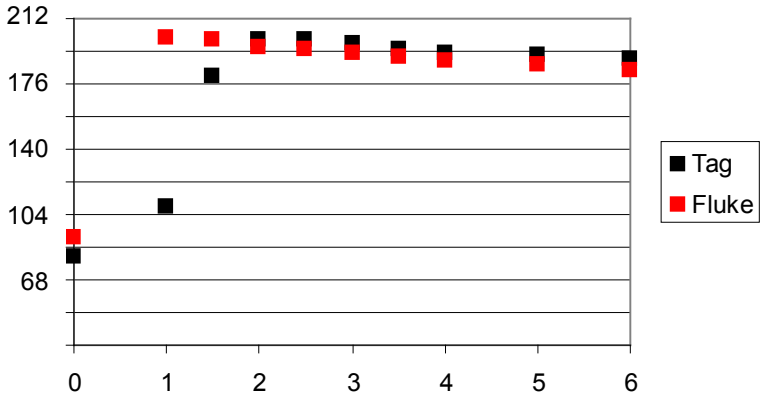

°C = (°F – 32)/1.8

Figure 93. Graph. Thermal response from tag 0A21 using hot HMA.

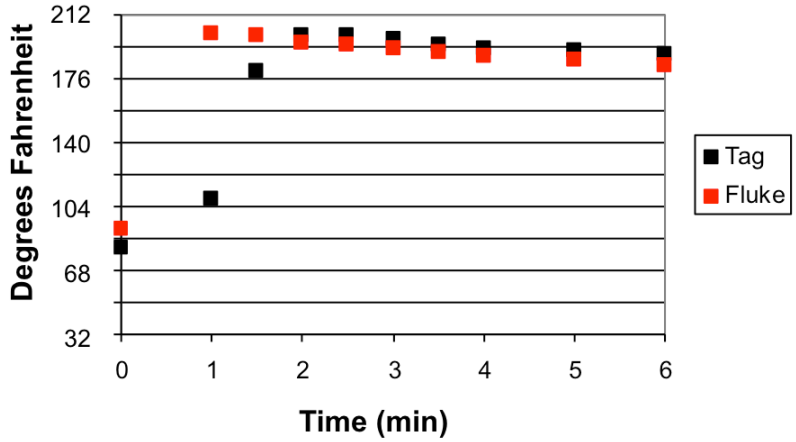

°C = (°F – 32)/1.8

Figure 94. Graph. Thermal response from tag 0443 using hot HMA.

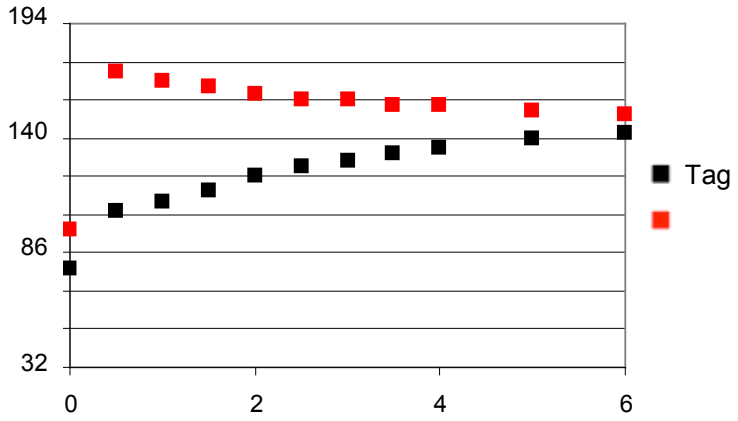

°C = (°F – 32)/1.8

Figure 95. Graph. Thermal response from tag 09FE using hot HMA.

Overall, the thermal sensitivity study suggests that, given an adequate amount of time after HMA placement before compaction, all of the tested SAW RFID tags have transient thermal response sufficiently rapid for field use. The unencapsulated monopole tag performed more effectively than the others. Nonetheless, further field evaluation of all of the tags is justified.

FIELD EVALUATION

Field trials were conducted to evaluate the suitability of SAW RFID technology for wireless measurement of in-place HMA temperatures during intelligent compaction. These trials, hosted by MDSHA in conjunction with the FHWA Intelligent Compaction Pooled Fund Study, were conducted on July 23, 2009, during placement of a 1.5 inches (38 mm) pavement overlay.[13]

Site Information

The project site for the field trials was located on United States Route 15/Maryland Route 340 in Frederick County, Maryland. More specifically, the site was located in the outer (right) northbound lane between Mt. Zion Road and the Jefferson Street Bridge. Figure 96 maps the general location of the project site.

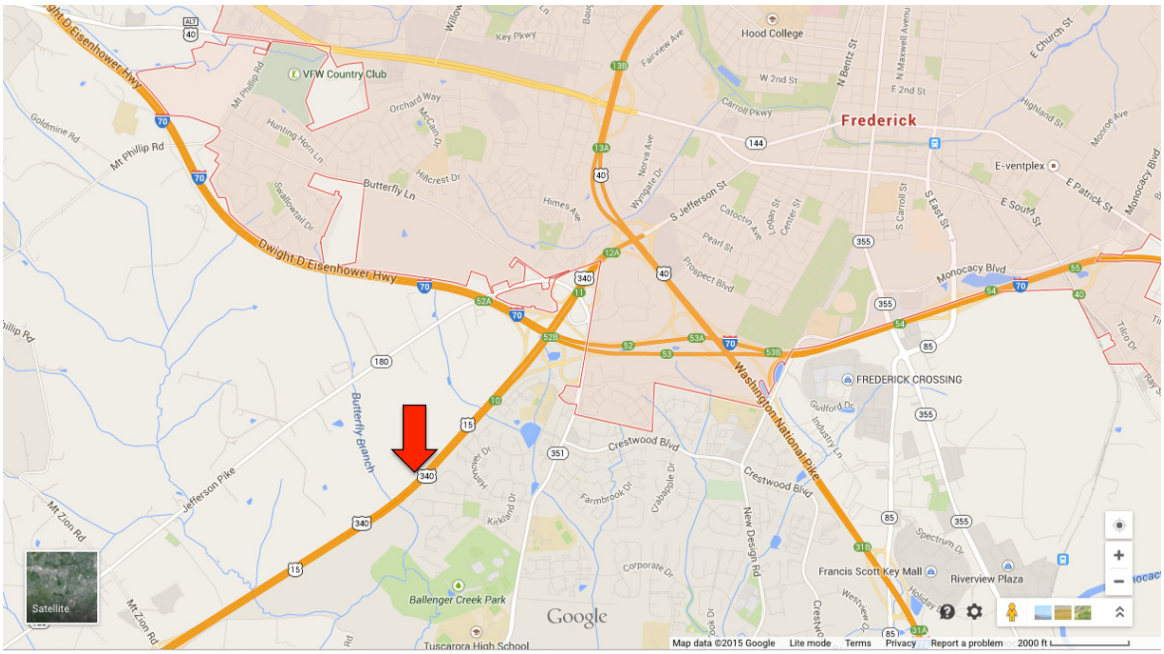

Original image: ©2015 Google®; map annotations provided by University of Maryland

Figure 96. Map. Approximate location of project site.[(24)]

Construction and activities related to the intelligent compaction field trial were conducted at the project site from about July 20 to July 24, 2009. An initial attempt was made on the evening of July 22 to perform the field evaluation of the SAW RFID temperature measurement system. However, all construction activities were cancelled because of an unexpected thunderstorm. The encapsulated tags for the field trial had already been affixed to the milled surface using epoxy putty before the storm. After cancellation, the tags were pried from the road surface and the epoxy putty was carefully ground off so that the tags could be reused on July 23. The field evaluation was completed on July 23 from about 0200 to 0300 h. Weather conditions were clear, mild, and windless. Table 18 summarizes weather data recorded just prior to testing from two nearby weather stations.

Table 18. Weather data recorded near the project site for July 22–23, 2009.

Time	Station	Temperature (°F)	Dew Point (°F)	Relative Humidity (%)	Wind Speed (mi/h)
20:55	Walnut Ridge	74.8	64.0	68	0
	Middletown	71.4	66.0	82	0
00:53	Walnut Ridge	71.4	63.0	75	0
	Middletown	70.5	64.9	82	0
01:47	Walnut Ridge	70.5	63.0	82	0
	Middletown	70.5	64.0	81	0

Note: Walnut Ridge and Middletown stations are about 8 (12.88 km) and 36 mi (57.96 km), respectively, from the project site.
°C = (°F – 32)/1.8
1 mi/h = 1.61 km/h

Testing Procedure

The test section was about 51 ft (15.5 m) long and was located near the interchange with Mt. Zion Road. Ten single patch tags and 30 monopole SAW RFID tags were pre-positioned ahead of the paver. In an effort to measure temperature through the depth of the overlay, three elevations were considered: bottom of the mat (elevation 0 inches), middle of the mat (elevation 0.75 inches (19 mm)), and surface of the mat (elevation 1.5 inches (38 mm)). The middle tags were elevated using a thicker layer of thermally conductive epoxy underneath the tag. Layout schematics for the test section are shown in figure 97 and figure 98.

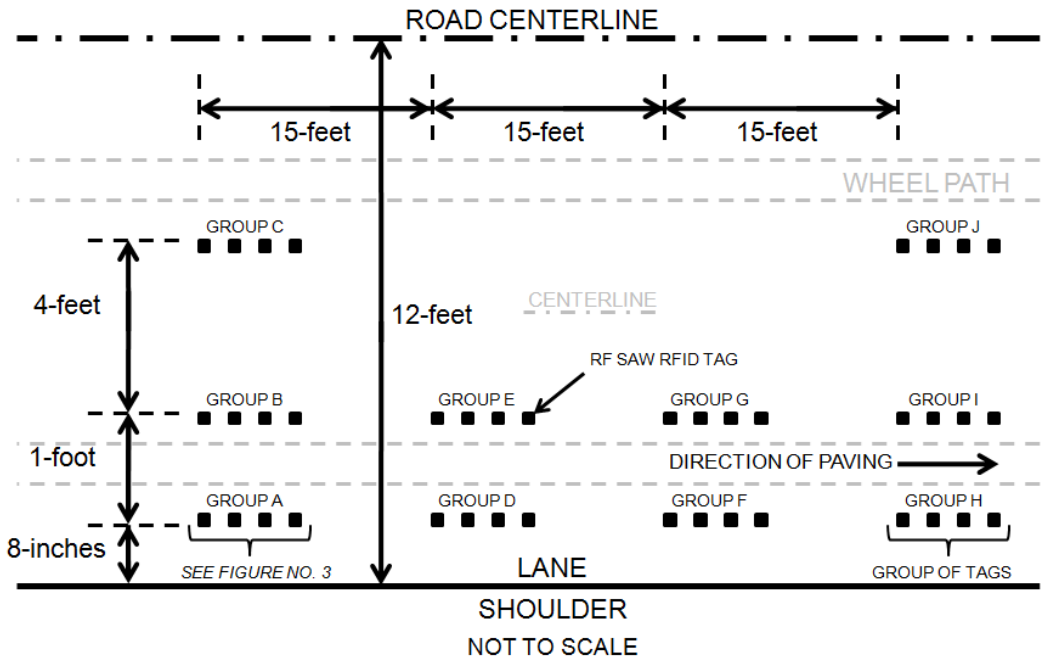

1 ft = 0.305 m

Figure 97. Drawing. Plan view of test section.

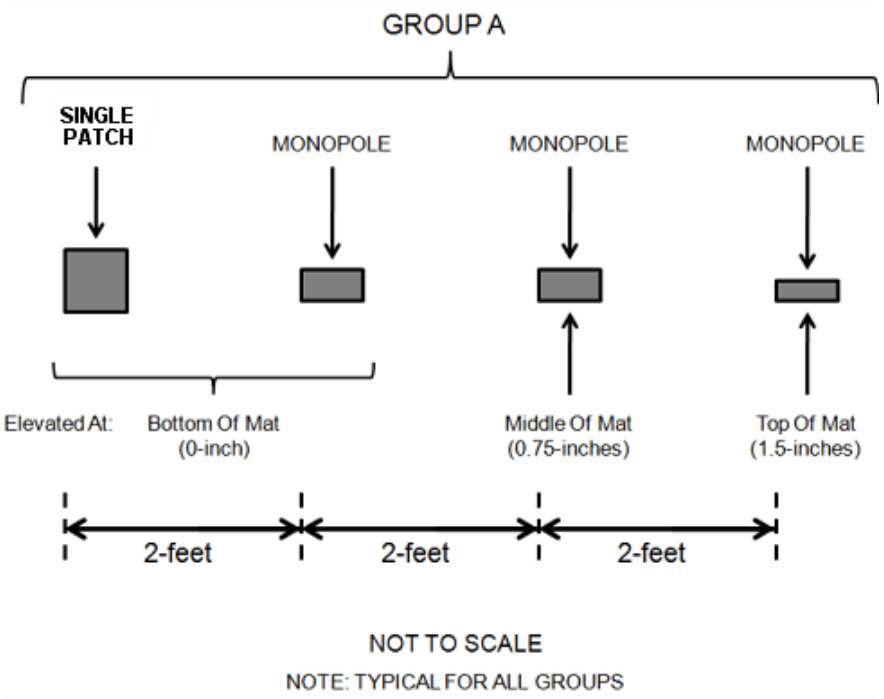

1 ft = 0.305 m
1 inch = 25.4 mm

Figure 98. Drawing. Detailed plan view of a single group of SAW RFID tags.

As previously described, all of the tags except for eight "top of mat" surface tags were encapsulated in a relatively rigid thermally conductive epoxy. All tags other than those used for the surface were affixed to the milled existing pavement surface using quick-hardening epoxy putty (Loctite® 5-Minute Epoxy Putty). The mounted tags were oriented so that their ceramic chip and antenna were facing upward to enhance their readability. The unencapsulated surface tags were placed face down into the asphalt by the contractor immediately after passage of the paver. Figure 99 shows the tags being placed on the milled surface.

The RF SAW tag reader and circularly polarized antenna were mounted on a long-handled wheeled carriage to read the tags from the side of the road during compaction operations. The antenna was elevated about 1 ft (0.3 m) above the pavement surface. The wheeled apparatus was manually operated to minimize any disturbance to the hot asphalt or disruption of the compaction operations while the lift was cooling and being compacted. The reader was cabled to a laptop computer that recorded temperature and tag signal strength during testing.

Figure 99. Photo. Placement of SAW RFID tags on surface of existing milled pavement.

The reader software requires that the operator specify a temperature window prior to reading the tags; the manufacturer recommends a 86 °F (30 °C) temperature window. This temperature window may be widened; however, the software signal processing time becomes longer. A longer signal processing time has been known to decrease the signal strength/response of the tag, especially when the tag is embedded in attenuating materials.

Thermal lag added another complication to obtaining good early temperature readings from the encapsulated tags immediately after they were covered with hot HMA. As described previously, thermal lag is the time required for the encapsulated tags to "heat up" to the temperature of the surrounding material. Results from the laboratory study suggested that the thermal lag for encapsulated tags is about 3 to 8 min, depending on the tag type; encapsulated single patch tags experience the longest thermal lag. The laboratory thermal sensitivity study also suggested that unencapsulated tags at the surface would exhibit only about 1 to 2 min of thermal lag.

The estimated temperature window immediately after placement of the overlay was set at 230 to 284 °F (110 to 140 °C). Initially, no response could be obtained from any tag. After the temperature window on the reader was adjusted downward to 176 to 230 °F (80 to 110 °C), some tags were read successfully at about 8 min after paving. The manufacturer-recommended temperature window of 86 °F (30 °C) was used throughout the field trials. However, during the initial heating of the tags (thermal lag) and rapid cooling of the mat immediately after placement, it proved difficult to adjust the temperature window on the reader quickly enough to capture the initial tag temperatures.

The wheeled reader and antenna apparatus was initially passed over the "Group A" tags (see figure 97 and figure 98), then "Group B," then "Group C," and so on, after which the cycle was

repeated. The data collected during testing included the tag identification number, the time/date stamp of the last reading during the antenna pass, the tag distance from the antenna at the last reading, and the temperature at the last reading. Note that even if multiple reads were obtained from a tag during a given pass, the reader software saved only the data from the last read. Four full cycles of readings from Groups A through I were performed until the mat had cooled sufficiently that the vibratory compactors moved on to other sections. Prior to each pass, the reader software temperature window was adjusted for the decreasing temperature conditions. Figure 100 shows the paving operation and test setup during construction.

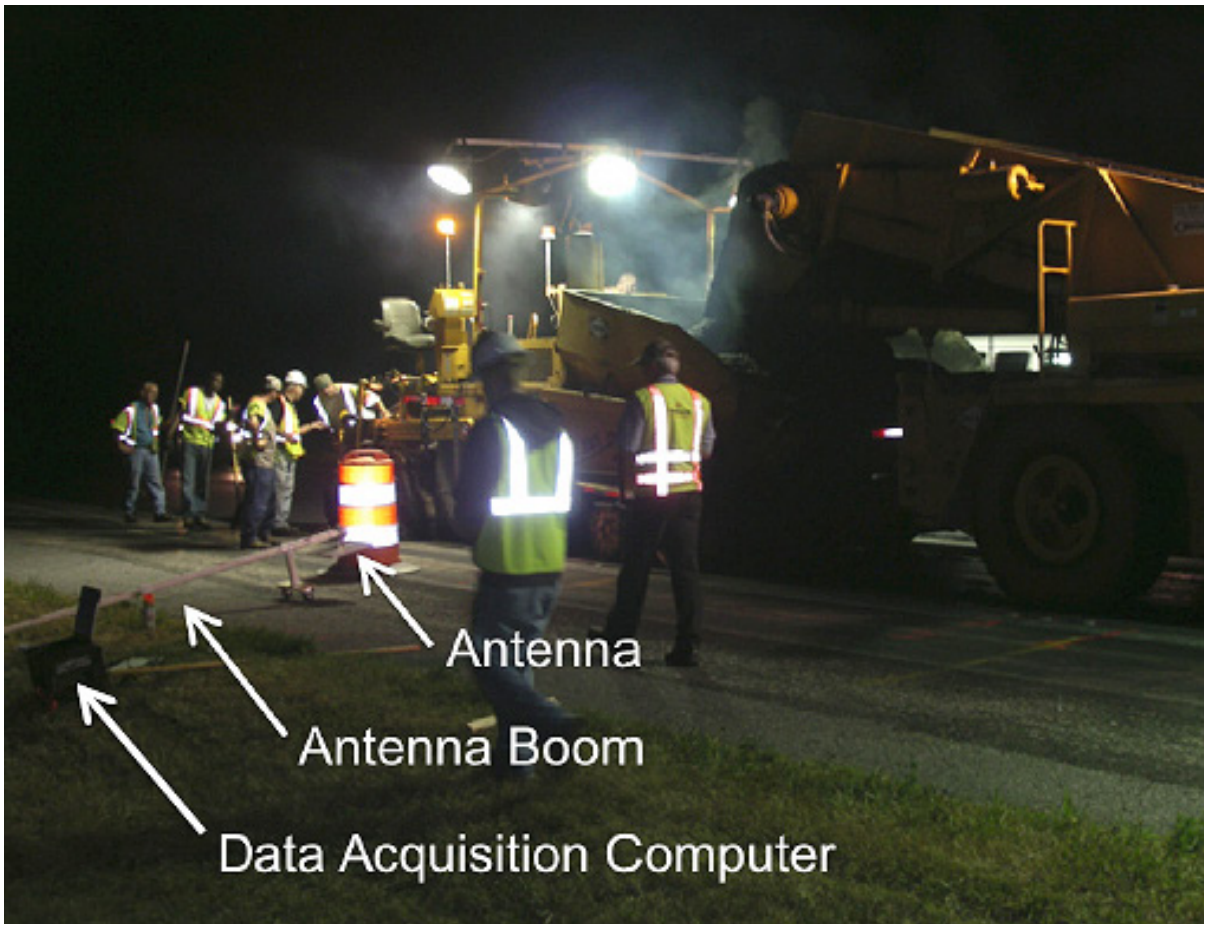

Figure 100. Photo. Paving operation and test setup during construction.

Field Test Results

After the hot-mix asphalt had been placed on the first groups of tags (Groups A through C), the vibratory compactors passed the testing area for a few minutes. Additional time was required to configure the reader software with a proper temperature window to read the tags. Consequently, the first tag reads were obtained about 8 min (± 1 min) after the tags were covered with asphalt. Readings were than taken for approximately the next hour, continuing after the vibratory compactors had moved on to subsequent sections of pavement.

Overall, the temperatures at the bottom of the mat decreased from 198 to 135 °F (92 to 57 °C) during the cooling period monitored in this study. At the middle of the mat and on the surface,

temperatures generally decreased from 208 to 133 °F (98 to 56 °C) and from 219 to 111 °F (104 to 44 °C), respectively. Table 19 summarizes the read success rates for the tags. Five of the 30 preplaced tags could not be read successfully during system testing prior to paving operations. This is likely owing to damage caused by their removal from the roadway surface the night before and/or their preparation for reuse by grinding off the hardened epoxy putty. The read rates after asphalt placement and during compaction increased from 28 percent during the first pass to 52 percent in the fourth. This should not, however, be interpreted as an increase in the inherent read rate with time. Rather, this increase is because it was easier to set an appropriate temperature window in the reader software during the slower cooling of the later passes than during the rapid cooling in the first pass.

Table 19. Tag read rates.

Paver Pass	Tag Count	Total Possible	Reading (percent)
Pre-Paving	25	30	83
Pass 1	11	40	28
Pass 2	19	40	48
Pass 3	22	40	55
Pass 4	21	40	52

Evaluations of the cooling HMA temperatures with depth and time were performed at two transverse cross sections: Groups A-D-F-H and B-E-G-I. Results from cross section B-E-G-I are described here; the results from cross section A-D-F-H were very similar. Plots illustrating temperature versus time since paving are given in figure 101 through figure 103 for the bottom, mid-thickness, and surface of the mat, respectively. "Time since paving" is the estimated elapsed time after the tags are covered with the asphalt by the paver.

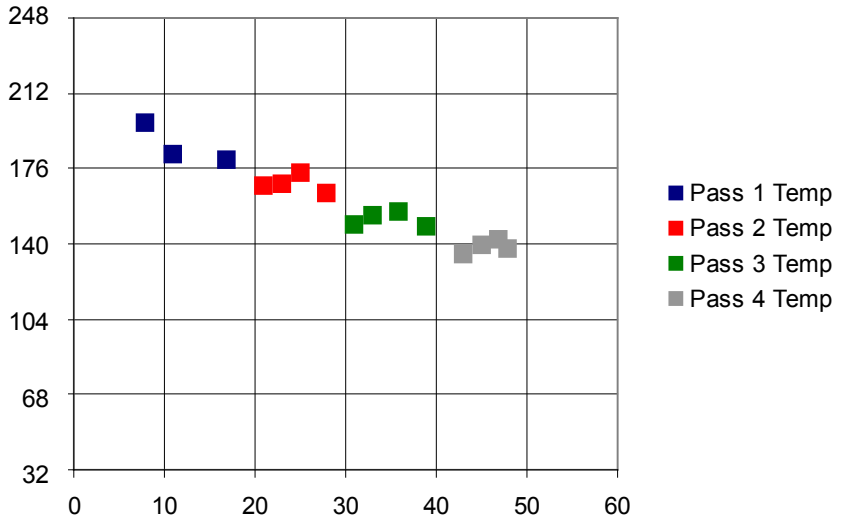

°C = (°F – 32)/1.8

Figure 101. Graph. Temperature versus time at bottom of mat (cross section B-E-G-I).

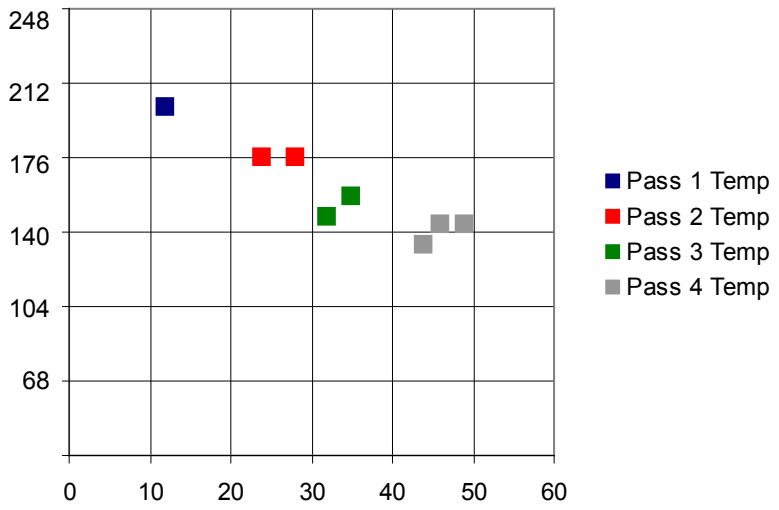

°C = (°F – 32)/1.8

Figure 102. Graph. Temperature versus time at middle of mat (cross section B-E-G-I).

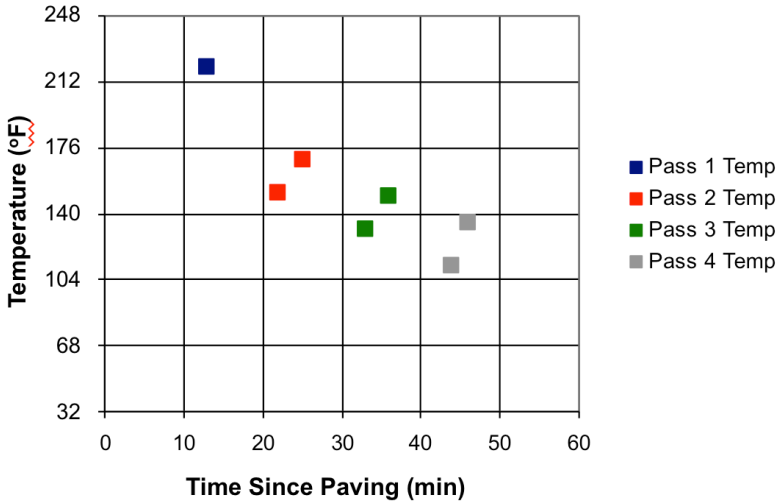

°C = (°F – 32)/1.8

Figure 103. Graph. Temperature versus time at surface of mat (cross section B-E-G-I).

As shown in the figures, the temperatures measured by the tags decreased with every compaction pass. Based on these test results and theoretical expectations for typical mat cooling trends, exponential regression lines were fit to the data. Figure 104 summarizes the cooling trends segregated by location within the mat thickness.

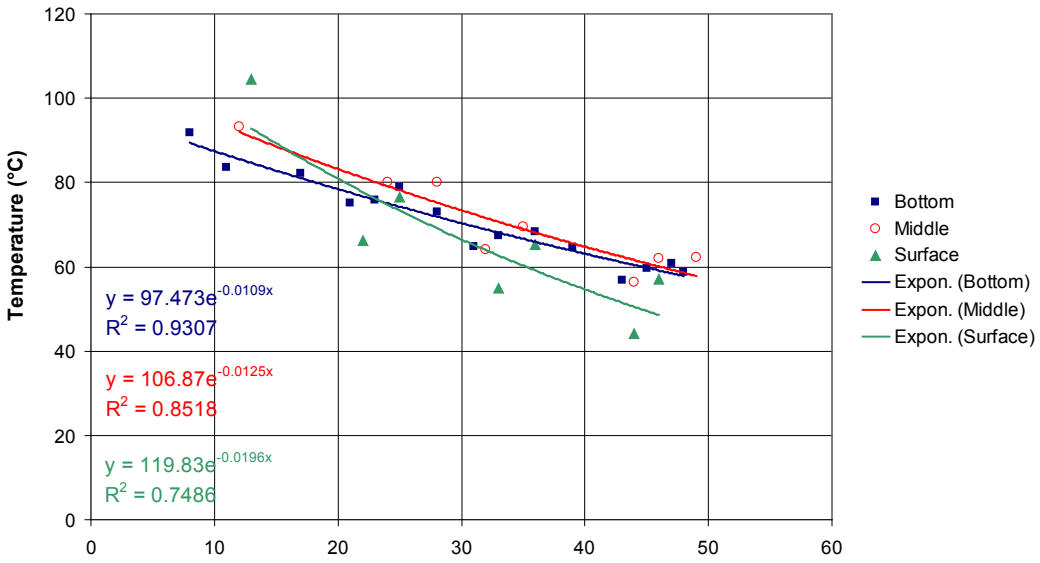

°F = (°C x 1.8) + 32

Figure 104. Graph. Temperature versus time segregated by location (cross section B-E-G-I).

The similarities between the regression lines shown on figure 104 are not suggestive of any systematic variations in temperature through the depth of the mat. This is likely because of the thinness of the overlay (1.5 inches (38 mm)) and other limitations of the test (inaccuracies in the depth of the tags and nonuniformity of initial paving temperatures). Therefore, all depth locations were combined, and a single exponential regression equation was fit to the combined dataset, as shown in figure 105.

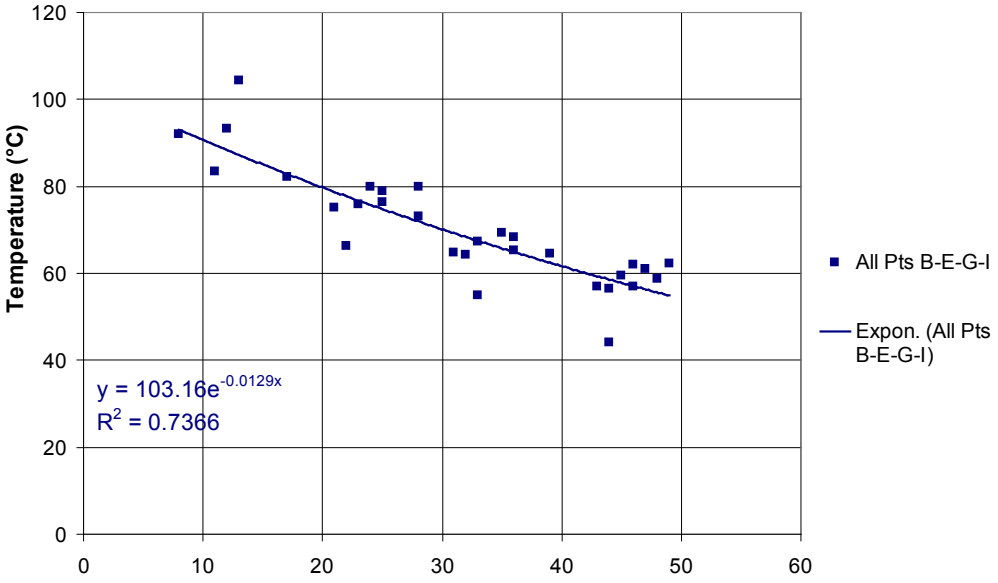

.

°F = (°C x 1.8) + 32

Figure 105. Graph. Temperature versus time averaged across depth (cross section B-E-G-I).

The exponential regression equation for the mat cooling at cross section B-E-G-I is shown in figure 106.

$$T = 103.16e^{-0.013t} \qquad R^2 = 0.737$$

Figure 106. Equation. Exponential cooling equation at cross section B-E-G-I.

The corresponding regression equation for the mat cooling at cross section A-D-F-H is shown in figure 107:

$$T = 101.87e^{-0.0096t} \qquad R^2 = 0.750$$

Figure 107. Equation. Exponential cooling equation at cross section A-D-F-H.

These regression equations for the combined data are the basis for evaluating the traditional mat cooling models from the literature.

Variability and Reliability

In an effort to determine the reliability of the field test results and the consistency of the data collected, the following additional evaluations were made:

- Comparison of measured temperatures reported by single patch and monopole SAW RFID tags placed at the same location at the bottom of the mat.
- Comparisons of surface temperatures measured with the SAW RFID tags against independent measurements using a Fluke® infrared thermometer.
- Additional laboratory testing to determine the variability of temperature measurements from the SAW RFID tags based on errors generated by the reader.

These variability and reliability analyses were performed on the temperature data recorded from cross sections B-E-G-I and A-D-F-H.

To determine whether there were any systematic differences between the single patch and monopole tags, pairs of each were placed at the bottom of the mat approximately 2 ft (0.6 m) apart within each group (see figure 97 and figure 98). A comparison of the temperatures measured by each tag type is presented in figure 108, figure 109, and table 20.

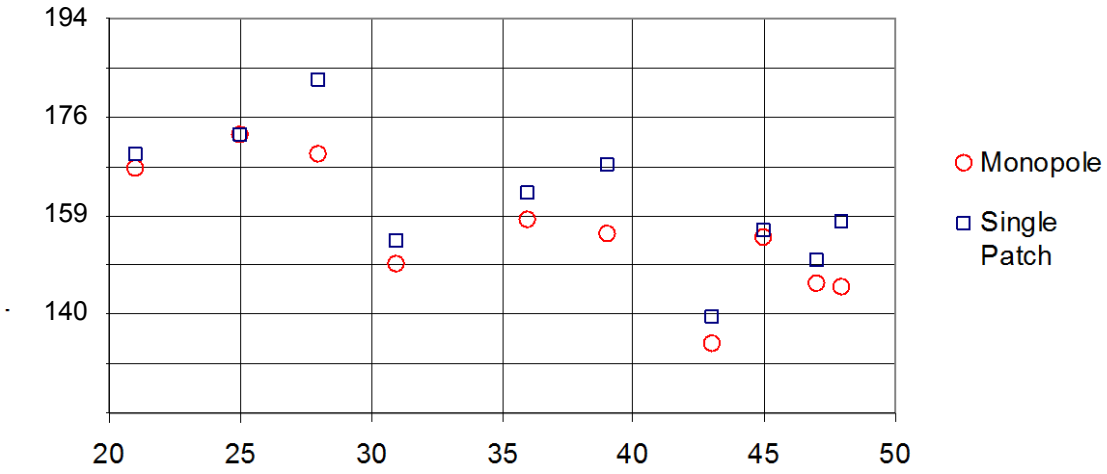

°C = (°F – 32)/1.8

Figure 108. Graph. Comparison of temperatures by tag type (cross section A-D-F-H, bottom of mat).

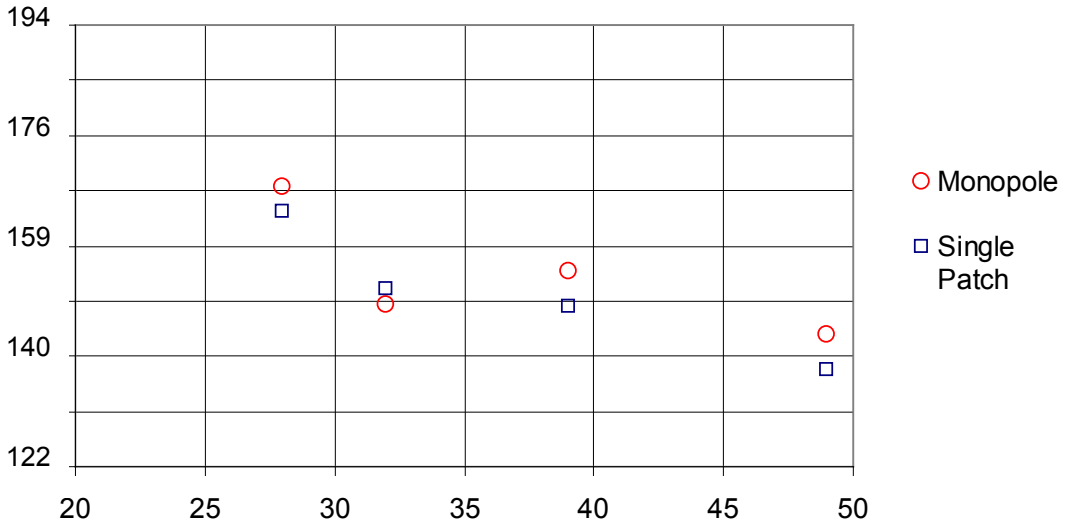

°C = (°F – 32)/1.8

Figure 109. Graph. Comparison of temperatures by tag type (cross section B-E-G-I, bottom of mat).

Table 20. Temperature comparisons at bottom of mat.

Cross Section A-D-F-H				Cross Section B-E-G-I			
Monopole Temperature (°F)	Single Patch Temperature (°F)	Time (min)	Difference (percent)	Monopole Temperature (°F)	Single Patch Temperature (°F)	Time (min)	Difference (percent)
166.5	169.0	21	1.84	167.5	163.6	28	2.92
172.8	172.8	25	0.00	148.5	151.0	32	2.12
169.2	182.7	28	8.96	153.9	148.1	39	4.73
149.0	153.3	31	3.56	143.4	137.7	49	5.17
157.1	162.0	36	3.74	—	—	—	—
154.8	167.2	39	9.19	—	——	—	—
134.6	139.3	43	4.36	—	—	—	—
153.9	155.1	45	1.02	—	—	—	—
145.6	149.9	47	3.66	—	—	—	—
144.9	156.7	48	9.52	—	—	—	—

— Indicates no data collected
°C = (°F – 32)/1.8

The maximum difference in temperature measured by the two types of tags at the bottom of the mat was about 9 percent for cross section A-D-F-H at 28, 39, and 48 min after paving. The average temperature difference for all of the tags was 4.6 percent at cross section A-D-F-H (standard deviation of 3.5 percent) and 3.7 percent at cross section B-E-G-I (standard deviation of 1.4 percent). These differing temperatures may be due to a general inaccuracy of the tags (possibly a systematic bias) or to spatial variability. However, on average, the temperatures were consistent within a 5-percent difference.

Comparisons were also made between surface temperatures measured using the SAW monopole RFID tags and independent measurements using a Fluke® infrared digital thermometer are summarized in figure 110 and table 21. More significant temperature variations are exhibited in this comparison; the maximum temperature difference was about 30 percent at 22 and 45 min and about 25 percent at 32 min. In addition, the difference is widely sporadic and inconsistent (ranging from approximately 7 to 30 percent). This may be the result of the different technologies between the Fluke® thermometer and the SAW RFID tags or spatial variability of the temperature distributions as the locations of the infrared readings were as much as several feet from the corresponding SAW RFID measurements. A more thorough explanation may require additional laboratory and/or field testing.

An additional laboratory study was performed to determine the inherent variability of the temperature measurements from the SAW RFID tags. The study was performed at constant room temperature. Repeated readings were taken to determine any fluctuating temperature readings caused by the SAW tags and reader rather than the environment. The result of the test found a negligible fluctuation of about ± 0.36 °F (± 0.2 °C). The manufacturer also states that transmission interferences (wireless communication and magnetic fields) may contribute to inaccuracies. However, this is unlikely to have been a major factor in the field trials.

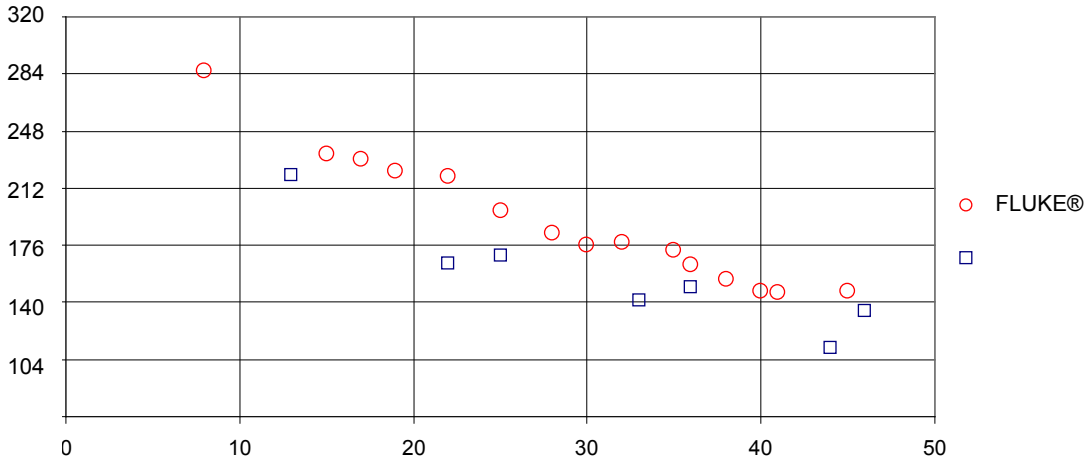

°C = (°F – 32)/1.8

Figure 110. Graph. Surface temperatures measured by SAW RFID tags versus Fluke® infrared thermometer.

Table 21. Temperature comparisons at top of mat.

Fluke® Readings		Surface Tag Readings		
Time (min)	Temperature (°F)	Time	Temperature (°F)	Difference (percent)
8	286	—	—	—
15	234	13	220	6.8
17	230	—	—	—
19	223	—	—	—
22	219	22	164	29.4
25	198	25	170	17.0
28	183	—	—	—
30	176	—	—	—
32	178	33	142	24.9
35	172	—	—	—
36	163	36	150	10.4
38	154	—	—	—
40	147	—	—	—
41	146	—	—	—
45	147	44	112	30.7

— Indicates data not available
°C = (°F – 32)/1.8

Conclusions: Field Evaluation

The overall findings from the field trials indicate that the SAW RFID tags can be used for measuring mat cooling temperatures during HMA construction. It is important, however, to understand that SAW RFID is still a developing technology—certain limitations and imperfections exist, but improvements in the technology are to be expected in the future. Specific conclusions related to various aspects of the field evaluation are described below.

Field Test Performance

- A temperature window must be specified in the RF SAW reader software to be able to read the in-place tags. This requirement may and did lead to operational issues in the field, particularly during the early stages of mat cooling when the temperature dropped rapidly, causing difficulty in setting the correct temperature window.

- The manufacturer recommends a 86 °F (30 °C) temperature window based on their calibration techniques at room temperature. The temperature window may be widened, but the software signal processing time then becomes longer and the signal strength/response of the tags decreases. The manufacturer's recommended temperature window of 86 °F (30 °C) was used for all of the field trials.

- There was difficulty differentiating physically damaged tags from those that simply could not be read immediately after paving/compaction. In other words, if a tag is nonresponsive to the reader, it might not be caused by destruction by vibratory compaction. It may be that the reader cannot get a response because the temperature window is incorrect or the tag signal is severely attenuated.

Field Test Results

- The field results generally show an exponential relationship between cooling temperatures and time. This generally agrees with theoretical considerations that suggest exponential cooling.

- No systematic temperature variations with depth were observed during mat cooling. In other words, the measured temperatures at the bottom, middle, and top of the asphalt mat, at any given location and time, were all within the variability range of the sensors. This may simply be a consequence of the thinness of the lift on this particular project.

Variability and Reliability

- Based on the comparative study at the bottom of the mat between the two types of tags (single patch and monopole) and previous laboratory testing, the temperatures recorded by the two tag types are reasonably consistent and accurate.

- The comparative study at the surface of the mat between the Fluke® infrared thermometer and monopole tag found inconsistencies between the two sets of readings. This may due to spatial variability. Additional field and/or laboratory testing are required for further explanation.

COMPARISONS BETWEEN PREDICTED AND MEASURED MAT COOLING

The mat cooling response measured using the SAW RFID tags is compared with the predicted temperatures versus time and depth from theoretical/numerical models. As will be described later, these comparisons require some field calibration of the model input parameters, given that there are no laboratory-measured values of the thermal properties for the mix placed at the field test site. The principal objectives of the comparisons between measured and predicted cooling response are the following:

- Determine whether the use of RFID technology to measure HMA cooling temperatures was accurate and successful.

- Identify improvements in the overall process of measuring mat cooling temperatures using RFID technology.

- Calibrate via a sensitivity analysis the values for the model input parameters that provide reasonable and close agreement with the field measured temperatures.

Analysis Inputs

The finite difference calculations for the analyses are based on figure 68 for the conduction calculations at the interior points and figure 72 for the heat balance at the mat surface. Table 22 summarizes the input parameter values used for the model predictions. These were selected based on recommendations from previous investigations and the results of the input parameter optimization presented later. Because the field construction was performed at night, the impacts of solar radiation (H_S) and absorptivity (a) are negligible. The convective heat transfer coefficient value corresponds to free convection at zero wind velocity. This is consistent with weather station data at the time of paving.

Table 22. Input parameters used in models.

Property	Units	Symbol	Used
Thermal conductivity	BTU/ft-h-°F	k	0.64
Thermal diffusivity	ft^2/h	α	0.0213
Convective heat transfer coefficient	Dimensionless	h	1.30
Thermal emissivity	Dimensionless	ε	0.95

1 BTU/ft-h-^oF = 1.73 W/m-^oK
1 ft^2/h = 0.093 m^2/h

The depth and time increments for the finite difference calculations are summarized in table 23. Temperatures are calculated every 0.25 inches (6.4 mm) of depth through the 1.5-inch (38-mm) overlay and for an additional 6 inches (150 mm) into the underlying asphalt base. This is assumed to be a sufficient depth across which conductive heat flows are negligible over the duration of the analyses. The time step shown in figure 111 was selected to satisfy the stability requirement for the Euler time integration algorithm:

$$\Delta t \leq \frac{\Delta y^2}{2\alpha}$$

Figure 111. Equation. Stability requirement for Euler time integration algorithm.

The temperature at the lower boundary was fixed at 81 °F and the ambient air temperature was set at 71 °F. The initial conditions are a uniform 305 °F temperature for the HMA in the overlay and a uniform 81 ^oF temperature in the underlying base asphalt. The base asphalt and ambient air temperatures were measured during the field trials. The initial HMA temperature of the overlay was provided by MDSHA.

Table 23. Input parameters used in finite difference solution.

Calculation Parameter	Minimum Value	Maximum Value	Step Increment
Depth step, Δy (inches)	0	7½	¼
Time step, Δt (min)	0	60	~ 0.3

1 inch = 25.4 mm

Predicted Mat Cooling Response

Figure 112 illustrates the predicted temperature versus time trends at the bottom, middle, and surface of the overlay and the average predicted temperature through the overlay thickness. As shown in the figure, the bottom of the mat expels the most heat initially, but as time elapses, the surface expels more heat than the bottom. These trends are consistent with those observed by Jordan and Thomas.[16] Figure 113 displays these cooling trends more explicitly as changes in temperature per time step versus time. The temperature at the bottom of the mat initially drops more than 20 °F (11.2 °C) and then exponentially drops another 1 °F (0.56 °C) over the rest of the cooling process. The temperature of the surface of the mat initially drops about 13 °F (7.2 °C) and then, at about 2 min, begins to expel more heat than the bottom of the mat.

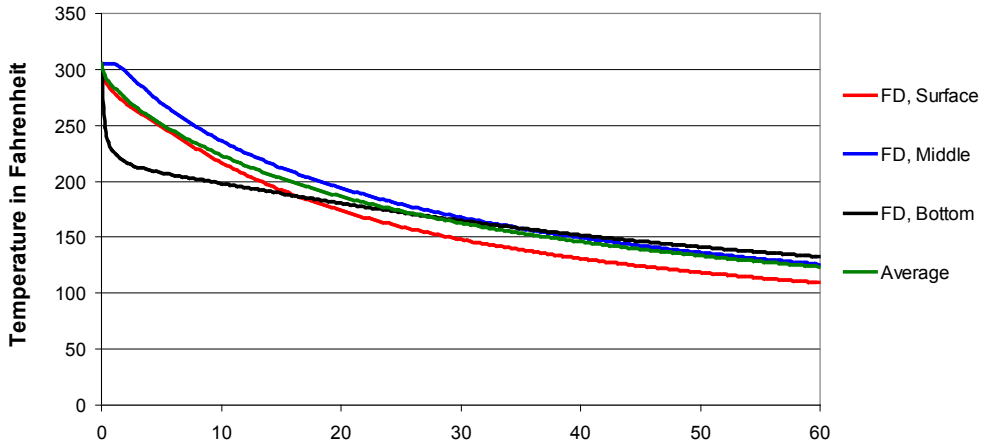

°C = (°F – 32)/1.8

Figure 112. Graph. Finite difference solutions for bottom, middle, and surface of mat.

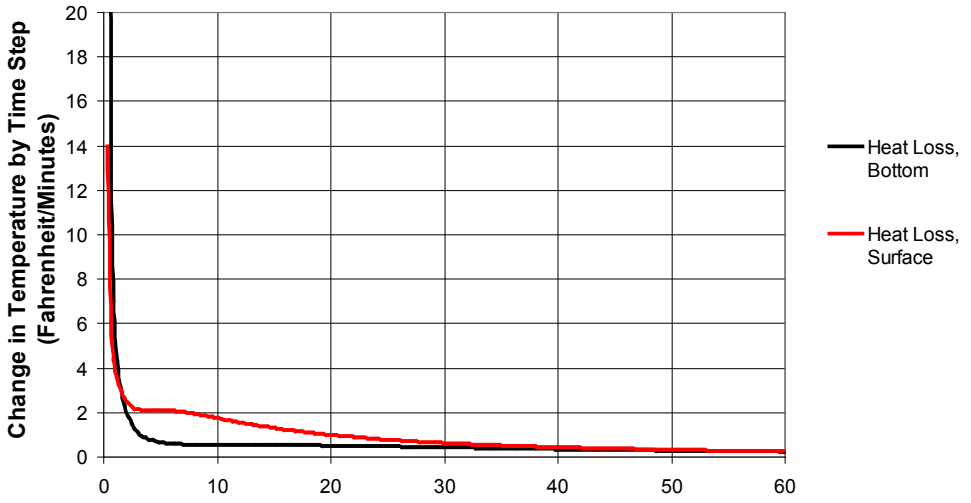

°C = (°F – 32)/1.8

Figure 113. Graph. Cooling trends at the bottom and surface of the asphalt mat.

Figure 114 displays the temperature trends of the asphalt base as it heats and then cools as a result of conductive heat transfer from/to the HMA overlay. The asphalt base has an initial temperature of 81 °F and, upon placement of the hot HMA overlay, rapidly heats up via conduction. Over time, as the HMA overlay cools by convection and radiation, the heated base material cools along with the overlay. These cooling trends are logical and match physical expectations.

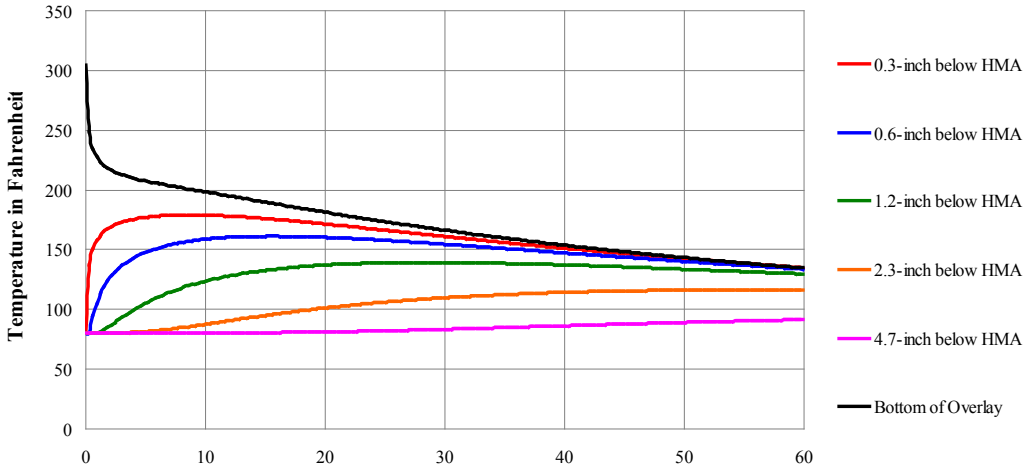

1 inch = 25.4 mm
°C = (°F – 32)/1.8

Figure 114. Graph. Base material temperatures cooling over time due to conductive heat transfer.

The decrease in temperature changes versus time at increasing depths within the base layer suggests that the arbitrary 6-inch (150-mm) depth for the lower fixed temperature boundary is

sufficiently distant. As additional confirmation, figure 115 compares predicted cooling curves assuming base thicknesses of 0, 1, 3, 6, and 8 inches (0 25, 75, 150, and 200 mm). The cooling curves stabilize once the thickness of the base material exceeds 3 inches (75 mm).

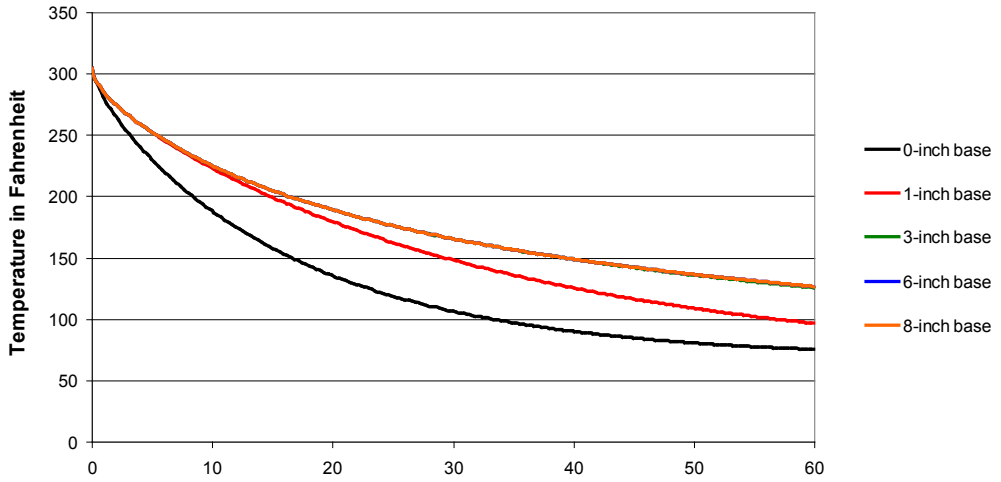

1 inch = 25.4 mm
°C = (°F – 32)/1.8

Figure 115. Graph. Impact of lower boundary depth on average predicted temperature profile.

The results in figure 112 through figure 115 all suggest that the finite difference solutions are correct and a relatively accurate representation of field conditions. Figure 116 and figure 117 compare the calculated temperature trends at the surface, middle, and bottom of the mat with the corresponding measured data from cross sections A-D-F-H and B-E-G-I, respectively. As an additional check on accuracy of the predictions, Figure 118 compares the calculated temperatures at the surface against measured values obtained using the Fluke® infrared thermometer.

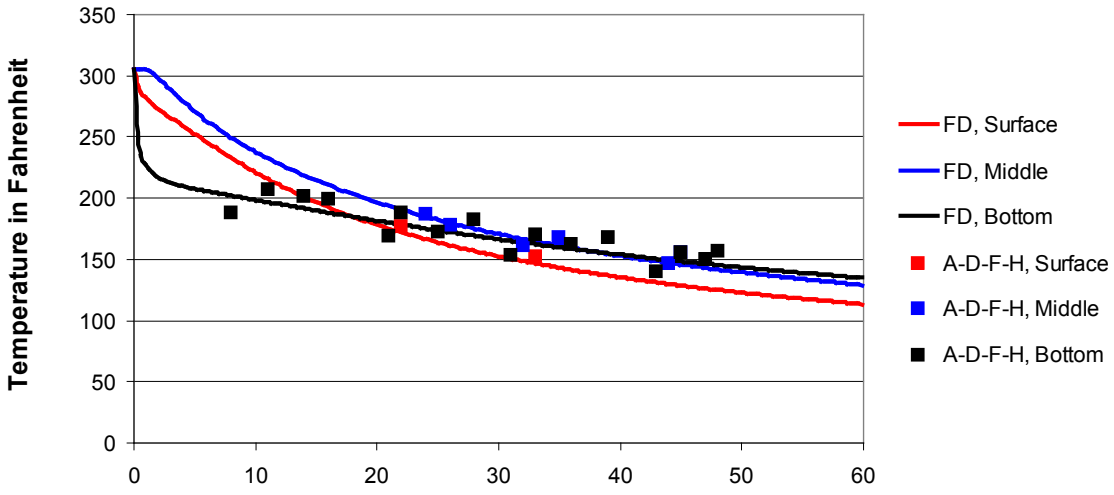

°C = (°F – 32)/1.8

Figure 116. Graph. Predicted versus measured temperatures at cross section A-D-F-H.

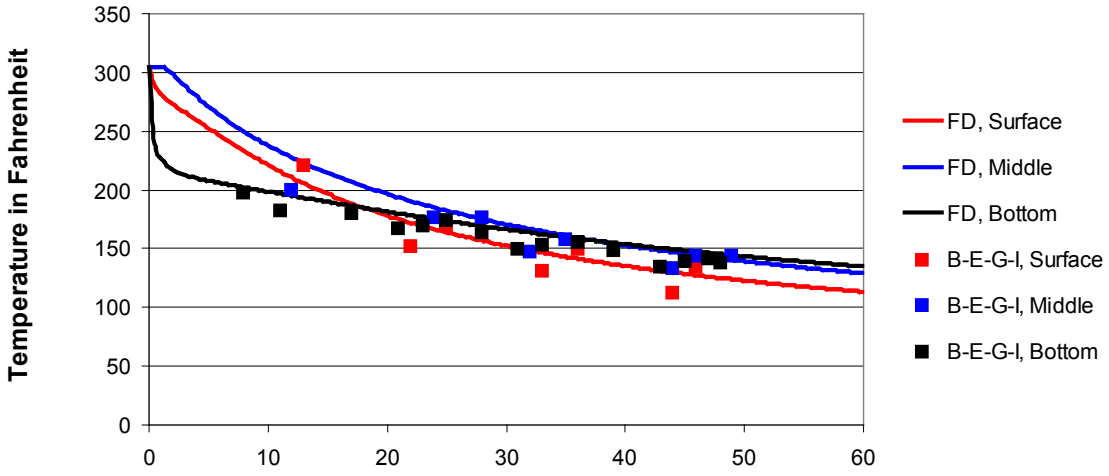

°C = (°F – 32)/1.8

Figure 117. Graph. Predicted versus measured temperatures at cross section B-E-G-I.

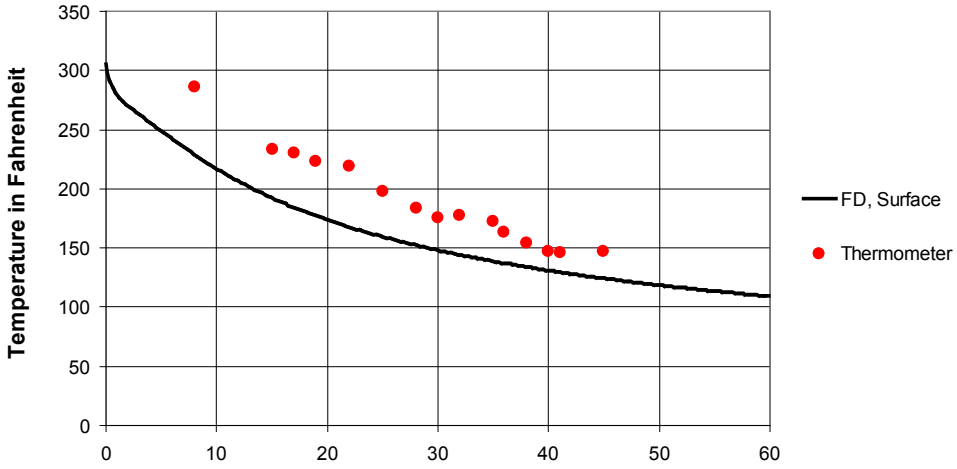

°C = (°F – 32)/1.8

Figure 118. Graph. Predicted versus measured surface temperatures.

The results in figure 116 and figure 117 show generally good agreement between measured and predicted temperatures over time. However, it is difficult to discern any systematic correlations between the calculated curves and the measured temperature values as a function of depth. This is most likely due to the thinness of the overlay and the imprecision in locating the RFID temperature sensors at specific depths. The comparison in figure 118 between the predicted temperatures at the surface and the measured values as obtained by the infrared thermometer are good in terms of trends, but the measured temperatures are consistently higher than the predicted values. This may indicate either errors in the finite difference predictions at the surface or, as

described previously, inaccuracies in the infrared temperature measurements due to spatial variability.

Because it was impossible to detect any systematic variations in measured temperatures through the depth, all depth locations were combined and fit with an exponential regression equation at each cross section as presented earlier in figure 106 and figure 107 for cross sections A-D-F-H and B-E-G-I, respectively. Figure 119 and figure 120 show the comparisons between the predicted temperatures and the exponential fits to the measured temperatures at the respective cross sections; figure 121shows the combined results from the two cross sections.

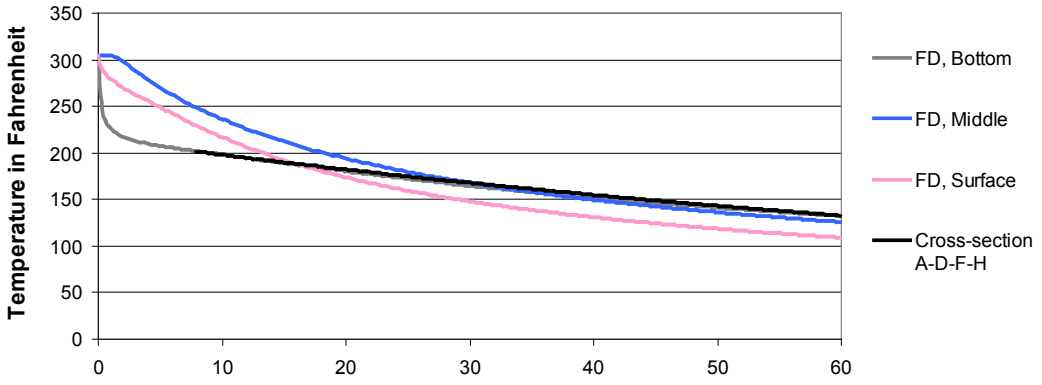

°C = (°F – 32)/1.8

Figure 119. Graph. Average measured versus predicted mat cooling at cross section A-D-F-H.

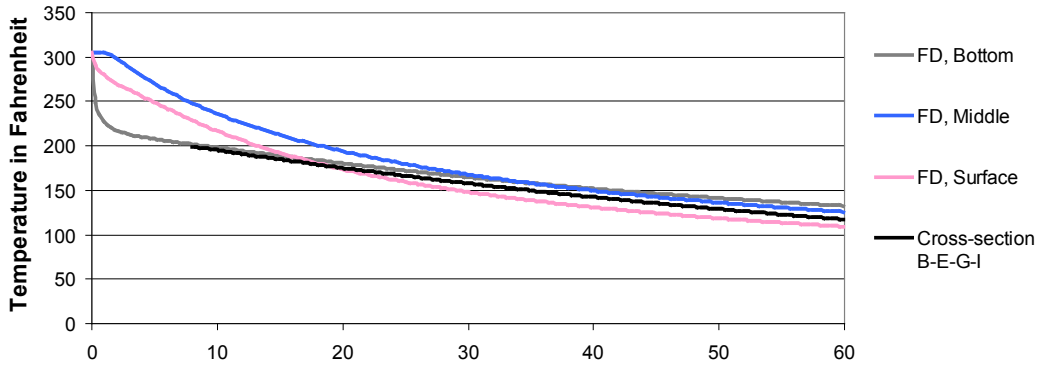

°C = (°F – 32)/1.8

Figure 120. Graph. Average measured versus predicted mat cooling at cross section B-E-G-I.

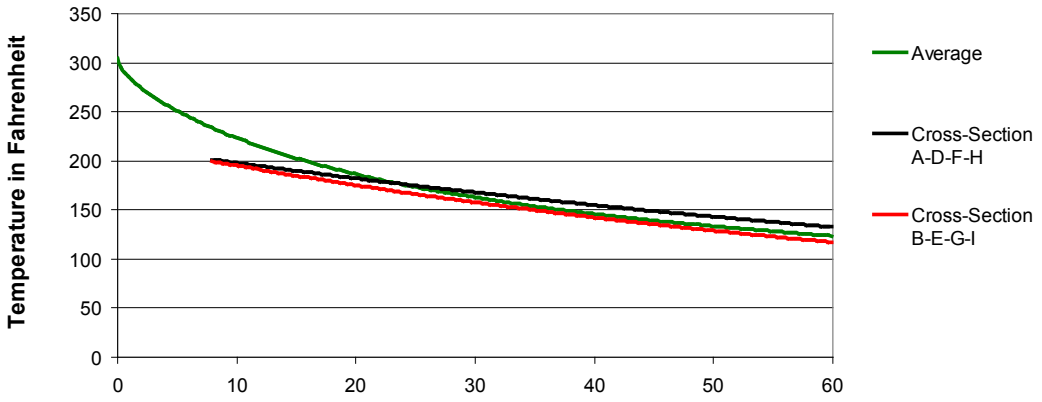

°C = (°F – 32)/1.8

Figure 121. Graph. Average measured versus average predicted mat cooling.

The following observations can be made from the results in figure 119 through figure 121:

- The curvatures of the measured exponential curves are relatively close to the calculated curve, with the exception of the early portion of the response. However, in terms of temperature accuracy, the average curve and exponential curves begin to show a close correlation only after about 15 to 20 min after paving. The early-stage comparisons are complicated by the fact that the tags did not return any data until about 8 min after paving. Nonetheless, it seems clear that the tag and calculated temperatures are not consistent in trend and curvature during the early stages of cooling. Further field investigations may be required determine the causes for this inconsistency.

- Experience suggests that an average mat temperature of 175 °F (79 °C) is the threshold below which compaction is no longer economical or may even be injurious to the pavement (e.g., because of aggregate breakage). Therefore, temperature data from the time of initial paving to when it reaches 175 °F (79 °C) are considered the most valuable. Figure 122 superimposes the 175 °F (79 °C) line on the data from figure 122. The predicted and measured temperature data show close agreement only for about the last 5 to 10 min before the curves meeting the 175 °F (79 °C) threshold.

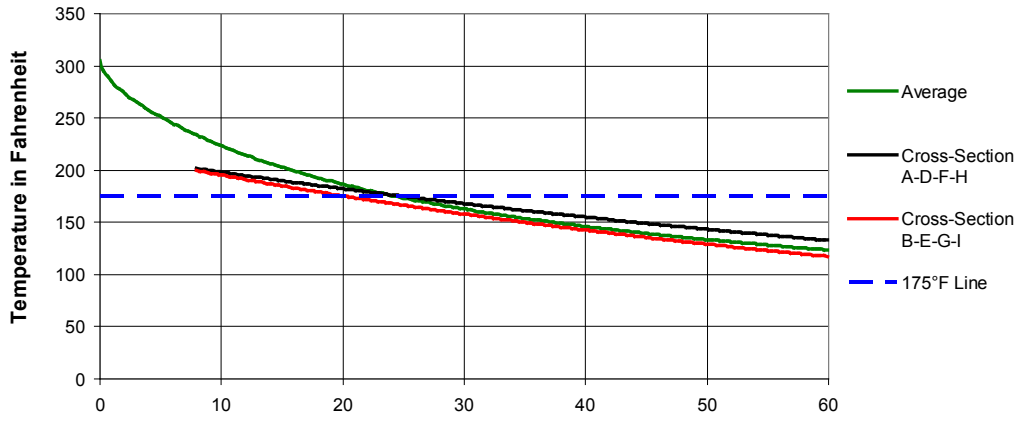

°C = (°F – 32)/1.8

Figure 122. Graph. Measured curves compared with calculated average curve with 175 °F line.

Conclusions: Comparisons Between Predicted and Measured Mat Cooling

The SAW RFID tags and equipment were successful in measuring the mat cooling temperatures during hot-mix asphalt placement. Comparisons with predictions from the finite difference computational models were generally favorable. However, there are inconsistencies between the predicted and measured temperatures, particularly during the early stages of the cooling response that may be due to limitations in technology, operator error, modeling error, or other causes. Further study is recommended to investigate and/or address the following:

- Recording temperature data immediately after paving rather than a few minutes afterward. This may be accomplished by preheating the tags to the initial asphalt temperature. The RF SAW reader software can then be adjusted more easily to read the tags immediately after paving.

- Improvement in the RF SAW reader and software to eliminate the need to set a temperature window.

- Performance of more field trials that incorporate traditional temperature measuring instrumentation (e.g., thermocouples). Comparing the SAW RFID with the traditional instrumentation should identify any limitations or inaccuracies in the SAW RFID technology in this application.

- Determine an encapsulation method and material that optimizes the functionality of the tag in terms of readability, thermal response, and physical survivability.

SENSITIVITY ANALYSIS AND CALIBRATION TECHNIQUES

No laboratory tests to determine the input parameter values for the mat cooling model were performed in this study. Instead, typical initial estimates of the input parameter values were obtained from the literature. However, these values varied widely among the citations, and the

appropriateness of some of the recommended values was suspect. A series of sensitivity and calibration analyses were therefore performed to determine better values for the model input parameters to use in the numerical simulations described in the preceding section. These analyses provided additional confidence and validation that the numerical solutions are logical and correct as well as producing field-calibrated values for the inputs. The following subsections detail sensitivity analyses for the following inputs: thermal diffusivity and thermal conductivity, convective heat transfer coefficient, and emissivity. A calibration procedure to determine the input parameter values that produce the best fit between the measured and calculated temperatures is also described. This field calibration technique enables accurate predictions from the mat cooling model in the absence of laboratory measured input parameters.

Thermal Diffusivity and Conductivity

As described earlier, Luca and Mrawira conducted laboratory experiments to identify thermal properties for Superpave mixtures.[21] They measured thermal diffusivity α and thermal conductivity k and compared their measured values with ranges cited in the literature (table 15 and table 16, respectively).

The sensitivity analyses aim to determine how changes in thermal diffusivity and conduction affect the curvature, rate of cooling, and other characteristics of the predicted cooling response. Note that changes in thermal diffusivity also imply changes in the analysis time step to satisfy the stability requirement for the Euler time-integration algorithm as given by figure 111.

As shown in table 15, Luca and Mrawira found that thermal diffusivity may range from 1.35×10^{-2} to 3.20×10^{-2} ft^2/h (1.25×10^{-3} to 2.98×10^{-3} m^2/h). Five sample values within this range were therefore selected for the sensitivity analysis: 1.35×10^{-2}, 1.56×10^{-2}, 2.13×10^{-2}, 2.24×10^{-2}, and 3.20×10^{-2} ft^2/h (1.25×10^{-3}, 1.45×10^{-3}, 1.98×10^{-3}, 2.08×10^{-3}, and 2.98×10^{-3} m^2/h). Similarly, Luca and Mrawira found that thermal conductivity may range from 0.58 to 2.24 BTU/ft-h-°F (1.0 to 3.9 W/m-°K) (table 16). Four sampled values within this range were therefore selected for the sensitivity analysis: 0.58, 0.64, 1.01, 1.19, and 2.24 BTU/ft-h-°F (1.00, 1.11, 1.75, 2.06, and 3.88 W/m-°K). Luca and Mrawira emphasized that thermal diffusivity and conductivity are generally difficult to predict and measure. Therefore, parameter values that fall outside the ranges in table 15 and table 16 should not be considered infeasible.

Figure 123 and figure 124 illustrate the results of the sensitivity analyses for thermal diffusivity and conductivity. Changing either the thermal diffusivity or the thermal conductivity values significantly affects the curvature and rate of cooling of the predicted mat cooling response. When interpreting the results in figure 123 and figure 124, it is important to remember that thermal diffusivity and conductivity are interrelated (see figure 65). Figure 123 shows that the rate of cooling increases with increasing thermal diffusivity. This is sensible; from figure 65, increasing α at constant k implies a decreasing specific heat capacity C_p, i.e., decreasing thermal inertia, hence a faster cooling rate. Figure 124 shows that the rate of cooling decreases with increasing thermal conductivity. At first glance, this appears paradoxical, because one would intuitively expect that an increased ability to conduct heat would lead to faster cooling. However, the observed behavior is indeed sensible given the relationship in figure 65: increasing k at constant α implies increasing specific heat capacity, i.e., increasing thermal inertia, hence a slower cooling rate.

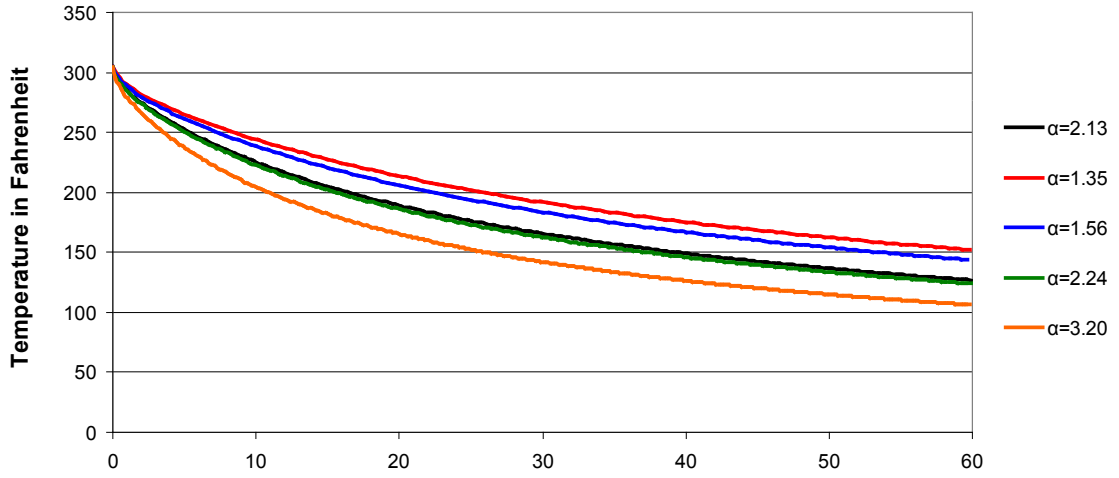

k = 0.64 BTU/ft-h-°F (1.10W/m-°K)
°C = (°F – 32)/1.8

Figure 123. Graph. Sensitivity analysis for thermal diffusivity.

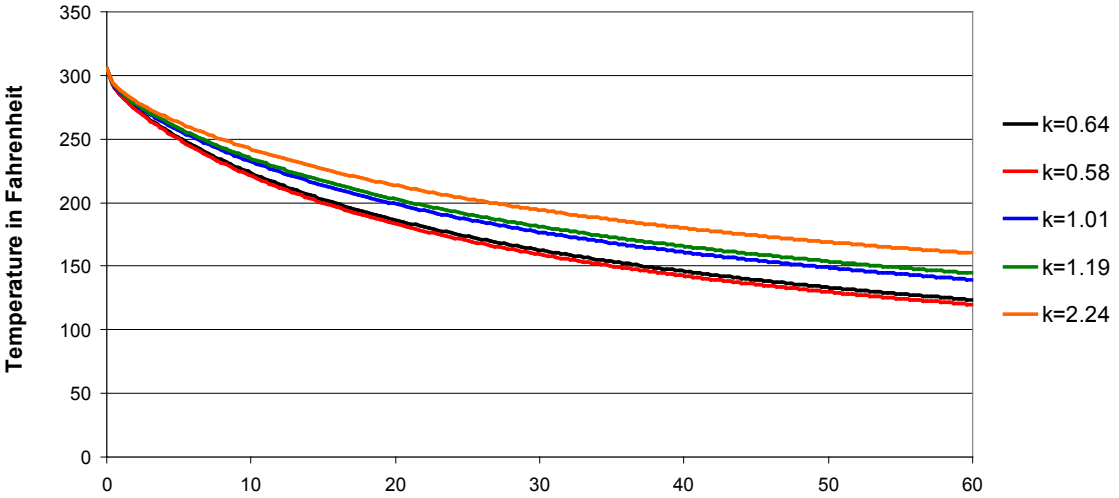

α = 2.13x10^{-2} ft^2/h (1.98x10^{-3} m^2/h)
°C = (°F – 32)/1.8

Figure 124. Graph. Sensitivity analysis for thermal conductivity.

Convective Heat Transfer Coefficient

Wolfe and Colony developed a relation for estimating convective heat transfer coefficients for an open highway construction environment that considered both free and forced convection principles.[17,18] After studying various methods for estimating the convective heat transfer coefficient h, Wolfe, Heath, and Colony recommended the relation in figure 73.[19]

The sensitivity analysis for the convective heat transfer coefficient aims to determine how changes in convection affect the curvature, rate of cooling, and other characteristics of the

predicted cooling response. Table 24 displays a series of increasing wind velocities and their correlating value for the convective heat transfer coefficient when using the equation in figure 73. These convective heat transfer coefficients are used as input parameters for the sensitivity analysis. Figure 125 illustrates the results.

Table 24. Comparison of convective heat transfer coefficients.

Wind Velocity (mi/h)	Convective Heat Coefficient. (h) (BTU/ft^2-h-°F)
0	1.30
2	2.34
4	3.05
6	3.68
8	4.25
10	4.79

1 BTU/ft-h-°F = 1.73 W/m-°K
1 mi/h = 1.61 km/h

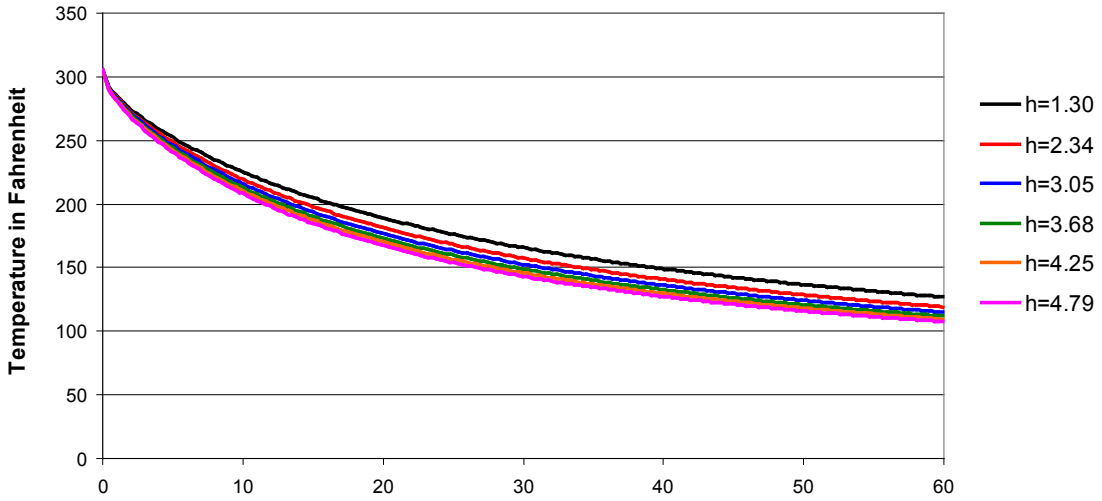

°C = (°F – 32)/1.8

Figure 125. Graph. Sensitivity analysis for the convective heat transfer coefficient.

Based on the results in figure 125, altering the convective heat transfer coefficient does affect the curvature and rate of cooling of the mat cooling model. However, it is less pronounced than in the case of thermal diffusivity (figure 123) or thermal conductivity (figure 124). As the convective heat transfer coefficient increases, the curvature and rate of cooling increases. This is sensible; an increasing convective heat transfer coefficient means that more heat is lost through the surface, which, in turn, will cause the mat to cool more quickly.

Emissivity

Emissivity is the pavement surface's relative ability to emit heat energy via radiation. It is defined as the ratio of the actual heat energy radiated by the pavement to the heat energy radiated

by an idealized object that emits all radiation at the given temperature, i.e., a "perfect radiator."[15] Wolfe and Colony recommend a relatively narrow range of 0.90 to 0.95 for the emissivity of an asphalt surface.[17] Therefore, a sensitivity analysis comparing values 0.90 through 0.95 was performed to determine its effect on the curvature, rate of cooling, and other characteristics of the predicted temperature response. The results displayed in figure 126 suggest that altering the input value for emissivity has little impact on the curvature and rate of cooling of the predicted cooling response.

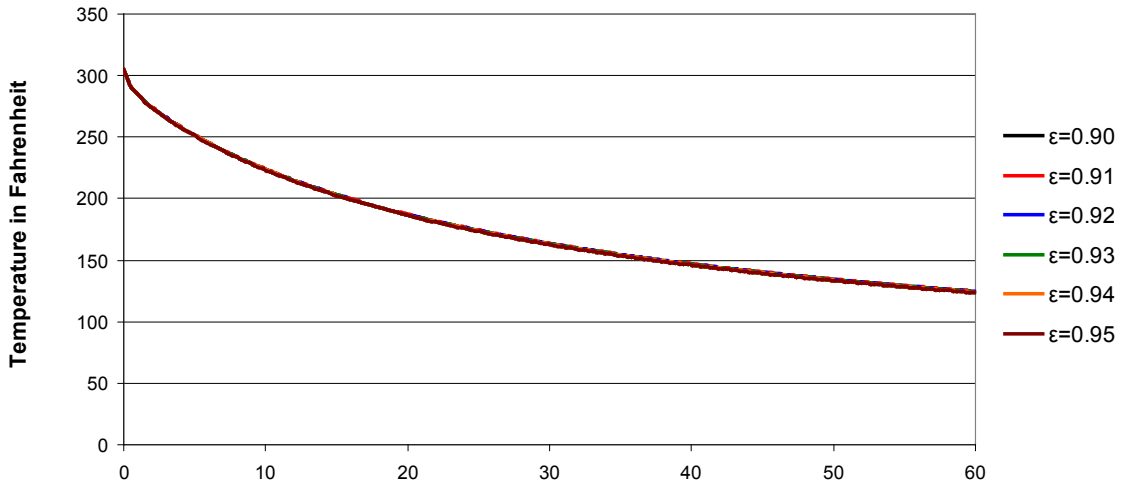

°C = (°F – 32)/1.8

Figure 126. Graph. Sensitivity analysis for emissivity.

Input Parameter Optimization Via Calibration

An optimization was performed on the input parameters using Microsoft® Excel Solver to determine the input values providing the best agreement between the measured and calculated temperatures. Based on the literature, it is known that the input parameters (thermal diffusivity, thermal conductivity, convective heat transfer coefficient, and emissivity) are not easily predicted or measured. Determination of these values through a field calibration process may expedite use of the mat cooling models by eliminating the need for laboratory testing to determine the input parameters.

To perform the optimization, the predicted temperatures from the mat cooling model are compared with the actual field-measured temperatures. The sum of the squared residual values between the predicted and measured temperatures is minimized in the Microsoft® Excel Solver tool by changing the input parameters for thermal diffusivity, thermal conductivity, convective heat transfer coefficient, and emissivity. Constraints are set within Solver to prevent negative values.

Two optimizations were performed: one that held the convective heat transfer coefficient *h* constant at 1.3 (figure 73 for the negligible wind speed observed in the field) and one that also optimizes *h*. Table 25 and table 26 summarize the results from both optimizations. Figure 127 compares the predicted cooling curves using the input values from the two optimizations. Both

sets of optimized input parameters produce identical calculated average cooling curves. Therefore, based on the sensitivity analysis and recommendations from the literature, the selected input parameters used in this study have been taken from table 25, with the value of the convective heat transfer coefficient as recommended by Wolfe, Heath, and Colony.[19] However, table 26 would have equally sufficed.

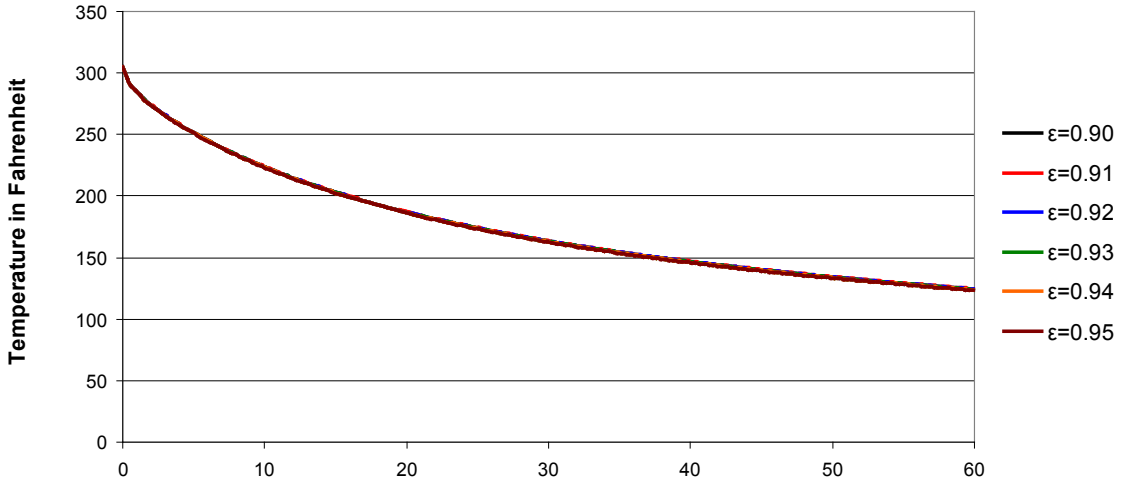

°C = (°F – 32)/1.8

Figure 127. Graph. Comparing both sets of optimized input parameters for the mat cooling model.

Table 25. Results of Optimization #1—*h* constant.

Property	Units	Symbol	Used
Thermal conductivity	BTU/ft-h-°F	k	0.64
Thermal diffusivity	ft^2/h	α	0.0213
Convective heat transfer coefficient	Dimensionless	h	1.30
Thermal emissivity	Dimensionless	ε	0.95

1 BTU/ft-h-°F = 1.73 W/m-°K
1 ft^2/h = 0.093 m^2/h

Table 26. Results of Optimization #2—*h* optimized.

Property	Units	Symbol	Used
Thermal conductivity	BTU/ft-h-°F	k	0.49
Thermal diffusivity	ft^2/h	α	0.0212
Convective heat transfer coefficient	Dimensionless	h	0.42
Thermal emissivity	Dimensionless	ε	0.93

1 BTU/ft-h-°F = 1.73 W/m-°K
1 ft^2/h = 0.093 m^2/h

These successful optimizations demonstrate that it is possible to field-calibrate thermal diffusivity, thermal conductivity, convective heat transfer coefficient, and emissivity. For a specific paving construction project, these input parameters can be determined by field

calibration to limited field temperature measurements at the beginning of the project, eliminating the need for complex laboratory testing.

Conclusions: Sensitivity Analysis and Calibration Techniques

Each of the major input parameters was analyzed for its individual impact on the predicted cooling response. These sensitivity analyses provide added confidence that the numerical solutions are logical and correct. The following results were obtained:

- **Thermal diffusivity**: Based on the results shown in figure 123, altering the thermal diffusivity significantly affects the curvature and rate of cooling of the predicted response. As the value for thermal diffusivity increases, the curvature and rate of cooling increases.

- **Thermal conductivity**: Based on figure 124, altering the thermal conductivity significantly affects the curvature and rate of cooling of the model. As the value for thermal conductivity increases, the curvature and rate of cooling decreases.

- **Convective heat transfer coefficient**: Based on the results shown in figure 125, altering the convective heat transfer coefficient affects the curvature and rate of cooling of the mat cooling model. As the value for the convective heat transfer coefficient increases, the curvature and rate of cooling increases.

- **Emissivity**: Based on the results shown in figure 126, altering the emissivity has little impact on the curvature and rate of cooling of the mat cooling model.

A field calibration procedure using the Microsoft® Excel Solver tool successfully determined the optimum input parameter values for this study. For a specific paving construction project, the thermal diffusivity, thermal conductivity, convective heat transfer coefficient, and emissivity values may be determined by calibration to limited field temperature measurements at the beginning of the project, eliminating the need for complex laboratory testing.

OVERALL CONCLUSIONS AND LESSONS LEARNED REGARDING TEMPERATURE MEASUREMENT

The overall purpose of this study was to evaluate RFID-based wireless temperature sensors and traditional asphalt mat cooling models to predict temperature versus depth and time to better interpret stiffness feedback data from intelligent compactors. This work was done in conjunction with the FHWA Pooled Fund Study on Intelligent Compaction.[25] More specifically, the objectives are as follows:

- Evaluate the feasibility of using SAW-based RFID technology to measure HMA temperatures via wireless sensors.

- Demonstrate, in the field, the survivability and temperature measurement capabilities of the SAW RFID sensors during a pavement overlay.

- Consolidate data to develop asphalt cooling curves of measured temperature versus time.

- Compare measured cooling response with predictions from theoretical mat cooling models.

- Perform a sensitivity analysis of the effect of relevant input parameters in the theoretical mat cooling models on the predicted cooling response. From the sensitivity analysis, explore field-calibration techniques to expedite the use of the mat cooling models without requiring laboratory measured input parameters.

Based on the evaluations and experiments performed in this thesis, the following conclusions were reached regarding the above-mentioned objectives:

Laboratory Evaluation

Through laboratory analysis and information from the literature, an encapsulation process was developed to protect the SAW RFID tags from physical damage (during construction) while promoting heat transfer. It is recommended that additional work be performed to determine the minimum thickness of the epoxy coating to optimize tag readability while ensuring survivability.

In terms of signal strength and readability, both the encapsulated monopole and patch antenna tags showed acceptable performance when encased in HMA specimens. The monopole tags, while more practical and compact in size, do not perform as reliably as the patch tags in terms of signal strength and readability. Both tags performed the best when aligned closely to "orientation #1/rotation #1" (see figure 85 and figure 86). Regarding thermal response, a thermal lag was observed after exposing the encapsulated tags to hot material. This lag is defined as the time required for the tag to "heat up" to match its environment. The encapsulated single patch tags required the longest thermal lag of about 5 min.

Field Evaluation

Overall, the findings from the field evaluation were that the RF SAW RFID tags can measure asphalt mat cooling temperatures during paving and compaction. It is important to note SAW RFID is a developing technology—certain constraints and imperfections exist, and improvements in the technology are expected in the future. The following subsections summarize the conclusions from the field evaluation in terms of field test performance, field test results, and variability and reliability:

Field Test Performance

The RF SAW tag reader requires a narrow temperature window to read the in-place tags. This requirement led to operational issues in the field, especially during the early stages of the asphalt cooling when temperatures dropped rapidly. The manufacturer recommends a 86 °F (30 °C) temperature window based on their calibration techniques at room temperature. It is recommended that additional future field tests be performed to more closely monitor the initial temperature of the HMA, perhaps by preheating the tags so that they can be read immediately after paving. Alternatively, the manufacturer of the SAW RFID technology could eliminate the use of a temperature window from the reader software.

There was also difficulty differentiating permanently damaged tags from those that simply could not be read immediately after paving/compaction. In other words, if a tag is nonresponsive to the RF SAW reader, it might not be caused by destruction due to high temperatures or vibratory compaction. It may be that the reader cannot get a response because the temperature window is incorrect or the tag's signal is severely attenuated.

Field Test Results

The field results generally show an exponential relationship between cooling temperatures and time. This generally agrees with theoretical considerations that suggest exponential cooling. No systematic temperature variations with depth were observed during mat cooling. In other words, the measured temperatures at the bottom, middle, and top of the asphalt mat, at any given location and time, were all within the variability range of the sensors. This may simply be a consequence of the thinness of the lift on this particular project.

Variability and Reliability

Based on the comparative study at the bottom of the mat between two sets of tags (single patch and monopole) and previous laboratory testing, the temperatures recorded by the two tag types are reasonably consistent and accurate. The comparative study at the surface of the mat between the Fluke® infrared thermometer and monopole tag found larger inconsistencies between the two sets of readings. This may be the result of testing at different locations on the mat surface. Additional field and/or laboratory testing are recommended to resolve this issue.

Comparisons Between Measured and Predicted Mat Cooling Response

RF SAW RFID tags and equipment can be used for measuring the mat cooling temperatures during hot-mix asphalt placement. Predicted temperatures from the theoretical heat transfer model (using input parameters obtained from the literature and through field calibration) agreed with field measurements. However, there are inconsistencies between the two that may either be due to limitations in the technology or to operator error. Further testing is recommended to investigate and remediate the following:

- Recording temperature data immediately after paving rather than a few minutes afterward. This may be accomplished by preheating the tags to the initial asphalt temperature—during laboratory testing, the tags exhibit a thermal lag in meeting their intended temperature. The RF SAW reader software can then be adjusted to read the tags accordingly; or simply improved by the manufacturer.

- Incorporating traditional thermocouple temperature sensors that have been used successfully in the past. Comparing the SAW RFID with the traditional equipment can better identify any limitations in the SAW RFID technology for this application.

- Refining the encapsulation process to optimize readability and survivability. During the field trials, there was difficulty differentiating physically damaged tags from those that simply could not be read immediately after paving/compaction. In other words, if a tag is nonresponsive to the reader, it might not be caused by destruction by vibratory

compaction. It may be that the reader cannot get a response because the temperature window is incorrect or the tag's signal is severely attenuated.

Sensitivity Analysis and Calibration Techniques

Sensitivity analyses were performed on key input parameters, and a field calibration procedure was developed to optimize the accuracy of the theoretical cooling response predictions. The following conclusions were drawn from these analyses:

- Increasing thermal diffusivity increases the curvature of the cooling curve and the rate of cooling.

- Increasing thermal conductivity reduces the curvature of the cooling curve and the rate of cooling.

- Increasing the convective heat transfer coefficient increases the curvature of the cooling curve and the rate of cooling.

- Emissivity has little impact on the predicted cooling response.

- The input parameter values for this study were determined through a field calibration process. Microsoft® Excel Solver can be used to optimize the thermal diffusivity, thermal conductivity, convective heat transfer coefficient, and emissivity values to minimize the discrepancies between predicted and measured temperatures. For any specific paving construction project, these input parameters can be determined by field calibration to limited field temperature measurements at the beginning of the project, eliminating the need for complex laboratory testing.

Lessons Learned

Based on the experiences and results of this study, the following lessons were learned:

- The encapsulation of the tags should be uniformly and minimally thin. In this study, the thickness of the encapsulant for each tag varied slightly, causing variability in the laboratory and field test results.

- To determine whether there is the possibility of systematic variation within a pavement layer, future testing should be performed on thicker pavement overlays. It was difficult to discern systematic variations in temperature versus depth for the very thin 1.5-inch (38-mm) overlay examined in this study.

- Future field trials should be performed under daytime conditions so that the solar absorption terms in the mat cooling models can be exercised and evaluated.

CHAPTER 7: EARLY DETECTION OF REFLECTION CRACKS

INTRODUCTION

HMA overlays are among the most common rehabilitation methods for a deteriorated pavement. A properly designed overlay increases the structural capacity of the pavement, inhibits water from penetrating into the subgrade, and restores friction resistance. Rehabilitation using HMA overlays is also advantageous because of the short construction time required, which minimizes travel delays for road users.

One of the most common distresses in HMA overlays is the development of new cracks in the overlay over the existing cracks or joints in the underlying deteriorated pavement. These are termed reflection cracks. Although reflection cracks can occur in HMA overlays over HMA pavements, they are most commonly experienced in HMA overlays over PCC pavements because of the regular transverse joints in the underlying layer. This latter type of reflection cracking is the focus here. Such cracks start at the bottom of the HMA layer at the joint locations between slabs and then propagate to the surface.

The two most critical movements of the concrete slabs are shown in figure 128. Horizontal movements are caused by changes in temperature; these cause Mode I or opening mode cracking. Vertical movements are caused by wheel loading; these cause Mode II or shear mode cracking. A good overview of Mode I and Mode II fracture mechanics can be found in Broek.[26]

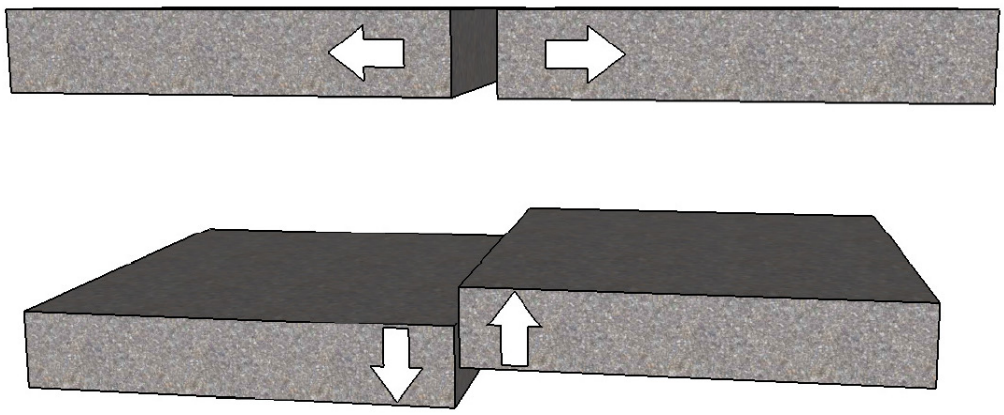

Figure 128. Drawing. Horizontal and vertical movement of concrete slabs causing Mode I and Mode II cracking.

Reflection cracks begin at the bottom of the HMA overlay and gradually grow toward the surface. Once the fully propagated reflection cracks are observed at the surface, the damage is done. Water can penetrate through the reflection cracks in the asphalt layer to the subgrade, decreasing its structural capacity. During low temperature conditions, the entrapped water in the cracks expands as a result of freezing, causing further crack growth. As these cracks get wider, smoothness decreases and damage to vehicles increases.

Early detection of reflection cracks before they reach the surface is especially important for warranty projects. Cui et al. provide an overview of the implementation of warranties on highway projects.[27] In 1990, FHWA initiated Special Experiment Project Number 14 to

encourage State transportation departments to implement contracting techniques that would lower overall project costs. By 2004, more than 30 States had used warranties in some of their projects. The use of warranties helps reduce lifecycle cost, improve quality, and encourage contractor innovation.

The warranty period for HMA overlays has typically been 2 to 4 years. Reflection cracking may start during this period but may not become visible at the surface until later. The use of crack sensors can give the State transportation departments the ability to detect reflection cracking early, enabling them to make a more informed decision on holding the contractor responsible for either repairing the damage if still under warranty or allowing the department more time to set aside sufficient funds to cover damages.

Some research has been conducted on the use of RFID tags to detect cracks. However, most has not gone beyond the proposal stage. Morita and Noguchi envisioned the use of RFID tags to detect structural cracks in combination with electrically conductive paint or an electrically conductive sheet affixed to the structure and connected to the RFID tag using copper wire.[28] When a crack initiates, the conductive paint breaks, resulting in an increase in resistance. The crack width could theoretically be predicted based on the reader–tag communication because the electrical resistance changes with varying crack width. However, Morita and Noguchi did not pursue this application any further than the proposal stage. Rather than using an RFID tag and reader, they directly measured the resistance of the electrically conductive paint strip as the crack propagated through the structure.

Wood and Neikirk proposed a passive sensor to provide information about the condition of welded connections in steel structures after earthquakes.[29] Although they acknowledged the possibility of using RFID technology for this application, they did not explore this idea and instead pursued evaluation of electronic article surveillance stickers. Neither Morita and Noguchi nor Wood and Neikirk went further than hypothesizing that RFID technology could work in detecting fatigue cracks in concrete or steel structures.

Growth of an initiated crack due to cyclic loading is classically expressed using Paris' Law.[30] As shown in figure 129, Paris' Law relates the rate of crack growth to repeated loading cycles:

$$\frac{dC}{dN} = A \cdot (\Delta K)^n$$

Figure 129. Equation. Paris's Law for crack growth.

Where:

C = crack length.
N = number of loading cycles.
A, n = fracture properties of HMA.
ΔK = change in stress intensity factor during cyclic loading.

The stress intensity factor is a measure of the driving force for crack propagation. It depends on the geometry of the structure, the loading conditions and magnitudes, and the crack length. The

stress intensity factor is very difficult to measure. In practice, it is often replaced by a proxy such as the CMOD.

Lee et al. measured crack opening and crack growth in conjunction with tests to determine the optimum rubblized depth for preventing reflection cracking.[31] The tests were conducted in Mode I bending loading on 12- by 8- by 2-inch (300- by 200- by 50-mm) asphalt slabs. Two PCC slabs were separated by 0.4 inches (10 mm) to simulate an open joint. The concrete slabs were, in turn, supported on an engineered synthetic rubber pad 1.2 inches (30 mm) thick to simulate the foundation conditions. A crack gauge was used to measure the horizontal deformation at mid-depth of the asphalt slab. The results of the horizontal deformation and vertical propagation of the crack were measured as a function of loading cycles. The crack was observed to have propagated about 60 percent through the 2-inch (50-mm) overlay at about 200,000 cycles. This corresponded to a horizontal deformation of about 0.018 inches (0.45 mm). This information provides some basis for estimating the range of displacement that must be considered during development of the crack sensor.

This chapter describes the conceptual development of an RFID-based wireless sensor to detect reflection cracks before they reach the surface of the pavement and become visible. One of the great advantages in trying to detect reflection cracks in pavements is that the potential crack locations are well defined (i.e., over the joints in the underlying slabs) as opposed to conventional fatigue cracks, which can develop almost anywhere. Because of the potentially very low cost of RFID crack detection systems, they could conceivably be placed at all potential reflection crack locations along an overlay rehabilitation project (i.e., at all joints in the underlying rigid pavement slabs).

The concept for the RFID-based wireless reflection crack sensor is to configure the RFID tag so that when a crack has grown to some critical length, the antenna circuit is broken, thus causing the tag to stop transmitting. Two possibilities where explored: a conductive paint that would crack at a certain strain, and an overlapped copper antenna “microswitch” that would open at a certain CMOD. Key factors in the sensor development are read range and survivability. In the field, the sensor must be readable through the thickness of the asphalt overlay and at least 1 to 2 ft (0.3 to 0.6 m) of air. The sensor must be able to survive the high temperatures and compaction stresses of paving operations.

As documented in this chapter, the RFID-based wireless crack detection system has been developed well beyond the basic conceptual stage. Prototypes were developed and successfully evaluated via laboratory testing and field trials. Unfortunately, project schedule and resources preluded comprehensive field evaluation over sufficiently long time periods to validate the ability of the system to detect early-onset reflection cracks under in-service pavement conditions.

CRACK DETECTION SENSOR DESIGN

The concept for early detection of reflection cracks is to adapt an RFID tag to “fail” in the sense that it can no longer be read once a significant crack initiates. To achieve this functionality, a short section of the antenna link is replaced with a conductive but frangible link. The modified RFID tag is placed above a joint in an existing PCC pavement layer before paving the HMA overlay. When the frangible antenna link fails at a prescribed strain level, the RFID tag stops

working, indicating the initiation of a reflection crack. RFID tags could be placed in pairs at the bottom of the HMA overlay, one crossing the joint in the underlying PCC slab and one parallel and slightly away from the joint. Failure of the tag crossing the joint while the companion tag remains readable would be a clear indicator of early reflection crack formation.

The RFID tags used for this project are the Avery Dennison™ AD-223 shown in figure 130. These are UHF Gen 2 tags with the Monza® 3 chip, the newest chip developed from Impinj®. The chip is cut from the tag, leaving about 0.075 inches (2 mm) of the original antenna as shown in figure 131. The modified antenna is then connected to the 0.075-inch (2-mm) stub. The reader used for all of the tests in this chapter is the Mercury® 5 ThingMagic reader.

The efficiency of an antenna is governed by its electrical reactance. Reactance is a measure of the effect of capacitance and inductance on a time-varying current. A half-wave dipole has a reactance of zero. A shorter than half-wave antenna has a capacitive reactance, and a longer one has an inductive reactance. In this chapter, all the read range tests have been conducted for a half-wave dipole and shorter.

When shortening the tag from the half-wave dipole, capacitive reactance is introduced, which causes deterioration of the tag's read range performance. This is because part of the signal is "wasted" as stored electromagnetic energy in the reactive capacitance.

Note: Overall tag length is approximately 6 inches (150 mm).

Figure 130. Photo. RFID tag AD-223.

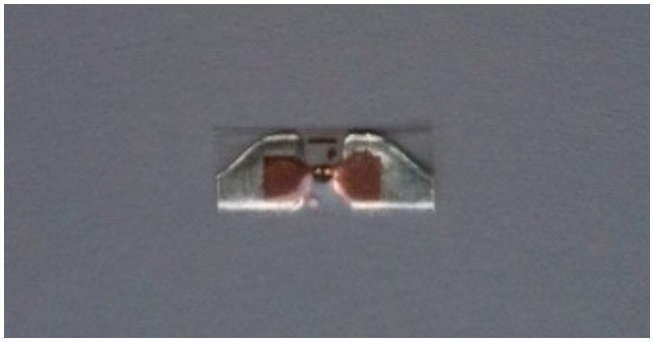

Figure 131. Photo. RFID chip with 0.075 inches (2 mm) of antenna on each side.

In practice, the length of the RFID dipole antenna can be shortened by introducing a frangible link that breaks at a target strain or displacement level. Two types of frangible antenna links were investigated. The first one is based on electrically conductive paint designed to break at a critical strain level. The second uses slightly overlapped metal strips to form a microswitch in the antenna that opens—i.e., breaks the antenna connection—at a critical CMOD. In both cases, the modified RFID tag is required to work/give a readable signal from a given distance before a crack has initiated and give no readable signal from the same distance after a crack has initiated but not yet appeared on the surface of the pavement.

Conductive Paint Antennae

Read Range

A conductive paint was initially thought to be the best choice for the frangible link, in large part because of the ease and flexibility of its application. The read ranges for three possible antenna configurations were evaluated: a loop antenna, a dipole antenna, and a C-shaped antenna.

As a first attempt, Aquadag® E™, a conductive carbon paint from M.E. Taylor Engineering, Inc., was used to paint a 0.2-inch (5-mm)-wide loop antenna connected to the RFID chip from the Avery Dennison™ tags. The loop antennae were painted on a flexible plastic substrate made from conventional transparency stock. Small dabs of a thicker silver conductive paint were used to create better connections between the Aquadag® E™ paint and the chip. Three tags were made with loop antennae of one wavelength, two wavelengths, and three wavelengths as shown in figure 132 through figure 134.

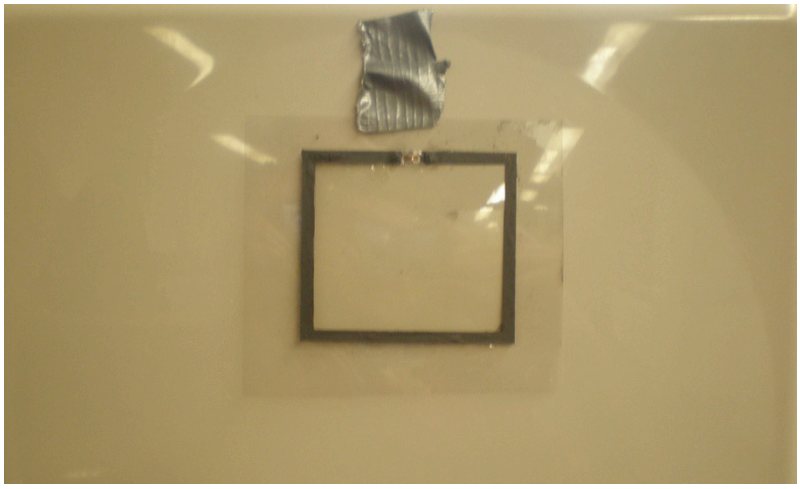

Figure 132. Photo. One-wavelength loop antenna.

Figure 133. Photo. Two-wavelength loop antenna.

Figure 134. Photo. Three-wavelength loop antenna.

The loop antennae were 0.2 inches (5 mm) wide and 12.9, 25.8, and 38.7 inches (328, 656, and 984 mm) in total length based on the wavelength calculation shown in figure 135:

$$\lambda = \frac{c}{v} = \frac{1.18 \times 10^{10}\ \text{inches/s}}{915 \times 10^{6}\ /\ \text{s}}$$

Figure 135. Equation. Wavelength calculation.

Where:

λ = wavelength.
c = speed of light = 1.18×10^{10} inches/s.
ν = frequency = 915 MHz for UHF tags.

The maximum read distance was evaluated for all tags, with results shown in table 27. All the readings were taken over 20-s intervals on the T (transmit) side of the antenna.

Table 27. Read range for the carbon paint loop antenna tags.

Number of Wavelengths	Maximum Read Distance	
	Inches	Meters
1	1.3	0.41
2	1.6	0.50
3	1.4	0.44

The maximum read range for the loop antennae through air was 1.6 ft (0.5 m), which is marginal in the field when the tag is placed at the bottom of the HMA overlay. In an effort to extend the read range, the loop antennae were replaced with dipole antennae. Typically, dipole antennae are created by two quarter-wavelength conductors extending from a central connection; this was done using the conductive paint. As with the loop antennae, silver paint was used to create better connections between the Aquadag® E™ paint and the chip. Figure 136 illustrates one of the fabricated dipole antennae and RFID chip. The maximum read distance for the dipole tag was approximately 4 ft (1.2 m).

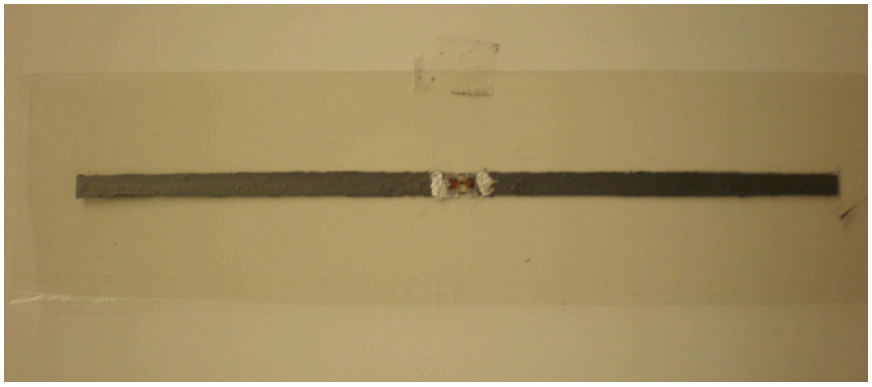

Figure 136. Photo. Dipole carbon paint antenna.

The read performance of the half-wavelength dipole tag was evaluated as one of the antenna legs was shortened to simulate breakage by a reflection crack. A series of 0.2-inch (5-mm) cuts were made on one side of the dipole antenna, and the effect on maximum read range was evaluated. The results are shown in table 28. It can be seen that the maximum read distance starts dropping significantly after the antenna is shortened to about half of its original length. If the antenna is cut at about 0.4 inches (10 mm) away from the chip, the tag cannot be read at a distance beyond about 1.3 ft (0.4 m). This would imply that if the antenna were kept at a distance of 1.6 ft (0.5 m) away from the embedded tag, the reader would be able to detect that the antenna had broken as a result of reflection cracking. A second dipole tag fabricated and tested in the same manner showed similar results.

Close examination of the read ranges for the modified tag after cutting one side of the antenna (table 28) shows that the read range did not drop as precipitously as expected as the antenna length was shortened. Even when there was only about 0.8 inches (20 mm) left on one side the tag, it could still be read from about 2.0 to 2.6 ft (0.6 to 0.8 m). The larger the drop in read range

after the antenna is broken, the easier it will be to detect whether a crack has initiated. For this reason, additional tests were conducted in which one side of the dipole antenna was already snipped at 0.8 inches (20 mm) as shown in figure 137. Read range was then measured as the other side of the antenna was progressively shortened. The antenna for these tests was made of silver conductive paint from Engineered Conductive Materials, LLC. The reason the tests were not continued with the carbon paint is because when one side of the antenna is only about 0.8 inches (20 mm) in the half-wavelength carbon dipole, the maximum read distance is approximately 2.3 ft (0.7 m). This particular silver paint was used because it was thought that it might give better read ranges.

Table 28. Read range for the carbon dipole tag with one side shortened.

Antenna Length (inches)	Maximum Read Distance (ft)
3.2	4.0
3.0	4.0
2.8	4.0
2.6	4.0
2.4	4.0
2.2	4.0
2.0	4.0
1.7	4.0
1.5	3.8
1.3	3.0
1.1	2.8
0.9	2.7
0.7	2.6
0.6	2.1
0.5	1.5
0.3	1.2
0.1	0.7
0	0

1 inch = 25.4 mm
1 ft = 0.305 m

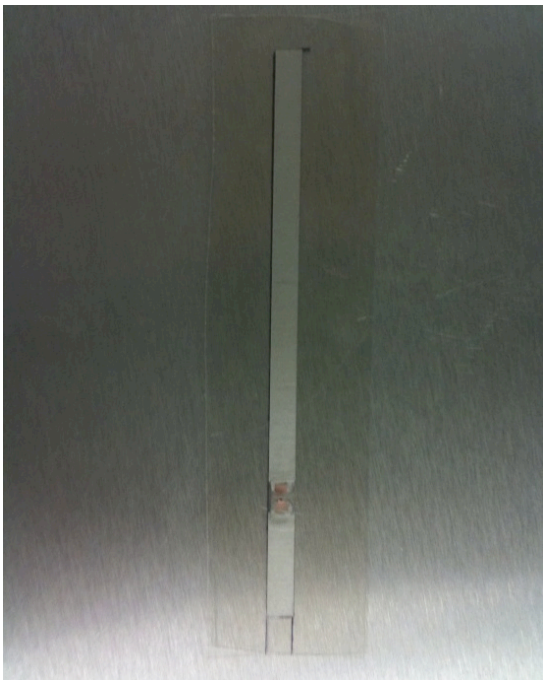

Figure 137. Photo. Silver dipole antenna with one side snipped at 0.8 inches (20 mm).

The results from these tests, summarized in table 29, show that it would be best to have both sides of the antenna break at a distance of 0.8 inches (20 mm) or less from the chip. Before failure, this tag could be detectable at a read range of about 4.2 ft (1.3 m); after failure, the read range is about an order of magnitude smaller. Another similar test with the same silver paint was conducted for another possible configuration, a C-shaped antenna instead of a straight dipole, as shown in figure 138. The maximum read range for this tag with no cuts to the antenna was about 8.2 ft (2.5 m). When one side of the antenna was trimmed to within 0.24 inches (6 mm) of the chip, the read range for the tag dropped to only about 1.5 ft (0.45 m). When both sides of the antenna were trimmed to within 0.24 inches (6 mm) of the chip, the tag could not be read at any distance. The reason for the C-shaped configuration is to cause the antenna to break simultaneously on both sides, which would give a much lower read range once the crack had initiated than if it broke only on one side. However, the C-shaped antenna also keeps the size of the tag comparatively small, raising the concern that it cannot cover the entire area where a reflective crack might occur. This does not make it a good candidate for the crack sensor application.

Table 29. Read range for the silver dipole antenna with one side fixed at 0.8 inches length while the other side is progressively shortened.

Left Side Antenna Length (inches)	Maximum Read Distance (ft)
3.2	4.2
3.0	4.0
2.8	3.8
2.6	2.8
2.4	2.7
2.2	2.5
2.0	2.1
1.9	2.0
1.7	1.4
1.5	1.2
1.3	1.1
1.1	1.0
0.9	0.8
0.7	0.4
0.5	0.3
0.3	0
0.1	0
0	0

1 inch = 25.4 mm
1 ft = 0.305 m

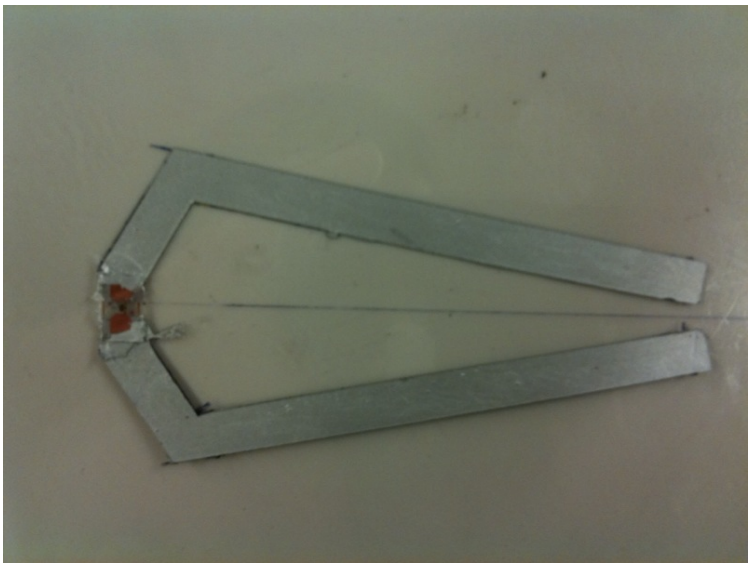

Figure 138. Photo. C-shaped silver dipole antenna.

The high conductivity of the silver paint allows evaluation of antenna effects for the "best case"—i.e., longest read range—conditions. However, as will be shown in a later section, the carbon paint was the only coating that broke anywhere near the target strain level and as a

consequence, it is the coating that must ultimately be used to modify the RFID tag. For this reason, more modified tags having carbon paint dipole antennae were constructed and tested. As expected, the read ranges of the tags with the carbon paint were not as long as for the silver dipole antennae because of the lower conductivity of the carbon compared with the silver. The maximum read range of the tags with the carbon dipole antennae in these new tests was only about 1.6 ft (0.5 m) compared with about 3.9 ft (1.2 m) for the silver. Although in earlier tests (table 28), the carbon paint dipole also read up to 3.9 ft (1.2 m), because of variations from tag to tag it would be more cautious to base the decisions on the worst results. To capitalize on the properties of both materials, tags with hybrid dipole antennae combining both silver and carbon paint were fabricated. The 0.8 inches (20 mm) of the antenna closest to the RFID chip was painted with carbon and the rest of the dipole length was painted with silver paint, as shown in figure 139. It was expected that this tag would have a maximum read range close to that of the pure silver dipole while at the same time have a frangible link at the critical location close to the chip that would fail at the target strain level. Read range test results for this hybrid silver and carbon dipole antenna tag are shown in table 30. The maximum read range before trimming the antenna length was 5.9 ft (1.8 m), comparable to the pure silver dipole antenna. The read range of the tag dropped by approximately 40 percent to 3.3 ft (1 m) or less as the remaining dipole leg was shortened to 0.8 inches (20 mm).

Figure 139. Photo. Silver and carbon dipole antenna.

Table 30. Read range for the silver and carbon dipole antenna as one side is shortened.

Antenna Length (inches)	Maximum Read Distance (ft)
3.2	5.7
3.0	5.7
2.8	5.7
2.6	5.7
2.4	5.3
2.2	4.4
2.0	4.4
1.9	4.2
1.7	4.0
1.5	4.0
1.3	4.0
1.1	4.0
0.9	3.9
0.7	2.9
0.5	2.8
0.3	2.1
0.1	1.3
0	0.4

1 inch = 25.4 mm
1 ft = 0.305 m

The conclusion from these read range tests is that the dipole configuration is best for the crack sensor. Also, because of its higher initial read range before breakage and low read distance after the carbon paint is broken, the hybrid silver and carbon dipole antenna provides the best configuration for the reflection crack sensor.

Fracture Strains

Initially, the critical strain at which the conductive paint was targeted to break was estimated to be about 1,000 με based on elastic strain distributions at the bottom of an asphalt layer. Consequently, tests were conducted to find a conductive paint that broke at about that strain level. Two carbon conductive paints, two conductive silver paints, and one conductive silver epoxy were tested in the laboratory to determine the strain at which they would break. Details of these paints are given in table 31. They were strained in a four-point bending test using an Instron® Model 1331 compression machine. A strip of each of the paints was painted on a plastic film. The painted film was then glued to the bottom of the beam. The adhesive used for this was SG496 (Omega® Engineering Inc.), a methyl-based cyanoacrylate 1-part glue commonly used for strain gages. A beam was fabricated from 7075-T6 aluminum, a material that remains elastic at strains up to 4,600 με. The calculated beam dimensions to reach the target strain of 1,000 με under reasonable applied load levels are shown in figure 140. An ohmmeter was used to measure the resistance in the painted strip of conductive paint to check for breakage. The complete test setup is shown in figure 141. Although the required critical strain was

1,000 με, the tests were run to the elastic limit of 4,600 με. Unfortunately, none of the cured conductive paints broke at this strain level.

Table 31. Description of the conductive paints tested to determine failure strains.

Name	Composition	Supplier
Aquadag® E™	Water-based colloidal graphite	M.E. Taylor Engineering, Inc.
Conductive Shielding Paint	Carbon paint	Stewart-MacDonald
Conductive Silver Paint	18-percent silver	M.E. Taylor Engineering, Inc.
Conductive Silver Pen	45- to 50-percent silver	M.E. Taylor Engineering, Inc.
Conductive Silver Epoxy	Two-part electrically conductive silver epoxy	M.E. Taylor Engineering, Inc.

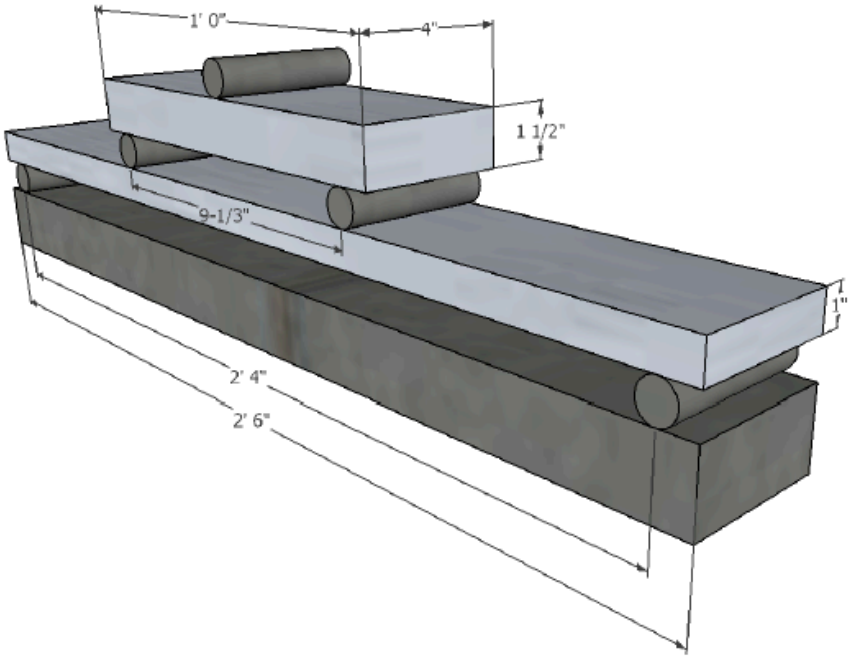

1 inch = 25.4 mm
1 ft = 0.305 m

Figure 140. Drawing. Beam dimensions for the four-point bending test.

Figure 141. Photo. Thin film test setup.

As a next step, another set of tests was developed to localize the strains similar to what occurs across the mouth of a fracture. Two polymethyl methacrylate (PMMA, trade name Plexiglas®) sheets were attached along the bottom of the beam; the sheets just touched each other, simulating the joints in the PCC slab in a pavement. This test specimen setup is shown in figure 142. Thin strips of the conductive paints were then painted across the simulated joint. The 18-percent silver conductive paint did not break. The carbon Aquadag® E™ conductive paint broke at about 300 με. Because the Aquadag® E™ paint actually broke, albeit at strain levels below the target, it was selected for the tag antenna studies described in the previous section.

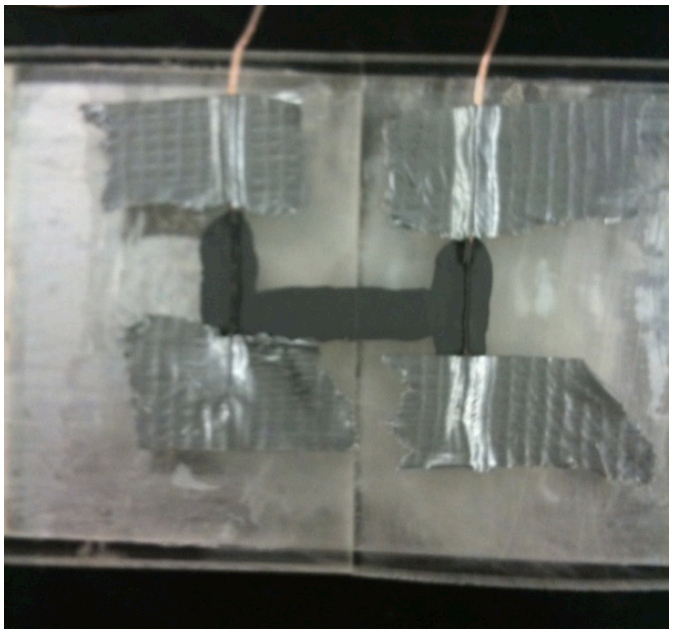

Figure 142. Photo. Painted Aquadag® E™ on the two abutting PMMA sheets.

Based on the read range tests from the previous sections, it was determined that the antenna needed to break close to the chip for the read distance to shorten significantly. In the PMMA plate test setup, the antenna would fail directly over the "pre-cracked" plates. However, this implies that in the field, one would need to paint directly on the top of PCC slabs or the underside of the overlay, which is not practical. A carrier for the paint was needed to force the maximum strains to occur next to the chip. Therefore, a new test configuration was developed. A 4- by 9-inch (100- by 230-mm) polycarbonate polymer (trade name Lexan) sheet was fabricated with a 3.5-inch (90-mm)-diameter hole in its center to act as a stress/strain raiser. The 3.5-inch (90-mm)-diameter hole in the 4-inch (100-mm)-wide Lexan sheet causes the elastic stresses and strains to increase by a factor of 10 in the ligaments at the edges of the hole. The plate length was chosen as 9 inches (230 mm) so that the Lexan sheet would fit between the middle rollers where the bending strains are constant in the four-point beam loading system. A continuous 0.2-inch (5-mm) strip of Aquadag® E™ was painted along one edge of the plate (including over the ligament on one side of the hole), and a dipole tag with a 0.2-inch (5-mm)-wide antenna strip of Aquadag® E™ was painted along the other, as shown in figure 143. The dipole tag was painted so that the chip was slightly offset from the highest strain location in the ligament at the edge of the hole in order to break the antenna close to the chip. Two ohmmeters were used to monitor the conductivity in the painted strips to determine breakage. The antenna of the dipole tag broke about 0.2 inches (5 mm) away from the thinnest part of the ligament at a strain of about 12,000 με (after adjustment for strain magnification effects). The antenna broke very close to the chip as expected, after which the tag could not be read at long range. The continuous strip of paint on the other side of the plate did not break during the test.

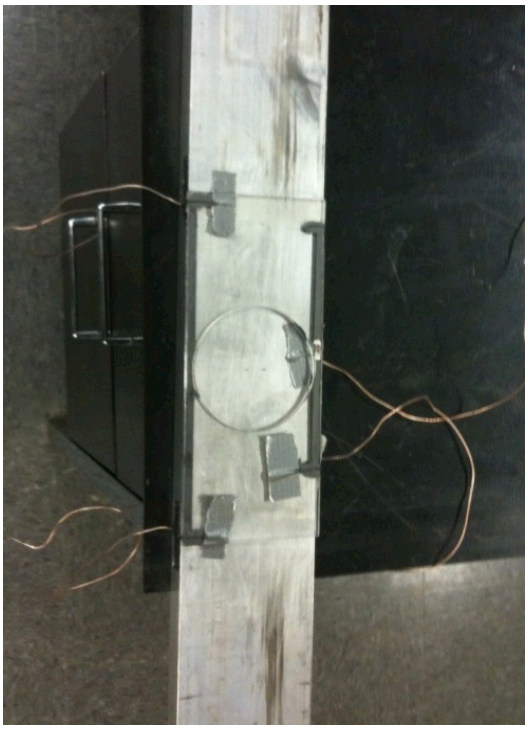

Figure 143. Photo. Painted dipole tag on one side and painted Aquadag® E™ only on other side of the polycarbonate sheet.

Based on insights from an additional literature search on measurement of CMOD, a reasonable estimate is that a reflection crack will have initiated and grown partially but not completely through an overlay at a CMOD on the order of 0.04 inches (1 mm). A CMOD of 0.04 inches (1 mm) over a gauge length of 4 inches (100 mm) corresponds to a strain of 10,000 με. These strain levels cannot be achieved with the bending beam apparatus except when using the polycarbonate sheet with the hole for concentrating and magnifying the stress and strain levels. However, this apparatus was problematic in practice because of difficulties in getting a secure attachment to the bottom of the aluminum beam. For these reasons, direct tension tests were conducted to determine the failure strains of the paints. Direct tension dogbone specimens were fabricated from polycarbonate with the dimensions shown in figure 144. Two tests could be conducted simultaneously on the same specimen by coating the opposite sides. The test setup is shown in figure 145 and figure 146. The tests were run in displacement control mode at a rate of 0.005 inches (0.127 mm) per min. Adhesion problems between the paint and the polycarbonate were observed in some of the previous bending tests; the paint in some cases would just fall off the polycarbonate sheet. To remedy this problem, the Aquadag® E™ carbon conductive paint was painted on a strip of watercolor art paper that had been glued to the polycarbonate specimen using strain gauge adhesive. The strips of paint were 0.2 inches (5 mm) wide. Figure 147 shows a typical strip of conductive paint on the polycarbonate specimen with wires for connecting the ohmmeters.

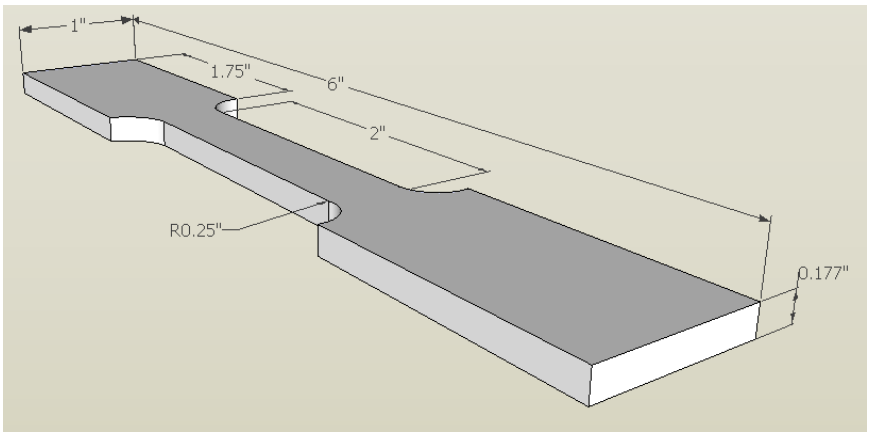

1 inch = 25.4 mm

Figure 144. Drawing. Dogbone specimen dimensions.

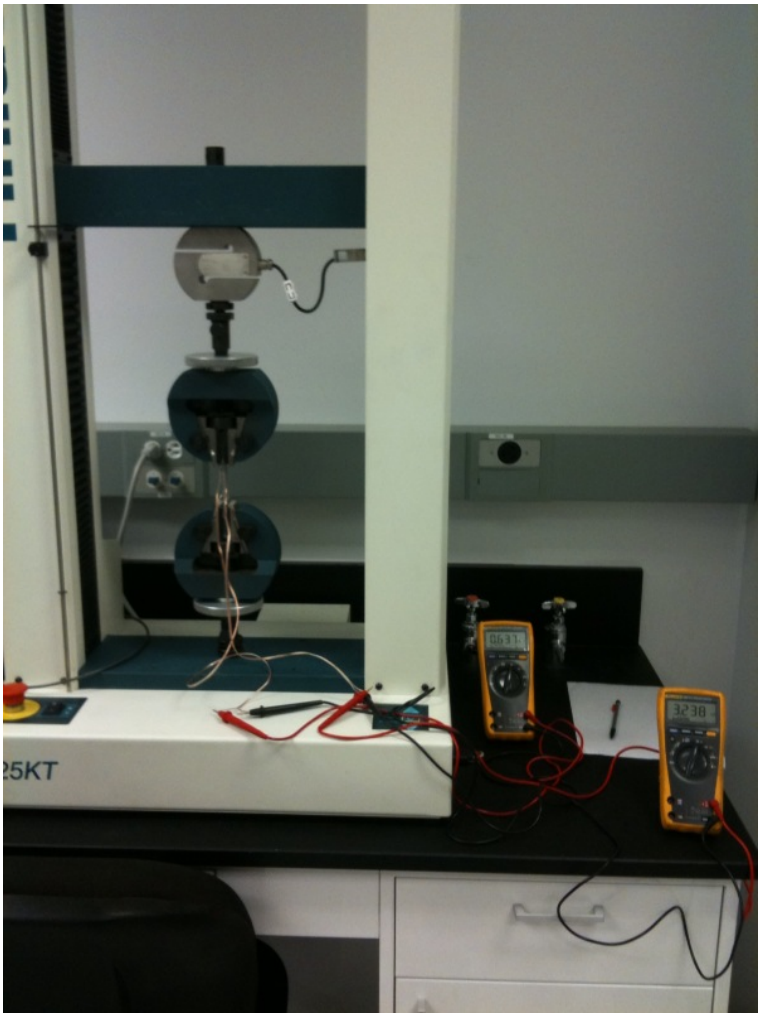

Figure 145. Photo. Direct tension test setup.

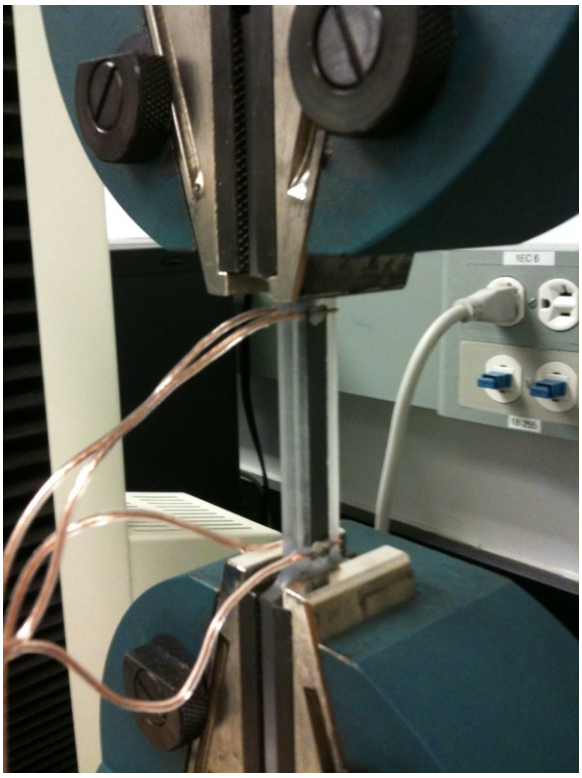

Figure 146. Photo. Direct tension test specimen attachment.

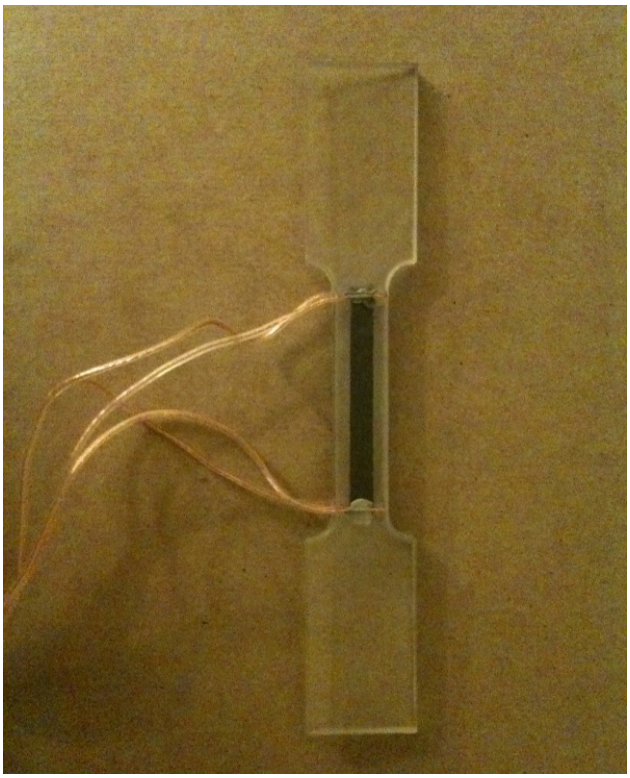

Figure 147. Photo. Conductive paint on the dogbone specimen.

The test was continued to a strain of 26,000 με, well above the strain at which reflection cracks should initiate in an HMA overlay. The carbon paint did not break. There was some concern that the watercolor paper might be creeping and that therefore the carbon paint was not experiencing the true applied strains. To account for this possibility, the test was repeated with two strips of carbon paint applied directly on the polycarbonate specimen after its surface had been roughed with extra-fine sandpaper to enhance adhesion. The painted strips were 0.2 inches (5 mm) wide, similar to the first test. This test was continued to a strain of 25,000 με, and the carbon paint still did not break, although some small cracks were visible.

One last tension test was conducted on the Aquadag® E™ carbon paint and the 18-percent silver conductive paint. The width of the painted strips was narrowed to 0.1 inch (2 mm) for this test on the assumption that a crack would propagate more easily over the narrower width. The test was run to 30,000 με without any breakage/conductivity fault in either the carbon or the silver paint.

The overall conclusion from all these tests is that while the carbon and the silver conductive paints can be used to make suitable antennae for the RFID chip, none was reliably brittle enough to serve as a frangible link. Therefore, the approach was changed from a strain-based brittle material concept to a simple displacement-based mechanical microswitch scheme for interrupting the antenna circuit, as explained in the following section.

Antennae With Mechanical "Microswitch"

The final crack sensor design was based on modifying the antenna of an existing RFID tag using electrically conductive metal strips that overlap just enough so that the antenna mechanically opens or disconnects when a crack occurs. Essentially, the RFID crack sensor will behave like a switch, so when a crack occurs, the antenna circuit is broken and the tag turns off and gives no signal.

It was decided that the crack sensor should be developed so that it detects cracks that have propagated through approximately 60 percent of the overlay. This corresponds to a 0.018-inch (0.45-mm) overlap in the antenna microswitch.[26] One of the main reasons for this decision was to keep the crack sensor manufacturing as simple as possible. As the target overlap gets small, the fabrication becomes more difficult.

A 36 gauge (0.005-inch (0.125-mm)-thick) copper sheet was cut into strips about 0.1 to 0.15 inches (2 to 3 mm) wide for creating the dipole antenna of the RFID tag. One side of the dipole was connected to the 0.1-inch (2-mm) stub of the original antenna using the two-part electrically conductive silver epoxy from M.E. Taylor Engineering, Inc., to assure a good connection. The other side of the dipole was fabricated to have a 0.018-inch (0.45-mm) overlap of the thin copper sheet over the stub of the original antenna.

To determine the best configuration of the dipole, read range studies were conducted for different antenna lengths as was done earlier with the conductive paint antenna. These tests were initially conducted in the Pavement Materials Laboratory at UMD. Because of inconsistencies in the indoor readings thought attributable to RF reflections from metal interior objects, the read range studies were moved outdoors to parking lot E behind the Engineering Laboratory Building at UMD to minimize any interference (figure 148). It was expected that the results would be less

variable and more reliable, and in addition, the outdoor conditions better represent the actual field scenario.

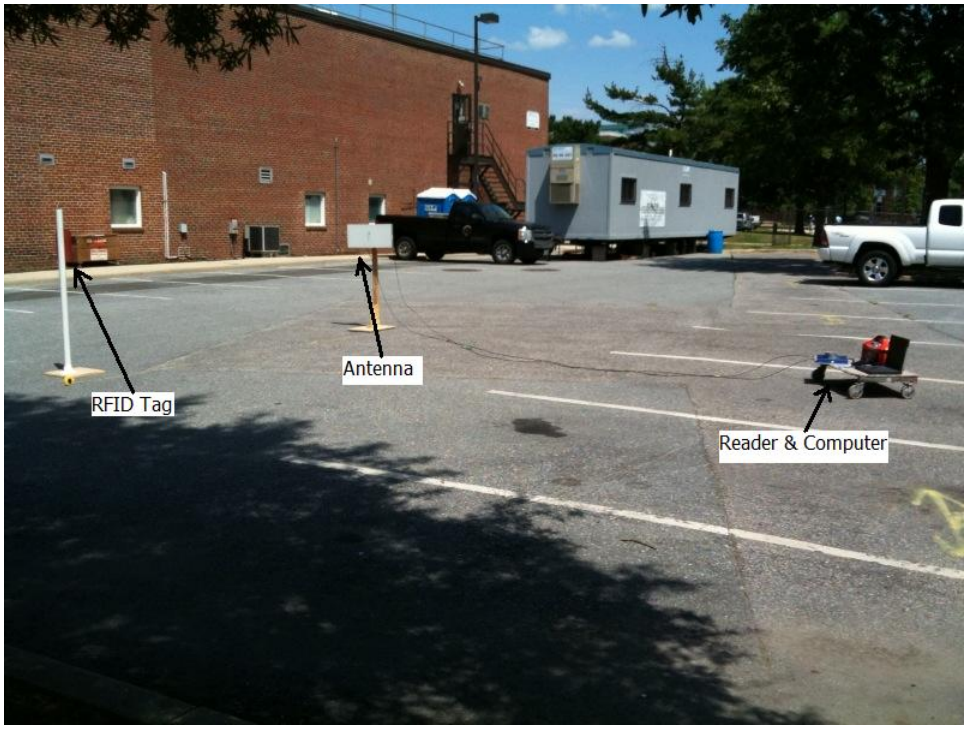

Figure 148. Photo. Read range tests in parking lot E.

The first set of tests was done for a symmetrical antenna, starting with a half-wavelength dipole with two sides of 3.2 inches (82 mm) each and then continuing by shortening each side of the dipole. For each length, readings were taken with one side alternately being connected and disconnected. The dipole tag was sandwiched between two thin polycarbonate pieces to keep it in place and to simulate the expected encapsulation of the sensor in the field. To create a good connection at the mechanical overlap, a wooden toothpick was sandwiched between the polycarbonate pieces on top of the overlap (figure 149). The readings were taken in four directions, north, south, east, and west. The tag was optimally placed in front of the transmit side of the antenna.

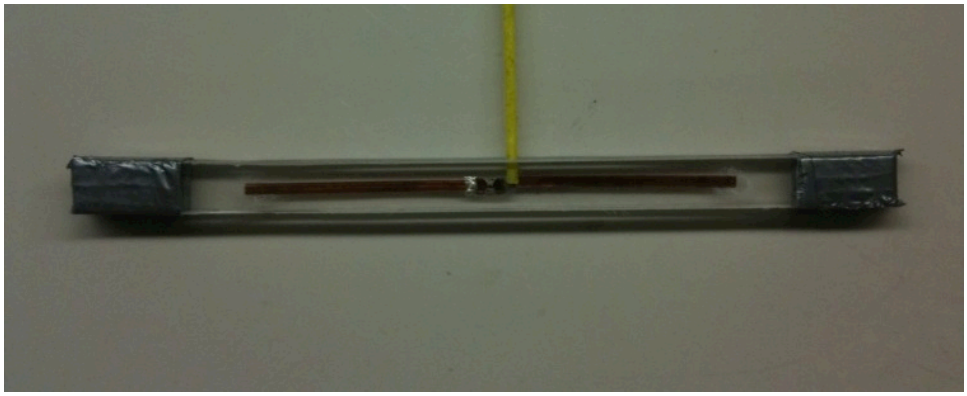

Figure 149. Photo. Symmetric dipole used in the read range study.

The results for the symmetrical dipole read range are shown in figure 150. The maximum read distances are very similar in all four directions. Except for a slight anomaly at 6.7 inches (170 mm), the maximum read distance consistently decreased as the total dipole length shortened. Some possible suitable configurations chosen from these results were the following:

- 4 inches (100 mm) dipole length;
  Connected read at 7.6 ft (2.3 m);
  Disconnected read at 1.6 ft (0.5 m).

- 3.5 inches (90 mm) dipole length;
  Connected read at 5.2 ft (1.6 m);
  Disconnected read at 1.3 ft (0.4 m).

- 3.1 inches (80 mm) dipole length;
  Connected read at 4.4 ft (1.35 m);
  Disconnected read at 1 ft (0.3 m).

Next, a read range study was conducted with one side of the dipole fixed at 3.2 inches (82 mm) and the side other starting at 2 inches (50 mm) and then progressively shortened. The longer 3.2-inch (82-mm) antenna leg contained the overlapped microswitch. The same testing method as for the symmetric antenna readings was followed. Readings were taken with the long side connected and disconnected. The dipole tag was put between two thin polycarbonate pieces and a toothpick was used as before to ensure a good connection at the overlapped microswitch (figure 151). The readings were taken in four directions, north, south, east, and west. Two replicate tags were tested to evaluate reproducibility. Again, the tags were placed in front of the transmit side of the antenna for all readings.

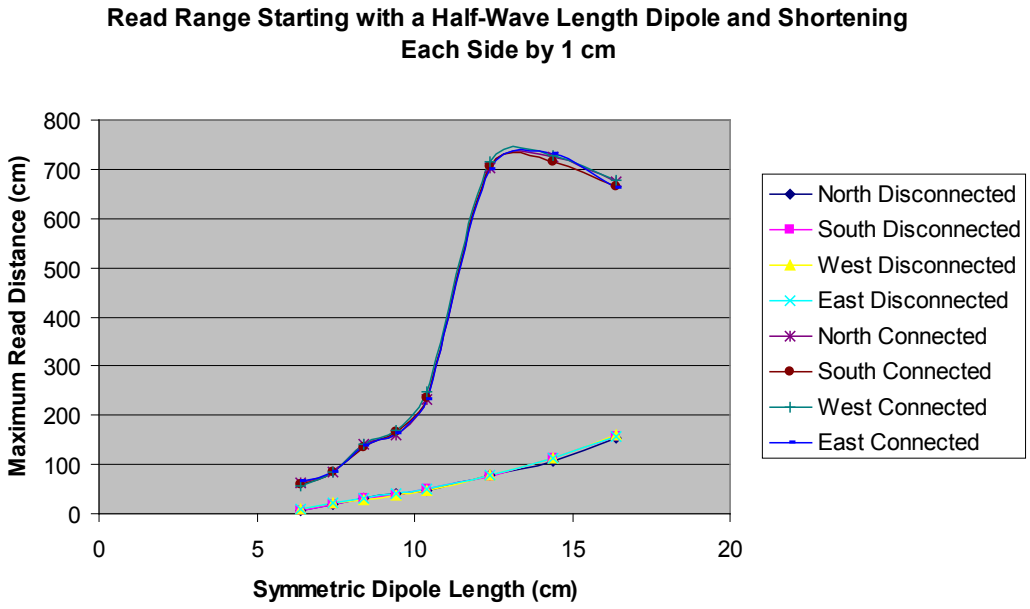

1 inch = 2.54 cm

Figure 150. Graph. Read range for the symmetric dipole in each direction connected and disconnected.

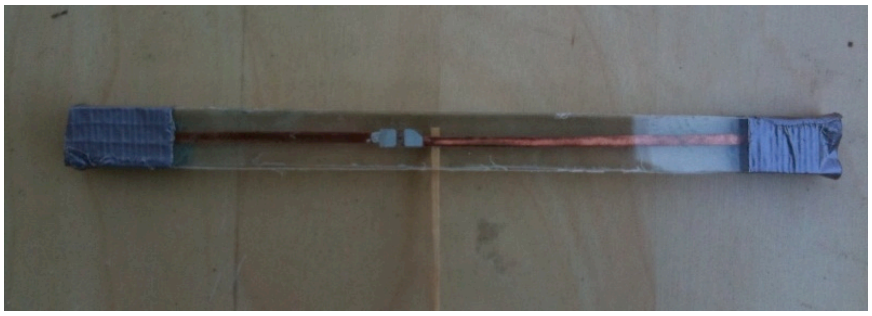

Figure 151. Photo. Asymmetric dipole used in the read range study.

The results of these tests are shown in figure 152 through figure 155. The read ranges for the four different directions were very similar, as were the readings from the two replicate tags. Based on these results, it was decided that the best dipole length for this application was 3.2 inches (82 mm) on one side and 0.6 inches (15 mm) on the other. This configuration, when connected, could be read at more than 7 ft (2.1 m) but only at less than 1 ft (0.3 m) when disconnected. This difference in read ranges is large enough for the antenna to be read from a moving vehicle when connected and not read from that same distance when disconnected. The 7-ft (2.1-m) read range when connected is actually greater than required in the field; however, this adds a safety margin to help ensure that the tag can be read even after possible signal attenuation through the HMA overlay.

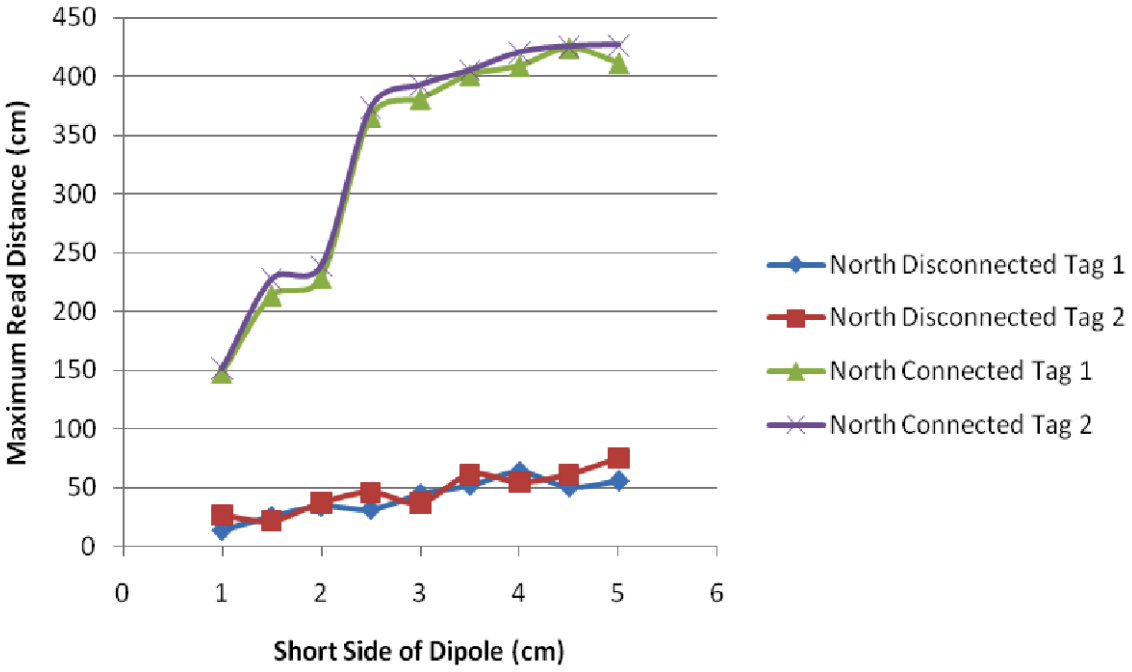

1 inch = 2.54 cm

Figure 152. Graph. Read range for tags disconnected and connected in the north direction.

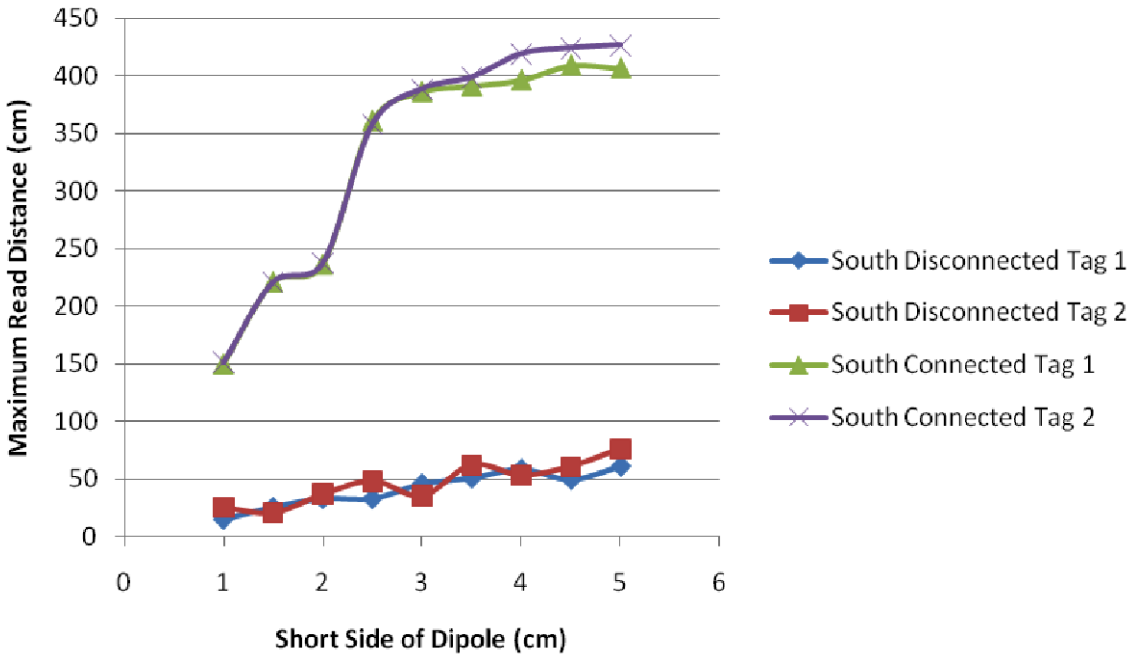

1 inch = 2.54 cm

Figure 153. Graph. Read range for tags disconnected and connected in the south direction.

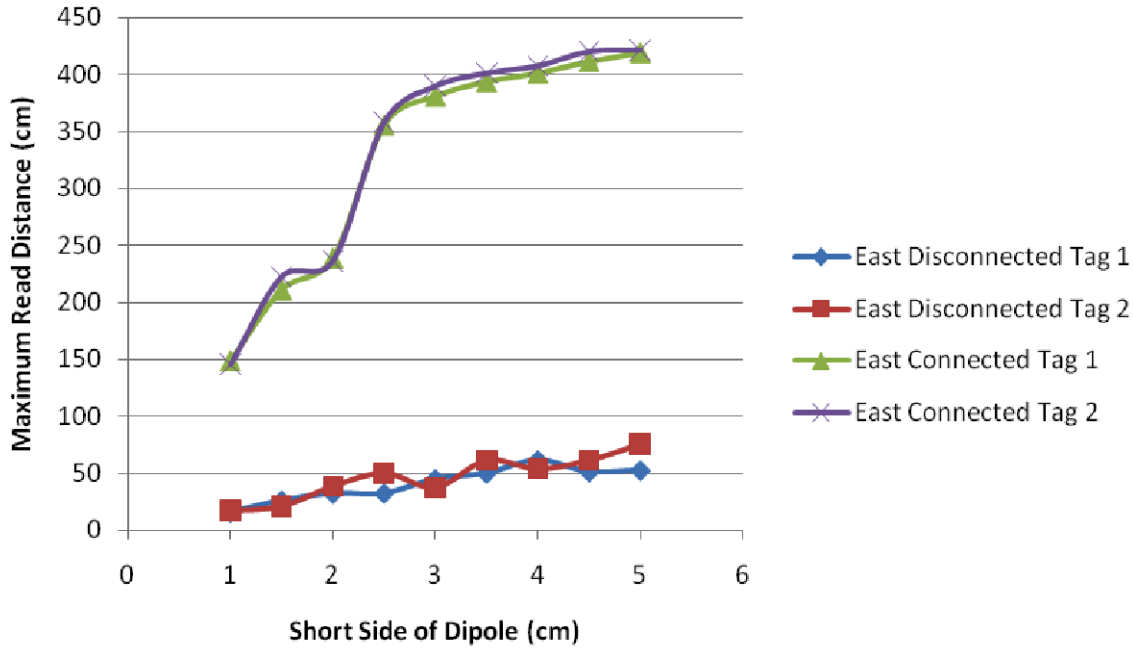

1 inch = 2.54 cm

Figure 154. Graph. Read range for tags disconnected and connected in the east direction.

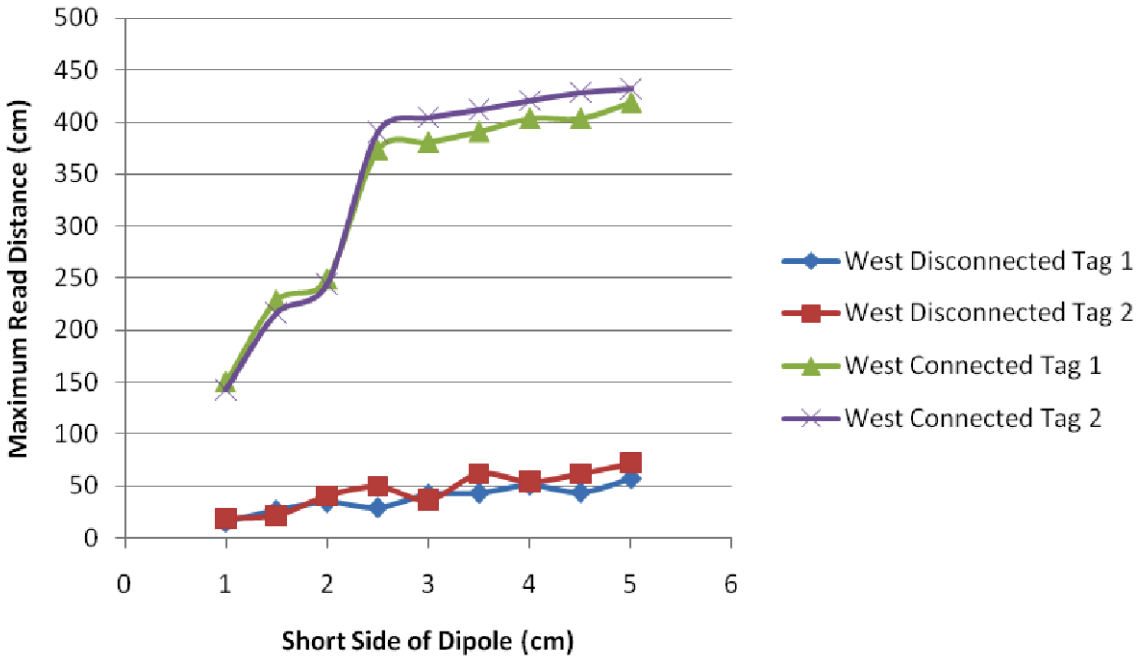

1 inch = 2.54 cm

Figure 155. Graph. Read range for tags disconnected and connected in the west direction.

PROTOTYPE DESIGN

Fabrication

Because the sensor must be placed on the surface of the existing pavement prior to the overlay, for practical field applications the RFID tag needs to be encapsulated to protect it from high temperatures and stresses during paving operations. However, the encapsulation must be able to transmit displacements to the antenna so that eventually the overlapped microswitch can open.

Polycarbonate (Lexan™) was used for the encapsulation. Its melting temperature is 513 °F (267 °C) and its glass transition temperature is 302 °F (150 °C), which are sufficient for paving conditions. The glue used for attaching the RFID tag to the polycarbonate and for assembling the polycarbonate parts was the SG496 strain gauge adhesive used previously in the laboratory studies.

The different parts used for encapsulating the tag are shown in figure 156, and the actual encapsulated tag is shown in figure 157. A 12-inch (300-mm)-long by 0.4-inch (10-mm)-wide piece of 0.095-inch (2.4-mm) thick polycarbonate was used as the top mounting plate for the RFID tag. This part transmits the crack opening movements in the overlay to the antenna. The 12-inch (300-mm) length is sufficient to span the area where the reflection crack might initiate. A longitudinal groove deep enough to fit the RFID tag is cut into the mounting plate and the dipole ends are glued in the groove. Two small 0.6- by 2.0-inch (15- by 50-mm) cross pieces of 0.18-inch (4.5-mm)-thick polycarbonate are glued to the end of the top mounting plate. The grooved polycarbonate bottom protection piece covers the dipole, and the mounting plate and is about 1.2 inches (30 mm) shorter than the top mounting plate. The bottom plate is glued only in one place to the top piece; the bottom plate provides a protection cover but does not interfere

with the movements in the top plate and the sensor. Only the two cross pieces of the assembled sensor are to be affixed to the underside of the asphalt overlay. Once a crack initiates, these cross pieces begin to spread, putting the sensor into tension and decreasing the overlap in the microswitch until it opens and the RFID tag stops giving a readable signal.

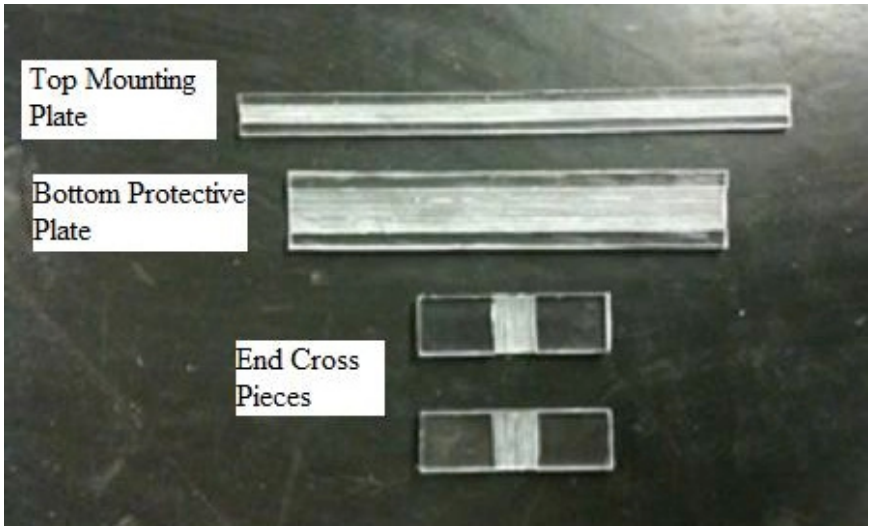

Figure 156. Photo. Parts for encapsulating the RFID tag.

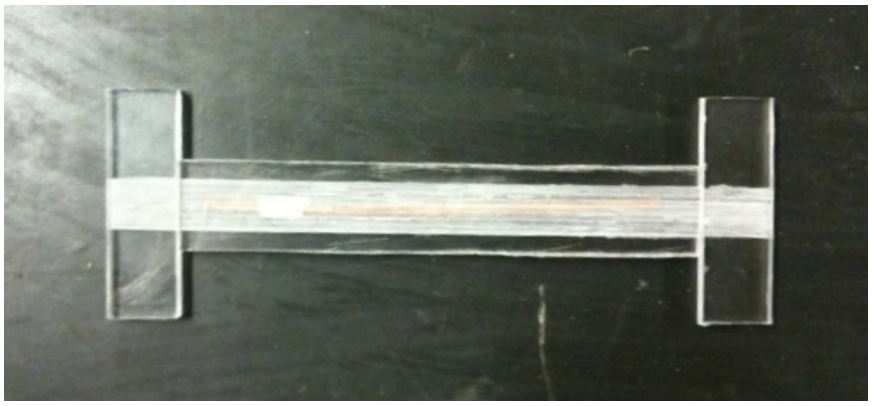

Figure 157. Photo. H-sensor for reflection crack detection.

Field Survivability and Read Range

Field tests were conducted to determine the survivability of these tags when subjected to high temperatures and compaction stresses during paving. Another objective of the field tests was to finalize the length of the antenna by evaluating read ranges of various lengths of tags through an asphalt overlay. This would give a better understanding how the tags perform through HMA as opposed to just air.

Eighteen RFID tags were prepared for the field tests. Two of them were encapsulated in the H-sensor configuration (figure 157). The other 16, however, were simply sandwiched between two 0.4–inch (10-mm)-wide polycarbonate plates, one of which was grooved so that the chip would not be damaged. These tags were used to evaluate the optimum antenna length. To determine

which antenna length would be the best for the crack sensor design, the maximum read distances for the connected case and disconnected case must be evaluated. The 16 tags were therefore paired in groups of two in which one tag was in the connected condition and the other disconnected. For simplicity, in the connected case, the copper antenna on either side of the chip was attached using conductive silver epoxy instead of overlapping one side. Six different lengths, as listed in table 32 , were evaluated. A 2-inch (50-mm) HMA milling and overlay project on Campus Drive at UMD was selected for the field trials. The encapsulated tags were placed longitudinally at 2-ft (0.6-m) intervals, as shown in figure 158. Quick set epoxy putty was used to make sure the tags were not displaced during the paving operations (figure 159 through figure 161).

Two days after the paving was completed, a read range study was conducted (figure 162). The number of successful reads over a 20-s interval was recorded. Although some tags were run over by equipment during the paving operations, only 1 tag of 18 failed to give any readings. The results for the maximum read distances for the tags are given in table 32. The 5-ft (1.5-m) height entries do not necessarily represent the maximum distance at which the tags could be read; 5 ft was just the highest distance above the pavement that could be achieved in the field. Establishing the actual maximum read distance beyond 5 ft was not necessary because a bumper-mounted reader antenna would not be at a higher distance than that above the pavement. Based on the results, the symmetric dipole with a 1.6-inch (40-mm) antenna on each side of the chip was determined to be the best configuration. When connected, it read at least 5 ft (1.5 m), and when disconnected, it read at only about 0.6 ft (0.2 m). If the reader antenna were mounted anywhere from 1.6 to 5 ft (0.5 to 1.5 m) above the pavement, the tag would give a signal when there was no crack and would not read once there was a crack in the pavement.

Figure 158. Photo. Encapsulated tags placed in the roadway prior to paving.

Figure 159. Photo. Close-up view of one of the encapsulated tags.

Figure 160. Photo. Two H-sensors in the pavement prior to paving.

Figure 161. Photo. Paving in progress.

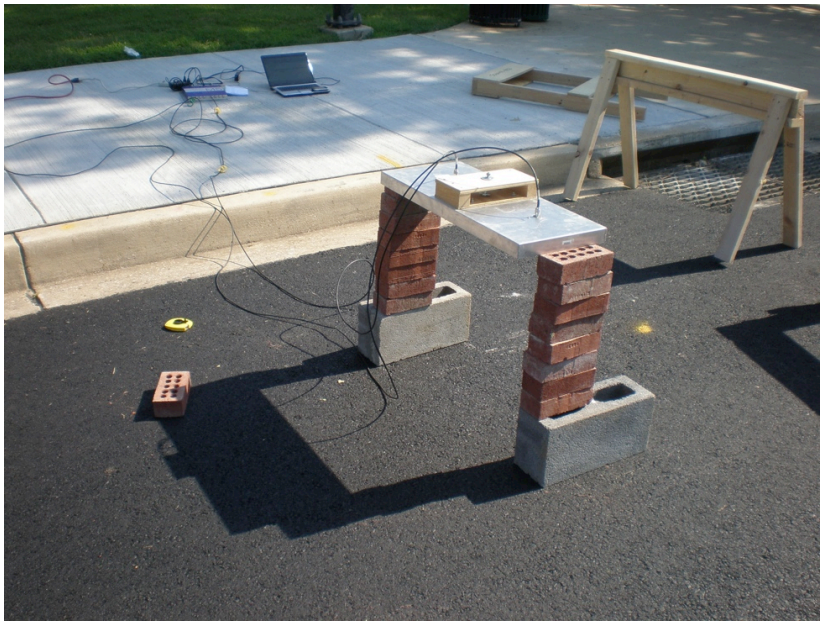

Figure 162. Photo. Read range test setup.

Table 32. Field test results.

RFID Tag	Maximum Read Distance (ft)	Number of Readings
8x8 C	1.0	14
8x8 D	2.2	9
6x6 D	2.4	4
8x8 C	5.0	9
8x8 D	3.3	9
6x6 C	4.2	12
6x6 D	3.1	9
5x5 C	5.0	16
5x5 D	1.5	15
4.5x4.5 C	**5.0**	**16**
4.5x4.5 D	**1.1**	**12**
4x4 C	5.0	17
4x4 D	0.6	17
8x1.5 C	3.5	16
8x1.5 D	1.1	16

C = connected antenna
D = disconnected antenna (simulating a crack)
Note: Bold font indicates optimum antenna configuration.
1 ft = 0.305 m

Laboratory Evaluation

A laboratory evaluation was undertaken to demonstrate that the crack sensor design can detect cracks in a 2-inch (50-mm) thick asphalt overlay. The end cross pieces of the encapsulated RFID tags were glued to the bottom of asphalt beams. The idea was that when the beam experienced a crack during three-point bending, the crack sensor microswitch would disconnect when the crack reached about 50 percent or more of the height of the beam.

The asphalt specimens were prepared at the standard fatigue tests size of 15 inches (380 mm) length, 2.5 inches (63 mm) width, and 2.0 inches (50 mm) height. The sides of the asphalt beams where painted white to make it easier to observe cracking. The ends of the copper antenna were glued to the grooved polycarbonate plate as shown in figure 163. Copper wires were glued to each side of the RFID tag antenna using conductive silver epoxy and then connected to an ohmmeter to measure resistance and determine at what point the conductivity was lost. The polycarbonate plate to which the RFID tag was glued was kept at a length equal to the effective length of the beam during bending. For the laboratory tests, the protective top cover for the tag was unnecessary and not used. However, to make sure the antenna overlap remained in place with a good connection, small polycarbonate pieces were glued across the groove over the microswitch.

Figure 163. Photo. RFID tag glued to the asphalt beam.

The specimens were then loaded for three-point bending using an Instron® compression machine. The tests were run in displacement control mode at a rate of 0.2 inches (5 mm) per minute. For the first three tests, the overlap of the copper antenna to the existing antenna was kept at about 0.02 inches (0.5 mm) as discussed previously. However, in all three instances the microswitch opened prior to a crack initiating. This could have been the result of several factors, including the slow loading rate used during the three-point bending, the properties of the beam, and other details of the test setup. For this reason, the third test was continued until the crack propagated 50 percent through the beam thickness even though the antenna was disconnected. Based on this test, it was determined that an antenna overlap of about 0.06 inches (1.5 mm) was required.

The next step was to run a test that would more closely represent the use of the crack sensor in the field. Instead of measuring resistance, the reader and antenna were positioned close to the bending machine. Although even in air the 1.6- by1.6-inch (40 by 40 mm) RFID tag could not be read from further away than 5 ft (1.5 m), in the laboratory during the test it was read at a distance more than 6 ft (1.8 m). This was most probably because of wave reflections coming from the metal machines surrounding the antenna. The antenna was placed 6 ft (1.8 m) away from the RFID tag. The connection was lost at a vertical displacement of the asphalt beam of about 0.8 inches (20 mm). At this point, the crack had propagated about 50 percent through the 2-inch (50-mm) beam thickness at a CMOD of between 0.1 to 0.15 inches (2 to 3 mm) (figure 164).

Figure 164. Photo. Crack propagation when the RFID tag stopped reading.

CONCLUSIONS AND RECOMMENDATIONS FOR REFLECTION CRACK DETECTION

Conclusions

HMA overlays are the most common rehabilitation methods for deteriorated pavements, and the most common distresses in these rehabilitated pavements are reflection cracks. The development of a crack sensor for detecting early onset of reflection cracks would be beneficial to State transportation departments because they could hold the contractor responsible for repairs in warranty construction projects, and it would help them plan better for future rehabilitation activities.

The reflection crack sensor concept is to implement a switch in the antenna circuit of the RFID tag: when there is no crack the RFID tag gives a signal that can be read at a distance, but after a crack forms, the signal becomes too weak to be read. The first design for the crack detection sensor employed conductive paint that would rupture at strain levels corresponding to a certain CMOD. The conductive paint dipoles had good read ranges, reaching about 6 ft (1.8 m). However, the drawback with the conductive paint was that none of the evaluated paints broke at the desired strain. The Aquadag® E™ carbon paint and the 18-percent silver paint survived strains up to 25,000 με without breaking.

The second sensor design was based on the use of copper antennae on both sides of the RFID tag, with one side having a mechanical overlap microswitch with the existing antenna cut from the original AD-223 RFID tags. A crack causes the antenna to be pulled in tension, eventually causing disconnection at the overlap microswitch and thus an open circuit in the antenna.

The RFID tag was encapsulated between polycarbonate protective covers to protect it from the high stresses and temperatures of paving operations. The ends of the copper modified antenna

were glued to the polycarbonate mounting plate, which is then affixed to the asphalt overlay. The plates both protect the tag and transmit displacements to the tag.

A survivability check of the encapsulated tags was conducted by embedding them in a 2-inch (50-mm)-thick overlay. Seventeen of 18 tags tested survived the paving operations; the tags could be read at distances of more than 5 ft in the optimal antenna configuration. Subsequent laboratory beam testing confirmed the concept of the overlapping copper antenna microswitch for the crack detection sensor. The sensor successfully detected the crack once it had grown to about 50 percent of the height of the beam.

As documented in this chapter, the RFID-based wireless crack detection system has been developed well beyond the basic conceptual stage. Prototypes were developed and successfully evaluated via laboratory testing and field trials. Unfortunately, project schedule and resources preluded comprehensive field evaluation over sufficiently long time periods to validate the ability of the system to detect early-onset reflection cracks under in service pavement conditions.

Recommendations

The tests to determine the amount of the overlap were conducted in a three-point bending configuration with a static load applied in the middle of the beam. This results in vertical deflections well beyond those expected in the field. Future tests should be conducted using a Texas Overlay Tester so that the beam fails in a way more similar to how the pavement would fail. Through these tests, the CMOD as a function of vertical crack propagation can be determined more accurately, and the overlap can be adjusted as needed. The flexibility of the design presented in this chapter allows one to use the sensor to detect small cracks or strains (less overlap) or detect larger cracks or strains (more overlap).

Laboratory testing using the Texas Overlay Tester should be followed by field trials on in-service pavements. The duration of these field trials would need to be on the order of 5 to 10 years to allow sufficient time for reflection cracks to initiate and propagate.

CHAPTER 8: GUIDANCE ON DATA INTEGRATION

INTRODUCTION

To ensure—and ideally to improve—the performance of asphalt pavements, it is vital that the influence of material properties on performance be clearly understood. Correlations between as-constructed properties of asphalt concrete in construction databases and field performance of pavements in PMSs can quantify the link between material quality and performance.

Unfortunately, the dissimilar ways in which these two sets of data are recorded with respect to location along the pavement alignment makes it difficult to establish these correlations. As depicted in figure 165, HMA concrete is produced at a production facility and then trucked to the highway construction site for offloading into the asphalt paver. HMA producers sample their production periodically from departing trucks and perform various QC tests to ensure that the mixture properties (gradation, volumetrics) remain within acceptable limits. As part of a QA program, agencies typically take additional samples for acceptance testing to corroborate the producer's QC test results and to establish pay factors. QC and acceptance samples are typically taken at specified tonnage intervals from delivery trucks as they leave the asphalt plant. For example, in Maryland, a minimum of one QC sample (volume sufficient for the full suite of tests) is typically taken for each 1,000-T (909-t) sublot of production. This corresponds roughly to one truck out of every 50 leaving the plant production or approximately 1.25 lane-mi (2 lane-km) of paving for a 2-inch (50-mm) overlay. Test results from this sample are assumed to be representative of the entire 1,000-T (909-t) sublot. One acceptance sample is also taken for each day's production (on the order of 4,000 T (3,636 t) or more). Additional in-place material sampling (cores for field density determination) is also typically performed on the compacted mat. All of these QA material property data can then be stored in the agency's materials management system (MMS) by lot and sublot.

PMS data, on the other hand, are collected at regular intervals during the pavement life after construction and referenced to a specific location in the roadway. For example, in Maryland, an automated distress measurement vehicle (figure 165) collects roughness, rutting, and visual distress data for the entire State highway network on a 2-year cycle. These pavement management data are automatically referenced to the milepoint (or, alternatively, geospatial) location along the roadway.

It is often desirable to compare the PMS distress data during the service life of the pavement with the material property data collected during construction—e.g., for forensic investigations into premature rutting, cracking, or other failures along a particular section of roadway. Unfortunately, at present there is no good practical way to determine precisely where in the roadway the sampled and tested lot/sublot of material was deposited. In many instances, the milepoint range for the entire 1,000 T (909 t) of production represented by the sampled truckload is not even recorded during construction. Unless the HMA QA data can also be tied to a spatial location along the pavement, it cannot be correlated with PMS data on anything better than a crude project-by-project basis.

These problems caused by mismatched referencing of pavement data were highlighted during a pilot implementation of the *HMAView* software by the MSHA. *HMAView* is a Web-based

application for integrating construction, materials, pavement management, and other pavement data.[27] For the pilot project implementation, the spatial location of the QA material property data measured during the original construction had to be laboriously and crudely estimated by hand.

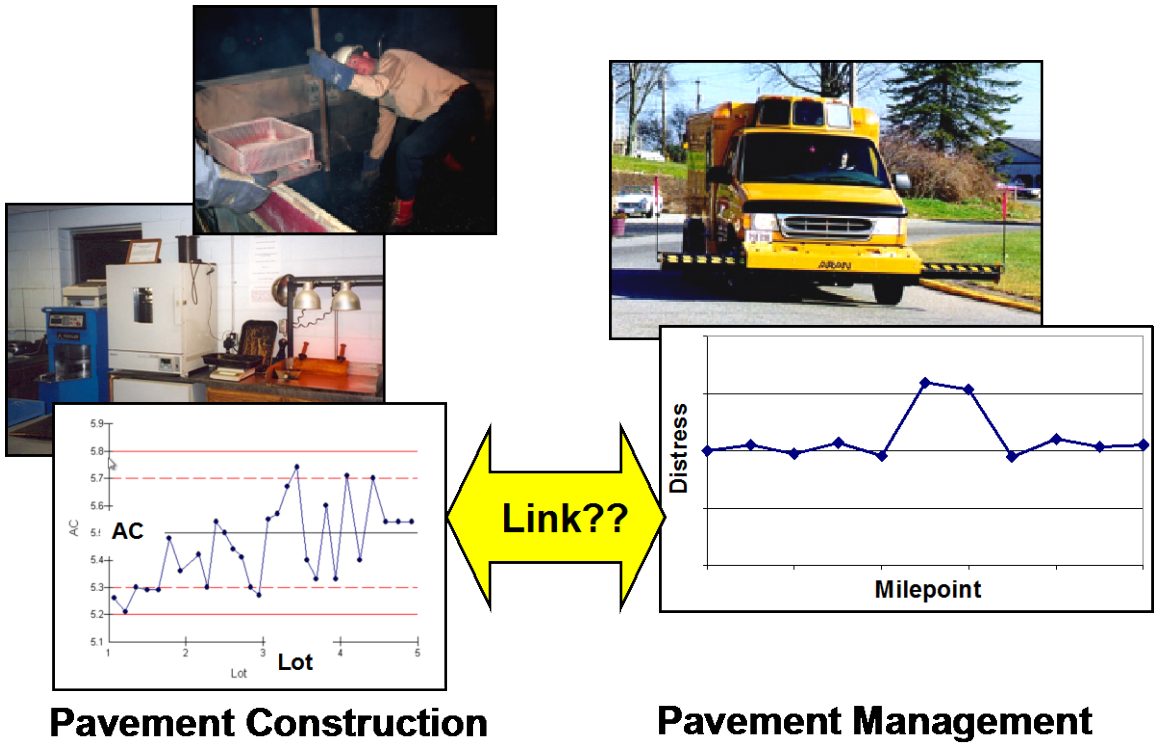

Figure 165. Illustration. Referencing problem in linking pavement construction and pavement management data.

As described in chapters 2 through 4 of this report, inexpensive expendable electronic sensors based on passive RFID technology can be used to identify or tag truckloads of hot mix asphalt as they leave the production plant. These sensors pass through the paver and are compacted into the finished mat. After construction, a vehicle-mounted or handheld scanner is used to electronically "read" the identity tags and cross reference them with latitude and longitude coordinates using GPS technology. These geospatially referenced MMS data can then be directly linked to as-constructed in-place test results and thus to future pavement performance data recorded in the agency's PMS, enabling robust statistical analyses of the correlations between material properties and observed performance.

The application of RFID technology for tracking HMA placement was the genesis for this entire research project. It is also the application that is most suited to near-term commercial implementation. Its major benefit is that it provides a simple and straightforward means for integrating an agency's QA materials property data with its pavement performance measurements. However, several steps are needed to enable this data integration. Given the wide range of materials and pavement management systems in use among the States, the implementation of these steps will be different for each agency. The general guidelines provided

in this chapter for the data integration steps can be adapted to each agency's specific database structures, policies, procedures, and information technology infrastructure.

GUIDELINES FOR INTEGRATING MMS AND PMS DATABASES

A wide variety of MMSs and PMSs have been implemented by highway agencies nationwide. In some cases, these systems may have been developed in-house, either by agency personnel or by consultants, and subsequently modified and extended over time. This makes it difficult to develop a "one size fits all" set of guidelines for integrating these two sets of data. Therefore, the approach adopted here is to outline the general set of issues that must be addressed when integrating these two data sources and to illustrate them, where possible, using application examples from AASHTOWare™'s SiteManager™ product, Fugro's Roadware/Vision software, the MSHA MarylandWare software, and other sources from the literature and, where appropriate, database examples using Microsoft® Access.[28,29] (The Microsoft® Access 2007 version is used.) The SiteManager™ and Roadware/Vision software, in particular, are used by a significant number of State transportation departments for materials management and pavement management/data display, respectively.

The basic components required for implementing an RFID-based HMA materials tracking system and for integrating MMS and PMS databases are as follows:

1. Linkage of RFID identifiers to material samples collected at the plant or in the field.

2. Linkage of GPS latitude and longitude coordinates to RFID identifier and thus to the material sample.

3. (Optional) Conversion of latitude/longitude to PMS location reference system (e.g., milepoints).

4. Extraction of MMS and PMS data by roadway location.

5. Display of extracted data for data analysis and other purposes.

Each of these components is discussed in more detail in the following subsections. The focus here is on QA material samples taken from RFID-tagged trucks as they leave the HMA production plant and the material property tests that are obtained from these samples. QA samples taken directly from the roadway are not considered here because the spatial location of these samples is known directly although they may not be recorded to allow linkage with the PMS. The terms used in these discussions are defined as follows:

- Tag: An RFID tag placed in a sampled transport truck as it leaves the HMA production plant. For redundancy, there will generally be multiple tags in a single transport truck.

- Tag ID: The digital identification label that is electronically coded into each RFID tag.

- Material sample (or sample): The material sampled from a single truck as it leaves the HMA production plant. It is assumed here for simplicity that there is one sample per truck, but the logic could be easily generalized to multiple samples per truck.

- Test: A QA material property test obtained for a material sample. There will in general be multiple QA material property tests (e.g., asphalt content, maximum specific gravity, etc.) associated with a material sample.

- Join: The relational database operation that combines information from multiple database tables based upon common data elements shared by the tables (e.g., ID fields).

Linkage of RFID Identifier to Material Samples

For redundancy, multiple RFID tags are deposited in each sampled truck as it leaves the plant because some of the tags may fail or be unreadable after being compacted into the roadway. In addition, multiple test specimens and test types may be associated with each sample in the MMS. The following two types of relationships must therefore be addressed:

- The many-to-one relationship between RFID tags and material samples.

- The one-to-many relationship between a material sample and the various test specimens that are prepared from the material sample.

Dealing with the second issue first, this classic one-to-many data relationship is incorporated directly into most MMSs, including the SiteManager™ Laboratory Inventory Management System (LIMS) module. In SiteManager™ LIMS, a sample ID is established first and then multiple test types are associated with it, as shown in figure 166. This can also be accomplished using a standard relational database join operation as illustrated schematically in figure 167 through **Figure** 169. The query, given both in terms of the Microsoft® Access 2007 query designer and its Structured Query Language equivalent, extracts the three material property values (two asphalt contents and one voids in the mineral aggregate measurement) from tests performed on material from sample 54321. Note that the query in figure 168 can be implemented in other and arguably more efficient ways; the particular query structure in figure 168 is designed to highlight the one-to-many relationship between material samples and material property tests.

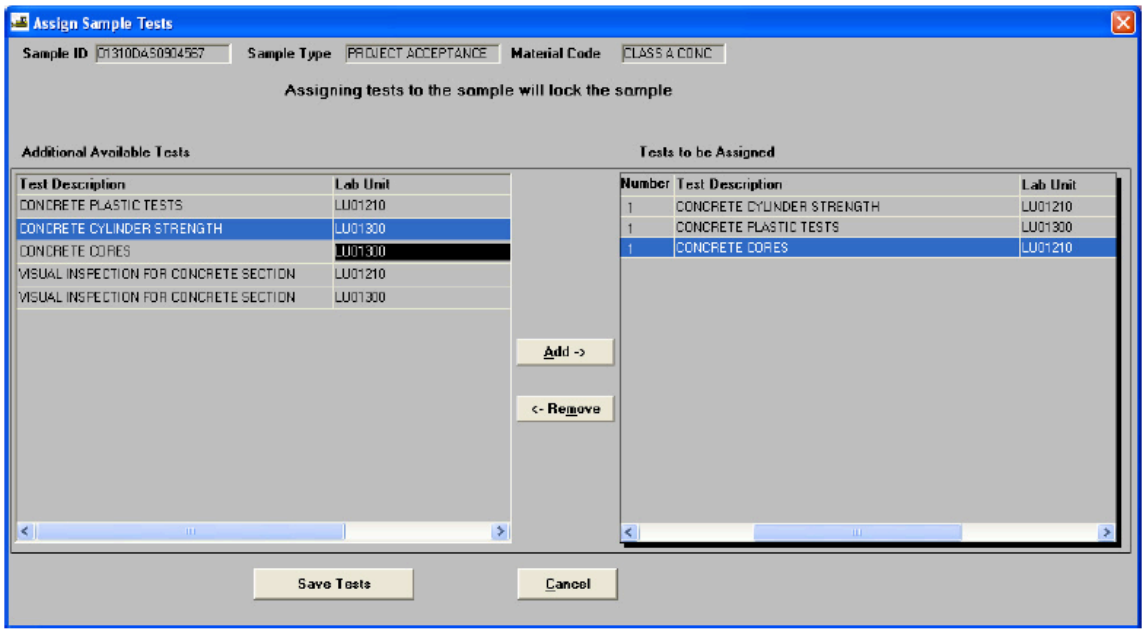

Figure 166. Screen Capture. Assign Sample Tests screen from SiteManager™ LIMS.

Samples

Sample_ID	Contract	Sample_Typ	Sample_Dat
54320	MD295-1234a	Loose HMA	8/18/2011
54321	MD295-1234a	Loose HMA	8/18/2011
54322	MD295-1234a	Loose HMA	8/18/2011

Tests

Test_ID	Test_Date	Prop_Type	Prop_Value
87650	8/20/2011	AC	4.3
87651	8/20/2011	AC	4.1
87652	8/21/2011	AC	4.6
87653	8/20/2011	VMA	15.6
87654	8/21/2011	VMA	14.8
87655	8/20/2011	AC	4.5

Test_Sample_Link

Test_ID	Sample_ID
87650	54321
87651	54321
87652	54322
87653	54321
87654	54320
87655	54320

Figure 167. Screen Capture. Schematic for associating a single sample (Sample_ID=54321) with multiple test specimens/material properties (Microsoft® Access 2007): Samples, Tests, and Test_Sample_Link tables.

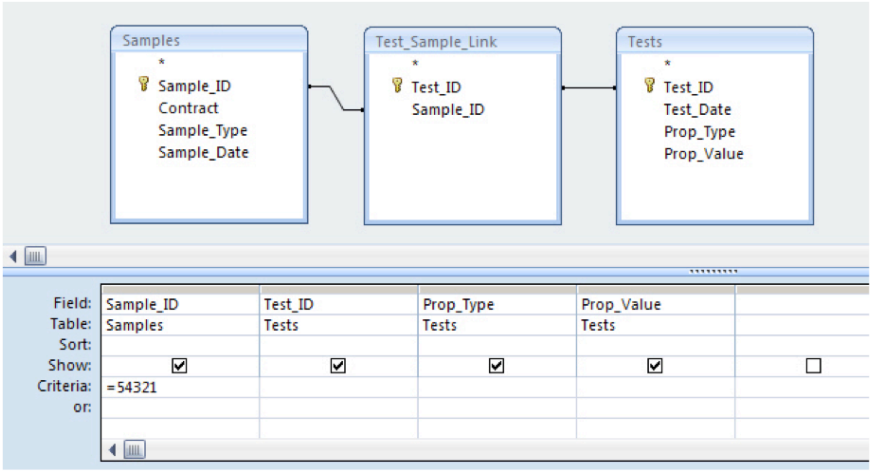


```
SELECT Samples.Sample_ID, Tests.Test_ID, Tests.Prop_Type, Tests.Prop_Value
FROM (Samples INNER JOIN Test_Sample_Link ON Samples.Sample_ID = Test_Sample_Link.Sample_ID)
INNER JOIN Tests ON Test_Sample_Link.Test_ID = Tests.Test_ID
WHERE (((Samples.Sample_ID)=54321));
```

Figure 168. Screen Capture. Schematic for associating a single sample (Sample_ID=54321) with multiple test specimens/material properties (Microsoft® Access 2007): Query.

Sample_ID	Test_ID	Prop_Type	Prop_Value
54321	87650	AC	4.3
54321	87651	AC	4.1
54321	87653	VMA	15.6

Figure 169. Screen Capture. Schematic for associating a single sample (Sample_ID=54321) with multiple test specimens/material properties (Microsoft® Access 2007): Query results.

The second issue of associating potentially multiple RFID tags IDs to a single material sample can be handled in either of two ways:

1. Because the multiple RFID tags are intended to be redundant, only one of the readable tags in the set can be selected as representing the entire set. The linkage between RFID tags and material samples then simplifies to a one-to-one relationship. The tag ID can then be simply included as another data element in the material samples table.

2. If it is desirable to maintain the redundancy between tags and samples, a linking table and associated join operations can be established between RFID tags and material samples and thus between tags and test specimens, as illustrated schematically in figure 170 through figure 172. The Tag_Sample_Link table captures the many-to-one relationship between tag IDs and samples. The query passes this additional information along, generating a table of tag IDs and the material property values measured for all tests from the sample associated with the tag IDs.

Tag_Sample_Link

Test_ID	Sample_ID
87650	54321
87651	54321
87652	54322
87653	54321
87654	54320
87655	54320

Figure 170. Screen Capture. Schematic for associating multiple RFID tags with a single material sample (Sample_ID=54321) having multiple test specimens/material properties (Microsoft® Access 2007): Tag_Sample_Link table (see figure 169 for other tables in query).

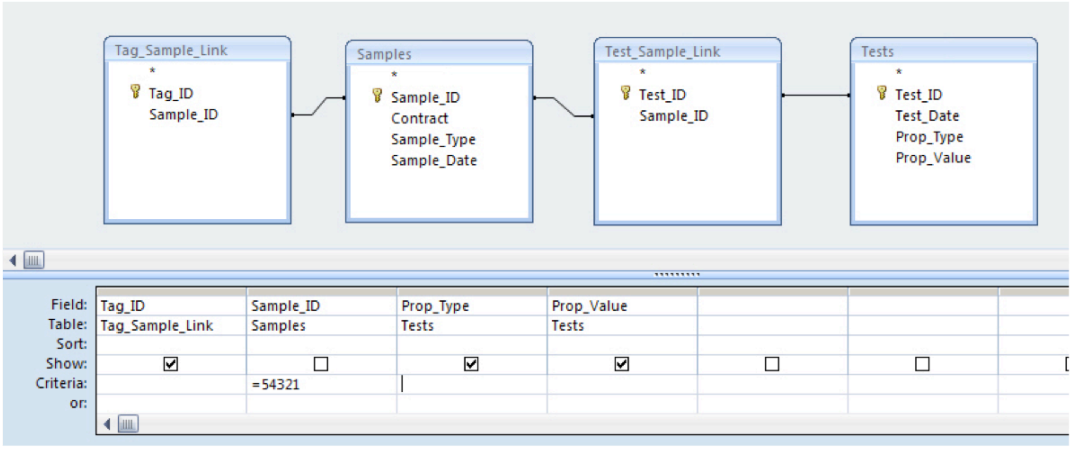


```
SELECT Tag_Sample_Link.Tag_ID, Tests.Prop_Type, Tests.Prop_Value
FROM ((Samples INNER JOIN Tag_Sample_Link ON Samples.Sample_ID = Tag_Sample_Link.Sample_ID)
INNER JOIN Test_Sample_Link ON Samples.Sample_ID = Test_Sample_Link.Sample_ID)
INNER JOIN Tests ON Test_Sample_Link.Test_ID = Tests.Test_ID
WHERE (((Samples.Sample_ID)=54321));
```

Figure 171. Screen Capture. Schematic for associating multiple RFID tags with a single material sample (Sample_ID=54321) having multiple test specimens/material properties (Microsoft® Access 2007): Query.

Tag_ID	Prop_Type	Prop_Value
100002	AC	4.3
100004	AC	4.3
100002	AC	4.1
100004	AC	4.1
100002	VMA	15.6
100004	VMA	15.6

Figure 172. Screen Capture. Schematic for associating multiple RFID tags with a single material sample (Sample_ID=54321) having multiple test specimens/material properties (Microsoft® Access 2007): Query results.

Linkage of GPS Coordinates to RFID Identifier/Material Sample

By definition, there is a one-to-one relationship between GPS coordinates and an RFID tag ID—i.e., the RFID tag can only be in one spatial location. The GPS coordinates can be entered directly into the Tags table after the tag has been interrogated by the vehicle-mounted reader and antenna system after construction.

The linkage of GPS coordinates to material samples is a bit more difficult. As described in the preceding section, there may be one or more RFID tag IDs associated with a single material sample. Consequently, there may be one or more sets of GPS coordinates associated with each single material sample. This issue can be addressed via one of three possible approaches:

1. Single RFID tag/single set of GPS coordinates: Most MMSs permit entry of one-to-one location links for material samples. The current version of the SiteManager™ LIMS and the MarylandWare QC/QA module permit direct entry of latitude and longitude for a sample; an example from the MarylandWare QC/QA module is shown in figure 173. The single set of latitude and longitude coordinates can be simply entered manually into the material sample screens. Alternatively, software utilities can be developed locally to automate entry of the latitude and longitude coordinates from the tags table.

2. Multiple RFID tags/sets of GPS coordinates: This can be handled in any of three ways:

    a. Because the multiple RFID tags are intended to be redundant, only one of the readable tags in the set can be selected as representing the entire set. The linkage between the GPS coordinates for the selected RFID tag and material samples then simplifies to a one-to-one relationship. Entry and storage of the GPS coordinates in this case is similar to that in the preceding item 1.

    b. Average or "best estimate" latitude and longitude values can be determined for the multiple redundant RFID tags associated with one sample. The linkage between the best-estimate GPS coordinates and material samples then simplifies to a one-to-one relationship. Entry and storage of the GPS coordinates in this case is similar to that in the preceding item 1.

    c. If it is desirable to maintain the redundancy between tags/sets of GPS coordinates and samples, a linking table and associated join operations can be established between the RFID tags/GPS coordinates and material samples and thus between tags/GPS coordinates and test specimens, as illustrated schematically in figure 174 through figure 176. The new Tags table contains the tag ID and associated latitude and longitude. The Tag_Sample_Link table captures the many-to-one relationship between tag IDs/GPS coordinates and samples. The query then uses this information to generate an output table listing for each tag the multiple material property test results determined from the material sample associated with that tag. As before, the query in figure 175 can be implemented in other and arguably more efficient ways; the particular query structure in figure 175 is designed to highlight the many-to-one relationship between RFID tags and material samples and the one-to-many relationship between material samples and material property tests.

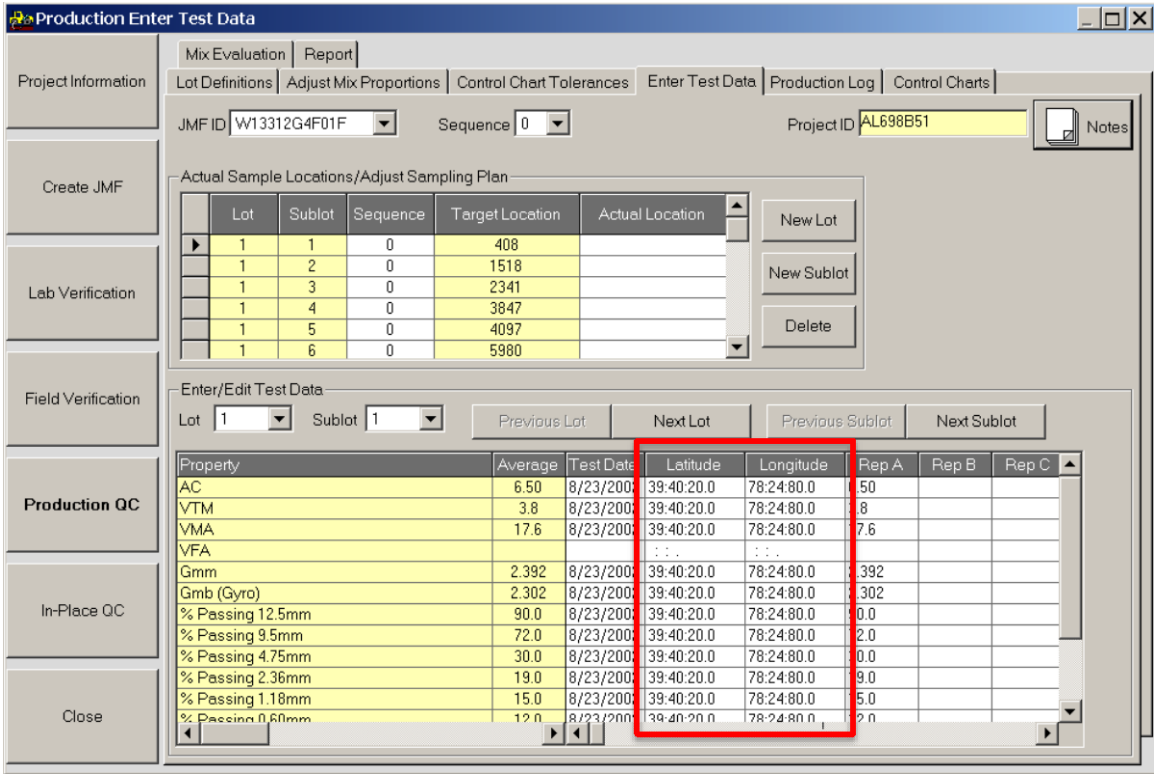

Figure 173. Screen Capture. MarylandWare example of direct entry of latitude and longitude location for a material sample (boxed area of screen).

Tags

Tag_ID	Latitude	Longitude
100001	39.512	-76.8432
100002	39.5826	-76.8444
100003	39.5831	-76.8456
100004	39.5824	-76.8446
100005	39.5833	-76.8454
100006	39.5829	-76.8458

Figure 174. Screen Capture. Schematic for associating multiple sets of GPS coordinates with a single material sample (Sample_ID=54321) having multiple test specimens: Tags table, augmented with GPS coordinates (see figure 167 and figure 170 for other tables in query).

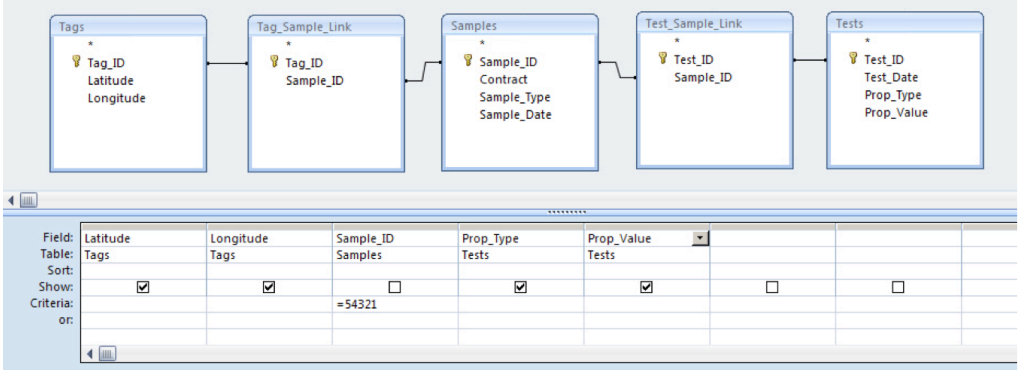


```
SELECT Tags.Latitude, Tags.Longitude, Tests.Prop_Type, Tests.Prop_Value
FROM (Tags INNER JOIN ((Samples INNER JOIN Tag_Sample_Link ON Samples.Sample_ID = Tag_Sample_Link.Sample_ID)
INNER JOIN Test_Sample_Link ON Samples.Sample_ID = Test_Sample_Link.Sample_ID) ON Tags.Tag_ID = Tag_Sample_Link.Tag_ID)
INNER JOIN Tests ON Test_Sample_Link.Test_ID = Tests.Test_ID
WHERE (((Samples.Sample_ID)=54321));
```

Figure 175. Screen Capture. Schematic for associating multiple sets of GPS coordinates with a single material sample (Sample_ID=54321) having multiple test specimens: Query.

Latitude	Longitude	Prop_Type	Prop_Value
39.5826	-76.8444	AC	4.3
39.5826	-76.8444	AC	4.1
39.5826	-76.8444	VMA	15.6
39.5824	-76.8446	AC	4.3
39.5824	-76.8446	AC	4.1
39.5824	-76.8446	VMA	15.6

Figure 176. Screen Capture. Schematic for associating multiple sets of GPS coordinates with a single material sample (Sample_ID=54321) having multiple test specimens: Query results.

Conversion of Latitude/Longitude to Roadway Location

The spatial referencing of the tags, and therefore of the associated material samples and material property test results in the MMS, are in terms of two-dimensional latitude and longitude. However, PMS data are most commonly spatially referenced in terms of linear milepoints along a route. Therefore, it is necessary to convert latitude and longitude to route and milepoint if the MMS data are to be combined with the PMS data. This is typically done by pairing GPS coordinates with milepoint locations at key points along the route and then interpolating. More information can be found in Schwartz and Bentahar and in O'Neill and Harper.[30,31]

Fortunately, most PMS software (including Roadware/Vision) already incorporates such coordinate conversion routines. In part, this is because some important PMS data elements—e.g., falling weight deflectometer test data as collected using Dynatest® and other common commercial systems—are spatially located automatically in terms of GPS coordinates. The material property data measured during construction can thus be exported from the MMS and imported into the PMS, and the PMS conversion routines can translate the GPS coordinates to milepoints. All MMSs and PMSs incorporate some type of data export/import routines, although

there may be formatting incompatibilities that would need to be resolved on an agency-by-agency basis.

Combining MMS and PMS Data by Location

Once the GPS coordinates for the MMS data have been converted to milepoints within the PMS, they can be extracted and combined with any desired PMS data elements. This would typically be done using the query facilities built into the PMS. Figure 177 through figure 179 illustrate schematically how to extract both MMS and PMS data along a particular section of roadway. New Route_No and Milepoint data elements have been added to the Tags table; the latitude and longitude coordinates and the PMS spatial reference conversion routines are used to generate the values for populating these data elements. The query in figure 177 through figure 179 is similar to that in figure 174 through figure 176, with the only difference being the reporting of route number and milepoint instead of latitude and longitude for each material property test value.

Tags

Tag_ID	Latitude	Longitude	Route_No	Milepoint
100001	39.5120	-76.8432	I-70	82.55
100002	39.5826	-76.8444	I-70	83.20
100003	39.5831	-76.8456	I-70	84.13
100004	39.5824	-76.8446	I-70	83.76
100005	39.5833	-76.8454	I-70	84.25
100006	39.5829	-76.8458	I-70	85.48

Figure 177. Screen Capture. Schematic for extracting MMS data along a portion of roadway (I-70 between milepoints 83 and 84): Tags table, augmented with milepoint data elements (see figure 167 and figure 170 for other tables in query).

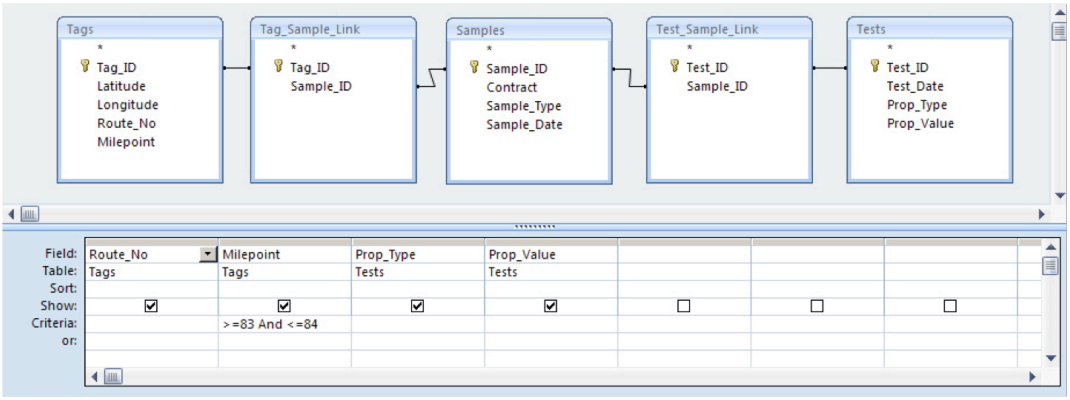


```
SELECT Tags.Route_No, Tags.Milepoint, Tests.Prop_Type, Tests.Prop_Value
FROM (Tags INNER JOIN ((Samples INNER JOIN Tag_Sample_Link ON Samples.Sample_ID=Tag_Sample_Link.Sample_ID)
INNER JOIN Test_Sample_Link ON Samples.Sample_ID=Test_Sample_Link.Sample_ID) ON Tags.Tag_ID=Tag_Sample_Link.Tag_ID)
INNER JOIN Tests ON Test_Sample_Link.Test_ID=Tests.Test_ID
WHERE (((Tags.Milepoint)>=83 And (Tags.Milepoint)<=84));
```

Figure 178. Screen Capture. Schematic for extracting MMS data along a portion of roadway (I-70 between milepoints 83 and 84): Query.

Route_No	Milepoint	Prop_Type	Prop_Value
I-70	83.20	AC	4.3
I-70	83.20	AC	4.1
I-70	83.20	VMA	15.6
I-70	83.76	AC	4.3
I-70	83.76	AC	4.1
I-70	83.76	VMA	15.6

Figure 179. Screen Capture. Schematic for extracting MMS data along a portion of roadway (I-70 between milepoints 83 and 84): Query results.

Figure 180 through figure 182 show a simple example query for extracting International Roughness Index (IRI) values from a PMS database. The output from the query lists the measured IRI values and associated milepoint along the specified section of roadway.

IRI

Route_No	Milepoint	Test_Date	IRI
I-70	82.5	09/29/11	109.5
I-70	82.6	09/29/11	109.8
I-70	82.7	09/29/11	106.5
I-70	82.8	09/29/11	108.4
I-70	82.9	09/29/11	103.2
I-70	83.0	09/29/11	100.1
I-70	83.1	09/29/11	104.2
I-70	83.2	09/29/11	102.6
I-70	83.3	09/29/11	105.5
I-70	83.4	09/29/11	106.6
I-70	83.5	09/29/11	105.8
I-70	83.6	09/29/11	103.5
I-70	83.7	09/29/11	104.4
I-70	83.8	09/29/11	109.2
I-70	83.9	09/29/11	112.3
I-70	84.0	09/29/11	108.0
I-70	84.1	09/29/11	107.3
I-70	84.2	09/29/11	102.7
I-70	84.3	09/29/11	103.8
I-70	84.4	09/29/11	106.7
I-70	84.5	09/29/11	108.3
I-70	84.6	09/29/11	100.6
I-70	84.7	09/29/11	103.1
I-70	84.8	09/29/11	104.2
I-70	84.9	09/29/11	102.5
I-70	85.0	09/29/11	103.5
I-70	85.1	09/29/11	105.7
I-70	85.2	09/29/11	101.3
I-70	85.3	09/29/11	104.4
I-70	85.4	09/29/11	104.0
I-70	85.5	09/29/11	108.1

Figure 180. Screen Capture. Schematic for extracting PMS data along a portion of roadway (I-70 between milepoints 83 and 84): IRI table.

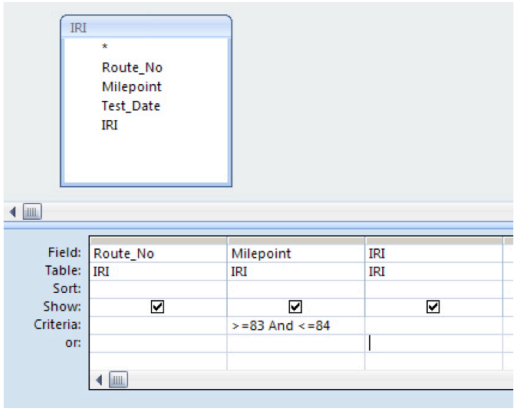


```
SELECT IRI.Route_No, IRI.Milepoint, IRI.IRI
FROM IRI
WHERE (((IRI.Milepoint)>=83 And (IRI.Milepoint)<=84));
```

Figure 181. Screen Capture. Schematic for extracting PMS data along a portion of roadway (I-70 between milepoints 83 and 84): Query.

Route_No	Milepoint	IRI
I-70	83.0	100.1
I-70	83.1	104.2
I-70	83.2	102.6
I-70	83.3	105.5
I-70	83.4	106.6
I-70	83.5	105.8
I-70	83.6	103.5
I-70	83.7	104.4
I-70	83.8	109.2
I-70	83.9	112.3
I-70	84.0	108.0

Figure 182. Screen Capture. Schematic for extracting PMS data along a portion of roadway (I-70 between milepoints 83 and 84): Query results.

Display of Extracted Data

Once the MMS and PMS data have been extracted as described in the preceding section, they can be displayed together, typically using the built-in data display routines in the PMS. Figure 183 shows a Roadware iVision display of multiple datasets versus milepoint location along the roadway. One of the data series in the lower left chart or the data series in the lower right chart in the figure could be replaced by one of the MMS data elements, e.g., asphalt content as measured during construction.

The exported MMS and PMS data can also be exported for subsequent external analyses. Most PMSs have the capability of exporting query results, often through some type of "report generator" feature. The available formats for the output data will vary from system to system.

Figure 184 is an example of using Microsoft® Excel for displaying the extracted PMS and MMS data. The PMS data elements (IRI) and MMS data elements (asphalt content) are displayed as separate series (and with separate y-axes). The data in figure 184 are consistent with those in the

earlier schematic examples in figure 177 through figure 182. An examination of figure 184 suggests that the localized higher roughness around milepoint 83.9 may be associated with a low and/or variable asphalt content. These types of insights, many of which will be far more powerful than in these simple examples, are the key benefits of integrating MMS and PMS data.

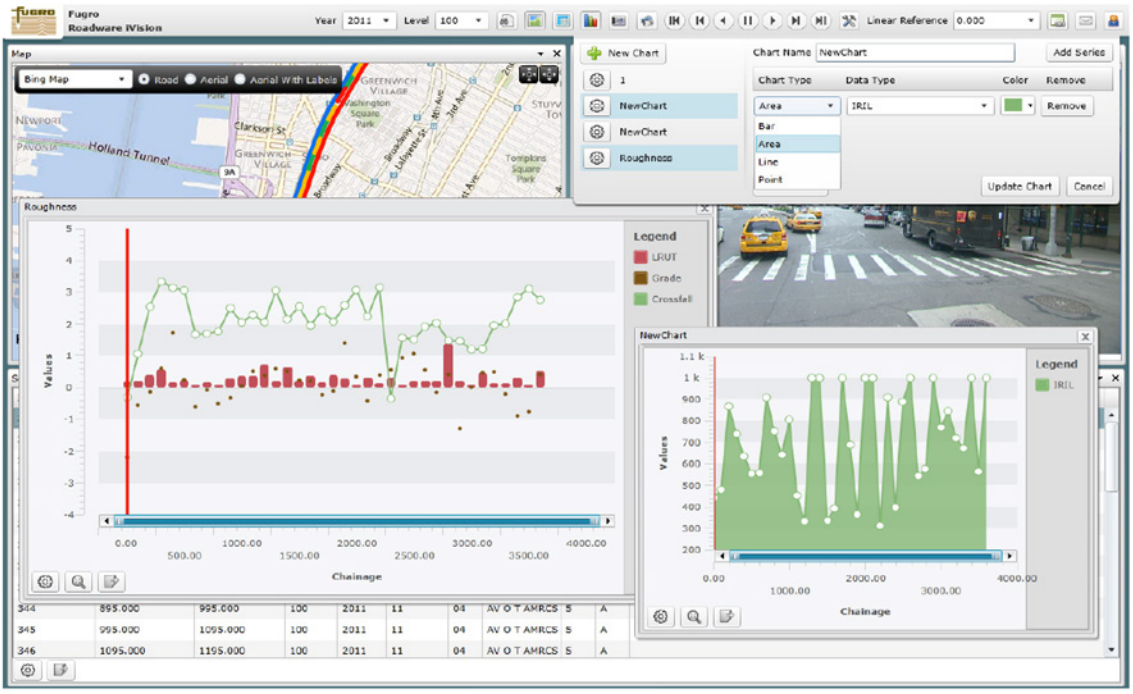

Figure 183. Screen Capture. Roadware iVision charts screenshot.[(29)]

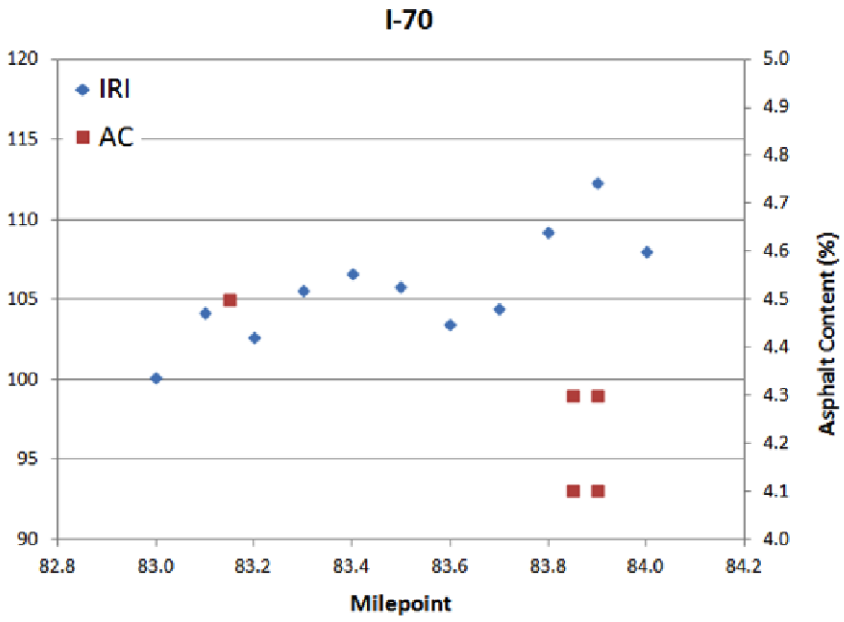

1 inch/mi = 0.041 m/km
1 mi = 1.61 km

Figure 184. Graph. Roughness (IRI) from PMS and asphalt content from MMS along a specified section of roadway (I-70 between milepoints 83 and 84).

DATA INTEGRATION SUMMARY

Maximum use of material property data collected during construction and pavement management data collected during service life is possible only when both sets of data can be related to a common spatial referencing system. Using RFID tags to track loads of sampled and tested material enables geospatial identification of the location of the delivered material in the pavement. These material properties can then be linked with the corresponding spatially located pavement performance data from the PMS.

Because of the wide variety of MMS and PMS used by agencies, it is possible only to outline the general steps to link these two datasets via geospatial coordinates. This chapter provides examples of the following necessary operations:

- Linkage of one or more RFID identifiers to material samples.
- Linkage of GPS coordinates to RFID identifier/material sample.
- Conversion of latitude/longitude to roadway location.
- Combining of MMS and PMS data by location.
- Display of extracted data.

The details of implementing these operations will depend on the particular MMS and PMS used by an agency.

CHAPTER 9: CONCLUSIONS

PROJECT OBJECTIVES

The original objective of this project was to demonstrate that inexpensive expendable radio RFID tags can be used to identify the spatial location along the pavement alignment of specific truckloads of HMA (or warm/cold mix asphalt) production. These tags are placed in the truckload as it leaves the production plant, pass through the paver, and are compacted into the finished mat. Cross referencing these tags with GPS latitude and longitude coordinates after construction allows spatial referencing of QA material property data measured at the production plant, enabling linkage to other spatially referenced in-place test results and PMS pavement performance data. This use of the large QA and PMS datasets already collected by highway agencies will permit more robust analyses and insights into the relationships between HMA material properties and actual pavement performance.

During the pursuit of this original objective, additional applications of RFID technologies to pavements were identified for evaluation:

- Evaluation of potential problems caused by surfaced tags.
- Exploration of SAW RFID technology for improved performance of small format tags.
- Demonstration of RFID tracking of placement of PCC loads in pavements.
- Provision of guidance to agencies on data integration.

These issues were pursued in the final phase of the project.

KEY FINDINGS

Key findings of this work are summarized here organized by the following topical areas:

- RFID tracking of HMA placement (chapters 2, 3, and 4).
- RFID tracking of PCC placement (chapter 5).
- Pavement temperature measurement using SAW RFID (chapter 6)
- Reflection crack detection (chapter 7).
- Guidance on data integration (chapter 8).

RFID Tracking of HMA Placement

The feasibility of using RFID tags to track HMA placement was evaluated via: 1) literature review, 2) identification of appropriate RFID technology, and 3) prototype tag development and evaluation. Key findings from the feasibility evaluation are as follows:

- UHF (860–960 MHz) passive RFID technology was determined to be best suited to the HMA paving application. The advantages of passive UHF RFID included small tag size, low cost, adequate read range, and wide commercial availability.

- A ThingMagic Mercury® 5 RFID system was evaluated as being most appropriate for use on this project and was therefore acquired.

- Suitable RFID tags of appropriate size were identified. These included Alien® Gen 2 1x1 and Alien® Gen 2 2x2 tags. The larger format Alien® Gen 2 2x2 tags had superior read performance and were adopted for most of the study. A UPM Raflatac® 1x2 tag was subsequently added to the study after the Alien® 1x1 tags were taken out of production by the manufacturer.

- An effective and inexpensive encapsulation system was developed that adequately protects the RFID tags from the temperatures and compaction stresses inherent in HMA transport and paving. The flexible RFID tag is curled inside a 3/4-inch (19-mm) nominal outside diameter CPVC pipe, which is subsequently filled with high-temperature epoxy (Cotronics® Durapot™ 866). An improved curing process for the epoxy was also developed that minimized the formation of air bubbles and void.

- The read ranges of the encapsulated tags were thoroughly evaluated. The read range for the Alien® 1x1 tags in the optimal circumferential orientation inside the CPVC pipe varied between 0.5 and 2 ft (0.15 and 0.6 m), which is inadequate for the intended application. The corresponding read range for the Alien® 2x2 tags varied between 5 and 9 ft (1.5 and 2.7 m), which is more than adequate for the HMA tracking application.

- Thermal and mechanical survivability of the encapsulated tags was evaluated in the laboratory via oven heating and gyratory compaction. The encapsulated tags survived oven heating for 1.5 h at temperatures up to 347 ^{o}F (175 ^{o}C), adequate for paving applications. Survival rate for combined thermal and mechanical effects was approximately 75 percent. This is sufficient for field application because multiple tags will be placed into each truckload of HMA for redundancy.

The encapsulated RFID tags were field tested to evaluate the following issues: survivability under real-world paving scenarios, read range under actual field conditions, required redundancy, construction practicality issues, and construction quality issues. The encapsulated RFID tags were evaluated at three parking lot locations on the UMD campus and in two stages in a new pavement constructed by the MSHA for the Hampstead Bypass. Key findings from the field trials are as follows:

- In the parking lot trials, the read success rate (percentage of tags that could be read) varied from about 60 percent for the Alien® 1x1 tags to 100 percent for the larger format Alien® 2x2 tags.

- In the Hampstead Bypass trial, the overall read success rates were slightly less than 20 percent for the UPM Raflatac® tags and between 60 and 80 percent for the larger Alien® 2x2 format.

- Read success rate decreased slightly with increasing vehicle speed. The read success rate at 45 mi/h (72 km/h) was approximately 65 percent of the rate at slow speeds.

- Approximately 15 percent of the RFID tags “floated” to the surface of the mat in all of the field trials.

The field trials confirmed the very high survival rate of the encapsulated tags. Read success rates varied significantly with tag size and less significantly on other details such as antenna configuration and vehicle speed. The field trials consistently demonstrated that post-construction read success rates of 60 to 80 percent or higher are achievable from a bumper-mounted antenna array, even on a vehicle moving at traffic speeds.

It was observed during the HMA field trials that some of the encapsulated RFID tags "floated" to the surface of the compacted mat. This raised the possibility of a decrease in in-place compacted density or an increase in the in situ permeability or both in the local region around the tag. Extensive density and permeability testing was performed to evaluate these possibilities. No localized decrease in density, increase in permeability, or any detrimental effects of the surfaced tags were found. There is the possibility for long-term deterioration around the tags due to degradation of the bonds between the asphalt binder and the CPVC pipe encapsulation. However, qualitative observations of the surfaced tags in Lot EE at the time of this writing show no evidence of deterioration over the intervening 6 years. These findings confirm that the encapsulated RFID tags are a successful low-impact and inexpensive technology for tracking placement of HMA in the roadway.

RFID Tracking of PCC Placement

The successful application of RFID tags to track placement of HMA immediately suggested the parallel use for PCC placement. Preliminary laboratory evaluation of concrete cylinders suggested that the Alien® Gen2 2x2 tags could be read through about 2 inches (50 mm) of concrete at a distance of up to 5 ft (1.5 m). The reconstruction of a section of I-90 near Syracuse, NY, provided an opportunity for field evaluation. A large number of RFID tags similar to those used in the HMA application were placed in the PCC delivery trucks as they left the batch plant near the paving site. These tags were deposited with the PCC ahead of the slip form paver and incorporated into the concrete slabs. Unfortunately, on the return visit to the site about 1 month after paving, none of the tags could be read. The causes of this surprising and disappointing result were investigated in the laboratory. The influences of aggregate, water, and cement on read range and read success were systematically investigated. The most plausible explanation supported by the laboratory results is that the hydrated cement paste causes the cured concrete to have a very high dielectric constant (about 20). The penetration depth (i.e., read range) of the UHF RFID radio waves diminishes sharply as the dielectric constant increases.

Pavement Temperature Measurement Using SAW RFID

SAW RFID technology has the intrinsic capability to measure thermal expansion and thus temperature. Real-time measurement of pavement temperature distributions is necessary to interpret the stiffness feedback data in intelligent compaction because the stiffness of HMA is extremely temperature dependent.

The temperature measurement capability of SAW RFID was evaluated through laboratory and field testing. For the field testing, various configurations of SAW RFID tags were encapsulated in thermally conductive epoxy, attached with quick-set epoxy to the surface of a milled existing pavement, and then covered with a 1.5-inch (38-mm) thick compacted HMA overlay. Although limitations of the SAW RFID reader system made it difficult to measure the temperature versus

time trends during the first few minutes after placement, mat temperatures were recorded starting at about 10 min after placement until the mat was too cool for continued compaction. The measured temperatures versus time compared favorably with predictions from analytical/ numerical models, and an approach for using the SAW RFID field temperature measurements for calibrating these analytical/numerical models is proposed. Overall, the SAW RFID technology has potential for in situ temperature measurement in HMA pavement layers.

Reflection Crack Detection

The development of an early onset reflection crack detector was originally intended as another application of the SAW RFID technology. However, it was subsequently determined that conventional RFID was a more appropriate technology choice, in part because of the current relatively high cost of SAW RFID tags.

The reflection crack sensor concept is to implement a switch in the antenna circuit of the RFID tag: when there is no crack, the RFID tag signal can be read at a distance, but after a crack forms, the signal becomes too weak to be read. A prototype reflection crack detector was developed and tested in the laboratory and, under more limited conditions, in the field. In the laboratory, the prototype detector was shown to be capable of detecting a reflection crack before it reached the pavement surface. The limited field trials also showed that the detector had the required survivability and read range for real-world applications. Seventeen of 18 tags tested in the field survived the paving operations, and the tags could be read at distances of more than 5 ft in the optimal antenna configuration. This approach shows considerable promise, but will require additional and more rigorous field evaluation that was beyond the scope and resources of the present project.

Guidance on Data Integration

Maximum use of material property data collected during construction and pavement management data collected during service life is possible only when both sets of data can be related to a common spatial referencing system. Using RFID tags to track loads of sampled and tested material enables geospatial identification of the location of the delivered material in the pavement. These material properties can then be linked with the corresponding spatially located pavement performance data from the PMS.

Because of the wide variety of MMSs and PMSs used by agencies, it is possible only to outline the general steps needed to link these two datasets via geospatial coordinates. Generic examples are provided for the following necessary operations:

- Linkage of one or more RFID identifiers to material samples.
- Linkage of GPS coordinates to RFID identifier/material sample.
- Conversion of latitude/longitude to roadway location.
- Combining of MMS and PMS data by location.
- Display of extracted data.

The details of implementing these operations will depend on the particular MMS and PMS used by an agency.

RECOMMENDATIONS FOR FUTURE WORK

Recommendations for follow-on work after this project include the following:

- Commercialization of the RFID system for tracking HMA placement. This research has demonstrated the success of the concept. However, it was impossible to generate commercial interest in it during the course of the project.

- Evaluation of other RFID systems (e.g., different frequency range, active instead of passive system, etc.) for use in tracking PCC placement. The high dielectric constant of the cement paste coating the aggregates in PCC makes it impossible to pass a sufficiently strong signal to/from the passive UHF RFID tags used so successfully for HMA tracking.

- For temperature measurement using SAW RFID tags, more work should be done to determine the minimum thickness of the epoxy coating to maximize tag readability and minimize thermal lag while still ensuring survivability. Additional work in collaboration with the SAW RFID system manufacturer is required to optimize the temperature window in the reader so that the early rapid cooling trends of the mat can be captured. Field trials should also be repeated on thicker HMA layers in which the variation of temperature with depth is more pronounced.

- Laboratory evaluation of the reflection crack detector should be conducted using a Texas Overlay Tester instead of three-point bending to better simulate how overlays fail. Through these tests, the CMOD as a function of vertical crack propagation can be determined more accurately, and the crack detector design can be adjusted as needed. Laboratory evaluation should then be followed by field trials on in-service pavements. The duration of these field trials would need to be on the order of 5 to 10 years to allow sufficient time for reflection cracks to initiate and propagate.

REFERENCES

1. Jaselskis, E.J., Anderson, M.R., Jahren, C.T., Rodrigues, Y., and Njos, S. (June 1995). "Radio-Frequency Identification Applications in the Construction Industry," *Journal of Construction Engineering and Management, 121*, 189–196.
2. Jaselskis E.J. and El-Misalami, T. (November/December 2003). "Implementing Radio Frequency Identification in the Construction Process," *Journal of Construction Engineering and Management, 129*, 680–688.
3. Sawyer, T. (2004). "Researchers are Getting Serious About Electronic Tracking Tags," *Engineering News Record, 253*, 28–29, December 13, 2004.
4. RF SAW Inc. (2010). *RF SAW—One Tag Worldwide.* Accessed July 12, 2012 (http://www.rfsaw.com).
5. Google®, Inc. (2015). *Map of Hampstead, MD.* Accessed March 6, 2015 (https://www.google.com/maps/place/Hampstead+Bypass,+Hampstead,+MD+21074/@39.5856963,-76.8458421,1784m/data=!3m1!1e3!4m2!3m1!1s0x89c841b72ab8394b:0x839adb14e013c04e)
6. Google®, Inc. (2015) *Satellite Image of the Parking Lot XX1 at the University of Maryland*. Accessed March 6, 2015 (https://www.google.com/maps/place/College+Park,+MD/@38.9897036,-76.9363343,112m/data=!3m1!1e3!4m2!3m1!1s0x89b7c41e0d714699:0xeb8c0de36dd36d95)
7. Google®, Inc. (2015) *Satellite Image of the Parking Lot EE at the University of Maryland*. Accessed March 6, 2015. (https://www.google.com/maps/place/College+Park,+MD/@38.9898521,-76.9378088,110m/data=!3m1!1e3!4m2!3m1!1s0x89b7c41e0d714699:0xeb8c0de36dd36d95)
8. Cooley, L.A. and Brown, E.R. (2000). "Selection and Evaluation of a Field Permeability Device for Asphalt Pavements," *Transportation Research Record, 1723*, 73–82.
9. Google®, Inc. (2015) *Satellite Image of the Syracuse NY study site*. Accessed March 6, 2015. (https://www.google.com/maps/place/792-1%2F2+N+Main+St,+North+Syracuse,+NY+13212/@43.0771507,-76.4817329,826m/data=!3m1!1e3!4m2!3m1!1s0x89d9ecfa084ee939:0x67388dce2149ecfc)
10. Ho, K.K.S. and Li, K.S. (2003). *Geotechnical Engineering*. Lisse: Swets and Zeitlinger B.V.
11. Zhang, X., Ding, X.Z., Ong, C.K., and Tan, B.T.G. (1996). "Dielectric and Electrical Properties of Ordinary Portland Cement and Slag Cement in the Early Hydration Period," *Journal of Materials Science, 31*, 1,345–1,352.
12. Wen, S. and Chung, D.D.L. (2001). "Effect of Admixtures on the Dielectric Constant of Cement Paste," *Cement and Concrete Research, 31*, 467–479.
13. FHWA (2012). *Accelerated Implementation of Intelligent Compaction Technology for Embankment Subgrade Soils, Aggregate Base, and Asphalt Pavement Material,* Report No. FHWA-HIF-2002-012, McLean, VA. Accessed July 12, 2012.
14. Corlew, J.S. and Dickson, P.F. (1968). "Methods for Calculating Temperature Profiles of Hot-Mix Asphalt Concrete as Related to the Construction of Asphalt Pavements," *Journal of the Association of Asphalt Paving Technologists, 37*, 101–140.

15. Holman, J. (2001). *Heat Transfer*, Ninth ed.: McGraw-Hill, Inc.
16. Jordan, P.G. and Thomas, M.E. (1976). *Prediction of Cooling Curves for Hot-Mix Paving Materials by a Computer Program*, Report LR 729, Transport and Road Research Laboratory.
17. Wolfe, R.K. and Colony, D.C. (1976). *Asphalt Colling Rates: A Computer Simulation Study*, Final Report on Project 2844, Ohio Department of Transportation.
18. Colony, D.C. and Wolfe, R.K. (May 1078). "Initial Cooling of Asphaltic Concrete Mats," *Journal of Transportation Engineering, 104*, 295–310.
19. Wolfe, R.K., Heath, G.L., and Colony, D.C. (January 1983). "Cooling Curve Prediction of Asphaltic Concrete," *Journal of Transportation Engineering, 109*, 137–147.
20. Kreith, F. and Black, W.Z. (1980). *Basic Heat Transfer*. New York: Harper & Row.
21. Luca J., and Mrawira, D. (January/February 2005). "New Measurement of Thermal Properties of Superpave Asphalt Concrete," *Journal of Materials in Civil Engineering, 17*, 72–79.
22. Fwa, T.F., Low, B.H., Tan, S.A. (1995), "Laboratory Determination of Thermal Properties of Asphalt Mixtures by Transient Heat Conduction Method," *Transportation Research Record,. 1492*, 118–128.
23. Highter, W.H. and Wall, D.J. (1983). "Properties of Some Asphaltic Concrete Mixes," in *AIAA 18th Thermophysics Conference*.
24. Google®, Inc. (2015) Map of US Route 15 project site. Accessed March 6, 2015 (https://www.google.com/maps/place/Frederick,+MD/@39.4094127,-77.4378708,14z/data=!4m2!3m1!1s0x89c9c50c8cbdaee3:0xda6247bdbd111c99)
25. The Transtec Group Inc. (2010). *Intelligent Compaction*. Available at http://www.intelligentcompaction.com
26. Broek D. (1982). *Elementary Engineering Fracture Mechanics*. The Hague: Martinus Mijhoff Publishers.
27. Cui, Q., Johnson, P.W., and Sees, E. (2008). "Long-Term Warranties on Highway Projects," Report 06109, University Transportation Center of Alabama, Birmingham AL.
28. Morita, K. and Noguchi, K. (2006). "Crack Detection Methods Using Radio Frequency Identification and Electrically Conductive Materials," *AIJ Journal of Technology and Design, 24*, 59–66.
29. Wood, S.L. and Neikirk D.P. (2001). "Development of a Passive Sensor to Detect Cracks in Welded Steel Construction," presented at the U.S.-Japan Workshop on Cooperative Research of Urban Earthquake Disasters, Seattle WA.
30. Paris, P. and Erdogan, F. (1963). "A Critical Analysis of Crack Propagation Laws," *Journal of Basic Engineering, 85*, 528–534.
31. Lee, S.W., Bae, J.M., Han, S.H., and Stoffels, S.M. (2007). "Evaluation of Optimum Rubblized Depth to Prevent Reflection Cracks," *Journal of Transportation Engineering, 133*(6), 355–361.
32. White, G.C., Mahoney, J.P., Turkiyyah, G.M., Wiloughby, K.A., and Brown, E.R. (2002). "Online Tools for Hot-Mix Asphalt Monitoring," *Transportation Research Record, 1813*, 124–232.
33. American Association of State Highway Transportation Officials. (2012). *AASHTOWare SiteManager Construction Management System*, July 23, 2012. Available at http://www.aashtoware.org/Pages/SiteManager.aspx

34. Fugro Roadware Inc. (2012),). *Fugro Roadware*. July 23, 2012. Available at http://www.roadware.com/
35. Schwartz, C.W. and Bentahar, N.L. (1995) "Joining Dynamically Segmented Infrastructure Data in Relational Database Systems," presented at the Computing in Civil Engineering: Proceedings of the 2nd Congress on Computing in Civil Engineering, New York.
36. O'Neill, W.A. and Harper, E. (1997). "Location Translation within a Geographic Information System," *Transportation Research Record, 1593*, 55–63.

ANNOTATED BIBLIOGRAPHY

Anonymous (2002). "Tracking Concrete Cubes for QA," *RFID Journal*, August 18, 2002. Available at http://www.rfidjournal.com/article/articleview/194.

RFID tags embedded in concrete test cubes were evaluated as an alternative to manual tracking to reduce human errors and costs for tracking QA test data. This "Cube Info" application employed passive 13.56 MHz tags with 228 bytes of storage. The tags were approximately the size of a quarter and were encapsulated in a hard plastic protective casing. A handheld reader/ writer was employed to scan the cubes at the job site and encode them with field information. Fixed reader/writers attached to the laboratory weigh scales and compression test machines were used to record QA test results. Read range is not reported in the article, but from the accompanying figures, it appears to be on the order of 1 m (3.28 ft).

Concrete mix information for an individual mixer truck was entered into the handheld reader/ writer via a barcode attached to the paper load slip. After a slump test was performed at the sight, the encapsulated active RFID tag was placed inside the freshly prepared 6-inch (152-mm) test cube. The handheld reader/writer then wrote the mix information, slump test results, and date to the active RFID tag. The cube was then sent to laboratory for curing. After curing, it was weighed, and the weight data were transferred from the weight machine RFID reader/writer to the tag embedded in the cube. A compression test was finally performed, and these results were also transferred by the associated RFID reader/writer to the tag. The protective plastic casing enabled the RFID tag to be retrieved intact after the test for download of the complete dataset. The encapsulated tags could be reused (more than 20 times). After verification of the test results, they were posted to a materials database and/or sent via email to the concrete producer and others.

The pilot implementation of the Cube Info system was reported as giving good results. No major technical problems were reported. Nonetheless, acceptance of this system does not appear to be speedy or widespread.

AXCESS, Inc. (2006). "AXCESS' Active RFID Solution Utilized by Bechtel to Automate HAZMAT Truck Payload Management," press release, May 9, 2006. Available at http://www.axcessinc.com/press/050509bechtel.doc.

In this application, RFID was used to monitor environmentally hazardous material movement with minimum hindrance in its transport. Active RFID tags were installed on trucks and drums. When the truck passed a weigh station, its load, contents, and other information was scanned and automatically uploaded to a database.

Collins, J. (2004). "Case Builds for RFID in Construction," *RFID Journal*, January 5, 2004. Available at http://www.rfidjournal.com/article/articleview/720/1/4/.

RFID technology was evaluated as an alternative to bar coding for tracking the shipment and delivery of metal pipes from a fabrication plant in Texas to a construction site. The RFID system consisted of active UHF (915 MHz) RFID tags from Identec® and Phase IV Engineering, an Identec® handheld reader connected to an iPaq™ personal digital assistant (PDA), and a

CargoWatch® stationary reader. Read-write range in noninterfering environments was approximately 328 ft (100 m). Only tag identification information was evaluated.

The focus of the study was to determine whether reliable readings could be obtained when the RFID tags were placed on a pipe surrounded by a large number of other pipes on the back of the truck. The tags were mounted on the pipes after loading onto the truck to avoid damage by the loading process. Two read modes were evaluated. Stationary loaded trucks were scanned by a worker with the handheld reader who moved around the truck trailer. Moving trucks were scanned as they were driven past a stationary reader location.

Tag reads for stationary trucks were 100-percent accurate up to a range of 10 ft (3.05 m). Accuracy dropped slightly for a moving truck passing the stationary reader. However, it rebounded to 100 percent when the truck stopped briefly near the stationary reader.

Ergin, E., and Hendrickson, C.T. (January 2007). "Utilization of Radio-Frequency Identification Tags for Transportation Infrastructure Management: Tracking Engineered-to-Order Elements and Materials Throughout Their Life-Cycles," ***Transportation Research Board 86th Annual Meeting*****, Washington, DC, Paper No. 07-2788.**

Information flow related to materials and components used in transportation infrastructure systems and their supply chains are plagued with inefficiencies caused by inadequate or late deliveries and installation of components at wrong locations. This paper provides a vision of how RFID tags could be used as a means to track components from long distances, store information on these components, and allow multiple parties to access this information. A requirements analysis and a limited set of field tests were performed to explore the technical feasibility of using RFID technology for these purposes. The experiments demonstrated that it was technically feasible to add intelligence to the components in transportation infrastructure systems to collect status information automatically within the supply chain.

Goodrum, P.M., McLaren, M.A., and Durfee, A. (2006). "The Application of Active Radio Frequency Identification Technology for Tool Tracking on Construction Job Sites," ***Automation in Construction*****,** ***15*****, 292–302.**

The objective of this study was to improve the tracking of handheld power tools on construction sites to make them more easily available to a worker when needed. Commonly used tools (corded hammer drill, portable band saw, reciprocating saw) at three construction projects were identified and tagged. Active UHF (915 MHz) RFID tags with lithium/thionyl chloride ($Li/SOCl_2$) and 32 Kb of memory were employed. The tags, approximately 1 by 5 inches in size, were mounted internally within the plastic tool housings. A handheld reader connected to a PDA was used to collect data.

Contractors were allowed to move tools freely according to their needs. Readings were taken every week at the job sites. Readings were taken while the tools were stored in top-opening metal gang (tool storage) boxes with the lid open. Reading distance and direction from the tools in the gang box were noted. Evaluation included read range, integrity of stored inventory and maintenance data on the tag, and ability of reader to update that data.

Readings in environmentally controlled laboratory conditions were successful up to ranges between 49.2 to 82 ft (15 to 25 m). This range dropped in the field to between 9.84 to 19.52 ft (3 to 9 m). The variation in the field read ranges was attributed to temperature influences and metal interference. The electromagnetic field produced by the tool itself did not affect the RFID signal. It was also noted that the active RFID could be short-circuited when drenched in water.

The largest read range decrease occurred at one site where temperatures fell to 10 °F (-12 °C). Battery performance in the active RFID tag was adversely affected by these low temperatures.

International Road Dynamics, Inc. (May 2004). "Wireless Concrete Maturity Meter," news release. Available at http://www.identecsolutions.com/fileadmin/user_upload/PDFs/case_studies/News_Release_ird_-_Wireless_Concrete_Maturity_MonitorV2_Eng.pdf.

Concrete maturity time was predicted using measured temperatures from an embedded RFID sensor and as input to predictive techniques such as the Equivalent Age (Arrhenius) and/or Nurse-Saul models. The RFID technology for this application consisted of an Identec® i-Q™ active UHF tag and a handheld reader. The system can read tags up to 8 inches inside concrete. This system, in conjunction with the predictive models, gave estimates of the compressive strength of concrete onsite. This was more accurate than laboratory techniques that did not share the same environmental and other conditions (e.g., volume) as onsite.

Johns Hopkins University Applied Physics Laboratory (January 2005). "New Sensors Promise to Drive Down Highway Maintenance Costs," news release. Available at http://www.jhuapl.edu/newscenter/aplnews/2002/highway.asp.

In this study, an RFID tag was combined with a conductivity sensor to monitor the corrosive environment in reinforced concrete bridge decks. The "Smart Aggregate" was a passive RFID tag roughly the size of a quarter that was encapsulated in a high compressive strength ceramic. During preliminary field trials, the Smart Aggregate tags were embedded in the concrete bridge deck for the Johns Hopkins/Gorman Road bridge over US Route 29 in Maryland. Results of these trials had not been located as of the time of this writing.

Jaselskis, E.J., Anderson, M.R., Jahren, C.T., Rodriguez, Y., and Njos, S. (June 1995). "Radio-Frequency Identification Applications in Construction Industry," *Journal of Construction Engineering and Management*, ASCE, *121*(2), 189–196.

This early paper on RFID applications in construction engineering begins with a basic description of the various technology options available and their respective advantages and limitations. Current and potential applications of this technology are then described. Although many of these applications are speculative, they suggest a broad impact of RFID technology in the construction industry.

Jaselskis, E.J., and El-Misalami, T. (November/December 2003). "Implementing Radio Frequency Identification in the Construction Process," *Journal of Construction Engineering and Management*,. *129*(6), 680–688. (see also Jaselskis, E.J., and El-Misalami, T. (2003). "RFID's Role in a Fully Integrated, Automated Project Process," *Construction Research Congress in Construction: Wind of Change: Integration and Automation*, ASCE.)

This paper is, in essence, an update of Jaselskis et al. (1995). The basic concepts and advantages and limitations of available RFID technologies are described. Key outcomes from a construction industry-RFID supplier workshop held to disseminate information and generate suitable application ideas in construction are summarized. This workshop generated one pilot application that was conducted to demonstrate the applicability of RFID to the material procurement process at a construction site. The pilot tests showed that RFID tags reduced the time required to download data into a company's material tracking system and reduced the potential for duplicate data entries. The application demonstrated the benefits of the technology in the materials receiving process.

Jaselskis, E.J., Grigas, J., and Brilingas, A. (September/October 2003). "Dielectric Properties of Asphalt Pavement," *Journal of Materials in Civil Engineering*, ASCE,*15*(5), 427–434.

Electromagnetic wave absorption, reflection, and transmission through asphalt concrete depend on the dielectric properties of the material. Asphalt concrete samples of different densities were studied in the frequency range from 100 Hz to 12 GHz to determine the temperature and frequency dependencies of the real and imaginary permittivity components. The principal findings were: 1) permittivity and loss depend on frequency and temperature, 2) permittivity increases with increasing pavement density, 3) permittivity slightly increases with temperature, 4) moisture strongly increases permittivity and loss at low frequencies and only slightly at high frequencies, and 5) the penetration depth of electromagnetic waves in asphalt pavements is about 4.72–5.51 inches (12–14 cm) at 8 GHz and only about 1.57 inches (4 cm) at 30 GHz. Although the focus of this study was on microwave transmission (frequencies between about 1 GHz and 300 GHz) to determine the density of in-place asphalt concrete, the data and results are also relevant to ground penetrating radar (frequencies between about 100 MHz and 1.6 GHz) and UHF RFID (frequency of approximately 900 MHz).

Naresh, A.L., and Jahren, C.T. (September 1997). "Communication and Tracking for Construction Vehicles," *Journal of Construction Engineering and Management*, ASCE, *123*(3), 261–268.

This survey article describes the potential efficiency benefits of advanced communication and tracking systems for construction vehicle fleets such as dump trucks, concrete trucks, low boy trailers, and scrapers. Three advanced systems are covered: signaling systems, continuous communication and tracking systems, and RFID. Implementation and potential value of these systems for construction fleet management are described in conceptual terms only.

O'Connor, M.C. (2006). "RFID Cures Concrete," *RFID Journal*, October 30, 2006. Available at http://www.rfidjournal.com/article/articleview/2673.

The time taken for concrete to mature depends on volume and temperature. As a consequence, test cylinders overestimate maturity time. The objective of this study was to measure the actual concrete maturity time onsite by employing temperature-sensing RFID technology.

The RFID technology employed in this application was an Identec® i-Q™ 915 MHz UHF active tag with an integrated temperature sensor. The RFID tag was placed in the wet concrete during construction. The temperature readings of concrete were transmitted to the handheld reader, which downloaded the information to a handheld computer capable of running concrete maturity time algorithms that model the relationship of maturity to temperature during curing. The RFID temperature sensor tag found that the required concrete strength at the actual site was achieved in only one-third of the time predicted by cylinder tests. This could significantly shorten the construction time for a building.

Peyret, F., and Tasky, R. (2004). "A Traceability System between Plant and Work Site for Asphalt Pavements," *Computer-Aided Civil and Infrastructure Engineering*, *19*, 54–63.

This study, conducted as part of the European Open System for Road Information Support project, evaluated the linkage of RFID and GPS technologies for associating asphalt mix data collected at the production plant with location of the material on the roadway. Of all of the material reviewed from the literature, this was the most relevant to the present project.

In this prototype system, the mix properties of a batch were stored in the plant computer. When a loaded transport truck fitted with an RFID tag left the plant, the plant computer transferred the mix properties, temperature, and weight of the load via the reader to the active RFID tag on the truck body. The paver at the job site was equipped with an RFID reader, GPS transponder, and a computer. When the transport truck arrived at the job site and unloaded into the paver, the paver instrumentation read the tag ID and other information and combined this information with GPS coordinates to record the starting and ending times and latitude/longitude coordinates along the roadway for that specific load

The RFID technology employed in this application consisted of an active UHF (866 MHz) RFID tag having an approximate size of 0.15 by 0.03 by 0.02 m. Reported read ranges were 49.1 ft (15 m) effective and 98.4 ft (30 m) nominal. The 13- by 0.82- by 1-ft (0.4- by 0.25- by 0.3-m) plant and paver antennas had coverage angles of approximately 120 degrees. An OMNISTAR® Differential GPS mounted on the paver was used to determine latitude, longitude, and time data.

During the prototype implementation, some minor information was lost from the tags, but this was judged to have no significant impact on the test results because such losses were anticipated in the prototype. There were some occasional difficulties obtaining an accurate GPS reading when the satellite signal was obstructed. The software for the prototype system was not fully integrated, and therefore the data reading and recording processes were not fully automated. This was to be remedied in future phases of the project. However, it is unclear whether these future phases were ever conducted. The authors have been contacted via email to learn whether any

additional work on the system has been completed, but no reply had been received at the time of this writing.

Sawyer, T. (2004). "Researchers Are Getting Serious About Electronic Tracking Tags," *Engineering News Record*, *253*(23), December 13, 2004, pp. 28–29.

This article describes how large construction firms have been employing RFID technology for a variety of applications, including automatic inventory control, automated tool check-out, and tracking of construction components in storage yards.

Song, J., Haas, C.T., and Caldas, C.H. (September 2006). "Tracking the Location of Materials on Construction Job Sites," *Journal of Construction Engineering and Management*, ASCE, *132*(9), 911–918. (See also Song, J., Haas, C.T., Caldas, C.H., and Liapi, K. (2005). "Locating Materials on Construction Site Using Proximity Techniques," *Construction Research Congress 2005: Broadening Perspectives*, ASCE.)

This paper presents an approach by which construction materials can be tagged and then automatically identified and tracked on construction sites without interfering with regular site operations. A construction supervisor equipped with a portable RFID reader and a GPS transponder roved the site. A combination of proximity of reads from discrete ranges allowed the construction material item to be located within a two-dimensional grid overlaying the construction site. Off-the-shelf RFID passive technology was employed in this study, but specifics were not provided regarding operating frequency or other parameters.

Stone, W.C., Pfeffer, L., and Furlani, K. (March 2000). "Automated Part Tracking on the Construction Job Site," *Robotics 2000*, ASCE Conference on Robotics for Challenging Environments, Albuquerque, NM. Available at
http://fire.nist.gov/bfrlpubs/build00/PDF/b00003.pdf**.**

This system design exercise was conducted as part of a National Institute of Standards and Technology initiative to develop Web-based techniques for tracking prefabricated components on construction site in real time. The basic concept was that each component to be shipped to a site was identified with a unique bar code or RFID tag. The bar code/RFID tag was scanned, and the identification information downloaded to a laptop when the component arrived on the job site. The component ID was then sent from laptop to the project database, where it was joined with the whole description of the component, e.g., from the manufacturer's specification book. The site inspector also entered the 3D coordinates of the component's onsite storage location using a 3D coordinate measuring tool. The component was tracked by sensors that automatically updated the project database. The project database information could be sent via the Web to a distant project management office, where all activity could be viewed in real time in three-dimensional space.

A pilot test monitored site activity from an office located approximately 0.621 mi 1(km) away from the job site. However, only barcodes were used in the pilot. Although not implemented, the author anticipated much better performance using RFID technology.

Swedberg, C. (2006). "RFID Markers Track Buried Cables at Atlanta Airport," *RFID Journal*, September 12, 2006. Available at http://www.rfidjournal.com/article/articleview/2647/.

This application focused on locating underground cables and pipes at the Atlanta airport using RFID. Ball markers containing RFID tags were used to store identification, location, and other information for each utility cable and pipe. Different categories of utility cables and pipes were assigned different RFID tag frequencies. Passive RFID tags with 256 bits of memory and operating frequencies ranging from 66 to 169 MHz were employed for this application. The system was reported to work well, with tags readable up to five ft underground.

Violino, B. (2007). "RFID Rocks at Graniterock," *RFID Journal*, January 22, 2007. Available at http://www.rfidjournal.com/article/articleview/2905/1/4/.

RFID technology was employed to improve efficiency of movement of trucks at Graniterock quarries. The system was based on a TransCore® IP Ltd. passive RFID tag (approximate dimensions of 2 by 12 inches (5 by 30.5 cm) scanned using a fixed location TransCore® reader. A key focus of this implementation was integration of the RFID data with other Graniterock® business operation software and databases.

The quarry operations staff was informed via telephone about the RFID tag identification, trucking company name, and other information as the truck approached the entrance. This information was fed into the operations database. As the truck entered the quarry weigh station, the fixed reader read the tag ID and combined this information with the empty truck weight and other information that was correlated with the pre-arrival information already stored in the database. As the loaded truck left, it again passed the reader, the tag ID was again read, and the corresponding loaded weight was automatically uploaded to the database. A hardcopy receipt/billing slip was printed for the truck operator.

Although the details of the reader configuration and read range are not stated, the test trials of the system were reported as very successful. There was an initial problem distinguishing incoming and outgoing trucks passing the fixed reader simultaneously, but this problem was resolved through modification of the direction and power of reader. Overall, Graniterock® found that the automated RFID system dramatically reduced human input (i.e., staff time) and produced significant time savings.

Wasserman, E. "Construction's Building Blocks: RFID," *RFID Journal*. Available at http://www.rfidjournal.com/magazine/article/2922/1/394/.

A nontechnical survey article describing several applications of RFID technologies to the construction industry.

Wessel, R. (2006). "RFID Chops Timber Costs," *RFID Journal*, April 3, 2006. Available at http://www.rfidjournal.com/article/articleview/2220/1/4/.

RFID technology was integrated into a Log Tracking System (LTS) to minimize logs lost in the forest and to improve the efficiency of timber log deliveries to sawmills. An RFID tag encased in a plastic nail was hammered into the base of a freshly cut log in the forest. The RFID

identification number was scanned and downloaded to a handheld computer where it was combined with other manually-entered characteristics of the log. These data were transmitted wirelessly to a central main database. After the trees had been transported from the forest to the roadside, the tag was again scanned, and the identification number transmitted to the main database. The main database compared the ID numbers of the cut logs from the forest against the ID numbers of the logs along the roadside to reduce the chances of leaving a log in the forest. The ID numbers of logs were again scanned at the time of loading into the haul trucks and when delivered to the sawmill.

The RFID technology employed in this application consisted of a passive 125 KHz tag encased in a special plastic nail. The plastic nail was made of polyamide reinforced with glass fiber and was approximately 0.2 inches (0.5 cm) in diameter by 1.4 inches (35.6 cm) long. A special hammer was used to drive the RFID nail. The handheld reader was attached to a wristband and was connected to a handheld computer. Maximum read range was 1.2 inches (3 cm), which seems marginal, but the nails were clearly visible in the ends of the logs at all steps and could therefore be easily located and read at close range. Other data regarding the log were entered into the handheld computer using a voice input system via a microphone attached to the logger's helmet. Data were transmitted wirelessly from the handheld computer using a wireless local area network connection or the GSM network.

The pilot implementation of this system was successful. No trunks were lost by using RFID. The LTS worked in rain and snow conditions. The RFID tags did have a small read range and stored only an identification number, but any enhancements would make the tags economically infeasible. One problem encountered early on was damage to the nails when they were hammered into the log, particularly if the log was frozen. A special hammer was developed to solve this problem.

HRDI-20/04-15(50)E